

THE BIOGEOCHEMICAL CYCLING OF DISSOLVED AND COLLOIDAL TRACE  
METALS IN THE WESTERN ARCTIC OCEAN

A Dissertation

by

LARAMIE THANIEL JENSEN

Submitted to the Office of Graduate and Professional Studies at Texas A&M University  
in partial fulfillment of the requirements for the degree of

DOCTOR OF PHILOSOPHY

Chair of Committee,	Jessica Fitzsimmons
Committee Members,	Rainer Amon
	Franco Marcantonio
	Peter Santschi
Head of Department,	Shari Yvon-Lewis

August 2020

Major Subject: Oceanography

Copyright 2020 Laramie Jensen

## ABSTRACT

The Arctic Ocean is characterized by broad continental shelves, large river inputs, sea ice coverage, and limited exchange with other major ocean basins. This provides a unique environment in which to examine the distribution of trace metal micronutrients such as Mn, Fe, Co, Ni, Cu, Zn, Cd, and Pb. Many trace metals are essential micronutrients for phytoplankton in the surface ocean, serving as metal centers for important metabolic reactions such as photosynthesis, nitrogen fixation, and carbon uptake. The distribution and behavior of these metals are relatively unexplored in the Arctic Ocean. However, this dataset collected within the international GEOTRACES program presents an opportunity to explore elemental cycling and size speciation on an unprecedented spatial scale in the Western Arctic Ocean. It also bridges together the overall dissolved, colloidal, and soluble size distribution of these trace metals. The colloidal size fraction (here defined between 0.003  $\mu\text{m}$  or 0.02  $\mu\text{m}$  and 0.20  $\mu\text{m}$ ) is an operationally defined component of the dissolved phase ( $<0.20\mu\text{m}$ ) that may be more bioavailable to phytoplankton and represents an intermediary between the soluble and the more refractory particulate phase. Our methodology allows us to combine and exploit the characteristics of multiple trace metals at once to expand our understanding of the biogeochemical processes governing the Arctic Ocean.

Overall, this work defined the unique behavior of trace metals in the Arctic Ocean. First, we outline our methodology, including the under-explored effects of storage on filtration and sorption to bottle walls, important tenets of the trace metal field.

We then spend the next three chapters outlining the unique cycling of different metals within the Western Arctic Ocean. First, we first examined the dissolved biogeochemical cycling of Zn, an essential micronutrient that often cycles with major macronutrients such as silicate. This study illuminated the role of the Chukchi Shelf as a major factor controlling the distribution of Zn. The Chukchi Shelf was also critical for Fe and Mn, where elevated concentrations on the shelf persisted offshore within a water mass known as the halocline and allowed us to explore scavenging rates for these important “scavengers of the sea.” Finally, metals such as Cu and Ni that typically share no relationship in the global ocean were surprisingly correlated in the Arctic Ocean, leading to a comparison between sources and sinks of these elements in the Arctic, such as major rivers, sea ice melt, and water mass advection. Finally, we describe the results of a comparison of metal size partitioning across cryospheric waters: snow, meltponds atop the sea ice, sea ice, and the underlying seawater. This study was an unprecedented opportunity to assess the effects of incubation and mixing of these pools on the size distribution of trace metals and how, if at all, the melting of sea ice and snow in the Arctic will affect the availability of trace metals to the surface Arctic Ocean. Overall, this dissertation attempts to determine what major processes affect dissolved and colloidal trace metals in the Arctic Ocean and how this connects to our global understanding of biogeochemical cycling.

## DEDICATION

I would like to dedicate this dissertation to my parents, Stephen Jensen and Alison Byerly, for their unwavering support and motivation. They instilled in me a love of learning and exploring from an early age that has not failed me yet. Thank you for believing in me.

## ACKNOWLEDGEMENTS

I would like to first and foremost thank and acknowledge my advisor Dr. Jessica Fitzsimmons without whom this work would not have been possible. Her vision and guidance helped me to make analyses and interpretations at every step of the way. She values mentorship and strives to put her students and their best interests first. Since Day 1 she has worked tirelessly to ensure that I got absolutely everything possible out of my PhD, including ample fieldwork experience, networking opportunities, and published papers. She encouraged me to be independent in my progress and confident in sharing my ideas and opinions. As a result, I am well poised to begin the next chapter of my career in science with a mentor and colleague I can count on. Thank you, Jess.

Thank you to my committee members, Rainer Amon, Franco Marcantonio, and Peter Santschi for their continued guidance and wisdom throughout my PhD. Thank you, as well, to my department head, Shari Yvon-Lewis for her support and leadership over the past five years.

This work would not have been made possible without the GEOTRACES program and leadership by the chief scientists of the 2015 U.S. Arctic GEOTRACES cruise David Kadko, William Landing, and Greg Cutter. Gabrielle Weiss, Simone Moos, Jessica Fitzsimmons, Neil Wyatt, Ana Aguilar-Islas, Robert Rember, and Chris Marsay sampled and subsampled Arctic samples in this dissertation. Nathan Lanning, Janelle Steffen, and Kimber De Salvo helped collect and process samples in Galveston Bay. A special thanks to my coauthors and collaborators in the first three chapters: Neil Wyatt,

Ben Twining, Pete Morton, Bill Landing, Sara Rauschenberg, Robert Sherrell, Jessica Fitzsimmons, Mariko Hatta, Chris Measures, Seth John, Ruifeng Zhang, Paula Pinedo-Gonzales, and Maja Heller.

A huge thank you to Luz Romero in the R. Ken Williams radiogenic laboratory for all of her patience, good humor, and assistance in running samples on the ICP-MS. I will always be grateful to her for her willingness to watch the instrument while I took breaks and endless hours of trouble-shooting when things were not going well.

Finally, a special thank you to my friends and TAMU family over the past five years who have made this work more enjoyable and this community something I am absolutely proud to be a part of every day. To my “Fitz Lab” labmates past and present, Kimber De Salvo, Janelle Steffen, and Nate Lanning, thank you for your unwavering friendship, love, and support, I could not have done this without you guys in my corner.

## CONTRIBUTORS AND FUNDING SOURCES

### **Contributors**

This work was supervised by a dissertation committee consisting of Professor Jessica Fitzsimmons of the Department of Oceanography and Professor(s) Franco Marcantonio of the Departments of Geology&Geophysics and Oceanography, Rainer Amon, and Peter Santschi both of the Departments of Oceanography (main campus) and Marine Science at Texas A&M Galveston.

### **Funding Sources**

Graduate study was supported by a Merit fellowship from Texas A&M University, Louis and Elizabeth Scherck fellowship, the M.T. Halbouty '30/AAPG Foundation Endowed fellowship, the Texas SeaGrant Grants-in-Aid of Graduate Research grant, a Texas A&M Triad Grant awarded to Jessica Fitzsimmons, Bella Chu, and Gerardo Gold-Buchot, and a grant by the National Science Foundation S-STEM scholar program courtesy of Drs Wilf Gardner and Mary Jo Richardson.

This work was also made possible in part by the NSF Division of Ocean Sciences (OCE) under Grant Number(s) 1434493 and 1713677 awarded to Drs Jessica Fitzsimmons and Robert Sherrell (Rutgers University) for work through the international GEOTRACES program. Its contents are solely the responsibility of the authors and do not necessarily represent the official views of the NSF.

## NOMENCLATURE

AB = Amundsen Basin

AL = Atlantic Layer

AMR/A-MR = Alpha-Mendelev Ridge

AOU = Apparent Oxygen Utilization

BNL = Benthic nepheloid layer

BSB = Barents Sea Branch

CB = Canada Basin

Cd = Cadmium

CFF = Cross flow filtration

cMe = Colloidal metal

Co = Cobalt

COC = Colloidal organic carbon

CTD = Conductivity, temperature, depth

Cu = Copper

DIN = Dissolved inorganic nitrogen

dMe = Dissolved metal

DNA = Deoxyribonucleic acid

HEPA = High-efficiency particulate air

DOC = Dissolved organic carbon

DOM = Dissolved organic matter

ESI = Elemental Scientific

Fe = Iron

FIA = Flow injection analysis

FSB = Fram Strait Branch

HCl = Hydrochloric acid

HDPE = High density polyethylene

HNLC = High-nutrient, low-chlorophyll

HNO<sub>3</sub> = Nitric acid

HR-ICP-MS = High resolution intercoupled plasma mass spectrometry

LDPE = Low density polyethylene

LHL = Lower halocline layer

LR = Lomonsov Ridge

LTERR = Long-term ecological research

ARSV = Antarctic research and supply vessel

MB = Makarov Basin

MIZ = Marginal ice zone

Mn = Manganese

nanoSIMS = Nanoscale secondary ion mass spectrometry

Ni = Nickel

NO<sub>3</sub><sup>-</sup>/N = Nitrate

OMZ = Oxygen minimum zone

Pb = Pb

PFA = Perfluoroalkoxy

PML = Polar mixed layer

$\text{PO}_4^{3-}/\text{P}$  = Phosphate

PTFE = Polytetrafluoroethylene

RSD = Relative standard deviation

RT = Room temperature

SA:V = Surface area: volume

SEPR = Southern East Pacific Rise

SIO ODF = Scripps Institute of Oceanography Oceanographic data facility

$\text{SiO}_4/\text{Si}$  = Silicate/silicic acid

sMe = Soluble metal

SXRF = Scanning X-ray fluorescence

TAMU = Texas A&M University

TPD = Transpolar drift

UHL = Upper halocline layer

USCGC = United States coast guard cutter

UV = Ultraviolet

Zn = Zinc

## TABLE OF CONTENTS

	Page
ABSTRACT .....	ii
DEDICATION .....	iv
ACKNOWLEDGEMENTS .....	v
CONTRIBUTORS AND FUNDING SOURCES.....	vii
NOMENCLATURE.....	viii
TABLE OF CONTENTS .....	xi
LIST OF FIGURES.....	xiv
LIST OF TABLES .....	xviii
1. INTRODUCTION.....	1
1.1. Overview .....	1
1.2. Background on trace metals .....	2
1.2.1. Size partitioning .....	7
1.2.2. Background on the Arctic Ocean .....	9
1.3. Project Summary .....	11
1.4. References .....	12
2. ASSESSMENT OF THE STABILITY, SORPTION, AND EXCHANGEABILITY OF MARINE DISSOLVED AND COLLOIDAL METALS .....	26
2.1. Overview .....	26
2.2. Introduction .....	27
2.3. Methods.....	32
2.3.1. Sample collection .....	32
2.3.2. Ultrafiltration methods .....	33
2.3.3. Experimental methods.....	35
2.3.4. Metal analysis.....	41
2.4. Results .....	44
2.4.1. Colloid preservation experiment: Can soluble/colloidal size partitioning be preserved over time by storing seawater frozen or at room temperature? .....	44

2.4.2. Colloid exchangeability experiment: Do colloids “grow back” after removal via ultrafiltration, and if so, how fast? .....	51
2.4.3. Adsorption experiment: How quickly are dissolved metals lost from solution to bottle wall adsorption in the absence of seawater acidification? .....	55
2.4.4. Desorption experiment: Once samples have been acidified, how quickly do metals desorb from bottle walls? .....	61
2.5. Discussion and implications .....	62
2.6. Conclusions .....	68
2.7. References .....	70
3. BIOGEOCHEMICAL CYCLING OF DISSOLVED ZINC IN THE WESTERN ARCTIC (ARCTIC GEOTRACES GN01).....	86
3.1. Overview .....	86
3.2. Introduction .....	87
3.3. Methods.....	91
3.3.1. Sample Collection .....	91
3.3.2. Zn analysis and Intercomparison.....	93
3.3.3. Temperature, Salinity, Nutrients, and Hydrography .....	98
3.3.4. SXRF Cell Stoichiometry Analyses .....	98
3.4. Results and Discussion.....	99
3.4.1. Hydrographic Setting .....	101
3.4.2. The sPML dZn Distribution .....	106
3.4.3. Halocline Zn Distribution.....	118
3.4.4. Atlantic Layer: FSB.....	122
3.4.5. Arctic Deep Water.....	125
3.4.6. Zn:Si Global Comparison.....	131
3.5. Conclusions .....	135
3.6. References .....	138
4. A COMPARISON OF MARINE FE AND MN CYCLING: U.S. ARCTIC GEOTRACES GN01 WESTERN ARCTIC CASE STUDY .....	162
4.1. Overview .....	162
4.2. Introduction .....	163
Iron (Fe) and manganese (Mn) are both essential micronutrients for marine.....	164
4.3. Sample Collection and Analysis Methods .....	168
4.3.1. Ultrafiltration.....	171
4.3.2. Dissolved analyses .....	172
4.3.3. Particulate analyses .....	174
4.3.4. Intercalibration of dissolved Fe and Mn datasets.....	175
4.3.5. Hydrographic analyses .....	177
4.4. Results .....	177
4.4.1. Hydrography.....	177

4.4.2. Overview of Fe and Mn observations .....	180
4.4.3. Oxidation differences between Fe and Mn along the Bering and Chukchi shelves .....	191
4.5. Discussion and Implications .....	208
4.6. Conclusions .....	214
4.7. References .....	215
5. A NOVEL RELATIONSHIP BETWEEN DISSOLVED COPPER AND NICKEL IN THE WESTERN ARCTIC OCEAN (GEOTRACES GN01).....	238
5.1. Introduction .....	238
5.2. Methods.....	243
5.2.1. Sample collection .....	243
5.2.2. Analysis.....	245
5.3. Results .....	246
5.3.1. Hydrography.....	246
5.3.2. Copper and Nickel in the Arctic Ocean.....	249
5.4. Discussion .....	267
5.4.1. What causes the Cu-Ni linear correlation in the Arctic?.....	268
5.4.2. Copper and Nickel global relationship.....	272
5.5. Conclusions .....	277
5.6. References .....	279
6. BIOGEOCHEMICAL CYCLING OF COLLOIDAL TRACE METALS IN THE ARCTIC CYROSPHERE .....	302
6.1. Introduction .....	302
6.2. Methods.....	308
6.2.1. Sample collection .....	308
6.2.2. Ultrafiltration.....	310
6.2.3. Analyses .....	312
6.3. Results .....	313
6.4. Discussion .....	322
6.4.1. Question 1: Do cryospheric freshwater pools have higher %colloids than seawater? .....	326
6.4.2. Question 2: Could aggregation and/or colloidal scavenging be a pathway for metal loss during the incubation of waters in cryospheric freshwater reservoirs before it is sourced to seawater?.....	330
6.5. Conclusions .....	339
6.6. References .....	341
7. SUMMARY AND CONCLUSIONS.....	355

## LIST OF FIGURES

	Page
Figure 1.1 Global comparison of Fe, Cu, Ni, Zn, Mn, Cd, and Pb in the Pacific (filled circles) and Atlantic (open circles). .....	4
Figure 1.2 Conceptual box model diagram for trace metal inventory in the ocean. ....	6
Figure 2.1 Schematic of the Colloid Preservation Experiment methods. ....	36
Figure 2.2 Schematic of the Colloid Exchangeability Experiment methods. ....	39
Figure 2.3 Schematic of the Adsorption (left) and Desorption (right) Experiment methods.....	42
Figure 2.4 Summary of all results of the Colloid Preservation Experiment. ....	46
Figure 2.5 Summary of all results of the Colloid Exchangeability Experiment across all metals.....	54
Figure 2.6 Results from the Adsorption (left) and Desorption (right) Experiments. ....	58
Figure 3.1 U.S. GEOTRACES Arctic GN01 transect with relevant stations, rivers, seas, and bathymetric features identified.....	92
Figure 3.2 Full-depth intercalibration between two SeaFAST pico isotope dilution methods.....	97
Figure 3.3 Global comparison of P, Si, and dZn profiles.....	100
Figure 3.4 Water mass characteristics for the northbound (left) and southbound (right) transects in the upper 500 m (top) and >500 m (bottom). ....	102
Figure 3.5 Upper 500 m of the northbound (left) and southbound (right) transects to characterize the halocline layers. ....	105
Figure 3.6 Characterization of dissolved zinc (dZn) in the surface Polar Mixed Layer (0–25 m).....	107
Figure 3.7 Chukchi Shelf (Stations 2–8 and 61–66) correlation between dZn and (a) Si ( $\mu\text{mol/kg}$ ) to show a remineralized nutrient source, (b) apparent oxygen utilization (AOU) to confirm a remineralization source, and (c) $\text{N}^{**}$ to show a remineralization source constrained to the sediments. ....	113
Figure 3.8 Plots of Zn:Si and Zn:C in Arctic cells.....	115

Figure 3.9 Plots of Zn in the LHL and UHL.....	122
Figure 3.10 Intermediate Atlantic layer dZn dynamics.....	125
Figure 3.11 Arctic deepwater dZn.....	126
Figure 3.12 Relationships between dissolved Zn and Si.....	130
Figure 3.13 Summary schematic of the major sources of dissolved zinc to the Western Arctic, where relative arrow size reflects the magnitude of the source.....	137
Figure 4.1 Schematic of the similarities and differences between Fe and Mn highlighted in this study.....	165
Figure 4.2 U.S. GEOTRACES Arctic GN01 transect with relevant stations, rivers, seas, and bathymetric features identified.....	170
Figure 4.3 Intercalibration across GN01.....	176
Figure 4.4 Sectional plots of a) dFe, b) dMn, c) pFe <sub>xs</sub> (particulate Fe excess), d) pMn <sub>xs</sub> (particulate Mn excess), e) salinity in the upper 400m.....	179
Figure 4.5 Surface (0-20m) plots of a) dFe, b) dMn, c) pFexs, d) pMnxs.....	181
Figure 4.6 Plots of a) %dFe = dFexs/(dFe + pFexs) and b) %dMn = dMnxs/(dMn + pMnxs) across the upper 400m of the transect.....	182
Figure 4.7 Plots of a) dissolved Fe, b) dissolved Mn, c) particulate Fe excess, and d) particulate Mn excess in the surface at MIZ.....	185
Figure 4.8 Major elements along the shelf and UHL.....	188
Figure 4.9 Plots in the upper 400 m of GN01 of Fe, Mn against macronutrients.....	189
Figure 4.10 Following the work of Rijkenberg et al. (2018) we calculated various Fe limitation scenarios along the GN01 transect in the upper 400m.....	192
Figure 4.11 Bering Strait/Chukchi Shelf station profiles of a) dFe b) dMn, c) pFe <sub>xs</sub> , d) pMn <sub>xs</sub> to show full range of elements at these important stations.....	193
Figure 4.12 Benthic sources along the shelf of Fe and Mn.....	194
Figure 4.13 Log-scale profiles of a) dFe, b) pFexs, c) dMn, d)pMnxs.....	196

Figure 4.14 Fe(II) oxidation half lives across the shelf and slope stations for the northbound (top panel, Stations 4-10) and southbound (bottom panel, Stations 57-66) transects.....	199
Figure 4.15 Dissolved Fe(II) measurements taken at Stations 61 (circles) and 66 (squares) are shown in black alongside overall dissolved Fe (all species, red).....	200
Figure 4.16 Log-scale transport plots of $\ln([\text{metal}])$ vs. distance from the 100 m isobath.....	203
Figure 4.17 Comparison of the Arctic Ocean (top, this study) with the North Atlantic (bottom, Fitzsimmons et al. 2015).....	207
Figure 4.18 Summary schematic of the major trends described in the text. ....	211
Figure 5.1 Linear correlation of Cu and Ni in the Western Arctic Ocean on GEOTRACES GN01 (excluding Station 1 in the Pacific). ....	242
Figure 5.2 U.S. GEOTRACES Arctic GN01 transect labeled with relevant stations, rivers, seas, and bathymetric features identified.....	244
Figure 5.3 Full depth sections of dissolved a) Ni and b) Cu across the GN01 transect.	248
Figure 5.4 Global comparison of the profile shapes of Cu (blue) and Ni (orange) .....	251
Figure 5.5 Plots of surface seawater Ni and Cu vs $f_{\text{sim}}$ and $f_{\text{met}}$ .....	253
Figure 5.6 Profile overlay of the concentrations of a) Cu and b) Ni across the entire transect in the upper 500 m of the water column.....	257
Figure 5.7 Ni and Cu across the Shelf and Strait. ....	259
Figure 5.8 Correlations between Cu, Ni, and Si within the halocline (Stations 8-19, 46-60).....	261
Figure 5.9 Plot of the distance from the shelf break vs natural log of a) Cu and b) Ni. ....	262
Figure 5.10 Plots of Cu and Ni within the Atlantic layer.....	264
Figure 5.11 Copper and nickel in Arctic deep water.....	265
Figure 5.12 Global comparison of Cu/Ni relationship to this study .....	274
Figure 6.1 Schematic of freshwater pools in the Arctic cryosphere. ....	304

Figure 6.2 Map of samples sites in this study as part of U.S. Arctic GEOTRACES GN01 cruise (2015). .....	309
Figure 6.3 Station 33 %Colloidal = [colloid]/[dissolved] for each metal (left) and the size partitioned concentrations (right) across each cryospheric pool. ....	318
Figure 6.4 Station 31 %Colloidal = [colloid]/[dissolved] for each metal (left) and the size partitioned concentrations (right) across each cryospheric pool. ....	319
Figure 6.5 Station 46 %Colloidal = [colloid]/[dissolved] for each metal (left) and the size partitioned concentrations (right) across each cryospheric pool. ....	320
Figure 6.6 Station 42 %Colloidal = [colloid]/[dissolved] for each metal (left) and the size partitioned concentrations (right) across each cryospheric pool. ....	323
Figure 6.7 Station 39 %Colloidal = [colloid]/[dissolved] for each metal (left) and the size partitioned concentrations (right) across each cryospheric pool. ....	324
Figure 6.8 Station 43 %Colloidal = [colloid]/[dissolved] for each metal (left) and the size partitioned concentrations (right) across each cryospheric pool. ....	325
Figure 6.9 Results of [colloid] and [soluble] concentrations in modeled (black) and measured (white) meltponds for Stations 33, 42, 43, and 46. ....	335

## LIST OF TABLES

	Page
Table 2.1 Summary of SAFe D1, blank, and limit of detection (LOD) results from this study compared to the May 2013 consensus values reported by GEOTRACES.....	43
Table 3.1 Measured Values for GEOTRACES Reference Materials SAFe D1 and D2 Across Three Labs and Two Analytical Methods. Reproduced with permission from Jensen et al. (2019).....	95
Table 4.1 Reported certified SAFe D1, D2, and S values as well as blanks and detection limits for dissolved Fe and Mn. ....	173
Table 4.2 Summary of log scale transport distance ( $d_{in}$ in km) values for this study (red) compared to literature values, primarily for Fe species.....	205
Table 5.1.1 Reported values of consensus SAFe D1, D2, and S solutions, as well as blanks and detection limits for dissolved Cu and Ni over the analytical sessions used for GN01 samples.....	246
Table 5.2 Table of global Cu-Ni slopes along zonal GEOTRACES transects. ....	277
Table 6.1 Values for SAFe D1 consensus materials for elements reported in this study (nmol/kg). ....	313
Table 6.2 Summary of %colloids within each pool (snow, melt pond, sea ice, and underlying seawater from 0-20m) and the number of measurements incorporated from each pool ( $n$ ). ....	316

# 1. INTRODUCTION

## 1.1. Overview

The Arctic Ocean presents a dynamic environment in which to study biogeochemical processes, particularly in light of ongoing climate change that disproportionately affects high latitude regions. The Arctic basin is enclosed and dominated by shelf area (>50%, (Jakobsson et al., 2004)) and receives geochemical input from a variety of sources such as rivers, continental margins, aerosol deposition, hydrothermal vents, and ice melt (Aagaard and Carmack, 1989; Aagaard and Roach, 1990; Edmonds et al., 2003; Rudels, 2010; Rudels, 2015). Importantly, it also serves as a site of mixing between the North Pacific and North Atlantic Oceans through restricted and shallow sills (50 m and 2600 m, respectively, (Talley et al., 2011)), in particular producing the outflow to the North Atlantic site of deep water formation (Dickson et al., 2002; Karcher et al., 2012). As important biogeochemical fluxes to the Arctic Ocean (river fluxes, precipitation, permafrost melt, sea ice melt, etc.) change with a warming climate, our understanding of trace metal distributions and their potential impacts on the global ocean become paramount.

This dissertation capitalizes on the work of the International GEOTRACES Program's effort to learn more about elemental cycling in the Arctic Ocean, especially how this unique and understudied basin connects to our growing understanding of the global distribution and cycling of trace elements and their isotopes. Notably, the biogeochemical cycling of trace metals in the Arctic appears inherently unique in the

Western Arctic Ocean, which is the site of the 2015 U.S. GEOTRACES cruise on which this dissertation is focused. Namely, the methodology described here is multielemental, producing rapid and precise determination of multiple analytes at once, which allows us to use our understanding of each metal's behavior and a suite of external chemical tracers to distinguish individual processes such as shelf input and circulation changes within a complex suite of processes. Likewise, the addition of ultrafiltration in this dataset allows us to probe the colloidal phase, an important intermediary between truly soluble and particulate trace metals, which can have different bioavailability and reactivity than its smaller, soluble-sized counterparts (Chen and Wang, 2001; Wang and Dei, 2003; Hassler and Schoemann, 2009; Hassler et al., 2011).

## **1.2. Background on trace metals**

Trace elements have long been used as tracers of processes in the ocean including, but not limited to, biological uptake, circulation, redox reactions, remineralization of organic matter, scavenging transformations, aerosol deposition, and riverine input (Bruland et al., 2014). Many trace metals serve as essential micronutrients for marine phytoplankton and thus are vital components of important metabolic processes such as photosynthesis, carbon assimilation and nitrogen fixation (Raven et al., 1999; Sunda, 2012; Twining and Baines, 2013). As such, these micronutrients are strongly linked to primary production and export of carbon to deep sea sediments (Aumont et al., 2015; Tagliabue et al., 2016). By analyzing a suite of bioactive and anthropogenic trace metals such as Fe, Mn, Co, Ni, Cu, Zn, and Pb here, we can enhance our understanding on the processes occurring at important interfaces such as at the

continental shelf, under sea ice, in estuaries, and even between ocean basins. This synergistic study is especially prescient in the Arctic Ocean where climate change is rapidly altering the biogeochemical landscape with potentially direct effects to the North Atlantic, our gateway to thermohaline circulation.

Classically, trace metals are grouped based on their typical profile shape across the global ocean. The three main categories are “nutrient-type”, following the distribution of major macronutrients with surface depletion and regeneration with depth; “scavenged-type”, defined as having relatively high surface concentrations and depletion with depth due to scavenging onto sinking particulate phases; and “hybrid-type”, which have characteristics of both “nutrient-type” and “scavenged-type” elements (Bruland et al., 2014). Common “nutrient-type” metals include Cd, Zn, and Ni, which typify a nutrient-like profile and follow the distributions of phosphate and silicate closely within the global ocean (Boyle et al., 1976; Sclater et al., 1976; Bruland, 1980; Bruland et al., 2014; Böning et al., 2015). Likewise, Co often follows macronutrient distributions and, while implicated in biological cycling (Sunda and Huntsman, 1995; Hawco and Saito, 2018), also shows signs of intense scavenging with depth (Saito et al., 2017; Hawco et al., 2018). Manganese typifies a scavenged-type profile with high surface concentrations due to slow oxidation kinetics (Stumm and Morgan, 1981) and photoreduction (Sunda et al., 1983; Sunda and Huntsman, 1994) but increased scavenging with depth (Balistrieri et al., 1981; Landing and Bruland, 1987). Iron, the most biologically required trace metal (Ho et al., 2003), is considered “hybrid-type” as it experiences both surface depletion and some regeneration during the remineralization of organic matter with depth, but also

has evidence of scavenging at depth (Landing and Bruland, 1987; Bruland et al., 2013), much like Cu, another essential micronutrient that has a unique, hybrid-type profile (Boyle et al., 1977; Jacquot and Moffett, 2015; Richon and Tagliabue, 2019).

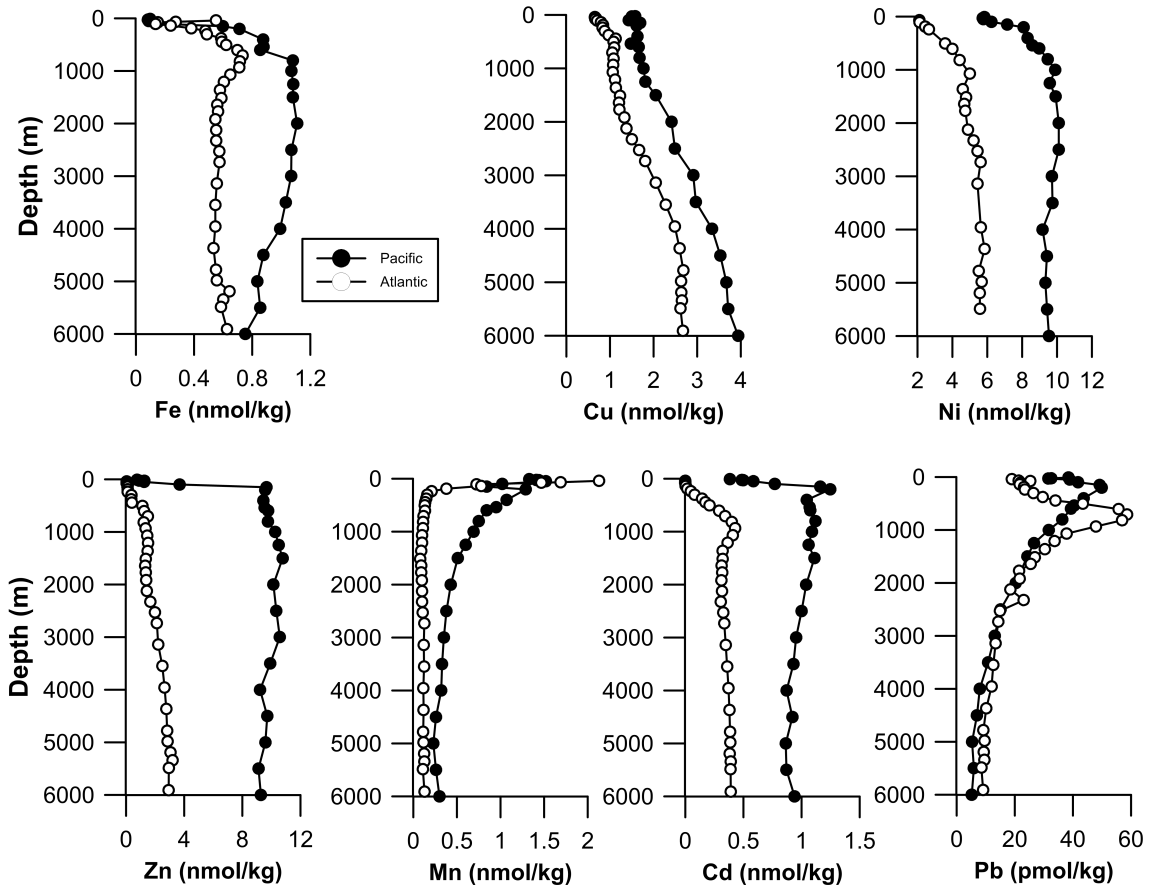


**Figure 1.1** Global comparison of Fe, Cu, Ni, Zn, Mn, Cd, and Pb in the Pacific (filled circles) and Atlantic (open circles). Subarctic North Pacific data is from GEOTRACES section GP02 (Station BD09, 47°N, 170.68°W), subtropical North Atlantic data is from GEOTRACES section GA03 (Station 20, 22.35°N, 35.87°W) (Schlitzer et al., 2018). Pacific waters remain nutrient-rich compared to the Atlantic waters due to the age of each basin as a result of thermohaline circulation.

These profiles are a combination of “sources and sinks” such as aerosol deposition, circulation, biouptake, scavenging, redox transformations, and regeneration of organic matter. Figure 1.1 shows typical profiles for each element in both the Atlantic and Pacific Oceans.

The defining elemental “personalities” translate to a changing inventory over thermohaline circulation. This is well-represented in Figure 1.1 where the concentrations for most “nutrient-type” trace metals are noticeably higher in the Pacific Ocean compared to the Atlantic Ocean due to the cumulative regeneration of nutrients and micronutrients in older Pacific waters compared to younger Atlantic waters. The ubiquitously low surface concentrations of micronutrients Fe, Zn, Ni, Cu, Co, and Cd are due to biological uptake in the surface waters (Sunda, 2012). These micronutrients are often recycled in the shallow euphotic zone (Hutchins and Bruland, 1994; Poorvin et al., 2004), but the majority sink vertically due to the settling of biogenic particles that can sorb or scavenge trace metals. These particles undergo bacterially mediated degradation giving rise to the subsurface enrichment due to regeneration that is seen in trace metal and nutrient profiles (Figure 1.1; (Sunda, 2012)). This process is inextricably linked to carbon cycling and export of carbon dioxide from the atmosphere to the ocean (Sigman and Boyle, 2000), highlighting the importance of understanding the processes governing trace metals in the global ocean. These processes, namely biouptake at the surface and regeneration with depth, shape our current view of trace metal cycling as well as lead them to be used as tracers along with nutrients. Additionally, profiles may be shaped by

scavenging onto sinking particles at the surface or with depth, linking them to abiotic uptake processes.

The interplay of various “sources and sinks” in controlling the distribution of trace metals in the water column leads us to conceptualize trace metals in the ocean as a box model, wherein the inventory inside of the box is a combination of source inputs and removal (Figure 1.2). This framework is especially helpful when navigating a novel study area, such as the Arctic Ocean, where hydrography is continuously monitored and relatively well understood but geochemical internal cycling is not constrained. Each source and sink controls the overall profile of different metal to different extents, and thus a multielemental comparison allows us to combine the unique behavior of each element to tease apart the major oceanographic processes acting in the Arctic Ocean. We also can explore the speciation and lability of dissolved trace metals in these various sources and sinks by employing ultrafiltration to examine size partitioning.

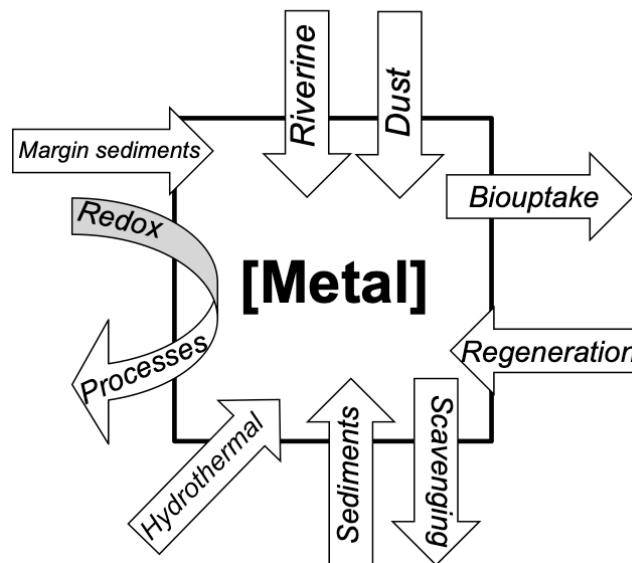


**Figure 1.2** Conceptual box model diagram for trace metal inventory in the ocean. Size of arrow or text has no bearing on the magnitude of the flux.

### 1.2.1. Size partitioning

The size partitioning of dissolved trace metals is important as it helps define differences in both the reactivity and bioavailability of dissolved metal complexes. Size definitions herein are operationally defined using the filter pore size; for instance, the dissolved phase is typically defined as what passes through a 0.2  $\mu\text{m}$  or 0.4  $\mu\text{m}$  filter, while the particulate phase is collected on those same filters (Bruland et al., 2014). Within the dissolved phase, we can further operationally define the smallest soluble phase as passing through a 0.02  $\mu\text{m}$  or 10 kDa ( $\sim 0.003 \mu\text{m}$ , (Erickson, 2009)) ultrafilter. Colloids, meaning “glue-like” (Graham, 1861), are generally thought of as the largest dissolved species (0.003-0.2  $\mu\text{m}$ ), whereas “soluble” species are considered truly dissolved ( $< 0.003 \mu\text{m}$ ). A more rigorous definition distinguishes colloids from soluble species at the size at which the internal characteristics of the dissolved matter become sufficiently different from its surroundings such that an interface between the two is formed (Wells, 2002). Additionally, the upper size limit is defined as when the force of gravity acts upon a colloid such that it begins to sink, typically via aggregation (Wells, 2002). Colloids are most often composed of macromolecules, making them primarily organic in nature (Guo and Santschi, 1997), although for metals they can be composed inorganic nanoparticles as well (Fitzsimmons et al., 2017). Typical sources of colloids vary from *in situ* formation such as from estuarine flocculation (Benner et al., 1992; Powell et al., 1996; Wen et al., 1999) to external supplies such as from sediment resuspension in coastal environments (Burdige et al., 1992; Guo and Santschi, 1997). However, the *in situ* cycling of aggregation-disaggregation dynamics dominate marine

colloid production in the water column (Burdige et al., 1992; Guo and Santschi, 1997; Wells, 2002).

Importantly, organic and inorganic colloids can contain trace metals such as Fe, and thus the speciation of dissolved Fe at any given location can affect the availability of these trace metals to phytoplankton, as well as the rates of other internal cycling processes such as scavenging. It is understood that the complexation of metals by organic ligands can increase their solubility and even accessibility to phytoplankton (Rue and Bruland, 1995; Gledhill and Buck, 2012). Colloids are also thought to be bioavailable to some degree (Chen and Wang, 2001; Chen et al., 2003; Wang and Dei, 2003). The bioavailability of the colloidal phase is critical to understanding its contribution to the dissolved phase, as bulk dissolved Fe concentration estimates of bioavailability may overestimate true Fe bioavailability. Currently, we assume that the colloidal trace metal fraction is ~50% of the dissolved phase, varying spatially and with depth in the global ocean (Fitzsimmons and Boyle, 2014a). Sources of Fe colloids to the ocean include dust deposition, continental margins, and hydrothermal vents, while colloidal Fe removal occurs primarily through biouptake, aggregation, or scavenging with depth (Fitzsimmons and Boyle, 2014a).

Recent studies have suggested that the proclivity of a metal to form colloids may be directly linked to their extent of organic complexation (Dammshäuser and Croot, 2012). To date, the majority of trace metal studies have focused on Fe, which has a significant colloidal phase and is >99% organically complexed in surface waters (Gledhill and Buck, 2012), but other metals such as Cu and Zn are known to be

complexed with organic ligands >99% or up to 97%, respectively, in surface seawater (Coale and Bruland, 1988; Wells et al., 1998). In coastal regimes colloids appear to be a significant but variable contributor to the dissolved phase for many trace metals: Ni 0-45%, Cu 35-64%, Cd 0-67%, Pb ~ 10%, Zn 0-36% (Wen et al., 1999; Wells, 2002), while Mn is thought to be largely soluble (Oldham et al., 2017). Importantly, the speciation of each metal may impart some proclivity to the colloidal phase (Byrne, 2002), but basin-wide studies of colloids beyond Fe are scarce. Additionally, while the filtration methods used are well constrained for Fe (Fitzsimmons and Boyle, 2014b), the effects of storage and prompt filtration have not previously been explored for other metals.

### **1.2.2. Background on the Arctic Ocean**

Trace metal studies in the Arctic Ocean began in the late 1970s with the LOREX, CESAR, Ymer and FRAM cruises (Moore, 1981; Danielsson and Westerlund, 1983; Yeats, 1988; Yeats and Westerlund, 1991). This provided the first full-water column profiles of the metals Fe, Mn, Cu, Ni, Cd, and Zn in the Eastern and Western Arctic Oceans. Due to sampling constraints, these studies most often involved single profiles through the ice of one or two trace metals and macronutrients that showed significant statistical spread due to contamination or movement of the ice. However, these studies elucidated important processes affecting trace metals in the Arctic Ocean such as advection from the Pacific and Atlantic Oceans, riverine sources, atmospheric deposition, chemical reactions occurring in shelf waters leading to removal at the

sediments, and advection of the shelf-derived halocline water mass (Yeats and Westerlund, 1991).

The Arctic remains a difficult region to traverse due to the presence of sea ice in the basin year-round, but with the advent of new icebreaker technology more recent studies have been focusing on Arctic trace metal biogeochemistry. Results from Fe studies in Arctic sea ice (Aguilar-Islas et al., 2008; Tovar-Sánchez et al., 2010), Eurasian basin seawater (Middag et al., 2011; Klunder et al., 2012b; Klunder et al., 2012a), and the Chukchi and Beaufort shelves (Nakayama et al., 2011; Cid et al., 2012; Nishimura et al., 2012; Aguilar-Islas et al., 2013; Kondo et al., 2016) have been invaluable in generating new hypotheses since the earlier studies in the 1980s for how metals behave in the Arctic. A few studies also provide new data on the other micronutrient metals such as Ni, Cd, Mn, and Zn (Cid et al., 2012; Kondo et al., 2016), but mostly on the continental shelves. The implementation of advanced sampling technology, such as the trace metal-clean CTD rosette (Cutter and Bruland, 2012), and more accurate and higher-throughput analytical techniques, such as with ICP-MS (Milne et al., 2010; Lagerström et al., 2013), have made high-quality, multielement datasets possible.

Despite a gap in chemical-focused studies, physical oceanographers continued to study the Arctic with an eye to climate change and its effect on the hydrography of the region. The hydrography of the Arctic appears to be changing (Rudels, 2015), with increased river input (Peterson et al., 2002) and sea ice melt (Perovich and Richter-Menge, 2015). Both of these processes are known to be sources of trace metals to the Arctic (Hölemann et al., 1999; Hölemann et al., 2005; Aguilar-Islas et al., 2008; Tovar-

Sánchez et al., 2010), not to mention the effect of freshwater input on stratification and circulation (Nummelin et al., 2016). We might expect that as the hydrography changes, the biogeochemistry will be affected as well (Macdonald et al., 2015). Previous studies did not have the spatial capacity to show the full effects of these changes moving offshore into the Western Arctic. This work endeavors to answer how metals are distributed in a changing Arctic, what their primary sources and sinks are, and how these distributions differ from the classic profiles seen in the more stable Pacific and Atlantic Oceans.

### **1.3. Project Summary**

This project seeks to explore a changing Arctic through the lens of trace metal biogeochemistry. The goal of this work is to utilize this unique, multielemental dataset to answer the following general research questions: 1) how do trace metals behave in the Arctic Ocean? 2) what sources and sinks in the Arctic control trace metal distribution? And 3) how does Arctic trace metal biogeochemistry align with what we expect to see globally? I will summarize the findings in five chapters. The first data chapter (Section 2) will assess how valid our commonplace sampling and storage procedures are, particularly with respect to the colloidal phase. The second chapter (Section 3) will discuss the micronutrient metal Zn in the Arctic Ocean, focusing on its unique distribution and the controlling processes that force its global relationship to the macronutrient silicate. The third chapter (Section 4) will focus on Fe and Mn, two elements considered to share similar sources and sinks in the global ocean, and the dynamics of their distribution on the shallow, productive continental shelves and

subsequent scavenging in the particle-poor Arctic basin. The fourth chapter (Section 5) examines Cu and Ni, two metals not often compared, and their remarkable linear correlation as a result of high surface and low deep water concentrations that are absent from global profiles. The final and fifth chapter (Section 6) explores a unique freshwater dataset of snow, melt pond, sea ice and underlying seawater size partitioning analyses that showcase typical seawater colloidal distributions for Fe, Zn, Ni, Cu, Cd, and Mn and how they may be affected by processes occurring within the cryosphere. In each section we answer what major sources and sinks control the dissolved and/or colloidal phases of these important trace metals and how this may be different from our global understanding of biogeochemical cycling in the context of a rapidly changing Arctic Ocean.

#### **1.4. References**

- Aagaard, K., and Ee C Carmack. 1989. "The role of sea ice and other fresh water in the Arctic circulation." *Journal of Geophysical Research: Oceans* 94 (C10):14485-14498.
- Aagaard, K, and AT Roach. 1990. "Arctic ocean-shelf exchange: Measurements in Barrow Canyon." *Journal of Geophysical Research: Oceans* 95 (C10):18163-18175.
- Aguilar-Islas, Ana M., Robert Rember, Shigeto Nishino, Takashi Kikuchi, and Motoyo Itoh. 2013. "Partitioning and lateral transport of iron to the Canada Basin." *Polar Science* 7 (2):82-99. doi: <http://dx.doi.org/10.1016/j.polar.2012.11.001>.

- Aguilar-Islas, A. M., R. D. Rember, C. W. Mordy, and J. Wu. 2008. "Sea ice-derived dissolved iron and its potential influence on the spring algal bloom in the Bering Sea." *Geophysical Research Letters* 35 (24):n/a-n/a. doi: 10.1029/2008GL035736.
- Aumont, Olivier, Christian Éthé, Alessandro Tagliabue, Laurent Bopp, and Marion Gehlen. 2015. "PISCES-v2: an ocean biogeochemical model for carbon and ecosystem studies." *Geoscientific Model Development* 8 (8):2465.
- Balistrieri, L, PG Brewer, and JW Murray. 1981. "Scavenging residence times of trace metals and surface chemistry of sinking particles in the deep ocean." *Deep Sea Research Part A. Oceanographic Research Papers* 28 (2):101-121.
- Benner, Ronald, Gerardo Chin-Leo, W Gardner, B Eadie, and J Cotner. 1992. "The fates and effects of riverine and shelf-derived DOM on Mississippi River plume/Gulf shelf processes." *Nutrient Enhanced Coastal Ocean Productivity. Publication Number TAMU-SG-92-109, Sea Grant Program, Texas A&M University, Galveston, Texas:84-94.*
- Böning, Philipp, Tim Shaw, Katharina Pahnke, and Hans-Jürgen Brumsack. 2015. "Nickel as indicator of fresh organic matter in upwelling sediments." *Geochimica et Cosmochimica Acta* 162:99-108. doi: <http://dx.doi.org/10.1016/j.gca.2015.04.027>.
- Boyle, E. A., FR Sclater, and JM Edmond. 1977. "The distribution of dissolved copper in the Pacific." *Earth and planetary science letters* 37 (1):38-54.

- Boyle, E. A., F. Sclater, and J. M. Edmond. 1976. "On the marine geochemistry of cadmium." *Nature* 263 (5572):42-44.
- Bruland, KW, R Middag, and MC Lohan. 2013. "Controls of trace metals in seawater."
- Bruland, K. W. 1980. "Oceanographic distributions of cadmium, zinc, nickel, and copper in the North Pacific." *Earth and Planetary Science Letters* 47 (2):176-198.
- Bruland, K. W., R. Middag, and M. C. Lohan. 2014. "8.2 - Controls of Trace Metals in Seawater." In *Treatise on Geochemistry (Second Edition)*, edited by Heinrich D. Holland and Karl K. Turekian, 19-51. Oxford: Elsevier.
- Burdige, David J, Marc J Alperin, Juliana Homstead, and Christopher S Martens. 1992. "The role of benthic fluxes of dissolved organic carbon in oceanic and sedimentary carbon cycling." *Geophysical Research Letters* 19 (18):1851-1854.
- Byrne, Robert H. 2002. "Inorganic speciation of dissolved elements in seawater: the influence of pH on concentration ratios." *Geochemical Transactions* 3 (1):11. doi: 10.1186/1467-4866-3-11.
- Chen, Min, Robert C. H. Dei, Wen-Xiong Wang, and Laodong Guo. 2003. "Marine diatom uptake of iron bound with natural colloids of different origins." *Marine Chemistry* 81 (3-4):177-189. doi: [http://dx.doi.org/10.1016/S0304-4203\(03\)00032-X](http://dx.doi.org/10.1016/S0304-4203(03)00032-X).
- Chen, Min, and Wen-Xiong Wang. 2001. "Bioavailability of natural colloid-bound iron to marine plankton: Influences of colloidal size and aging." *Limnology and Oceanography* 46 (8):1956-1967. doi: 10.4319/lo.2001.46.8.1956.

- Cid, Abigail Parcasio, Seiji Nakatsuka, and Yoshiki Sohrin. 2012. "Stoichiometry among bioactive trace metals in the Chukchi and Beaufort Seas." *Journal of oceanography* 68 (6):985-1001.
- Coale, Kenneth H., and Kenneth W. Bruland. 1988. "Copper complexation in the Northeast Pacific." *Limnology and Oceanography* 33 (5):1084-1101. doi: 10.4319/lo.1988.33.5.1084.
- Cutter, Gregory A., and Kenneth W. Bruland. 2012. "Rapid and noncontaminating sampling system for trace elements in global ocean surveys." *Limnology and Oceanography: Methods* 10 (6):425-436. doi: doi:10.4319/lom.2012.10.425.
- Dammshäuser, Anna, and Peter L. Croot. 2012. "Low colloidal associations of aluminium and titanium in surface waters of the tropical Atlantic." *Geochimica et Cosmochimica Acta* 96:304-318. doi: <http://dx.doi.org/10.1016/j.gca.2012.07.032>.
- Danielsson, Lars-Göran, and Stig Westerlund. 1983. "Trace Metals in the Arctic Ocean." In *Trace Metals in Sea Water*, edited by C. S. Wong, Edward Boyle, Kenneth W. Bruland, J. D. Burton and Edward D. Goldberg, 85-95. Boston, MA: Springer US.
- Dickson, Bob, Igor Yashayaev, Jens Meincke, Bill Turrell, Stephen Dye, and Juergen Holfort. 2002. "Rapid freshening of the deep North Atlantic Ocean over the past four decades." *Nature* 416 (6883):832.
- Edmonds, H. N., P. J. Michael, E. T. Baker, D. P. Connelly, J. E. Snow, C. H. Langmuir, H. J. B. Dick, R. Mühe, C. R. German, and D. W. Graham. 2003. "Discovery of

- abundant hydrothermal venting on the ultraslow-spreading Gakkel ridge in the Arctic Ocean." *Nature* 421:252. doi: 10.1038/nature01351  
<https://www.nature.com/articles/nature01351#supplementary-information>.
- Erickson, Harold P. 2009. "Size and Shape of Protein Molecules at the Nanometer Level Determined by Sedimentation, Gel Filtration, and Electron Microscopy." *Biological Procedures Online* 11 (1):32. doi: 10.1007/s12575-009-9008-x.
- Fitzsimmons, Jessica N, and Edward A Boyle. 2014. "Assessment and comparison of Anopore and cross flow filtration methods for the determination of dissolved iron size fractionation into soluble and colloidal phases in seawater." *Limnol. Oceanogr. Methods* 12:246-263.
- Fitzsimmons, Jessica N., and Edward A. Boyle. 2014. "Both soluble and colloidal iron phases control dissolved iron variability in the tropical North Atlantic Ocean." *Geochimica et Cosmochimica Acta* 125:539-550. doi:  
<http://dx.doi.org/10.1016/j.gca.2013.10.032>.
- Fitzsimmons, Jessica N., Seth G John, Christopher M Marsay, Colleen L Hoffman, Sarah L Nicholas, Brandy M Toner, Christopher R German, and Robert M Sherrell. 2017. "Iron persistence in a distal hydrothermal plume supported by dissolved–particulate exchange." *Nature Geoscience* 10 (3):195.
- Gledhill, Martha, and Kristen N. Buck. 2012. "The Organic Complexation of Iron in the Marine Environment: A Review." *Frontiers in Microbiology* 3:69. doi:  
10.3389/fmicb.2012.00069.

- Graham, Thomas. 1861. "X. Liquid diffusion applied to analysis." *Philosophical transactions of the Royal Society of London* 151:183-224.
- Guo, Laodong, and Peter H. Santschi. 1997. "Composition and cycling of colloids in marine environments." *Reviews of Geophysics* 35 (1):17-40. doi: doi:10.1029/96RG03195.
- Hassler, C. S., and V. Schoemann. 2009. "Bioavailability of organically bound Fe to model phytoplankton of the Southern Ocean." *Biogeosciences* 6 (10):2281-2296. doi: 10.5194/bg-6-2281-2009.
- Hassler, C.S., Véronique Schoemann, Carol Mancuso Nichols, Edward C. V. Butler, and Philip W. Boyd. 2011. "Saccharides enhance iron bioavailability to Southern Ocean phytoplankton." *Proceedings of the National Academy of Sciences* 108 (3):1076-1081. doi: 10.1073/pnas.1010963108.
- Hawco, Nicholas J, Phoebe J Lam, Jong-Mi Lee, Daniel C Ohnemus, Abigail E Noble, Neil J Wyatt, Maeve C Lohan, and Mak A Saito. 2018. "Cobalt scavenging in the mesopelagic ocean and its influence on global mass balance: Synthesizing water column and sedimentary fluxes." *Marine Chemistry* 201:151-166.
- Hawco, Nicholas J, and Mak A Saito. 2018. "Competitive inhibition of cobalt uptake by zinc and manganese in a pacific Prochlorococcus strain: Insights into metal homeostasis in a streamlined oligotrophic cyanobacterium." *Limnology and Oceanography* 63 (5):2229-2249.

- Ho, Tung-Yuan, Antonietta Quigg, Zoe V Finkel, Allen J Milligan, Kevin Wyman, Paul G Falkowski, and François MM Morel. 2003. "The elemental composition of some marine phytoplankton." *Journal of phycology* 39 (6):1145-1159.
- Hölemann, JA, M Schirmacher, and A Prange. 1999. "Dissolved and particulate major and trace elements in newly formed ice from the Laptev Sea (Transdrift III, October 1995)." In *Land-Ocean Systems in the Siberian Arctic*, 101-111. Springer.
- Hölemann, J. A., M. Schirmacher, and A. Prange. 2005. "Seasonal variability of trace metals in the Lena River and the southeastern Laptev Sea: Impact of the spring freshet." *Global and Planetary Change* 48 (1–3):112-125. doi: <http://dx.doi.org/10.1016/j.gloplacha.2004.12.008>.
- Hutchins, DA, and KW Bruland. 1994. "Grazer-mediated regeneration and assimilation of Fe, Zn and Mn from planktonic prey." *Marine Ecology Progress Series*:259-269.
- Jacquot, Jeremy E., and James W. Moffett. 2015. "Copper distribution and speciation across the International GEOTRACES Section GA03." *Deep Sea Research Part II: Topical Studies in Oceanography* 116:187-207. doi: <https://doi.org/10.1016/j.dsr2.2014.11.013>.
- Jakobsson, M, A Grantz, Y Kristoffersen, R Macnab, RW MacDonald, E Sakshaug, R Stein, and W Jokat. 2004. "The Arctic Ocean: Boundary conditions and background information." In *The organic carbon cycle in the Arctic Ocean*, 1-32. Springer.

- Karcher, Michael, John N Smith, Frank Kauker, Rüdiger Gerdes, and William M Smethie. 2012. "Recent changes in Arctic Ocean circulation revealed by iodine-129 observations and modeling." *Journal of Geophysical Research: Oceans* 117 (C8).
- Klunder, M. B., D. Bauch, P. Laan, H. J. W. de Baar, S. van Heuven, and S. Ober. 2012. "Dissolved iron in the Arctic shelf seas and surface waters of the central Arctic Ocean: Impact of Arctic river water and ice-melt." *Journal of Geophysical Research: Oceans* 117 (C1):n/a-n/a. doi: 10.1029/2011JC007133.
- Klunder, M. B., P. Laan, R. Middag, H. J. W. de Baar, and K. Bakker. 2012. "Dissolved iron in the Arctic Ocean: Important role of hydrothermal sources, shelf input and scavenging removal." *Journal of Geophysical Research: Oceans* 117 (C4):n/a-n/a. doi: 10.1029/2011JC007135.
- Kondo, Yoshiko, Hajime Obata, Nanako Hioki, Atsushi Ooki, Shigeto Nishino, Takashi Kikuchi, and Kenshi Kuma. 2016. "Transport of trace metals (Mn, Fe, Ni, Zn and Cd) in the western Arctic Ocean (Chukchi Sea and Canada Basin) in late summer 2012." *Deep Sea Research Part I: Oceanographic Research Papers* 116:236-252. doi: <http://dx.doi.org/10.1016/j.dsr.2016.08.010>.
- Lagerström, Maria, M. Field, Marie Seguret, Fisher E, Clark, and Robert Sherrell. 2013. "Automated on-line flow-injection ICP-MS determination of trace metals (Mn, Fe, Co, Ni, Cu and Zn) in open ocean seawater: Application to the GEOTRACES program." *Marine Chemistry* 155:71-80. doi: 10.1016/j.marchem.2013.06.001.

- Landing, William M, and Kenneth W Bruland. 1987. "The contrasting biogeochemistry of iron and manganese in the Pacific Ocean." *Geochimica et Cosmochimica Acta* 51 (1):29-43.
- Macdonald, RW, ZA Kuzyk, and SC Johannessen. 2015. "It is not just about the ice: a geochemical perspective on the changing Arctic Ocean." *Journal of Environmental Studies and Sciences* 5 (3):288-301.
- Middag, R., H. J. W. de Baar, P. Laan, and M. B. Klunder. 2011. "Fluvial and hydrothermal input of manganese into the Arctic Ocean." *Geochimica et Cosmochimica Acta* 75 (9):2393-2408. doi:  
<http://dx.doi.org/10.1016/j.gca.2011.02.011>.
- Milne, Angela, William Landing, Michael Bizimis, and Peter Morton. 2010. "Determination of Mn, Fe, Co, Ni, Cu, Zn, Cd and Pb in seawater using high resolution magnetic sector inductively coupled mass spectrometry (HR-ICP-MS)." *Analytica Chimica Acta* 665 (2):200-207. doi:  
<https://doi.org/10.1016/j.aca.2010.03.027>.
- Moore, R. M. 1981. "Oceanographic distributions of zinc, cadmium, copper and aluminium in waters of the central arctic." *Geochimica et Cosmochimica Acta* 45 (12):2475-2482. doi: [http://dx.doi.org/10.1016/0016-7037\(81\)90099-5](http://dx.doi.org/10.1016/0016-7037(81)90099-5).
- Nakayama, Yuta, Satoshi Fujita, Kenshi Kuma, and Koji Shimada. 2011. "Iron and humic-type fluorescent dissolved organic matter in the Chukchi Sea and Canada Basin of the western Arctic Ocean." *Journal of Geophysical Research: Oceans* 116 (C7):n/a-n/a. doi: 10.1029/2010JC006779.

- Nishimura, Shotaroh, Kenshi Kuma, Satoko Ishikawa, Aya Omata, and Sei-ichi Saitoh. 2012. "Iron, nutrients, and humic-type fluorescent dissolved organic matter in the northern Bering Sea shelf, Bering Strait, and Chukchi Sea." *Journal of Geophysical Research: Oceans* 117 (C2):n/a-n/a. doi: 10.1029/2011JC007355.
- Nummelin, Aleksii, Mehmet Ilicak, Camille Li, and Lars H Smedsrud. 2016. "Consequences of future increased Arctic runoff on Arctic Ocean stratification, circulation, and sea ice cover." *Journal of Geophysical Research: Oceans* 121 (1):617-637.
- Oldham, Véronique E., Alfonso Mucci, Bradley M. Tebo, and George W. Luther Iii. 2017. "Soluble Mn(III)–L complexes are abundant in oxygenated waters and stabilized by humic ligands." *Geochimica et Cosmochimica Acta* 199:238-246. doi: <http://dx.doi.org/10.1016/j.gca.2016.11.043>.
- Perovich, Donald K., and Jacqueline A. Richter-Menge. 2015. "Regional variability in sea ice melt in a changing Arctic." *Philosophical Transactions of the Royal Society A: Mathematical, Physical and Engineering Sciences* 373 (2045). doi: 10.1098/rsta.2014.0165.
- Peterson, Bruce J., Robert M. Holmes, James W. McClelland, Charles J. Vörösmarty, Richard B. Lammers, Alexander I. Shiklomanov, Igor A. Shiklomanov, and Stefan Rahmstorf. 2002. "Increasing River Discharge to the Arctic Ocean." *Science* 298 (5601):2171-2173. doi: 10.1126/science.1077445.

- Poorvin, Leo, Johanna M Rinta-Kanto, David A Hutchins, and Steven W Wilhelm. 2004. "Viral release of iron and its bioavailability to marine plankton." *Limnology and Oceanography* 49 (5):1734-1741.
- Powell, Rodney T, William M Landing, and James E Bauer. 1996. "Colloidal trace metals, organic carbon and nitrogen in a southeastern US estuary." *Marine Chemistry* 55 (1-2):165-176.
- Raven, John A, Michael CW Evans, and Rebecca E Korb. 1999. "The role of trace metals in photosynthetic electron transport in O<sub>2</sub>-evolving organisms." *Photosynthesis research* 60 (2-3):111-150.
- Richon, Camille, and Alessandro Tagliabue. 2019. "Insights Into the Major Processes Driving the Global Distribution of Copper in the Ocean From a Global Model." *Global Biogeochemical Cycles* 33 (12):1594-1610. doi: 10.1029/2019gb006280.
- Rudels, Bert. 2010. "Constraints on exchanges in the Arctic Mediterranean—do they exist and can they be of use?" *Tellus A: Dynamic Meteorology and Oceanography* 62 (2):109-122.
- Rudels, B. 2015. "Arctic Ocean circulation, processes and water masses: A description of observations and ideas with focus on the period prior to the International Polar Year 2007–2009." *Progress in Oceanography* 132:22-67. doi: <http://dx.doi.org/10.1016/j.pocean.2013.11.006>.
- Rue, Eden L, and Kenneth W Bruland. 1995. "Complexation of iron (III) by natural organic ligands in the Central North Pacific as determined by a new competitive

ligand equilibration/adsorptive cathodic stripping voltammetric method."

*Marine chemistry* 50 (1-4):117-138.

Saito, Mak A, Abigail E Noble, Nicholas Hawco, Benjamin S Twining, Daniel C

Ohnemus, Seth G John, Phoebe Lam, Tim M Conway, Rod Johnson, and Dawn

Moran. 2017. "The acceleration of dissolved cobalt's ecological stoichiometry

due to biological uptake, remineralization, and scavenging in the Atlantic

Ocean." *Biogeosciences* 14 (20):4637.

Sclater, FR, Edward Boyle, and JM Edmond. 1976. "On the marine geochemistry of

nickel." *Earth and Planetary Science Letters* 31 (1):119-128.

Sigman, Daniel M, and Edward A Boyle. 2000. "Glacial/interglacial variations in

atmospheric carbon dioxide." *Nature* 407 (6806):859.

Stumm, W, and JJ Morgan. 1981. "Aquatic Chemistry, 780 pp." *J. Wiley & Sons*.

Sunda, WG, SA Huntsman, and GR Harvey. 1983. "Photoreduction of manganese

oxides in seawater and its geochemical and biological implications." *Nature* 301

(5897):234-236.

Sunda, William G. 2012. "Feedback interactions between trace metal nutrients and

phytoplankton in the ocean." *Frontiers in Microbiology* 3. doi:

10.3389/fmicb.2012.00204.

Sunda, William G, and Susan A Huntsman. 1994. "Photoreduction of manganese oxides

in seawater." *Marine chemistry* 46 (1-2):133-152.

- Sunda, William G., and Susan A. Huntsman. 1995. "Cobalt and zinc interreplacement in marine phytoplankton: Biological and geochemical implications." *Limnology and Oceanography* 40 (8):1404-1417. doi: doi:10.4319/lo.1995.40.8.1404.
- Tagliabue, Alessandro, Olivier Aumont, Ros DeAth, John P Dunne, Stephanie Dutkiewicz, Eric Galbraith, Kazuhiro Misumi, J Keith Moore, Andy Ridgwell, and Elliot Sherman. 2016. "How well do global ocean biogeochemistry models simulate dissolved iron distributions?" *Global Biogeochemical Cycles* 30 (2):149-174.
- Talley, Lynne D., George L. Pickard, William J. Emery, and James H. Swift. 2011. "Chapter 12 - Arctic Ocean and Nordic Seas." In *Descriptive Physical Oceanography (Sixth Edition)*, 401-436. Boston: Academic Press.
- Tovar-Sánchez, Antonio, Carlos M. Duarte, Juan C. Alonso, Silvia Lacorte, Romà Tauler, and Cristobal Galbán-Malagón. 2010. "Impacts of metals and nutrients released from melting multiyear Arctic sea ice." *Journal of Geophysical Research: Oceans* 115 (C7):n/a-n/a. doi: 10.1029/2009JC005685.
- Twining, B. S., and Stephen B Baines. 2013. "The trace metal composition of marine phytoplankton." *Annual review of marine science* 5:191-215.
- Wang, Wen-Xiong, and Robert CH Dei. 2003. "Bioavailability of iron complexed with organic colloids to the cyanobacteria *Synechococcus* and *Trichodesmium*." *Aquatic Microbial Ecology* 33 (3):247-259.
- Wells, Mark L. 2002. "Marine colloids and trace metals." *Biogeochemistry of marine dissolved organic matter*:367-404.

- Wells, Mark L., Peter B Kozelka, and Kenneth W Bruland. 1998. "The complexation of dissolved Cu, Zn, Cd and Pb by soluble and colloidal organic matter in Narragansett Bay, RI." *Marine Chemistry* 62 (3-4):203-217.
- Wen, Liang-Saw, Peter Santschi, Gary Gill, and Christopher Paternostro. 1999. "Estuarine trace metal distributions in Galveston Bay: importance of colloidal forms in the speciation of the dissolved phase." *Marine Chemistry* 63 (3-4):185-212. doi: [http://dx.doi.org/10.1016/S0304-4203\(98\)00062-0](http://dx.doi.org/10.1016/S0304-4203(98)00062-0).
- Yeats, Philip A. 1988. "Manganese, nickel, zinc and cadmium distributions at the Fram-3 and Cesar Ice Camps in the Arctic Ocean." *Oceanologica acta* 11 (4):383-388.
- Yeats, Philip A., and Stig Westerlund. 1991. "Trace metal distributions at an Arctic Ocean ice island." *Marine Chemistry* 33 (3):261-277. doi: [http://dx.doi.org/10.1016/0304-4203\(91\)90071-4](http://dx.doi.org/10.1016/0304-4203(91)90071-4).

## 2. ASSESSMENT OF THE STABILITY, SORPTION, AND EXCHANGEABILITY OF MARINE DISSOLVED AND COLLOIDAL METALS\*

### 2.1. Overview

The size partitioning of dissolved trace metals is an important factor for determining reactivity and bioavailability of metals in marine environments. This, alongside the advent of more routine shipboard ultrafiltration procedures, has led to increased attention in determining the colloidal phase of metals such as Fe in seawater. While clean and efficient filtration, prompt acidification, and proper storage have long been tenets of trace metal biogeochemistry, few studies aim to quantify the kinetics of colloidal exchange and metal adsorption to bottle walls during storage and acidification. This study evaluates the effect of storage conditions on colloidal size partitioning, the kinetics of colloid exchange over time, and the timescale of bottle wall adsorption and desorption for dissolved Fe, Cu, Ni, Zn, Cd, Pb, Mn and Co. We report that preservation of dissolved size partitioning is possible only for Fe and only under frozen conditions. All metals except Mn and Cd show regeneration of the colloidal phase following its removal in as short as 14 h, validating the importance of prompt ultrafiltration. Adsorption of metals to bottle walls is a well-known sampling artifact often cited for Fe and assumed to be potentially significant for other metals as well. However, only Fe and Co showed significant proclivity to adsorption onto low density polyethylene bottle

---

\* This article was published in *Marine Chemistry*, 220, L.T. Jensen, N.J. Wyatt, W.M. Landing, J.N. Fitzsimmons, Assessment of the stability, sorption, and exchangeability of marine dissolved and colloidal metals, Copyright Elsevier 2020.

walls, sorbing a maximum of 91 and 72% over 40 months, respectively. After 20 weeks of acidification neither Fe nor Co desorbed to their original concentrations, leading to an acidified storage recommendation of 30 weeks prior to analyses following storage of unacidified samples for long periods of time. This study provides empirical recommendations for colloidal and dissolved trace metal methodology while also paving the way for much-needed future methods testing.

## **2.2. Introduction**

Colloids represent a dynamic class of compounds that exert control on the fate (transport, reactivity, and bioavailability) of trace metals in seawater. A colloid is distinguished from a truly dissolved species (here called “soluble” species) based on its size, where the transition from soluble to colloidal compounds theoretically occurs when the internal characteristics of a compound become significantly differentiated from the solution such that an interface is established (Wells, 2002). This surficial interface is critical for the adsorption of trace metals, and given the larger relative surface area of colloids compared to their particulate analogs, colloids can serve as an important adsorptive sink for metals from the dissolved phase. Moreover, given the physical inclination of colloids to aggregate (Honeyman and Santschi, 1988), adsorption followed by colloidal aggregation can serve as an important output vector of metals from the ocean when they ultimately sink as particles to the sediments. Thus, colloids play an important role in marine biogeochemistry as an intermediary in the continuum of size fractions in seawater and, as aggregators, as a part of the “scavenging” removal of elements from the ocean.

Additionally, the reactivity and bioavailability of trace metals in the ocean is closely tied to their physicochemical speciation. For iron (Fe), which is the best studied of the micronutrient metals, species in the smallest soluble size fraction (typically < 3 nm) have been established as the most bioavailable to marine phytoplankton, although larger Fe colloids (3–200 nm) are also thought to be bioavailable, depending on their chemical composition (Chen and Wang, 2001; Chen et al., 2003; Hassler et al., 2011). The colloidal distributions of other metals have been investigated in some earlier studies but remain poorly constrained in open ocean regions, with significant variability dependent on ultrafiltration method used and region studied (Buesseler et al., 1996; Wen et al., 1999; Doucet et al., 2007). However, it remains clear that the size and chemical composition of colloids play important roles in the bioavailability and reactivity of dissolved trace metals in seawater.

Over the last few decades, several isolation methods have been applied to the sampling of marine colloids: solid-phase extraction (Louchouart et al., 2000), flow field-flow fractionation (FFFF) (Stolpe et al., 2010; Baalousha et al., 2011), chromatography (Minor et al., 2002), gel filtration and stirred-cell ultrafiltration (Guo and Santschi, 2007), as well as more recent methods such as Vivaspin centrifuge ultrafilters (Schlosser et al., 2013). However, ultrafiltration methods such as Anopore filtration (0.02  $\mu\text{m}$  pore size cutoff) and the widely used cross flow filtration (1–1000 kDa) are now among the more common methods for metal colloid studies as they allow large quantities of water to be filtered at once over a large range of sizes (Buesseler et al., 1996; Guo and Santschi, 2007; Fitzsimmons and Boyle, 2014b). These have led to a

multitude of global ocean investigations of the size partitioning of dissolved Fe (synthesized in (Fitzsimmons and Boyle, 2014a; von der Heyden and Roychoudhury, 2015)), which have shown that the size partitioning varies spatially and is critically dependent on which pore size cutoff is used, since the size distribution of Fe colloids is itself dynamic (Stolpe et al., 2010; Baalousha et al., 2011). Unfortunately, few studies have compared colloidal metal concentrations across a range of ultrafiltration pore sizes in seawater at the same sites (Larsson et al., 2002; Ingri et al., 2004; Fitzsimmons and Boyle, 2014a), likely because of the time-consuming nature of ultrafiltration itself. This would help reveal the true size distribution of marine colloidal metals.

As is true for any operationally-defined method, it is important to rigorously calibrate the method and test for potential artifacts so that different users can expect to acquire the same results. For colloid ultrafiltration methods, methodological artifacts can arise after initial particulate removal via bulk filtration ( $> 0.2 \mu\text{m}$  pore size), which is required since particles can clog ultrafilters and/or serve as sorptive surfaces, both before and during the slow ultrafiltration process. Some of these artifacts were reviewed during an intercomparison exercise early in the development of colloidal methods (Buesseler et al., 1996) as well as during later studies (Chen et al., 2004; Schlosser et al., 2013; Fitzsimmons and Boyle, 2014b). For metals, the most significant concerns addressed were contamination and recovery differences across ultrafilters (Reitmeyer et al., 1996). While a subset of these ultrafilters have been vetted and are in regular use today (Larsson et al., 2002; Fitzsimmons and Boyle, 2014a; Fitzsimmons et al., 2015b), potential artifacts still exist and warrant further constraint, including the underexplored

kinetics of colloidal exchange with other solution components and/or with bottle walls, which are especially critical when it can take tens of minutes to many hours to ultrafilter a single seawater sample.

Previous studies have demonstrated that sorption and desorption from colloidal complexes is highly dependent on pH, ionic strength of the solution, temperature, and particularly the composition of particles, leading to exchange on the timescale of hours to days (Scheinost et al., 2001; Roberts et al., 2003). Marine colloids are thought to be primarily organic in nature, comprising a combination of humic-type substances and products of biological activity such as exopolymeric substances (Gaffney et al., 1996; Ron and Rosenberg, 2001) and, more generically, dissolved organic matter (DOM) (Santschi, 2018). Dissolved organic carbon (DOC) in particular is subject to rapid turnover, leading to a size-reactivity spectrum that is a crucial component of the global carbon cycle (Baskaran et al., 1992; Benner et al., 1992; Santschi et al., 1995; Guo and Santschi, 1997; Opsahl and Benner, 1997; Wen et al., 1997; Benner and Amon, 2015). If metals are bound to or otherwise incorporated within these organic colloids, they would be more vulnerable to exchange over short timescales.

Sorption of trace metals to sub-sampling bottle walls during storage also represents a potential artifact affecting measurements in seawater. The loss of various trace metals to bottle walls during storage is well documented (Masseie et al., 1981), references therein), leading to the standardization of storage procedures that typically involve acidification of samples prior to analysis (Pellenbarg and Church, 1978; Bruland and Rue, 2001; Lohan et al., 2005). Furthermore, the bottle material and

physicochemical speciation of each metal are known to affect the overall bottle wall sorption loss (Starik et al., 1963; James and Healy, 1972a; Pellenbarg and Church, 1978; Fischer et al., 2007). While previous studies have elucidated losses of dissolved, soluble, and colloidal Fe to bottle wall sorption (Schlosser et al., 2011; Fitzsimmons and Boyle, 2012), no recent rigorous kinetic testing has been performed to examine adsorptive loss of other trace metals to bottle walls. Moreover, trace metals such as manganese (Mn), cobalt (Co), nickel (Ni), copper (Cu), zinc (Zn), and cadmium (Cd) each have different inorganic speciation in seawater compared with Fe (Byrne, 2002), as well as varying degrees of complexation to ligands (Bruland et al., 2013). Thus, we might expect that adsorption and subsequent desorption of these metals would be different from Fe and dependent on their speciation at seawater pH, leading to important considerations of the timing of sample acidification and analysis, and for colloids, the slow ultrafiltration process. Naturally, these concerns raise questions of whether seawater samples can be preserved for ultrafiltration back in the lab, when more time and supplies would allow for better streamlining of the ultrafiltration process.

Here, we report the results of four experiments designed to answer questions related to the kinetics of colloidal metal exchange and adsorption to bottle walls, as well as the efficacy of preserving the colloidal size partitioning of metal samples: 1) a “Colloid Preservation Experiment” to assess the ability to preserve multi-metal marine colloidal size partitioning under room temperature and frozen conditions over several weeks, 2) a “Colloid Exchangeability Experiment” to assess the timescale of colloid re-formation rates from the soluble phase at room temperature over several days, 3) a

“Bottle Adsorption Kinetics Experiment” to assess the timescale of adsorption onto low density polyethylene (LDPE) bottle walls using two different bottle volumes, and 4) a “Bottle Desorption Kinetics Experiment” to assess the timescale of desorption from the same LDPE bottle walls. We analyzed these experimental treatments for their Fe concentrations but also, for the first time, extended our measurements to the size partitioning of Mn, Co, Ni, Cu, Zn, Cd, and lead (Pb). The goal of these experiments was to provide recommendations regarding sample storage prior to acidification, constraints on how long samples can be stored before ultrafiltration, and the influence of the ultrafiltration processing time itself, in order to avoid artifacts during future field studies.

## **2.3. Methods**

### **2.3.1. Sample collection**

Water used for these experiments was collected on three research cruises: 1) in September 2015 during the U.S. Arctic GEOTRACES GN01 cruise (Station 52: 77.50°N, 148.01°W, 100 m depth) aboard the USCGC *Healy* for the Bottle Adsorption/Desorption Kinetics Experiments, 2) in January 2016 in the Southern Ocean during the Palmer Long-Term Ecosystem Research (Pal-LTER) cruise aboard the ARSV *Laurence McKinley Gould* (Station 600.040: -64.93°N, 64.40°W, 1320 m depth for the Colloid Preservation Experiment; and Station 200.000: -67.77°N, -69.95°W, 682 m depth for the Colloid Exchangeability Experiment), and 3) in June 2018 on a Galveston Bay cruise aboard the R/V *Trident* (Station 3, 29.45°N, 94.87°W, 1 m depth) for the Colloid Preservation Experiment. Briefly, samples collected aboard the ARSV *Laurence M. Gould* were collected using a trace metal clean CTD rosette loaded with 12 × 12 L

Niskin-X bottles from stations close to the coast thought to be rich in colloids. Samples collected aboard the USCGC *Healy* followed established trace metal sampling protocols (Cutter et al., 2010) using a trace-metal clean Seabird CTD rosette mounted with 24 × 12 L GO-FLO (General Oceanics) bottles. The surface-water samples from Galveston Bay were collected using a trace-metal clean PTFE double diaphragm pump (Cole Parmer) fitted with acid-cleaned Bev-A-Line tubing (1/4 in, Cole Parmer) at stations thought to be rich in colloids. In all cases, samples were initially filtered through 0.2 µm AcroPak-200 polyethersulfone membrane filter capsules (Pall) and collected, following three 10% volume rinses, into LDPE Nalgene bottles previously cleaned using hydrochloric acid (HCl, trace metal grade, 1 M) and ultrapure Milli-Q (MQ, Millipore) water at 60 °C (Fitzsimmons and Boyle, 2012).

### **2.3.2. Ultrafiltration methods**

In each of the colloidal preservation and exchangeability experiments, standard protocol for the ultrafiltration of seawater was completed using a trace metal clean cross flow filtration system (CFF) (Fitzsimmons and Boyle, 2014b). This CFF system employed a Millipore Pellicon XL regenerated cellulose filter with a nominal weight cutoff of 10 kDa (~3 nm for spherical proteins, (Erickson, 2009)) and a Cole Parmer Masterflex pump with all fluorinated ethylene propylene (FEP) tubing. Prior to the research cruises, new Pellicon filters were first cleaned with 1 L of 0.24 M HCl (Optima Fisher Scientific), which was allowed to recirculate through the system for 1 h. The system was then flushed with at least 500 mL of ultrapure 0.024 M HCl and stored in 0.0024 M HCl until use. Prior to each use, 500 mL of dilute (~0.005 M) HCl was

circulated through the system followed by 100–500 mL of sample seawater (as much as the experimental volume allowed) to condition the system and allow for an accurate flow rate calibration. Total flow rate was calibrated to 25 mL/min, and permeate and retentate flows were subsequently equalized to 12.5 mL/min and recorded for accurate determination of the colloid concentration factor and recovery.

In this paper, all ultrafiltration via CFF was “single-pass,” meaning that the retentate solutions were not recycled back into the feed solution for cumulative ultrafiltration; instead, we treat all results as traditional filtrations but with a small pore size, which minimizes artifacts associated with common CFF approaches that pass sample retentate over the same filter multiple times. Critically, by maximizing flow rate through our CFF system, we minimize the height of our concentration polarization layer and associated filtration biases that were observed in early CFF ultrafiltration experiments for metals (Buffle et al., 1992). Also, by keeping sample volumes low and acid cleaning well between samples, we avoid variations in the permeate metal concentrations over time, which were often observed in earlier studies (e.g. (Wen et al., 1996)). In our system, soluble metal (sMe) concentrations are therefore defined as the concentration measured in the permeate solution, or what passes through the 10 kDa ( $\sim 0.003 \mu\text{m}$ ) membrane. Colloidal metal (cMe) concentrations are calculated as the mass balance difference between dissolved metal (dMe) and sMe concentrations ( $(\text{cMe}) = (\text{dMe}) - (\text{sMe})$ ), which assumes that any metal lost to the CFF system (during imperfect recovery from the CFF system) is lost from the colloidal size fraction only, not the soluble size fraction. This was confirmed in Fitzsimmons and Boyle (2014a) for Fe

using Pellicon CFF filters, where Fe losses were attributed mostly to colloidal Fe trapping inside the membrane itself. The cMe fraction is calculated as the cMe concentration divided by the dMe concentration ( $\%cMe = (cMe) / (dMe)$ ). The recovery is calculated as in Fitzsimmons and Boyle (2014a) and assesses the metal yield in the permeate + concentrated retentate solutions compared to the initial dMe concentration fed into the CFF system.

### **2.3.3. Experimental methods**

#### **2.3.3.1. Colloid preservation experiment**

Water collected from a near-bottom depth of 1320 m near Palmer Station (West Antarctic Peninsula) was used to assess whether seawater samples can be preserved over time for cMe size partitioning determination (Figure 2.1). Four 250 mL bottles, two 60 mL bottles, and one 4 L bottle of 0.2  $\mu\text{m}$  -filtered (Acropak 200, Pall) seawater were filled directly from a trace metal clean Niskin-X bottle following three 10% rinses of all bottles, caps, and threads. The two 60 mL bottles were immediately acidified and represent the initial dissolved metal concentrations (T0). The 4 L bottle was left at room temperature for immediate ultrafiltration into two 60 mL permeate (P T0) and two 60 mL retentate (R T0) solutions. Two 250 mL bottles were preserved in the dark (black bag) at room temperature (RT), and the remaining two 250 mL bottles were preserved in the dark at  $-20\text{ }^{\circ}\text{C}$  (frozen) and thawed to room temperature before ultrafiltration.

To assess the colloidal size partitioning, ultrafiltration of the 250 mL preserved (frozen or RT) samples was completed after 7 days (T7) and after 21 days (T21), using the CFF methods above.

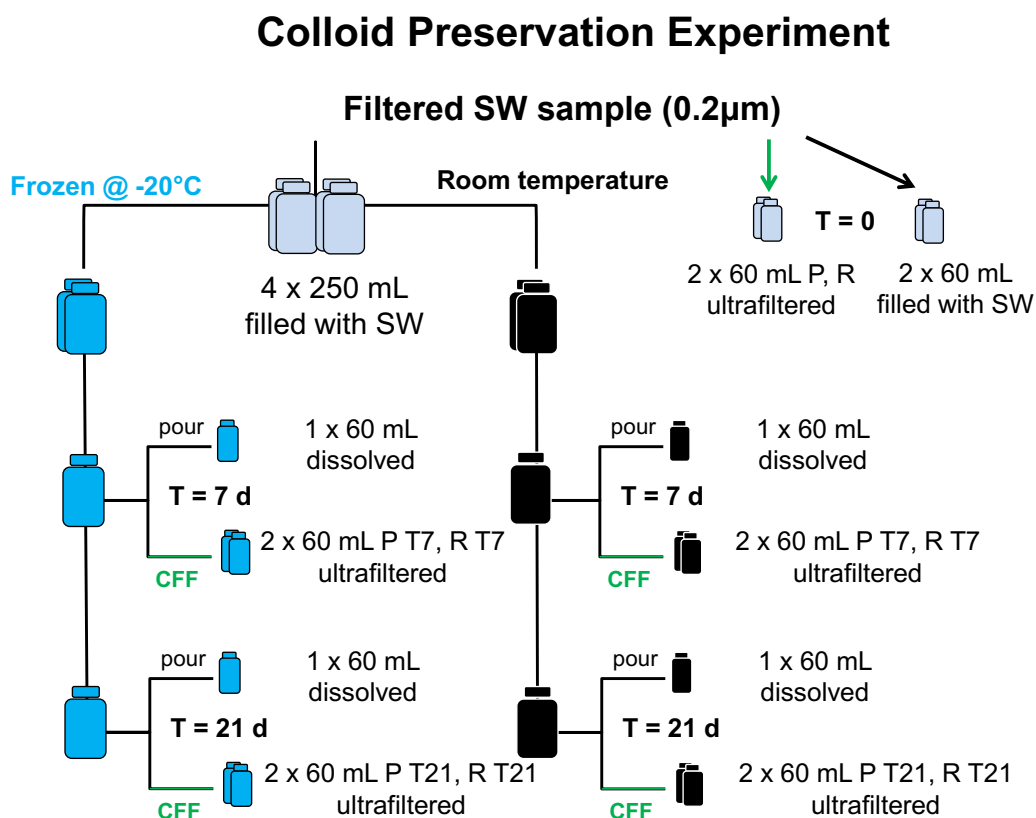


**Figure 2.1** Schematic of the Colloid Preservation Experiment methods. All samples came from the same, homogenized seawater sample (a single Niskin-X bottle in the Southern Ocean or a carboy in Galveston Bay). Blue bottles indicate samples frozen at  $-20^{\circ}\text{C}$ , while black bottles indicate samples kept at room temperature in the dark. “Pour” indicates samples that were directly poured from the corresponding 250 mL sample. “CFF” indicates when samples were ultrafiltered to permeate (P) or retentate (R) solutions. The Southern Ocean experiment had three timepoints: T0, T = 7 days, T = 21 days, while the Galveston Bay experiment had four timepoints: T0, T = 2 days, T = 9 days, T = 23 days.

Each time point yielded one 60 mL bottle of non-filtered, “poured” seawater, to record the dMe concentrations remaining in the bottle at that time point (minus any adsorption to bottle walls), one 60 mL bottle that was filled with CFF-ultrafiltered permeate solution (P), which contains no colloids and only truly soluble species, and one 60 mL bottle that was filled with ultrafiltered retentate solution (R), which contained some soluble species and the concentrated colloids (for CFF recovery determination).

We repeated this experiment with additional replicates and time points using the same procedure but with surface water collected from Galveston Bay. To better constrain the variability imparted by the CFF ultrafiltration itself, triplicate initial dMe (T0) were collected as well as triplicate CFF-ultrafiltered permeate (P T0) and retentate (R T0) samples. Replicate 250 mL samples were stored frozen and at room temperature and were then ultrafiltered after 2 days in duplicate (T2), after 9 days (T9, only one replicate each), and after 23 days (T23, one replicate for room temperature, duplicate for frozen treatment). All samples in both experiments were acidified to 0.012 M HCl (Optima) following their final filtration.

### **2.3.3.2. Colloid exchangeability**

Water collected from a near-bottom depth (682 m) in Marguerite Bay on the West Antarctic Peninsula was used to determine colloid metal exchangeability (“re-formation”) kinetics using the methods illustrated in Figure 2.2. Water was filtered directly from a trace metal clean Niskin-X bottle through a 0.2  $\mu\text{m}$  filter (Acropak 200, Pall) into a 4 L LDPE bottle following three 10% rinses of the bottle, cap, and threads. This filtered seawater was immediately sub-sampled into two 60 mL bottles for dMe

determination (T0), whilst additional seawater was immediately ultrafiltered into two 60 mL bottles for permeate (P T0) and two 60 mL bottles for retentate (R T0), as well as one 2 L bottle of just permeate solution. The 2 L bottle was the “incubation bottle” in which colloids were initially removed but might be re-forming (“exchanging with” or “aggregating from” the soluble phase) over time. This bottle was stored in the dark at room temperature until further processing at each time point.

After 14 h, seawater from the bulk 2 L permeate sample was poured into 60 mL bottles (P T14 “pour”) to capture the dMe concentrations in the bulk 2 L bottle, which excludes any metals lost to bottle wall adsorption. Solution from the 2 L bulk bottle was ultrafiltered again into permeate and retentate fractions (PP, PR at T14). This procedure was repeated at 24, 48, and 70 h (T24, T48, and T70, respectively). All 60 mL samples were subsequently acidified to 0.012 M HCl (Optima).

## Colloid Exchangeability Experiment

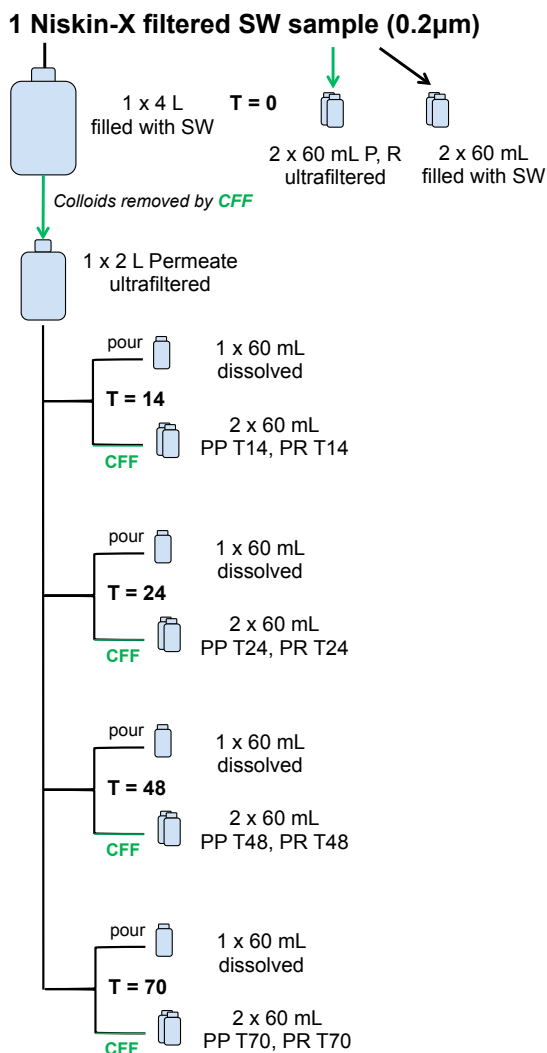


**Figure 2.2** Schematic of the Colloid Exchangeability Experiment methods. All samples came from the same, original Niskin-X 12 L bottle. “Pour” indicates that samples were directly poured from the corresponding 2 L sample. “CFF” indicates when samples were ultrafiltered to permeate (P) or retentate (R) solutions. All time points originated from the same, homogenized 2 L permeate sample, which had the colloids removed by ultrafiltration at  $T = 0$ .

### 2.3.3.3. Adsorption/desorption

Adsorption and desorption of metals was tested using LDPE bottles of two volumes, 250 mL and 125 mL, to quantify any effect of surface area to volume ratio

(SA:V) on metal adsorption. Seawater for these experiments was collected at 100 m depth in the Western Arctic Ocean.

For the adsorption experiment (Figure 2.3), seawater was filtered from a GO-FLO bottle through a 0.2  $\mu\text{m}$  filter (Acropak-200, Pall) into a trace metal clean 10 L carboy, homogenized, and then immediately subsampled into eighteen 250 mL bottles and eighteen 125 mL bottles following three 10% rinses of the insides, caps, and threads, with no headspace. For the initial time point (T<sub>0</sub>), three 250 mL and three 125 mL bottles were immediately acidified (0.024 M HCl, Optima). The remaining bottles were stored unacidified at room temperature in the dark (black bags) for different time periods during which metals could adsorb to the bottle walls. At each subsequent time point, three 250 mL and three 125 mL samples were poured into new, acid-cleaned 250 and 125 mL bottles, respectively, and acidified, which leaves any metals adsorbed to the original bottle walls in the original bottles. This was repeated at 4, 8, 16, and 24 h. Additionally, three 250 mL and three 125 mL samples were set aside as “long term” storage time points. They were transferred to new bottles and acidified (0.024 M HCl, Optima) at ~40 months.

For the desorption experiment (Figure 2.3), water collected from the same depth was 0.2  $\mu\text{m}$  filtered from a separate GO-FLO bottle and placed into another 10 L carboy, homogenized, and then directly subsampled into twelve 250 mL bottles and twelve 125 mL bottles following three 10% rinses of the insides, caps, and threads, with no headspace. All bottles were left at room temperature in the dark, unacidified (to allow for metal adsorption to bottle walls) for ~22 months until acidification (0.012 M HCl,

Optima). Immediately following acidification, two 250 mL and two 125 mL bottles were poured off into four fresh 250 mL bottles, representing the initial time point (T0). This T0 time point captured any dMe remaining in solution as well as any dMe that had rapidly desorbed from bottle walls following acidification. This process of pouring into a new clean bottle was repeated after 1, 3, 7.5, 12, and 20 weeks to measure the kinetics of metal desorption from bottle walls as a function of bottle SA:V ratio.

#### **2.3.4. Metal analysis**

Samples were analyzed for Mn, Fe, Co, Ni, Cu, Zn, Cd, and Pb at least 1 month following acidification using an offline isotope dilution and pre-concentration method on a SeaFAST-pico system (ESI, Omaha), modified from Lagerström et al. (2013). This method is described for Zn in Jensen et al. (2019) but is expanded here for the other metals. Briefly, a 10 mL sample aliquot was weighed and spiked with an isotope spike mixture containing  $[^{57}\text{Fe}] = 480.5 \text{ nM}$ ,  $[^{62}\text{Ni}] = 1455.8 \text{ nM}$ ,  $[^{65}\text{Cu}] = 687.5 \text{ nM}$ ,  $[^{68}\text{Zn}] = 709.6 \text{ nM}$ ,  $[^{206}\text{Pb}] = 44.7 \text{ nM}$ , and  $[^{114}\text{Cd}] = 449.6 \text{ nM}$  and loaded into the SeaFAST system. For monoisotopic metals Mn and Co, a standard was created where  $[\text{Mn}] = 452.80 \text{ nmol/kg}$ , and  $[\text{Co}] = 12.01 \text{ nmol/kg}$ , and this standard was used to create a 6-point standard curve spanning 0 to 10 nmol/kg for Mn and 0 to 0.27 nmol/kg for Co. It is important to note here that samples were not UV oxidized and thus the Co measured represents the “labile” fraction.

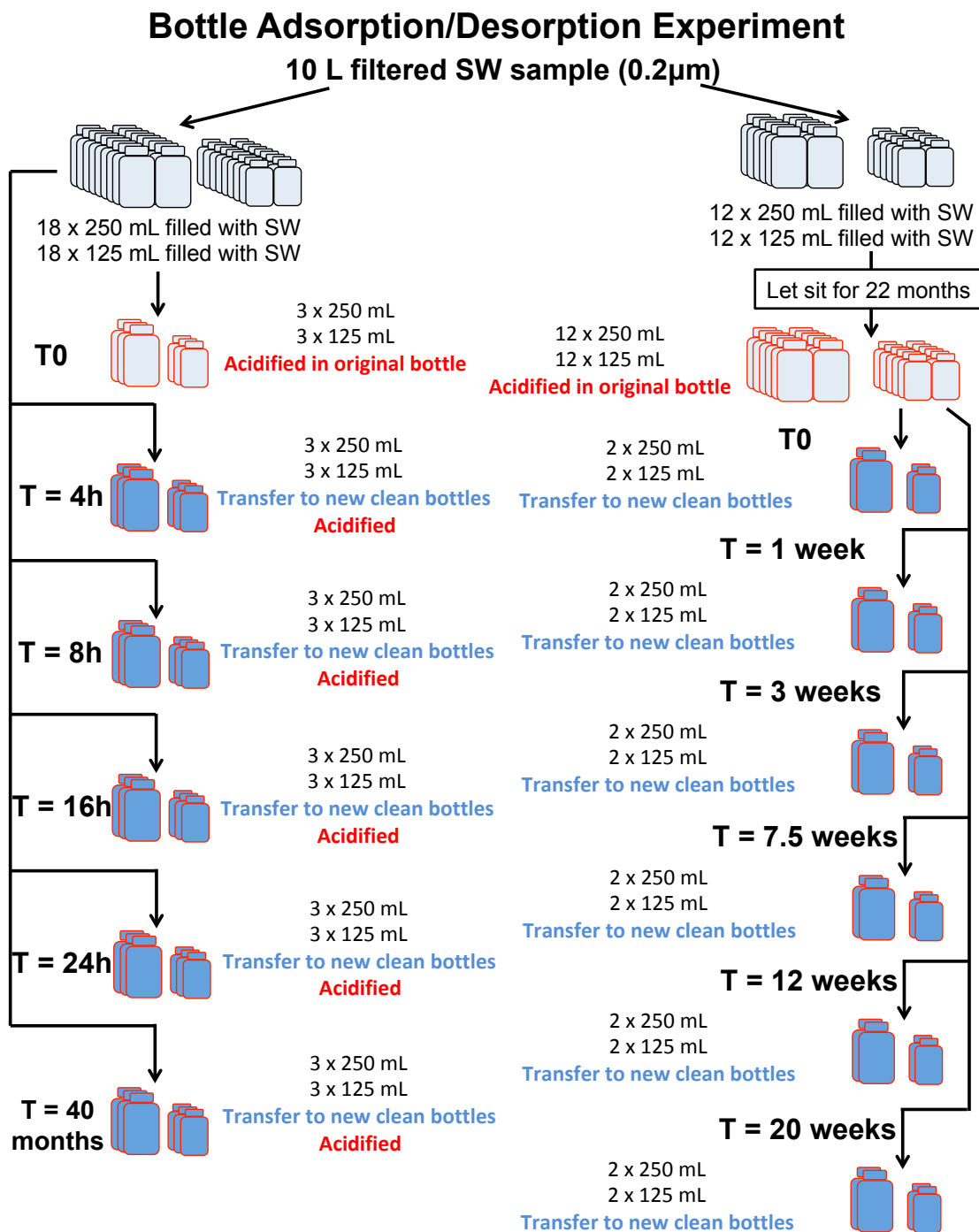


**Figure 2.3** Schematic of the Adsorption (left) and Desorption (right) Experiment methods. The water for both was taken from the same depth but two separate GO-Flo bottles. The time points for the Adsorption Experiment are in hours, except for the final time point of 40 months. Dark blue bottles indicate transfer to new, acid-cleaned bottles. Red (outlined) bottles indicate acidification. Note that the adsorption experiment was performed in triplicate while the desorption experiment was performed in duplicate, both over two bottle sizes: 125 mL and 250 mL.

Samples were then buffered in line with an ammonium acetate buffer (Optima, Fisher Scientific) prepared to pH ~7.4, which when mixed with the 10 mL of spiked sample at a flow rate of 350  $\mu\text{L}/\text{min}$  results in a buffered sample pH of  $6.2 \pm 0.3$  (Sohrin et al., 2008). This solution was immediately loaded onto a column containing Nobias-chelate PA1 resin and rinsed with ultrapure water to remove salts. The sample was subsequently back-eluted with 10% (v/v) nitric acid (Optima, Fisher Scientific) to yield 400  $\mu\text{L}$  of eluent, representing a 25-fold sample pre-concentration. These eluents were analyzed in low (Pb and Cd) and medium (Fe, Zn, Ni, Mn, Cu, and Co) resolution on a Thermo Element XR high resolution inductively coupled plasma mass spectrometer (HR-ICP-MS) at Texas A&M University in the R. Ken Williams Radiogenic Isotope Facility. Table 2.1 summarizes the detection limit and reference sample analyses to demonstrate the accuracy and precision of the measurements.

**Table 2.1** Summary of SAFe D1, blank, and limit of detection (LOD) results from this study compared to the May 2013 consensus values reported by GEOTRACES. All values are reported in  $\text{nmol}/\text{kg}$ . Reproduced with permission from Jensen et al. (2020).

Parameter	dFe	dZn	dNi	dCu	dCd	dPb	dMn	dCo
SAFe D1	nmol/kg							
Average	0.604	7.395	8.584	2.087	1.045	0.023	0.409	0.032
Stdev	0.063	0.212	0.098	0.063	0.006	0.003	0.009	0.001
n	8	10	10	10	10	10	9	8
Consensus	0.670	7.400	8.580	2.270	0.991	0.0277	0.35	0.045
Consensus stdev	0.040	0.350	0.260	0.110	0.031	0.0026	0.05	0.005
Average blank	0.056	0.069	0.014	0.008	0.0003	0.0002	0.002	0.0004
Blank stdev	0.010	0.011	0.003	0.003	0.0001	0.00004	0.001	0.0002
LOD	0.031	0.033	0.010	0.008	0.0002	0.00012	0.002	0.0005
n	4	4	4	4	4	4	4	4

## **2.4. Results**

### **2.4.1. Colloid preservation experiment: Can soluble/colloidal size partitioning be preserved over time by storing seawater frozen or at room temperature?**

The goal of this experiment was to assess whether the natural size partitioning of marine metals into soluble and colloidal fractions could be preserved prior to ultrafiltration over a timescale of weeks under room temperature or frozen conditions. This would allow seawater to be collected in the field, stored using an ideal preservation method, and then ultrafiltered back in the laboratory when more time allows for optimal ultrafiltration conditions. This experiment was completed twice: first using water from the West Antarctic Peninsula continental shelf (the Southern Ocean experiment using near-bottom seawater in Palmer Canyon), and then with increased experimental replication using surface water from Galveston Bay, Texas.

In the Southern Ocean experiment (Figure 2.4; salinity = 34.70,  $T = 1.48$  °C), the samples stored at room temperature exhibited a statistically significant decrease ( $t$ -test, two-tailed, heteroscedastic,  $p < .05$ ) in dFe concentration of 75% after just 7 days, likely from adsorption of dFe to bottle walls (see Adsorption Experiment results below), and continued to decrease through 21 days. In contrast, when stored frozen, the initial dFe concentration was fairly well preserved over 21 days, with no significant decrease (< 5%), suggesting that wall adsorption does not occur to a significant extent if seawater is frozen immediately. Additionally, when frozen the dFe size partitioning was also well preserved compared to initial ultrafiltration. This can be seen by relatively constant sFe concentrations over time and comparable % cFe after 7 days (63%) and even 21 days

(67%), compared to the initial partitioning ( $62 \pm 2\%$ ). These results suggest that freezing filtered seawater can preserve both the dFe concentration and its size partitioning into soluble/colloidal fractions relatively well (compared to samples ultrafiltered immediately) over the timescale of weeks. In contrast, storing samples at room temperature allows for wall adsorption that prevents the preservation of dFe concentrations over time.

To compare these results to a seawater sample with different physicochemical Fe speciation, the experiment was repeated in Galveston Bay (Figure 2.4; salinity = 26.50,  $T = 30.93$  °C) with two improvements: 1) more size partitioning replicates at each time point to improve statistical strength in comparisons between time points, and 2) more sampling time points: T2 at 2 days, T10 at 10 days, and T23 at 23 days, which is most similar to the T21 time point from the first Southern Ocean experiment. Unlike in the Southern Ocean experiment, dFe concentrations were not as well preserved even when frozen (Figure 2.4a, right), dropping 17% from  $2.36 \pm 0.04$  nmol/kg ( $n = 3$ ) to 1.99 nmol/kg in the frozen treatment after 10 days; this is similar magnitude to the dFe loss observed in the room temperature treatment. However, despite these dFe losses, the size partitioning of dFe was well maintained over time in both the room temperature and frozen treatments, with the exception of two likely contaminated permeate samples (RT T2 and frozen T10, which were anomalous for several metals).

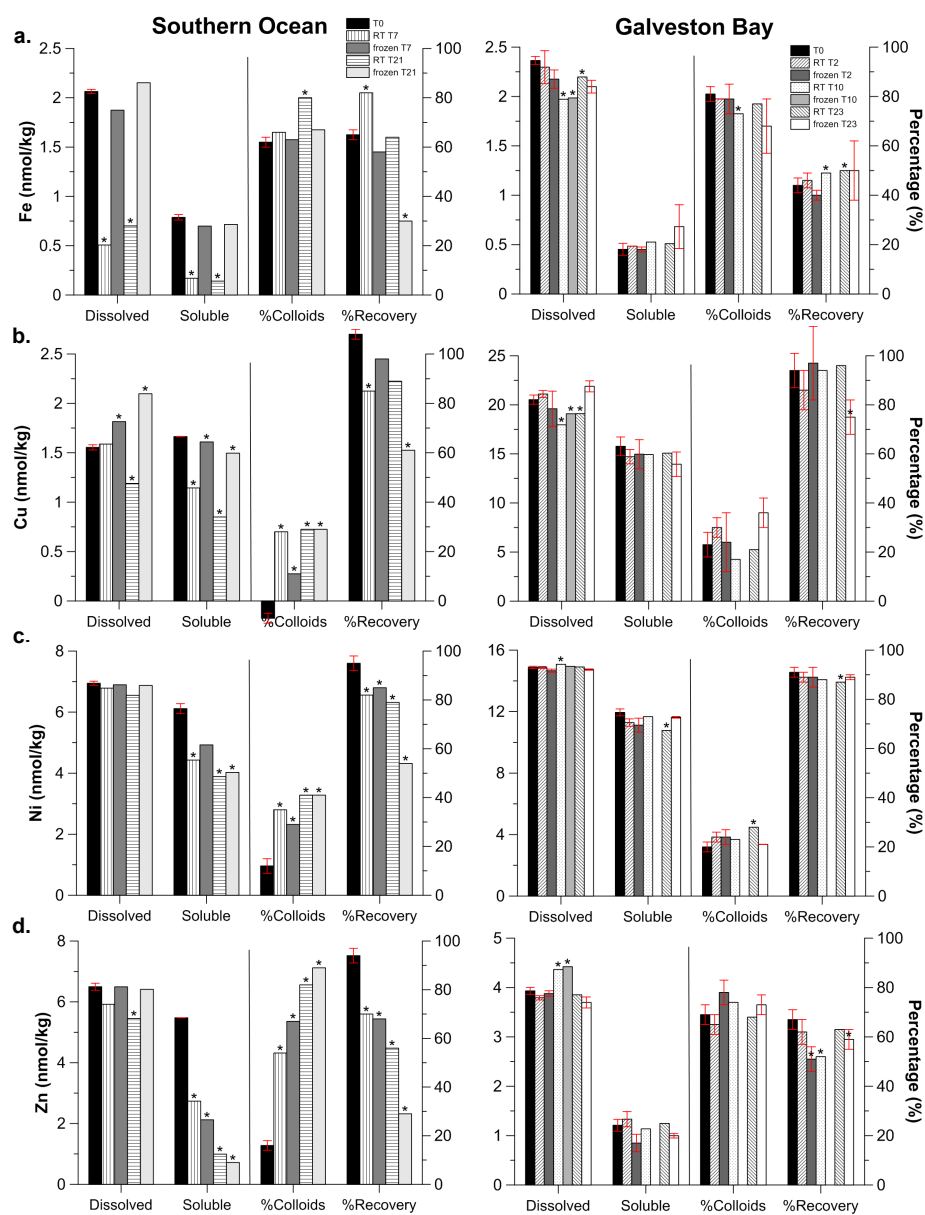


**Figure 2.4** Summary of all results of the Colloid Preservation Experiment. The left hand and right hand columns represent the initial Southern Ocean and subsequent Galveston Bay experiments, respectively. The legend for all treatment types is included in panel (a), where black is the initial seawater sample. The black line separates where the left-hand axes (concentration) are applicable to the “Dissolved” and “Permeate” groups of data from where the right-hand axes (percentage) are applicable to the “% Colloids” and “% Recovery” groups of data. The red error bars represent standard deviation over replicate bottles within a given time point. The frozen 9 day time point in the Galveston Bay experiment are removed for permeate concentration, % colloids and % recovery due to clear contamination of the permeate solution across all metal types. \* indicates a result that is significantly different from the initial (T0) result, used a two-tailed heteroscedastic  $t$ -test ( $p < .05$ ).

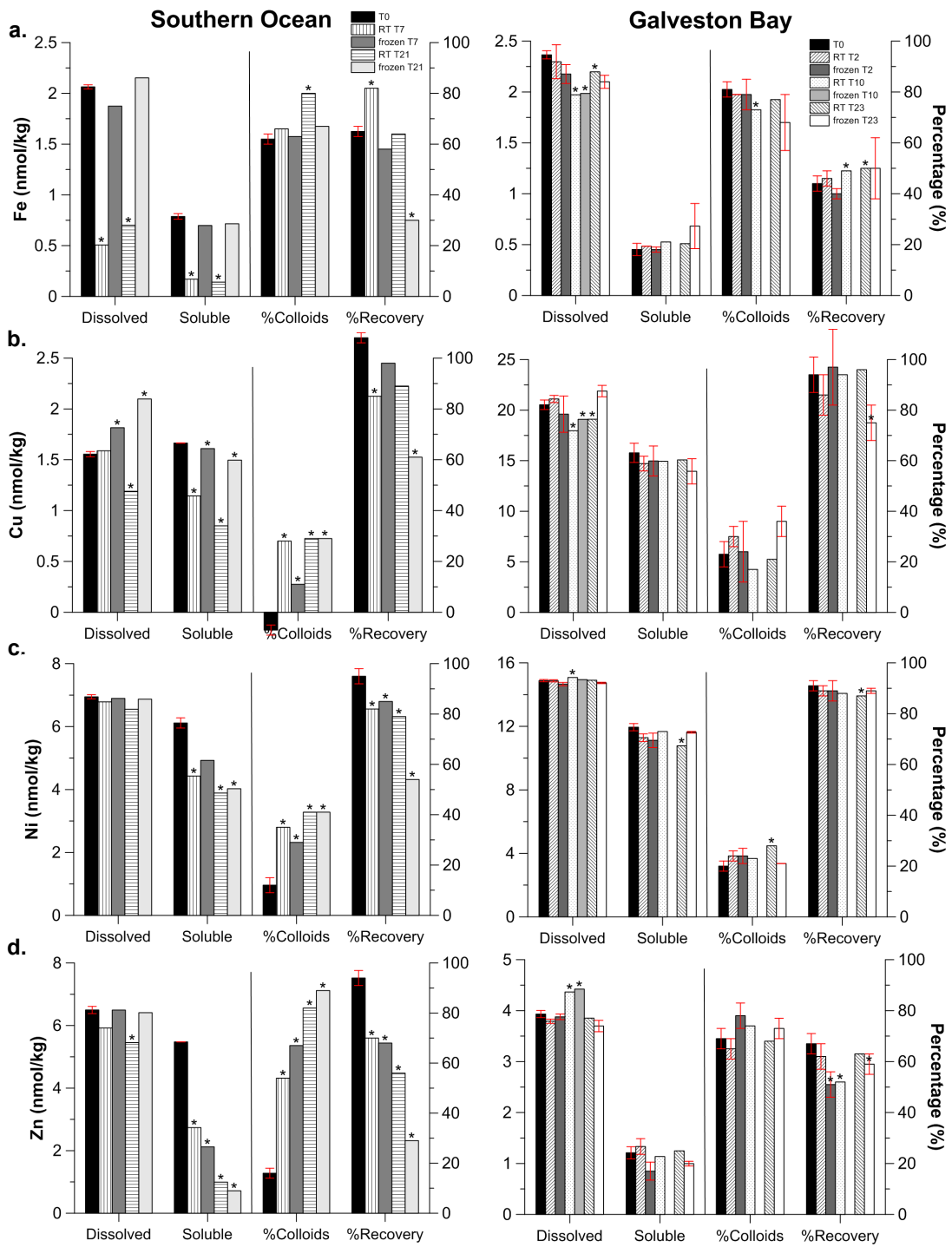


Figure 2.4 Continued.

Like Fe, Mn and Co both show little sorption loss to bottle walls (<10%) in the frozen treatment compared to room temperature (Figure 2.4), making the frozen storage method the best method for size partitioning preservation of these metals. However, while Zn, Ni, Cu, Cd, and Pb display minimal change in their dissolved concentrations over time, they all suffer reductions in permeate “soluble” concentrations, usually even by 7 days. Thus, colloids were being generated in solution due to aggregation over the duration of the experiment. This was especially true for Cd, which showed substantial colloidal aggregation from 0 to > 20% colloidal Cd at the Galveston Bay site. However, in the Southern Ocean experiment, this was also true for Ni and particularly true for Zn and Pb, where the colloid fraction increased from ~20% to > 90% by 21 days. Interestingly, this effect was more prominent for frozen samples (Figure 2.4d and e, respectively).<sup>[1]</sup><sub>SEP</sub> What explains the poor preservation of dMe size partitioning for all metals besides Fe, Mn, and Co under frozen conditions? Several factors must be considered, including metal sorption to bottle walls (which could favor soluble or colloidal metals), natural colloidal aggregation over time (which could be dependent on preservation conditions including temperature), and artifacts related to the ultrafiltration process. While we explore bottle wall adsorption and colloidal formation kinetics in detail in the next two experiments, we will first preview some patterns here based on these initial Colloid Preservation Experiments. Sorption to bottle walls was evident in the room temperature treatments for dissolved Fe, Zn, Co, Pb, Ni, and Mn, but was much more severe for Fe and Co (66% and 69% after 21 days, respectively) than for Pb (25%),

Zn (16%), Ni (6%), and Mn (4%). We also note that these statistics are for the Southern Ocean samples, which in general showed more bottle wall adsorption than the Galveston Bay samples. This can be attributed to differences between sites in either initial sample temperature and/or physicochemical metal speciation. It is known that sorption of metals to bottle walls is an exothermic process that is hastened in samples kept at colder temperatures (Bartell et al., 1951; Fitzsimmons and Boyle, 2012). It is not clear whether smaller soluble-sized or colloidal-sized species are favored during bottle wall adsorption, since for Co and Mn the dissolved and permeate concentrations appeared to decrease by similar amounts, implicating soluble Co and Mn in wall sorption, but for the other metals (Zn, Ni and Pb in particular) the permeate concentrations decreased much more than the dissolved concentrations, possibly implicating wall sorption of the soluble phase or colloid formation. Additionally, soluble-colloidal exchange cannot be precluded, making any pattern difficult to attribute specifically to adsorption of soluble or colloidal metals alone. It should also be noted that for the two metals with the greatest ingrowth of colloids over time (Zn and Pb) in the Preservation Experiment, the recovery of these metals through the CFF system also decreased over time from > 90% in samples ultrafiltered immediately (T0) to < 30% recovery after 21 days for the Southern Ocean samples. Thus, some of the “colloidal ingrowth” in these experiments could be misattributed and instead be caused by increasing soluble metal losses to the CFF system over time. The behavior of metals other than Fe in these CFF filters has not been well constrained, as the original CFF methods development and testing focused solely on Fe (Fitzsimmons and Boyle, 2014b). In fact, an earlier study by (Wen et al., 1996) using a

recirculating CFF system with different ultrafilter materials found molecular weight shifts in trace metal colloids during storage at room temperature, indicating potential aggregation over the course of hours at room temperature. However, even within our own experiments, it would appear that aged samples do not perform as reliably in the CFF system compared to fresh samples, since reductions in recovery were observed for all of the dissolved metals measured in the Southern Ocean experiment as a result of sample storage. In contrast, CFF recovery was generally higher and overall much more constant in the higher temperature Galveston Bay samples. Notably, the differences in recovery under frozen or room temperature conditions was not statistically different for any of the metals, so while we suggest here that there is a sample temperature effect on CFF recovery, which may help explain the differences between the Southern Ocean vs. Galveston Bay results, we cannot conclusively prove temperature causation.

In summary, the differences in dissolved metal concentrations and size partitioning preservation between the Southern Ocean and Galveston Bay samples can likely be attributed to two major factors: natural physicochemical speciation differences between samples and ultrafiltration artifacts. Natural physicochemical speciation refers to the native physical and chemical forms that the colloids originally had in seawater. In the Southern Ocean, previous studies point to potential sedimentary sources and/or resuspension supplying both particulate and dissolved Fe to Palmer Canyon bottom waters (Sherrell et al., 2018), as well as a high abundance of Fe-binding ligands with benthic sources (Gerringa et al., 2008) that may serve to stabilize dFe. In contrast, in an estuarine environment such as Galveston Bay, we would expect many inorganic dFe

nanoparticles coated in humic-like organics (Powell et al., 1996; Wen et al., 2008). These two samples thus have quite different physicochemical metal speciation and thus it is not surprising that they behave differently upon preservation or when processed using our CFF system. Furthermore, prior studies have suggested that Fe solubility increases at colder temperatures and that dFe samples that were frozen and thawed have a higher solubility (Schlosser et al., 2012). In this case, Fe would be more prone to stay solubilized under frozen conditions but also natively in a cold climate. This would in turn play into any filtration artifacts, which may be influenced by the original physicochemical speciation of the sample, as well as how it behaves when aged/warmed over time (Schlosser et al., 2011).

#### **2.4.2. Colloid exchangeability experiment: Do colloids “grow back” after removal via ultrafiltration, and if so, how fast?**

The goal of this experiment was to determine the rate of potential colloid re-formation (aggregation from soluble phase) at room temperature over 70 h after all colloids were removed from a near-bottom Southern Ocean sample via ultrafiltration. Aggregation of material from the soluble to the colloidal size fraction could be stimulated by interactions with the bottle walls, organic coagulation (Wilkinson et al., 1997), gel formation (Chin et al., 1998), and/or the so-called “Brownian pumping” of soluble-sized species (Honeyman and Santschi, 1989; Wen et al., 1997). At each time point after colloids were removed from the permeate solution at T<sub>0</sub>, any potential adsorption to bottle walls was monitored by pouring off a subsample of the original permeate solution, and then this original permeate solution was also re-ultrafiltered to

assess whether colloids had re-formed over time. If there was no generation of colloids, the re-ultrafiltered permeate should have equaled the “poured” permeate concentration at each time point. This was only true for dissolved Mn and Cd, which had negligible colloids in the original sample, and no additional colloids formed over the 70 h time period that was studied (Figure 2.5d, h).

However, for Fe, Co, Ni, Cu, Zn, and Pb, additional colloids were generated by aggregation over the 70 h experiment after they were removed at T0 (Figure 2.5). For Fe, the Southern Ocean sample originally had 58% of its dFe in the colloidal size fraction ( $c\text{Fe} = 0.75 \text{ nmol/kg}$ ), and after the colloids were removed at T0, cFe returned to 40% of dissolved after only 14 h ( $c\text{Fe} = 0.21 \text{ nmol/kg}$ ) and eventually exceeded the original fraction to 74% after 70 h ( $c\text{Fe} = 0.46 \text{ nmol/kg}$ ). Additional results from an identical experiment at Station ALOHA (22.75°N, 158.00°W, 24 September 2013, 800 m; sampling methods in (Fitzsimmons et al., 2015a)) demonstrated that Fe colloids can re-aggregate in as little as 3 h and approach the initial % colloidal partitioning after only 22 h (Figure 2.5e). This supports the conclusion that cFe aggregation occurs almost immediately and continues over time, likely attributed to interactions between the soluble and colloidal organic compounds that complex Fe in seawater, as well as possible self-assembly (Ding et al., 2008). While we do not have direct chemical speciation measurements at these near-bottom study sites, the only available literature data from surface waters of the West Antarctic Peninsula and coastal Antarctica indicate that ligands that may form complexes with Fe are present but are often saturated and

thus not uniformly in excess of Fe in this region in the surface ocean (Buck et al., 2010; Thuróczy et al., 2012).

The colloidal Fe re-aggregation kinetics pattern was replicated for Ni and Zn, except that for Ni and Zn both the colloidal concentrations and % colloidal Ni and Zn exceeded the original levels by 14 and 24 h, respectively; in contrast, it took Fe 70 h to exceed the original 58% cFe. Thus, Ni and Zn were particularly affected by the removal of colloidal species at the start of the experiment, and their re-aggregation kinetics were especially fast. This must be related to Ni and Zn themselves and/ or the organic ligands that bind them (Van den Berg and Nimmo, 1987; Bruland, 1989), since Fe, Cu, and Pb did not behave similarly in the same samples. For Cu and Pb, colloids did re-aggregate by 14 h following colloid removal, but cCu never reached its original % colloidal Cu, even after 70 h, while dPb quickly returned to the size partitioning of the original samples.

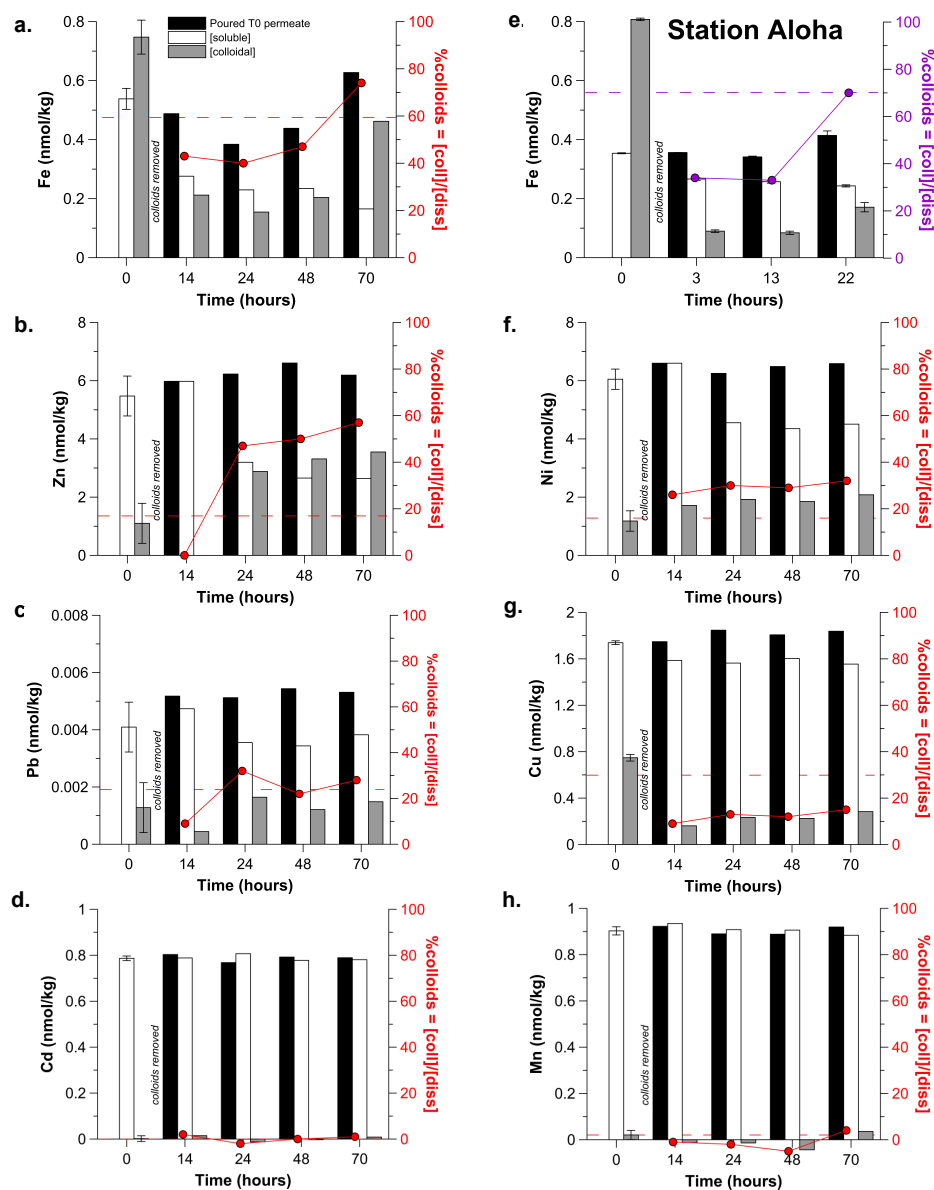


**Figure 2.5** Summary of all results of the Colloid Exchangeability Experiment across all metals. The legend for all treatment types is included in panel (a), where black bars are the initial permeate solution concentration re-poured at each subsequent time point to monitor for wall loss (compared to the white bar at T0, which is the initial permeate soluble metal concentration). White bars at non-zero timepoints are the re-ultrafiltered soluble concentrations, and grey bars are the re-ultrafiltered colloidal concentrations, obtained by subtracting the white bar from the black bar. Overlaid in red is the % colloidal metal (cMe/dFe; right axis) at each time point. The T0 time point contains the initial size partitioning of the seawater sample, and the initial % colloids is indicated by the dashed red line. Panel (e) shows unpublished data for Fe from a prototype of this experiment using water from 800 m depth at Station ALOHA, showing similar trends for Fe across a comparable timescale.

Thus, it appears that the metals studied here that have a substantial natural colloidal fraction in seawater (Fe, Cu, Zn, Ni, and Pb) will reaggregate to form colloids in as short as 14 h. However, the extent to which those colloids re-form varies, as often the re-formed % colloidal metal and the colloidal metal concentrations do not match the initial results. We hypothesize that organic aggregation/coagulation kinetics are involved, since the one element most likely to exist as a free cation (Mn, (Oldham et al., 2017)) showed no colloidal character in these samples. Fe and Cu are both thought to be bound > 99.9% by organic ligands in seawater (Rue and Bruland, 1995; Wu and Luther III, 1995; Moffett and Dupont, 2007), yet Cu did not re-form colloids to the same extent as Fe. Our knowledge of organic complexation of some of the other metals, like Zn, Cd, and Pb, however, is too poor to speculate further on the direct pathways of colloidal aggregation, except to say that organic aggregation is likely involved and our data demonstrate the extent to which these metals can re-aggregate.

#### **2.4.3. Adsorption experiment: How quickly are dissolved metals lost from solution to bottle wall adsorption in the absence of seawater acidification?**

The goal of this experiment was to quantify the rate of adsorptive loss of metals onto LDPE bottle walls over 24 h, which is a relevant timescale during which filtered seawater might be stored in holding bottles awaiting further processing. The results are shown in Figure 2.6, where the % dMe change from the initial concentration (indicated by a grey bar) are shown. Triplicate sampling allowed obviously contaminated samples to be removed from the averages used to calculate % metal loss to bottle walls.

Prior studies on bottles made of plastics other than LDPE indicate that the higher SA:V of smaller bottles will cause greater adsorptive Fe losses (Fischer et al., 2007; Fitzsimmons and Boyle, 2012). Indeed, the SA:V ratio of our 125 mL bottles is higher than our 250 mL bottles ( $0.838 \text{ cm}^{-1}$  versus  $0.760 \text{ cm}^{-1}$ ), providing more area per volume onto which metals can adsorb. The Adsorption Experiment data here on LDPE bottles show that, as expected, more adsorption occurred in the smaller 125 mL bottles compared to the 250 mL bottles for Co, Cu, Zn and Ni over 40 months. DFe also showed higher % loss onto the 125 mL bottles until 40 months, when surprisingly the adsorption onto 250 mL bottle walls (91% loss) surpassed that on the 125 mL bottle walls (75%). This could indicate that the dependence of bottle sorption on SA:V ratio is not the most significant factor in sorption, particularly when the SA:V ratios are comparable, as in our 125 and 250 mL bottles. However, these results do support prior suggestions that if storage in a plastic bottle over time is necessary, it is preferable to use larger bottle sizes (lower SA:V) to help reduce metal sorption losses to bottle walls.

Prior studies also suggest that metal sorption to bottle walls appears to be affected by bottle material. For example, Fe adsorbed the most over  $\sim 72$  h in quartz bottles (99%, (Fischer et al., 2007)), compared to HDPE bottles (29–60%, (Schlosser et al., 2011; Fitzsimmons and Boyle, 2012)), and PTFE bottles (40–60%, (Schlosser and Croot, 2008)) in prior studies. Adsorption onto LDPE bottles had not been explored previously, despite their being the bottle of choice for marine trace metal studies since the GEOTRACES era (Cutter et al., 2010), yet the second result of our Adsorption Experiment showed that LDPE bottle walls did promote some wall adsorption of dFe

over 24 h, which continued until 40 months after sample collection for both sizes. Our data show that sorptive losses from unacidified samples to LDPE bottles are generally low over the first 24 h and only statistically significant for dissolved Fe, Co, Ni, Zn, and Cd after 40 months (Figure 2.6).

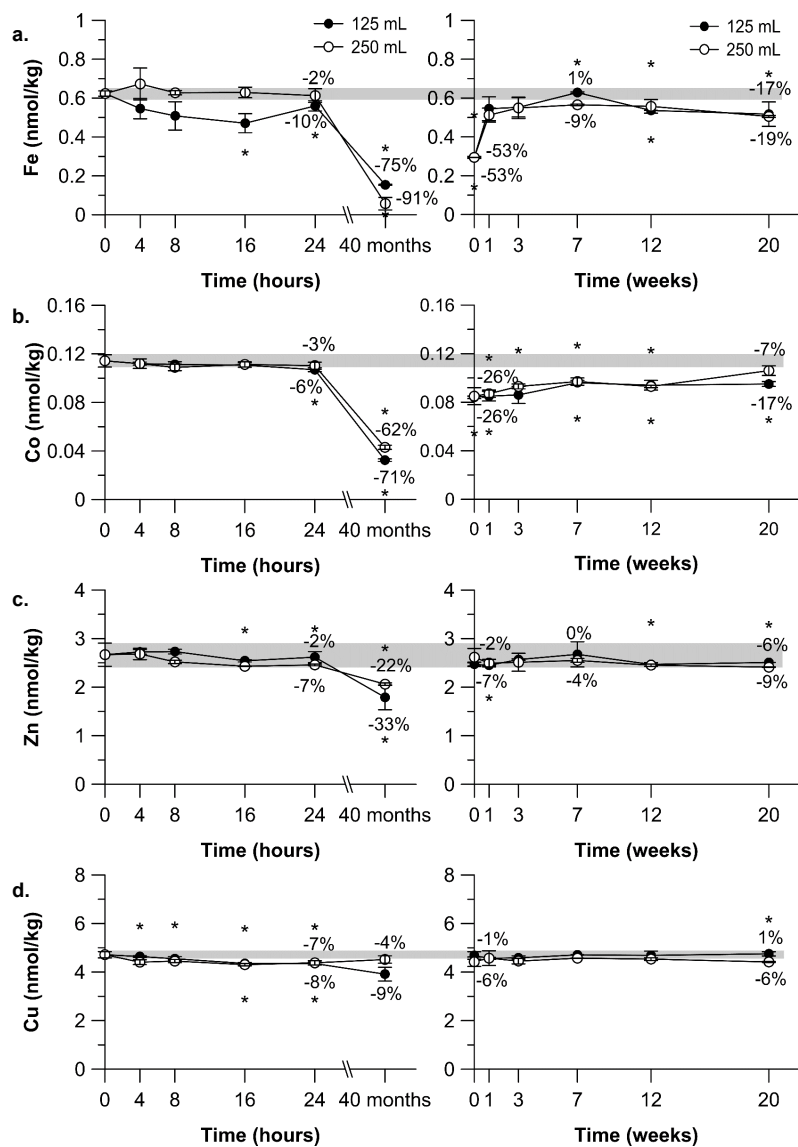


**Figure 2.6** Results from the Adsorption (left) and Desorption (right) Experiments. Water was collected at 100 m depth in the Arctic Ocean and filtered immediately upon collection and stored in the dark at room temperature for 22 months. The grey bar indicates the average value of the initial dissolved metal concentration for the seawater used in these experiments, and the width reflects the standard deviation in those initial measurements. 125 mL sample treatments are shown as a closed circle, while 250 mL sample treatments are shown as an open circle. The annotations refer to the % change in concentration from the average initial dMe concentration (grey bar) at select time points. \* indicates a result that is statistically significant from the initial (T = 0) adsorption result (grey bar), used a two-tailed heteroscedastic t-test ( $p < .05$ ). Asterisk above the data is for 250 mL treatment and below is for the 125 mL treatment. Pb has been excluded due to poor experimental reproducibility.

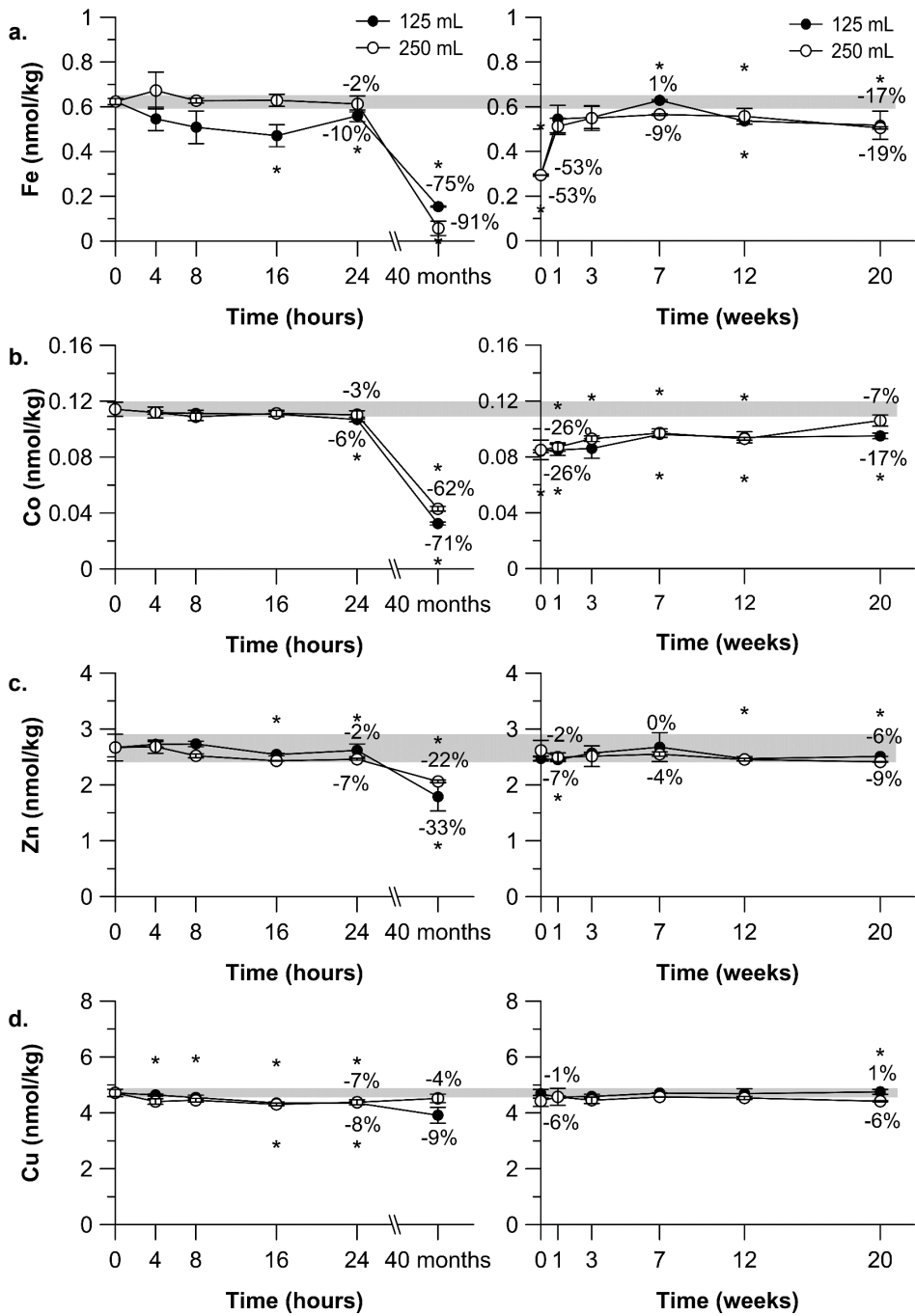


Figure 2.6 Continued.

Previously, dFe was adsorbed to HDPE bottle walls at a ratio of 0.878% per SA:V ( $\text{cm}^{-1}$ ) ratio (Fitzsimmons and Boyle, 2012) over 15.5 h, which would predict that 0.20 and 0.15 nmol/kg of dFe would have adsorbed onto 125 mL and 250 mL HDPE bottle walls by 16 h. However, only 0.16 and 0 nmol/kg were actually adsorbed, respectively, onto the LDPE bottle walls used in this study after 16 h, indicating that adsorption of metals to LDPE bottle walls is lower than adsorption to HDPE bottle walls, even with identical acid cleaning.

The third result of the Adsorption Experiment was that wall adsorption to LDPE bottles can now be extended to other metals beyond Fe, with significant losses observed over just 16 h for dissolved Co, Ni, Cu, Zn, and Cd (Figure 2.6). While wall losses of dFe have been studied in the past, losses of the other metals have been poorly constrained in any bottle type. Of the available data, one study showed that dCu had an adsorptive loss of 1.6% onto fluorinated ethylene (poly)propylene Nalgene bottles over the course of 2 h, while dCd showed almost no adsorption in seawater samples spiked with Cu, Cd, and Pb (Cuculić and Branica, 1996). No conclusive kinetic data for dissolved Ni, Mn, Zn, or Co exists from prior studies despite the fact that we now routinely collect and measure these dissolved metals in seawater. In this study, dissolved Fe, Co, and Zn showed the largest losses over 40 months in both bottle sizes, ranging from 22 to 91% loss (Figure 2.6 a,b,c). Ni and Cu also showed modest losses over this timescale (6 to 8% and 4 to 9% loss, respectively), despite showing almost no loss for Ni after 24 h. Wall losses of dissolved Mn and Cd were negligible ( $< 5\%$ ), even after being left unacidified for 40 months.

#### **2.4.4. Desorption experiment: Once samples have been acidified, how quickly do metals desorb from bottle walls?**

The goal of this experiment was to examine the kinetics of metal desorption from 125 and 250 mL LDPE bottle walls and thus assess how long samples that are thought to have suffered losses to bottle walls must be acidified to desorb the metals. We set up both the Adsorption and Desorption Experiments using seawater from the same 100 m depth in the Arctic Ocean so that we could compare concentrations at time points in both experiments to the same concentration (T0 of adsorption experiment, Figure 2.6, grey bar), which was the initial filtered seawater acidified immediately upon collection. The Desorption Experiment bottles were left unacidified for 22 months during which time metals were allowed to adsorb onto the bottle walls.

The Adsorption Experiment showed that dissolved Fe, Co, Ni, Cu and Zn were significantly adsorbed to LDPE bottle walls after spending 40 months unacidified; however, the Desorption Experiment showed that the desorption kinetics of each of these metals back to their initial concentration varied significantly. For instance, 30–40% of the dissolved Fe and Co that had adsorbed over 40 months desorbed immediately, but remained 7–19% lower than their initial concentrations 20 weeks after acidification (Figure 2.6a, b); thus, we never recovered all of the lost Fe or Co. DFe also showed some temporally variable desorption or exchange, as it desorbed to within 11% of the initial concentration by 12 weeks only to fall again to 19% below the initial concentration at 20 weeks. In contrast, dissolved Ni, Cu, and Zn all desorbed back to within  $\pm 10\%$  of the original sample concentration immediately upon acidification.

However, all three were still significantly different from the initial concentration after 20 weeks in the 250 mL bottles only. Dissolved Cd and Mn had insignificant desorption rates, but they also had insignificant adsorption to bottle walls, indicating that the timescale of acidification plays little to no role in the storage and analyses of these two metals.

## **2.5. Discussion and implications**

Based on the experimental results described above, we first make several recommendations for the collection and handling of dissolved and particularly colloidal trace metals samples in seawater. Then, we discuss some implications for the physicochemical speciation of dissolved metals in the ocean.

We recommend that:

1. Seawater should only be preserved for Fe size partitioning, not the size partitioning of any of the other metals, and only if stored seawater samples are preserved frozen at  $-20\text{ }^{\circ}\text{C}$  immediately upon collection;
2. Careful attention be given to the source and thus potential native conditions/physicochemical speciation of samples analyzed for metal size partitioning, as this appears to affect the preservation of metal speciation over time as well as colloid recovery during the ultrafiltration process;
3. Filtered seawater samples that require ultrafiltration should be ultrafiltered as soon as possible but no later than 24 h after initial filtration in order to avoid wall adsorption to bottle walls and/or exchange between the soluble and colloidal size fractions;

4. Seawater samples that will be stored in 125 mL or 250 mL LDPE bottles should be acidified as soon as possible (within a few hours at most) to avoid adsorptive wall losses of dissolved Fe and Co, which are difficult to recover;
5. Seawater samples that have suffered significant wall losses should not be analyzed for dissolved Fe or Co concentrations unless they have been acidified for at least 30 weeks, which is 1.5 times the maximum desorption timescale that we tested for dissolved Fe and Co;
6. If analyzing metals other than dissolved Fe and Co, 12 weeks of acidification is sufficient for complete desorption of most metals, and analysis after shorter timescales is acceptable if samples were not left unacidified for very long.

Additionally, looking across the experiments, a few conclusions about natural marine colloidal metal size partitioning can also be made. First, the colloidal preservation experiment showed contrasting size partitioning and preservation behavior of metals collected from different locations (West Antarctic Peninsula vs. Galveston Bay), suggesting that the inherent differences in physicochemical speciation at different locations largely affect the kinetics of metal exchangeability in seawater. As noted above, this is particularly noticeable in the preservation of dZn size partitioning (Figure 2.4d), where a statistically significant aggregation into colloids in both the frozen and room temperature treatment was observed in the Southern Ocean bottom water, while there was no discernible change in the % cZn over the same timescale in Galveston Bay estuarine surface water. This pattern was also true for Cu and Ni (Figure

2.4 b-c), indicative of a more stable equilibrium between the soluble and colloidal phases in Galveston Bay waters.

We also found that colloids tended to be more abundant in Galveston Bay, consistent with the literature (Guo and Santschi, 1997; Wen et al., 1999), suggesting a permanent sedimentary, riverine, or *in situ* flocculation source that maintains the presence of colloids at this estuarine site. The fact that metal preservation was so consistent in Galveston Bay, with little apparent wall loss or exchange, indicates that the ligands or other compounds involved in forming colloidal metals in Galveston Bay are very different from those in the Southern Ocean samples. The prior work of Wen et al. (1999) in the Galveston Bay estuary showed high % colloids for Fe, Cu, Zn, and Pb (55 to 91%) as well as an average 55% contribution of colloids to the organic carbon phase into which many metal-binding ligands might fall. Wen et al. (1999) further estimated that only 1% of the surface sites in the very abundant colloidal organic carbon (COC) phase would be sufficient to complex all trace metals, which is supported by a strong correlation between COC and colloidal Co, Ni, Cu, Zn, Cd. Wen et al. (1999) also report a large contribution of freshwater colloids associated with both metal and organic carbon phases in Galveston Bay, which is important as river water appears a major component of the Galveston Bay water collected during this study (salinity 26.5). This contribution from rivers has been shown to be a significant source of colloidal metals such as Fe, Ni and Cu in particular (Powell et al., 1996), which when combined with the increased colloidal complexation capacity observed between COC and some metals, may be

responsible for the different partitioning behaviors we observed in our two preservation experiments.

Second, we may interpret the differences in colloidal behavior in the Southern Ocean vs. Galveston Bay experiments as anecdotal evidence that cold seawater samples do not perform as well in the CFF system. As noted above, the temperature and salinity of a sample will have an effect on the overall initial physicochemical speciation of the sample. For example, the Southern Ocean metals other than Fe, in general, did not have well-preserved size partitioning, while Galveston Bay (25 °C warmer and fresher) showed much better stability of size partitioning of these same metals over time. Additionally, the frozen and then thawed samples showed relatively poorer recovery in the Galveston Bay experiment, perhaps a function of having been stored at a colder temperature. Previous studies have shown that frozen and thawed samples may increase the solubility of Fe over time [Schlosser et al., 2011), which would have a direct effect on speciation measurements and recovery.

Third, while it is common practice to freeze and thaw unacidified samples as a way of preserving DOC concentrations (Fellman et al., 2008), ligand concentrations (Apte et al., 1990), and even chemical speciation of trace metals when immediate analyses are not possible (Capodaglio et al., 1995; Buck et al., 2012), there may actually be artifacts in physicochemical speciation that arise simply from the freeze-thaw process itself. Previous studies have found that some sampling and storage artifacts, such as adsorption to bottle walls, are in fact increased under cold conditions (Fitzsimmons and Boyle, 2012). While we observed no change in dFe concentration or size partitioning

using frozen samples over 3 weeks in the Colloid Preservation Experiments, we cannot rule out that the process of freezing and thawing may have some effect on the kinetics of exchange between soluble and colloidal compounds in any seawater sample. This could include the possibility of self-aggregation or self-assembly (Ding et al., 2008; Verdugo et al., 2008) that may be a side effect of the freezing process or a natural function of these organic colloids.

Fourth, the results of all of our experiments show that the kinetics of colloidal exchange and metal adsorption are variable across different metals. Many factors contribute to this variability, such as the chemistry of the metal, the characteristics of the solution (in this case unacidified seawater) including organic ligand concentrations, the properties of the container, and other external factors such as temperature (Massee et al., 1981). We can apply some of these parameters directly to our study. For instance, adsorption to plastics such as polyethylene is initially motivated by hydrophobic and/or van der Waal's attraction of metal complexes with the hydrophobic plastic surface, perhaps encouraging greater adsorption of metals bound by organic compounds with hydrophobic "tails." Indeed, metals like Fe, Co, Zn, and Cu, all of which are organically complexed in seawater (Bruland et al., 2013), showed more significant (4–91%) adsorption in our experiments over 40 months and even 24 h compared to metals commonly found as free ions in seawater like Mn (Byrne, 2002). However, experiments from decades ago have shown that sustained cationic adsorption to plastic surfaces is a product of ion exchange with hydroxide groups in the inner charged layer of polyethylene's double-charged surface layer (Beneš and Smetana, 1969). Thus, it is

expected that hydrolyzed metals will adsorb more rapidly compared to free ions (Starik et al., 1963; James and Healy, 1972b), leading us to hypothesize that hydrolyzable metals or metals with significant organic complexation, like Fe, will show a greater loss to bottle walls over time. Additionally, organic complexation may indicate a proclivity to enter the colloidal phase (Dammshäuser and Croot, 2012), as demonstrated for metals such as Fe where colloids are a significant component of the dissolved phase (Fitzsimmons and Boyle, 2014a). There is often more consistent partitioning between soluble and colloidal phases for organically complexed metals such as Ni and Cu across the global ocean (Jensen and Fitzsimmons, unpublished). Thus, any ingrowth of colloids over 70 h is significant. Likewise, metals such as Mn that typically exist largely or entirely in the soluble phase showed no colloidal growth and were preserved for the dissolved phase under frozen conditions.

Finally, very little work, to the authors' knowledge, has directly examined metal desorption kinetics from sample bottle walls, although early studies stressed the importance of acid cleaning sampling containers and materials before use to prevent desorption of metal contaminants from bottle manufacture (Batley and Gardner, 1977; Ross, 1986). It is well known that protons significantly disrupt the binding of metals to common ligand groups (Doucet et al., 2007), making acidification commonplace in long-term sample storage. We found that while adsorption was significant for Fe and Co over even 24 h, desorption remained slow and incomplete after 20 weeks. In contrast, Cu did not show significant adsorption, but also did not completely desorb over the full 20 weeks. Therefore, we recommend preventing samples from experiencing significant

adsorption to bottle walls, since it can be hard to recover these metals even after extended time acidified. In the event that bottle wall adsorption does occur, we recommend allowing samples to sit acidified for at least 30 weeks in order to maximize the probability of metal remobilization.

## **2.6. Conclusions**

The accurate determination of trace metal concentrations and physicochemical speciation in seawater has progressed over the last few decades as clean sampling and storage procedures have been increasingly optimized. However, there are still challenges and unanswered questions regarding filtration and sample processing that warrant further examination, particularly in the context of multi-elemental analyses. For instance, while ultrafiltration to determine the colloidal concentrations of trace metals has received increased attention in the oceanographic literature (Guo and Santschi, 2007 and references therein), the timescale of storage prior to filtration and the potential effects this has on measured size fractionation remain poorly known. Additionally, important contributing factors to measuring dissolved and colloidal metal concentrations over time will include sampling and storage artifacts such as adsorption to bottle walls. Combining these issues, this study sought to answer four major questions: 1) Can we preserve the size partitioning of trace metals over time under frozen or room temperature conditions?, 2) Do colloids “grow in” over time following removal, and if so, how fast?, 3) How fast do metals adsorb to bottle walls in the absence of acidification?, and 4) Once samples are acidified, how quickly do metals desorb from bottle walls? The results of these experiments allowed us to make several recommendations involving sample storage and

proposed timing of ultrafiltration and analyses. For example, it is evident from the Colloid Preservation Experiment that only the size partitioning of Fe (and perhaps labile Co) can be preserved under frozen conditions. Notably, this experiment also demonstrated that the natural physicochemical speciation of waters will give rise to differential exchange between the soluble and colloidal phases and thus effect their ability to be preserved. In the Colloid Exchangeability Experiment, it was clear that in most cases metal colloids (once removed) do grow back via aggregation from the soluble phase, often exceeding the initial colloidal fraction. Prior work suggested that metal-organic complexation in seawater may impart a proclivity for trace metals to form colloids (Dammshäuser and Croot, 2012). Thus it is not surprising that Fe, Ni, Cu and Zn, which are all thought to be organically complexed in seawater, regenerated colloids in as short as 14 h, whereas Mn, which is thought to exist mostly as a free cation and weak chloride complexes in solution, did not aggregate into colloids. It is difficult to conclude from this study why colloids might re-form and reach higher proportions compared to their original natural partitioning, but future work might combine chemical speciation measurements with these colloid re-aggregation kinetics to investigate the mechanisms responsible for re-aggregation.

The results of the Bottle Adsorption and Desorption experiment simply add to what we already knew about adsorption kinetics of Fe, namely that the adsorption rate is dependent on both bottle material and SA:V ratio. It is evident that smaller bottles with higher SA:V ratios promote more sorption, not just for Fe, but also for Co, Ni, Cu, and Zn. We also saw less sorption using LPDE bottles compared to previous studies that

used HDPE bottles (Fischer et al., 2007; Schlosser et al., 2011; Fitzsimmons and Boyle, 2012). Even so, over 24 h, dissolved Fe, Co, Cu, and Zn all showed significant adsorption to LDPE bottle walls, demonstrating that any further sample processing, such as ultrafiltration, should occur as soon as possible after sample collection in order to avoid metal adsorption artifacts.

Based on the results of the desorption experiment we conclude that 20 weeks (5 months) may not be long enough to completely desorb dissolved Fe and Co (the two metals that were the most susceptible to adsorption) from LDPE bottles. However, it is important to note that our samples were stored unacidified for 22 months prior to acidification, which is much longer than most oceanographers wait to acidify after sample collection. It would be informative to conduct experiments to learn whether storage time prior to acidification plays a role in setting the desorption time scale. Finally, because we observed different behaviors and different kinetics for different metals in different water types, our recommendations on how to avoid artifacts in trace metal speciation measurements should be supplemented with further experimentation under one's "local" conditions of water chemistry and temperature when sample processing and sample acidification cannot be conducted as soon as possible after collection.

## **2.7. References**

Apte, S. C., M. J. Gardner, J. E. Ravenscroft, and J. A. Turrell. 1990. "Examination of the range of copper complexing ligands in natural waters using a combination of

- cathodic stripping voltammetry and computer simulation." *Analytica Chimica Acta* 235:287-297. doi: [https://doi.org/10.1016/S0003-2670\(00\)82086-3](https://doi.org/10.1016/S0003-2670(00)82086-3).
- Baalousha, M., B. Stolpe, and J. R. Lead. 2011. "Flow field-flow fractionation for the analysis and characterization of natural colloids and manufactured nanoparticles in environmental systems: A critical review." *Journal of Chromatography A* 1218 (27):4078-4103. doi: <https://doi.org/10.1016/j.chroma.2011.04.063>.
- Bartell, F. E., Tudor L. Thomas, and Ying Fu. 1951. "Thermodynamics of Adsorption from Solutions. IV. Temperature Dependence of Adsorption." *The Journal of Physical Chemistry* 55 (9):1456-1462. doi: 10.1021/j150492a005.
- Baskaran, M., P. H. Santschi, G. Benoit, and B. D. Honeyman. 1992. "Scavenging of thorium isotopes by colloids in seawater of the Gulf of Mexico." *Geochimica et Cosmochimica Acta* 56 (9):3375-3388. doi: [https://doi.org/10.1016/0016-7037\(92\)90385-V](https://doi.org/10.1016/0016-7037(92)90385-V).
- Batley, G. E., and D. Gardner. 1977. "Sampling and storage of natural waters for trace metal analysis." *Water Research* 11 (9):745-756. doi: [https://doi.org/10.1016/0043-1354\(77\)90042-2](https://doi.org/10.1016/0043-1354(77)90042-2).
- Beneš, P, and J Smetana. 1969. "Radiochemical study of the sorption of trace elements. IV. Adsorption of iron on polyethylene and its state in aqueous solutions." *Collection of Czechoslovak Chemical Communications* 34 (5):1360-1374.
- Benner, Ronald, J. Dean Pakulski, Matthew McCarthy, John I Hedges, and PATRICK G. HATCHER. 1992. "Bulk Chemical Characteristics of Dissolved Organic

- Matter in the Ocean." *Science* 255 (5051):1561-1564. doi:  
10.1126/science.255.5051.1561.
- Bruland, KW, R Middag, and MC Lohan. 2013. "Controls of trace metals in seawater."
- Bruland, K. W. 1989. "Complexation of zinc by natural organic ligands in the central North Pacific." *Limnology and Oceanography* 34 (2):269-285. doi:  
10.4319/lo.1989.34.2.0269.
- Bruland, K. W., and EDEN L Rue. 2001. "Iron: Analytical methods for the determination of concentrations and speciation." *The Biogeochemistry of Iron in Seawater*:255-289.
- Buck, K. N., James Moffett, Katherine A Barbeau, Randelle M Bundy, Yoshiko Kondo, and Jingfeng Wu. 2012. "The organic complexation of iron and copper: an intercomparison of competitive ligand exchange-adsorptive cathodic stripping voltammetry (CLE-ACSV) techniques." *Limnology and Oceanography: Methods* 10 (7):496-515.
- Buck, Kristen N., Karen E. Selph, and Katherine A. Barbeau. 2010. "Iron-binding ligand production and copper speciation in an incubation experiment of Antarctic Peninsula shelf waters from the Bransfield Strait, Southern Ocean." *Marine Chemistry* 122 (1):148-159. doi:  
<https://doi.org/10.1016/j.marchem.2010.06.002>.
- Buesseler, K. O., J. E. Bauer, R. F. Chen, T. I. Eglinton, O. Gustafsson, W. Landing, K. Mopper, S. B. Moran, P. H. Santschi, R. VernonClark, and M. L. Wells. 1996. "An intercomparison of cross-flow filtration techniques used for sampling

- marine colloids: Overview and organic carbon results." *Marine Chemistry* 55 (1):1-31. doi: [https://doi.org/10.1016/S0304-4203\(96\)00046-1](https://doi.org/10.1016/S0304-4203(96)00046-1).
- Buffle, J., D. Perret, and M. Newman. 1992. "The use of filtration and ultrafiltration for size fractionation of aquatic particles, colloids, and macromolecules." In *Environmental particles. IUPAC series on environmental analytical and physical chemistry*, edited by J. Buffle and Herman P. Van Leeuwen, 171-230. Lewis Publishers.
- Byrne, Robert H. 2002. "Inorganic speciation of dissolved elements in seawater: the influence of pH on concentration ratios." *Geochemical Transactions* 3 (1):11. doi: 10.1186/1467-4866-3-11.
- Capodaglio, G, G Scarponi, G Toscano, C Barbante, and P Cescon. 1995. "Speciation of trace metals in seawater by anodic stripping voltammetry: critical analytical steps." *Fresenius' journal of analytical chemistry* 351 (4-5):386-392.
- Chen, Min, Robert C. H. Dei, Wen-Xiong Wang, and Laodong Guo. 2003. "Marine diatom uptake of iron bound with natural colloids of different origins." *Marine Chemistry* 81 (3-4):177-189. doi: [http://dx.doi.org/10.1016/S0304-4203\(03\)00032-X](http://dx.doi.org/10.1016/S0304-4203(03)00032-X).
- Chen, Min, and Wen-Xiong Wang. 2001. "Bioavailability of natural colloid-bound iron to marine plankton: Influences of colloidal size and aging." *Limnology and Oceanography* 46 (8):1956-1967. doi: 10.4319/lo.2001.46.8.1956.

- Chen, Min, Wen-Xiong Wang, and Laodong Guo. 2004. "Phase partitioning and solubility of iron in natural seawater controlled by dissolved organic matter." *Global Biogeochemical Cycles* 18 (4). doi: 10.1029/2003gb002160.
- Chin, Wei-Chun, Mónica V. Orellana, and Pedro Verdugo. 1998. "Spontaneous assembly of marine dissolved organic matter into polymer gels." *Nature* 391 (6667):568-572. doi: 10.1038/35345.
- Cuculić, Vlado, and Marko Branica. 1996. "Adsorption of trace metals from sea-water onto solid surfaces: analysis by anodic stripping voltammetry." *Analyst* 121 (8):1127-1131. doi: 10.1039/AN9962101127.
- Cutter, G, P Andersson, Lou Codispoti, P Croot, R Francois, MC Lohan, H Obata, and Michiel Rutgers vd Loeff. 2010. Sampling and sample-handling protocols for GEOTRACES cruises. GEOTRACES.
- Dammshäuser, Anna, and Peter L. Croot. 2012. "Low colloidal associations of aluminium and titanium in surface waters of the tropical Atlantic." *Geochimica et Cosmochimica Acta* 96:304-318. doi: <http://dx.doi.org/10.1016/j.gca.2012.07.032>.
- Ding, Yong-Xue, Wei-Chun Chin, Anthony Rodriguez, Chin-Chang Hung, Peter H. Santschi, and Pedro Verdugo. 2008. "Amphiphilic exopolymers from *Sagittula stellata* induce DOM self-assembly and formation of marine microgels." *Marine Chemistry* 112 (1):11-19. doi: <https://doi.org/10.1016/j.marchem.2008.05.003>.

- Doucet, Frederic J, Jamie R Lead, and Peter H Santschi. 2007. "Colloid-trace element interactions in aquatic systems." *IUPAC SERIES ON ANALYTICAL AND PHYSICAL CHEMISTRY OF ENVIRONMENTAL SYSTEMS* 10:95.
- Erickson, Harold P. 2009. "Size and Shape of Protein Molecules at the Nanometer Level Determined by Sedimentation, Gel Filtration, and Electron Microscopy." *Biological Procedures Online* 11 (1):32. doi: 10.1007/s12575-009-9008-x.
- Fellman, Jason B., David V. D'Amore, and Eran Hood. 2008. "An evaluation of freezing as a preservation technique for analyzing dissolved organic C, N and P in surface water samples." *Science of The Total Environment* 392 (2):305-312. doi: <https://doi.org/10.1016/j.scitotenv.2007.11.027>.
- Fischer, A. C., J. J. Kroon, T. G. Verburg, T. Teunissen, and H. Th Wolterbeek. 2007. "On the relevance of iron adsorption to container materials in small-volume experiments on iron marine chemistry: <sup>55</sup>Fe-aided assessment of capacity, affinity and kinetics." *Marine Chemistry* 107 (4):533-546. doi: <https://doi.org/10.1016/j.marchem.2007.08.004>.
- Fitzsimmons, Jessica N., and Edward A. Boyle. 2012. "An intercalibration between the GEOTRACES GO-FLO and the MITESS/Vanes sampling systems for dissolved iron concentration analyses (and a closer look at adsorption effects)." *Limnology and Oceanography: Methods* 10 (6):437-450. doi: 10.4319/lom.2012.10.437.
- Fitzsimmons, Jessica N, and Edward A Boyle. 2014. "Assessment and comparison of Anopore and cross flow filtration methods for the determination of dissolved

iron size fractionation into soluble and colloidal phases in seawater." *Limnol. Oceanogr. Methods* 12:246-263.

Fitzsimmons, Jessica N., and Edward A. Boyle. 2014. "Both soluble and colloidal iron phases control dissolved iron variability in the tropical North Atlantic Ocean." *Geochimica et Cosmochimica Acta* 125:539-550. doi: <http://dx.doi.org/10.1016/j.gca.2013.10.032>.

Fitzsimmons, Jessica N., G. G. Carrasco, J. Wu, S. Roshan, M. Hatta, C. I. Measures, T. M. Conway, S. G. John, and E. A. Boyle. 2015. "Partitioning of dissolved iron and iron isotopes into soluble and colloidal phases along the GA03 GEOTRACES North Atlantic Transect." *Deep-Sea Research Part II: Topical Studies in Oceanography* 116:130-151. doi: 10.1016/j.dsr2.2014.11.014.

Fitzsimmons, Jessica N, Christopher T Hayes, Sherain N Al-Subiai, Ruifeng Zhang, Peter L Morton, Rachel E Weisend, François Ascani, and Edward A Boyle. 2015. "Daily to decadal variability of size-fractionated iron and iron-binding ligands at the Hawaii Ocean Time-series Station ALOHA." *Geochimica et Cosmochimica Acta* 171:303-324.

Gaffney, Jeffrey S, Nancy A Marley, and Sue B Clark. 1996. "Humic and fulvic acids: isolation, structure, and environmental role."

Gerringa, L. J. A., S. Blain, P. Laan, G. Sarthou, M. J. W. Veldhuis, C. P. D. Brussaard, E. Viollier, and K. R. Timmermans. 2008. "Fe-binding dissolved organic ligands near the Kerguelen Archipelago in the Southern Ocean (Indian sector)." *Deep*

- Sea Research Part II: Topical Studies in Oceanography* 55 (5):606-621. doi:  
<https://doi.org/10.1016/j.dsr2.2007.12.007>.
- Guo, Laodong, and Peter H. Santschi. 1997. "Composition and cycling of colloids in marine environments." *Reviews of Geophysics* 35 (1):17-40. doi:  
doi:10.1029/96RG03195.
- Guo, Laodong, and P. H. Santschi. 2007. "Ultrafiltration and its Applications to Sampling and Characterisation of Aquatic Colloids." In *Environmental Colloids and Particles*, edited by J. Buffle, H.P. Van Leeuwen, Kevin J. Wilkinson and Jamie R Lead.
- Hassler, C.S., Véronique Schoemann, Carol Mancuso Nichols, Edward C. V. Butler, and Philip W. Boyd. 2011. "Saccharides enhance iron bioavailability to Southern Ocean phytoplankton." *Proceedings of the National Academy of Sciences* 108 (3):1076-1081. doi: 10.1073/pnas.1010963108.
- Honeyman, BD, and PH Santschi. 1989. "A Brownian-pumping model for oceanic trace metal scavenging: evidence from Th isotopes." *Journal of Marine Research* 47 (4):951-992.
- Honeyman, Bruce D., and Peter H. Santschi. 1988. "Metals in aquatic systems." *Environmental Science & Technology* 22 (8):862-871. doi:  
10.1021/es00173a002.
- Ingri, Johan, Susanna Nordling, Jenny Larsson, Jenny Rönnegård, Nina Nilsson, Ilia Rodushkin, Ralf Dahlgvist, Per Andersson, and Örjan Gustafsson. 2004. "Size distribution of colloidal trace metals and organic carbon during a coastal bloom

- in the Baltic Sea." *Marine Chemistry* 91 (1):117-130. doi:  
<https://doi.org/10.1016/j.marchem.2004.06.009>.
- James, Robert O., and Thomas W. Healy. 1972. "Adsorption of hydrolyzable metal ions at the oxide—water interface. I. Co(II) adsorption on SiO<sub>2</sub> and TiO<sub>2</sub> as model systems." *Journal of Colloid and Interface Science* 40 (1):42-52. doi:  
[http://dx.doi.org/10.1016/0021-9797\(72\)90172-5](http://dx.doi.org/10.1016/0021-9797(72)90172-5).
- James, Robert O., and Thomas W. Healy. 1972. "Adsorption of hydrolyzable metal ions at the oxide—water interface. III. A thermodynamic model of adsorption." *Journal of Colloid and Interface Science* 40 (1):65-81. doi:  
[https://doi.org/10.1016/0021-9797\(72\)90174-9](https://doi.org/10.1016/0021-9797(72)90174-9).
- Jensen, L. T., N. J. Wyatt, B. S. Twining, S. Rauschenberg, W. M. Landing, R. M. Sherrell, and J. N. Fitzsimmons. "Biogeochemical cycling of dissolved zinc in the Western Arctic (Arctic GEOTRACES GN01)." *Global Biogeochemical Cycles* 0 (ja). doi: doi:10.1029/2018GB005975.
- Lagerström, M. E., M. P. Field, M. Séguret, L. Fischer, S. Hann, and R. M. Sherrell. 2013. "Automated on-line flow-injection ICP-MS determination of trace metals (Mn, Fe, Co, Ni, Cu and Zn) in open ocean seawater: Application to the GEOTRACES program." *Marine Chemistry* 155 (0):71-80. doi:  
<http://dx.doi.org/10.1016/j.marchem.2013.06.001>.
- Larsson, Jenny, Örjan Gustafsson, and Johan Ingri. 2002. "Evaluation and Optimization of Two Complementary Cross-Flow Ultrafiltration Systems toward Isolation of

- Coastal Surface Water Colloids." *Environmental Science & Technology* 36 (10):2236-2241. doi: 10.1021/es010325v.
- Lohan, Maeve C., Ana M. Aguilar-Islas, Robert P. Franks, and Kenneth W. Bruland. 2005. "Determination of iron and copper in seawater at pH 1.7 with a new commercially available chelating resin, NTA Superflow." *Analytica Chimica Acta* 530 (1):121-129. doi: <https://doi.org/10.1016/j.aca.2004.09.005>.
- Louchouart, Patrick, Steve Opsahl, and Ronald Benner. 2000. "Isolation and quantification of dissolved lignin from natural waters using solid-phase extraction and GC/MS." *Analytical Chemistry* 72 (13):2780-2787.
- Massee, R., F. J. M. J. Maessen, and J. J. M. De goeij. 1981. "Losses of silver, arsenic, cadmium, selenium and zinc traces from distilled water and artificial sea-water by sorption on various container surfaces." *Analytica Chimica Acta* 127:181-193. doi: [https://doi.org/10.1016/S0003-2670\(01\)83974-X](https://doi.org/10.1016/S0003-2670(01)83974-X).
- Minor, EC, J-P Simjouw, JJ Boon, AE Kerkhoff, and J Van der Horst. 2002. "Estuarine/marine UDOM as characterized by size-exclusion chromatography and organic mass spectrometry." *Marine Chemistry* 78 (2-3):75-102.
- Moffett, James W, and Christopher Dupont. 2007. "Cu complexation by organic ligands in the sub-arctic NW Pacific and Bering Sea." *Deep Sea Research Part I: Oceanographic Research Papers* 54 (4):586-595.
- Oldham, Véronique E., Alfonso Mucci, Bradley M. Tebo, and George W. Luther Iii. 2017. "Soluble Mn(III)-L complexes are abundant in oxygenated waters and

stabilized by humic ligands." *Geochimica et Cosmochimica Acta* 199:238-246.  
doi: <http://dx.doi.org/10.1016/j.gca.2016.11.043>.

Opsahl, Stephen, and Ronald Benner. 1997. "Distribution and cycling of terrigenous dissolved organic matter in the ocean." *Nature* 386 (6624):480-482. doi: 10.1038/386480a0.

Pellenbarg, R. E., and T. M. Church. 1978. "Storage and processing of estuarine water samples for trace metal analysis by atomic absorption spectrometry." *Analytica Chimica Acta* 97 (1):81-86. doi: [https://doi.org/10.1016/S0003-2670\(01\)83277-3](https://doi.org/10.1016/S0003-2670(01)83277-3).

Powell, Rodney T, William M Landing, and James E Bauer. 1996. "Colloidal trace metals, organic carbon and nitrogen in a southeastern US estuary." *Marine Chemistry* 55 (1-2):165-176.

Reitmeyer, Rebecca, Rodney T Powell, William M Landing, and Christopher I Measures. 1996. "Colloidal aluminum and iron in seawater: An intercomparison between various cross-flow ultrafiltration systems." *Marine Chemistry* 55 (1-2):75-91.

Roberts, Darryl R, Robert G Ford, and Donald L Sparks. 2003. "Kinetics and mechanisms of Zn complexation on metal oxides using EXAFS spectroscopy." *Journal of Colloid and Interface Science* 263 (2):364-376.

Ron, Eliora Z, and Eugene Rosenberg. 2001. "Natural roles of biosurfactants: Minireview." *Environmental microbiology* 3 (4):229-236.

- Ross, Howard B. 1986. "The importance of reducing sample contamination in routine monitoring of trace metals in atmospheric precipitation." *Atmospheric Environment (1967)* 20 (2):401-405. doi: [https://doi.org/10.1016/0004-6981\(86\)90044-2](https://doi.org/10.1016/0004-6981(86)90044-2).
- Rue, Eden L, and Kenneth W Bruland. 1995. "Complexation of iron (III) by natural organic ligands in the Central North Pacific as determined by a new competitive ligand equilibration/adsorptive cathodic stripping voltammetric method." *Marine chemistry* 50 (1-4):117-138.
- Santschi, Peter H. 2018. "Marine colloids, agents of the self-cleansing capacity of aquatic systems: Historical perspective and new discoveries." *Marine Chemistry* 207:124-135. doi: <https://doi.org/10.1016/j.marchem.2018.11.003>.
- Santschi, Peter H, Laodong Guo, M Baskaran, Susan Trumbore, John Southon, Thomas S Bianchi, Bruce Honeyman, and Luis Cifuentes. 1995. "Isotopic evidence for the contemporary origin of high-molecular weight organic matter in oceanic environments." *Geochimica et Cosmochimica Acta* 59 (3):625-631.
- Scheinost, Andreas C, Sven Abend, Kaumudi I Pandya, and Donald L Sparks. 2001. "Kinetic controls on Cu and Pb sorption by ferrihydrite." *Environmental Science & Technology* 35 (6):1090-1096.
- Schlosser, Christian, and Peter L Croot. 2008. "Application of cross-flow filtration for determining the solubility of iron species in open ocean seawater." *Limnology and Oceanography: Methods* 6 (11):630-642.

- Schlosser, C., C. L. De La Rocha, and P. L. Croot. 2011. "Effects of iron surface adsorption and sample handling on iron solubility measurements." *Marine Chemistry* 127 (1):48-55. doi: <https://doi.org/10.1016/j.marchem.2011.07.008>.
- Schlosser, Christian, Christina L. De La Rocha, Peter Streu, and Peter L. Croot. 2012. "Solubility of iron in the Southern Ocean." *Limnology and Oceanography* 57 (3):684-697. doi: 10.4319/lo.2012.57.3.0684.
- Schlosser, Christian, Peter Streu, and Peter L Croot. 2013. "Vivaspin ultrafiltration: A new approach for high resolution measurements of colloidal and soluble iron species." *Limnology and Oceanography: Methods* 11 (4):187-201.
- Sherrell, Robert M., Amber L. Annett, Jessica N. Fitzsimmons, Vincent J. Rocanova, and Michael P. Meredith. 2018. "A "shallow bathtub ring" of local sedimentary iron input maintains the Palmer Deep biological hotspot on the West Antarctic Peninsula shelf." *Philosophical Transactions of the Royal Society A: Mathematical, Physical and Engineering Sciences* 376 (2122):20170171. doi: [doi:10.1098/rsta.2017.0171](https://doi.org/10.1098/rsta.2017.0171).
- Sohrin, Yoshiki, Shouhei Urushihara, Seiji Nakatsuka, Tomohiro Kono, Eri Higo, Tomoharu Minami, Kazuhiro Norisuye, and Shigeo Umetani. 2008. "Multielemental Determination of GEOTRACES Key Trace Metals in Seawater by ICPMS after Preconcentration Using an Ethylenediaminetriacetic Acid Chelating Resin." *Analytical Chemistry* 80 (16):6267-6273. doi: [10.1021/ac800500f](https://doi.org/10.1021/ac800500f).

- Starik, IE, VN Scebetkobskij, and IA Skulskij. 1963. "The absorption of radioactive isotopes on polymer adsorbents that are not ion-exchangers III." *Radiokhimiya* 4:393-398.
- Stolpe, Björn, Laodong Guo, Alan M. Shiller, and Martin Hassellöv. 2010. "Size and composition of colloidal organic matter and trace elements in the Mississippi River, Pearl River and the northern Gulf of Mexico, as characterized by flow field-flow fractionation." *Marine Chemistry* 118 (3):119-128. doi: <https://doi.org/10.1016/j.marchem.2009.11.007>.
- Thuróczy, Charles-Edouard, Anne-Carlijn Alderkamp, Patrick Laan, Loes J. A. Gerringa, Matthew M. Mills, Gert L. Van Dijken, Hein J. W. De Baar, and Kevin R. Arrigo. 2012. "Key role of organic complexation of iron in sustaining phytoplankton blooms in the Pine Island and Amundsen Polynyas (Southern Ocean)." *Deep Sea Research Part II: Topical Studies in Oceanography* 71-76:49-60. doi: <https://doi.org/10.1016/j.dsr2.2012.03.009>.
- Van den Berg, CMG, and M Nimmo. 1987. "Determination of interactions of nickel with dissolved organic material in seawater using cathodic stripping voltammetry." *Science of the Total Environment* 60:185-195.
- Verdugo, Pedro, Monica V. Orellana, Wei-Chun Chin, Timothy W. Petersen, Ger van den Eng, Ronald Benner, and John I. Hedges. 2008. "Marine biopolymer self-assembly: implications for carbon cycling in the ocean." *Faraday Discussions* 139 (0):393-398. doi: 10.1039/B800149A.

- von der Heyden, B. P., and A. N. Roychoudhury. 2015. "A review of colloidal iron partitioning and distribution in the open ocean." *Marine Chemistry* 177:9-19. doi: <https://doi.org/10.1016/j.marchem.2015.05.010>.
- Wells, Mark L. 2002. "Marine colloids and trace metals." *Biogeochemistry of marine dissolved organic matter*:367-404.
- Wen, Liang-Saw, Peter Santschi, Gary Gill, and Christopher Paternostro. 1999. "Estuarine trace metal distributions in Galveston Bay: importance of colloidal forms in the speciation of the dissolved phase." *Marine Chemistry* 63 (3-4):185-212. doi: [http://dx.doi.org/10.1016/S0304-4203\(98\)00062-0](http://dx.doi.org/10.1016/S0304-4203(98)00062-0).
- Wen, Liang-Saw, Peter H Santschi, and Degui Tang. 1997. "Interactions between radioactively labeled colloids and natural particles: Evidence for colloidal pumping." *Geochimica et Cosmochimica Acta* 61 (14):2867-2878.
- Wen, Liang-Saw, Mary C. Stordal, Degui Tang, Gary A. Gill, and Peter H. Santschi. 1996. "An ultraclean cross-flow ultrafiltration technique for the study of trace metal phase speciation in seawater." *Marine Chemistry* 55 (1):129-152. doi: [https://doi.org/10.1016/S0304-4203\(96\)00052-7](https://doi.org/10.1016/S0304-4203(96)00052-7).
- Wen, Liang-Saw, Kent W. Warnken, and Peter H. Santschi. 2008. "The role of organic carbon, iron, and aluminium oxyhydroxides as trace metal carriers: Comparison between the Trinity River and the Trinity River Estuary (Galveston Bay, Texas)." *Marine Chemistry* 112 (1):20-37. doi: <https://doi.org/10.1016/j.marchem.2008.06.003>.

Wilkinson, K. J., J. C. Negre, and J. Buffle. 1997. "Coagulation of colloidal material in surface waters: the role of natural organic matter." *Journal of Contaminant Hydrology* 26 (1):229-243. doi: [https://doi.org/10.1016/S0169-7722\(96\)00071-X](https://doi.org/10.1016/S0169-7722(96)00071-X).

Wu, Jingfeng, and George W Luther III. 1995. "Complexation of Fe (III) by natural organic ligands in the Northwest Atlantic Ocean by a competitive ligand equilibration method and a kinetic approach." *Marine Chemistry* 50 (1-4):159-177.

### 3. BIOGEOCHEMICAL CYCLING OF DISSOLVED ZINC IN THE WESTERN ARCTIC (ARCTIC GEOTRACES GN01)\*

#### 3.1. Overview

The biogeochemical cycling of dissolved zinc (dZn) was investigated in the Western Arctic along the U.S. GEOTRACES GN01 section. Vertical profiles of dZn in the Arctic are strikingly different than the classic “nutrient-type” profile commonly seen in the Atlantic and Pacific Oceans, instead exhibiting higher surface concentrations (~1.1 nmol/kg), a shallow subsurface absolute maximum (~4–6 nmol/kg) at 200 m coincident with a macronutrient maximum, and low deep water concentrations (~1.3 nmol/kg) that are homogeneous with depth. In contrast to other ocean basins, typical inputs such as rivers, atmospheric inputs, and especially deep remineralization are insignificant in the Arctic. Instead, we demonstrate that dZn distributions in the Arctic are controlled primarily by (1) shelf fluxes following the sediment remineralization of high Zn:C and Zn:Si cells and the seaward advection of those fluxes and (2) mixing of dZn from source waters such as the Atlantic and Pacific Oceans rather than vertical biological regeneration of dZn. This results in both the unique profile shapes and the largely decoupled relationship between dZn and Si found in the Arctic. We found a weak dZn:Si

---

\* Reprinted with permission from “Biogeochemical Cycling of Dissolved Zinc in the Western Arctic (Arctic GEOTRACES GN01)” by L.T. Jensen, N.J. Wyatt, B.S. Twining, S. Rauschenberg, W.M. Landing, R.M. Sherrell, J.N. Fitzsimmons, 2019. *Global Biogeochemical Cycles*, 33, Copyright 2019 by American Geophysical Union.

regression in the full water column (0.077 nmol/ $\mu$ mol,  $r^2= 0.58$ ) that is higher than the global slope (0.059 nmol/ $\mu$ mol,  $r^2 = 0.94$ ) because of the shelf-derived halocline dZn enrichments. We hypothesize that the decoupling of Zn:Si in Western Arctic deep waters results primarily from a past ventilation event with unique preformed Zn:Si stoichiometries.

### **3.2. Introduction**

Zinc (Zn) is an essential physiological nutrient for marine microorganisms, supporting carbon and organic phosphorus acquisition, protein structure, and DNA replication (Morel, 2008). The availability of Zn has been shown to regulate microbial activity in laboratory culture experiments (Sunda and Huntsman, 1995; Shaked et al., 2006; Cox and Saito, 2013) and, more recently, in natural ocean systems (Crawford et al., 2003; Franck et al., 2003; Jakuba et al., 2012; Mahaffey et al., 2014). This has increased awareness of the important role for Zn in oceanic primary production and carbon export. While the extent to which surface dissolved Zn (dZn) concentrations limit oceanic primary production remains unclear, investigations of the processes that mediate Zn's surface water inputs and removal fluxes, deep water regeneration, and surface resupply are at the forefront of modern trace metal biogeochemistry (Little et al., 2014; Wyatt et al., 2014; Little et al., 2016; Boyd et al., 2017; Vance et al., 2017).

Globally, the vertical oceanic distribution of dZn resembles that of the macronutrients, with surface depletion resulting from biological uptake and high concentrations at depth from regeneration (Schlitzer et al., 2018). In most oceanic surface waters, dZn concentrations are typically  $< 0.2$  nmol/kg (Lohan et al., 2002;

Gosnell et al., 2012; Conway and John, 2014; Wyatt et al., 2014), and dZn is strongly complexed (> 95%) by organic ligands (Bruland, 1989; Ellwood and Van den Berg, 2000; Jakuba et al., 2012). In the deep ocean, dZn concentrations increase from 2 nmol/kg in the North Atlantic (Conway and John, 2014) to around 10 nmol/kg in the North Pacific (Bruland, 1980; Franck et al., 2003) as water masses age and accumulate Zn from regenerated material. However, this simplistic uptake and regeneration-based paradigm for oceanic Zn cycling is often insufficient to explain observational data, where a complex array of physical and biogeochemical interactions, including external inputs and horizontal mixing (Roshan and Wu, 2015; Kondo et al., 2016; Vance et al., 2017), scavenging onto organic matter (John and Conway, 2014), and authigenic Zn sulfide precipitation (Conway and John, 2015; Janssen and Cullen, 2015) may also be important.

Riverine inputs are widely regarded as the dominant source of dZn to the oceans, based on a global riverine Zn flux of  $5.9 \times 10^8$  mol/yr that is an order of magnitude higher than the atmospheric flux (Little et al., 2014). There is also evidence for a hydrothermal source of Zn (Conway and John, 2014; Roshan and Wu, 2015; Roshan et al., 2016), although the significance of this flux to the global ocean dZn inventory remains uncertain because of the paucity of far-field hydrothermal measurements. The principle removal mechanism for Zn from the oceanic inventory is the burial of organic and authigenic material in seafloor sediments (Little et al., 2014; Little et al., 2016). The large sedimentary Zn inventory (Cai et al., 2011; Trefry et al., 2014) may act as a source

of Zn to the water column under certain conditions (Conway and John, 2015; Kondo et al., 2016).

Zn also exhibits a remarkably tight correlation with dissolved silicate (Si) in the Atlantic, Pacific, and Southern Oceans, showing a deeper remineralization depth than nitrate (N) and phosphate (P) (Schlitzer et al., 2018). This would imply that the oceanic cycle of Zn is dominated by uptake into and regeneration from diatom siliceous tests, which are regenerated more slowly during sinking through the water column than intracellular organic matter (Zhao et al., 2014). However, the vast majority of Zn in diatoms is associated with N and P in organic tissues (Twining et al., 2004; Twining and Baines, 2013; Twining et al., 2015) and not diatom opal (1–3 % of total cellular Zn inventory) (Ellwood and Hunter, 2000; Jaccard et al., 2009), and thus Zn should be regenerated from this organic matter in the upper ocean alongside P rather than opal-derived Si (Twining et al., 2014). A more recent hypothesis suggests that the strong Zn-Si correlation across the major oceans is instead explained by extreme drawdown of Zn and Si relative to P by diatoms in the surface Southern Ocean, and it is the lateral transport and modification of these Zn- and Si-depleted waters that sets the unusual Zn-Si-P stoichiometry in global nutricline waters (Ellwood, 2008; Wyatt et al., 2014; Vance et al., 2017; Weber et al., 2018). Many of our global conclusions on Zn biogeochemistry have come from studies in low and mid-latitudes, with relatively little work done in the polar oceans (Cid et al., 2012; Kondo et al., 2016). Given the interconnections between the polar and lower latitude oceans through deep and intermediate water formation and

circulation, knowledge of polar ocean Zn biogeochemistry is critical to understanding its potential impact on Zn distributions across the global ocean.

Here, we investigate the dominant biogeochemical processes controlling the Zn distribution in the Arctic Ocean, where until very recently only four profiles of Zn had been published decades ago (Moore, 1981; Danielsson and Westerlund, 1983; Yeats, 1988; Yeats and Westerlund, 1991). The Arctic Ocean is a small, enclosed basin accounting for ~3% of the global ocean by area (Chang and Devol, 2009), where circulation is driven by a unique bottom bathymetry. Approximately 50% of its surface area overlies continental shelves (Jakobsson et al., 2004) such that margin processes play a much greater role in regulating trace metal distributions than in other major oceans (Cid et al., 2012; Kondo et al., 2016). The Arctic communicates with the North Atlantic Ocean through the deep Fram Strait and also receives inputs from the North Pacific through the shallow and narrow Bering Strait. A common tracer of Pacific waters in the Arctic is elevated Si concentration (Jones and Anderson, 1986), and since Si and Zn are well correlated in the global ocean, we hypothesized that Zn might also be a Pacific water tracer. Cid et al. (2012) and Kondo et al. (2016) recently identified a dZn concentration maximum associated with the macronutrient maximum of the upper halocline, suggesting that dZn distributions are generally controlled by the same biological cycles influencing the macronutrients compared to the shelf-based sources and/or removal processes suggested for iron (Cid et al., 2012; Aguilar-Islas et al., 2013; Hioki et al., 2014; Kondo et al., 2016). However, the mechanism for the transport of Zn from the shelves into the interior Arctic Ocean remains unclear.

We report the full water column distribution of dZn for the Western Arctic Ocean during late summer 2015 sampled along the U.S. GEOTRACES GN01 section. In contrast to other ocean basins, Zn sources such as atmospheric inputs and especially deep remineralization are less significant in the open Arctic. We show that mixing between North Pacific and North Atlantic source waters, as well as the influence of shelf sediment remineralization sources, dominates dZn biogeochemistry. These measurements are timely, given on-going climate change in the Arctic, as they provide a baseline for interpreting observations of Arctic biogeochemistry upon future environmental change.

### **3.3. Methods**

#### **3.3.1. Sample Collection**

Seawater samples were collected during the 2015 US Arctic GEOTRACES (GN01) cruise aboard the USCGC *Healy* (HLY1502), which departed from Dutch Harbor, AK, on 9 August 2015 and returned 12 October 2015. The cruise track (Figure 3.1 began in the North Pacific (~60°N, Station 1), traversed the Bering Shelf (Stations 2–3) and through the Bering Strait (Stations 4–5), across the Chukchi Shelf (Stations 6–8), and northward along ~170°W (“northbound”, Stations 10–30) to the North Pole (Station 32). The cruise track then returned south along 150°W (“southbound”, Stations 33–57) and ended on the Chukchi Shelf (Stations 61–66). There was increased sampling resolution along the shelf-break (Stations 8–14 and 57–66) for a total of 23 full-depth trace metal stations, 4 shallow-depth ice hole stations (Stations 31, 33, 39, 43), and 4 mid-depth marginal ice zone stations (Stations 8, 51, 53, 54).

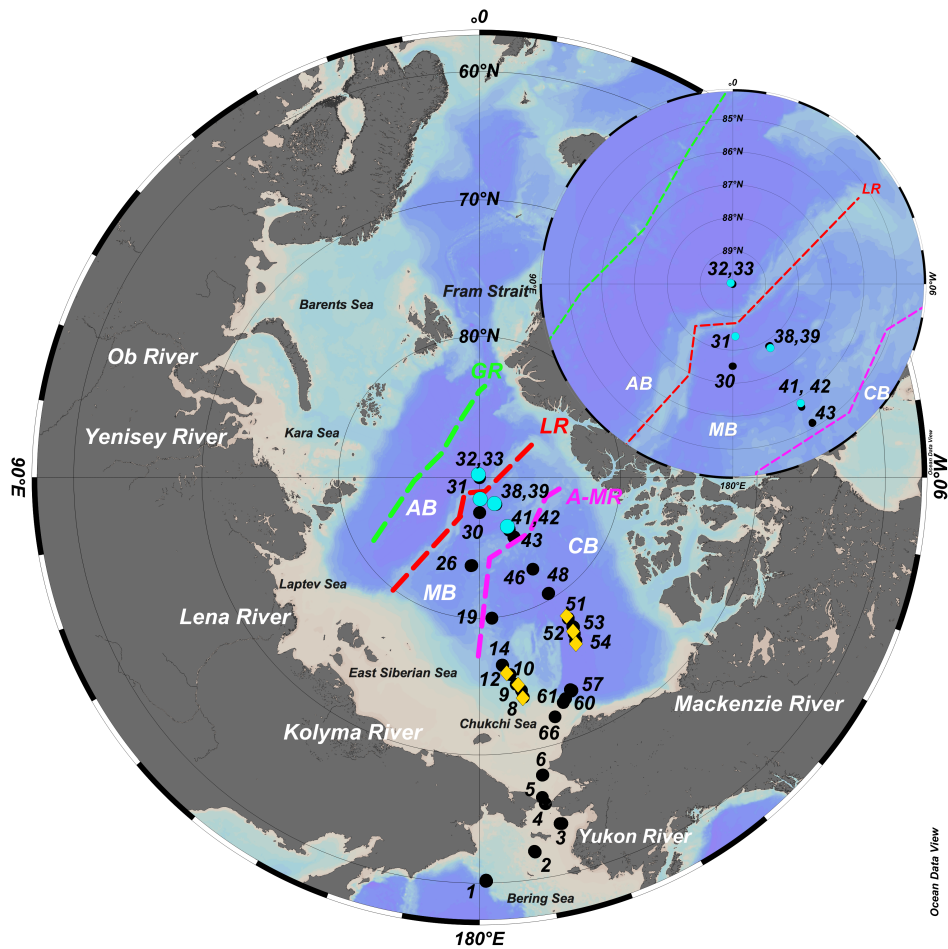


**Figure 3.1** U.S. GEOTRACES Arctic GN01 transect with relevant stations, rivers, seas, and bathymetric features identified. Blue dots = ice Stations 31, 33, 39, and 42; orange diamonds = MIZ Stations 8, 9, 10, 12, 52, 53, and 54; black dots = full-depth stations. AB = Amundsen Basin, MB = Makarov Basin, CB = Canada Basin, GR = Gakkel Ridge, LR = Lomonosov Ridge, A-MR = Alpha-Mendeleev Ridge. Station 1 is used as a North Pacific end member analog. Stations 1–3 are considered “Bering Shelf.” Stations 4 and 5 are considered “Bering Strait.” Stations (6–9, 61–66) are considered “Chukchi Shelf.” Stations 10–31 are “northbound” transect, Station 32 is the North Pole, and Stations 38–60 are “southbound” transect. Inset shows detail to differentiate ice stations from full-depth stations.

Seawater sample collection followed established GEOTRACES sampling protocols (Cutter et al., 2010). Briefly, seawater was collected using a trace-metal clean

Seabird carousel/CTD with a Vectran cable and 24 x 12 L Go-Flo bottles. Two bottles were tripped per depth on ascent at ~3 m/min. Upon recovery, each Go-Flo was pressurized to ~0.5 atm. with HEPA-filtered air and fitted with a 0.2  $\mu\text{m}$  AcroPak-200 polyethersulfone membrane filter capsule (Pall), and seawater was filtered into 250 mL LDPE Nalgene bottles following three 10% volume rinses of the bottle, cap, and threads. Bottles were cleaned prior to sampling using established protocols with hydrochloric acid (trace metal grade HCl, 1M) and ultrapure Milli-Q (MQ) water at 60°C (Fitzsimmons and Boyle, 2012). Samples were acidified to pH 1.8 (FIA, 0.024 M using quartz-distilled HCl) and 2.0 (ICP-MS, 0.012 M using Optima, Fisher Scientific) and stored at room temperature.

Near surface seawater samples were collected through holes in sea ice floes (Stations 31, 33, 39, 43) at 1, 5, and 20 m using a polypropylene high-head battery-powered enclosed motor centrifugal pump with ½-inch FEP-lined Tygon tubing (Cole Parmer). Samples were collected and filtered (0.2  $\mu\text{m}$ , AcroPak) on the ice into a 25 L acid-cleaned carboy and were subsampled into clean 250 mL LDPE Nalgene bottles, acidified, and stored as above.

### **3.3.2. Zn analysis and Intercomparison**

#### **3.3.2.1. FIA**

Dissolved Zn analysis was performed on-board ship using flow injection analysis (FIA) with fluorimetric detection, under a HEPA filter unit within a shipboard purpose-built clean environment. The FIA system was a modified version of the system described in Nowicki et al. (1994) and more recently in Wyatt et al. (2014) using the fluorescent

binding ligand p-tosyl-8-aminoquinoline (pTAQ). Briefly, the sample was buffered in-line to pH 5.0 using 0.3 M ammonium acetate (Optima, Fisher Scientific), yielding a final concentration of 0.12 M ammonium acetate in the samples, before Zn(II) was selectively pre-concentrated for one minute onto the cation exchange resin Toyopearl AF-Chelate 650 M. Interfering seawater constituents were removed from the resin by rinsing for 30 seconds with 0.08 M ammonium acetate before the Zn(II) was liberated from the resin using 0.08 M quartz-distilled HCl (q-HCl). The eluent was mixed with a 50  $\mu$ M pTAQ (Sigma-Aldrich) solution, and the fluorescent emission of the Zn-pTAQ complex was detected using a Shimadzu RF-10Ax1 fluorimeter with excitation and emission wavelengths set to 377 and 495 nm respectively.

Zinc standards (0–8 nmol/kg) were prepared in 0.2  $\mu$ m filtered, low-Zn surface seawater. The analytical blank, determined by loading acidified (0.024 M q-HCl, pH 1.7) ultrapure water treated as a sample, was typically < 0.15 nmol/kg. The limit of detection ( $3 \times \sigma$  of the lowest standard addition) was < 0.05 nmol/kg for a one minute load time, while the relative standard deviation (RSD) for replicate analyses was 0–5 %. The accuracy of the analytical method was validated by quantification of dZn in the SAFe D2 reference sample (Table 3.1, “FIA”).

Cadmium is also known to form a fluorescent complex with the reagent pTAQ. The Cd interference for the method was investigated by spiking low-Zn seawater with single and combination additions of Zn and Cd (1–10 nmol/kg from 1000 ppm Zn(II) and Cd(II) ICP-MS standards). The Cd interference from this standard matrix was estimated to be equivalent to ~4.5 % of the analytical signal. This interference was

corrected using the Cd concentration for each sample, measured using a  $^{111}\text{Cd}$  isotope spike at Texas A&M University (TAMU) simultaneously with Zn, as described below in section 3.2.2.2.

**Table 3.1** Measured Values for GEOTRACES Reference Materials SAFe D1 and D2 Across Three Labs and Two Analytical Methods. Reproduced with permission from Jensen et al. (2019).

Reference material	Measured value	Consensus value (May 2013)
SAFe D1 (SeaFAST TAMU)	7.37 ( $\pm 0.27$ ) nmol/kg, $n = 43$	7.40 ( $\pm 0.35$ ) nmol/kg
SAFe D1 (SeaFAST Rutgers)	7.32 ( $\pm 0.15$ ) nmol/kg, $n = 4$	
SAFE D2 (SeaFAST TAMU)	7.36 ( $\pm 0.23$ ) nmol/kg, $n = 43$	7.43 ( $\pm 0.25$ ) nmol/kg
SAFe D2 (FIA FSU)	7.30 ( $\pm 0.23$ ) nmol/kg, $n = 10$	

*Note.* FIA = flow injection analysis; FSU = Florida State University; TAMU = Texas A&M University.

### 3.3.2.2. SeaFAST/ICP-MS

At least 9 months after acidification, samples were analyzed for their Zn concentration at TAMU using isotope dilution and Zn pre-concentration on a SeaFAST-pico system (ESI, Omaha, NE) following a modified, offline version of Lagerström et al. (2013). An acidified seawater sample (10 mL) was weighed and then spiked with  $^{68}\text{Zn}$  and loaded into the SeaFAST autosampler, which automates mixing with a 5.90 N ammonium acetate buffer (Optima, Fisher Scientific) to adjust to an optimal pH around 6.5 (Sohrin et al., 2008). The buffered sample-spike mixture was then loaded onto a 200  $\mu\text{L}$  column filled with Nobias-chelate PA1 resin, followed by rinsing with ultrapure water to remove salts. The Zn collected on the column was then eluted using 1.6 M  $\text{HNO}_3$  (Optima, Fisher Scientific). Rather than online elution directly into the ICP-MS,

400  $\mu\text{L}$  of eluent was captured (for a 25-fold pre-concentration) in acid-cleaned 1.5 mL centrifuge tubes (Mircrowtube®) and stored up to 1 week before analysis. Elemental analysis was accomplished in medium resolution on a Thermo Finnigan Element XR high-resolution inductively coupled plasma mass spectrometer (HR-ICP-MS) housed at the R. Ken Williams Radiogenic Isotope Facility. At least 20 procedural blanks composed of acidified (0.012 M HCl Optima, Fisher Scientific), ultrapure MQ water (Element-POD, Millipore) for every 40 seawater samples were run through the spike, pre-concentration, and analysis sequence to evaluate the contribution of dZn from reagents and the SeaFAST system. Blanks for dZn averaged 0.18 nmol/kg and generally decreased over time with increased SeaFAST system usage, becoming as low as 0.050 nmol/kg in the later analytical sessions. The detection limit of this method, taken as  $3 \times \sigma$  of the procedural blanks, averaged 0.07 nmol/kg over all runs. The accuracy of the analytical method was validated by quantification of dZn in the SAFe D1 and D2 reference samples (Table 3.1, “SeaFAST (TAMU)”). Precision was evaluated over replicate analyses ( $n = 96$ ) of random samples within the dataset, yielding an RSD of 0–6%, compared to 3% precision in the SAFe D1 and D2 standards.

### **3.3.2.3. Intercomparison of Subsampling and Analytical Techniques**

An intercomparison of dZn concentrations between Texas A&M University (TAMU), Florida State University (FSU), and Rutgers University was performed in order to assess the reliability and accuracy of the FIA and SeaFAST methods (Figure 3.2). Unique seawater samples from Station 19 were collected by both FSU and TAMU teams on the Arctic cruise, and subsequently aliquots from TAMU were sent to Rutgers

for evaluation by their methods. Analytically, FSU performed the FIA dZn analysis, while both TAMU and Rutgers employed the SeaFAST-pico isotope dilution technique, with analysis on different HR-ICP-MS instruments (for Rutgers on a Finnigan MAT Element 1 HR-ICP-MS, procedural blank = 0.06 nmol/kg).

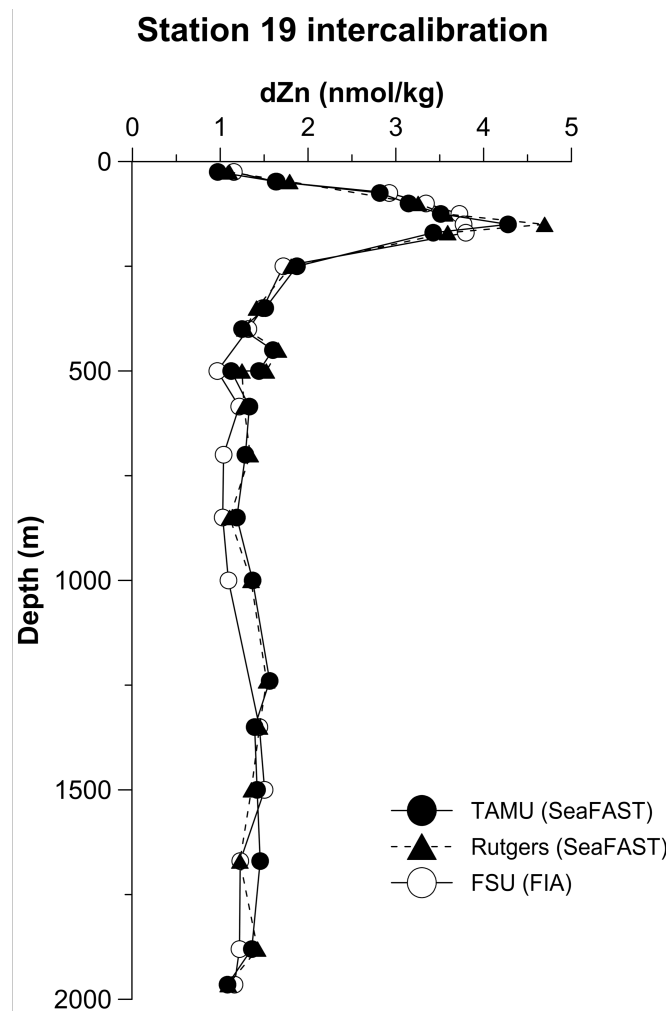


**Figure 3.2** Full-depth intercalibration between two SeaFAST pico isotope dilution methods from TAMU (filled circles) and Rutgers (filled triangles), and FIA fluorometric methods at FSU (open circles). The results from Station 19 showed an average relative standard deviation of 6% across the three labs. FIA; FSU = Florida State University; TAMU = Texas A&M University.

In general, the data generated by the three different laboratories agree well, with an average RSD of 6%, except at depths 450 and 500 m. This RSD agreed well with the reported precision for each method, as stated above.

### **3.3.3. Temperature, Salinity, Nutrients, and Hydrography**

Temperature and pressure were determined by the trace metal CTD sensors (Seabird 911+). Bottle salinity was measured on unfiltered subsamples using a shipboard Guildline Autosal 8400B salinometer at room temperature, while dissolved oxygen analyses were performed using a modified Winkler titration (Carpenter, 1965; Culberson et al., 1991) with water taken from a separate cast and CTD operated by the Scripps Institution of Oceanography (SIO). Dissolved macronutrients nitrate, nitrite, phosphate, and silicate were analyzed shipboard at room temperature on a Seal Analytical continuous-flow AutoAnalyzer 3 following the methods described in the GO-SHIP repeat hydrography manual (Hydes et al., 2010). All isosurface and contoured sections in this paper were prepared using the Ocean Data View software (Schlitzer, 2016).

### **3.3.4. SXRF Cell Stoichiometry Analyses**

Single-cell SXRF samples were collected from the surface mixed layer using the GEOTRACES rosette. Unfiltered water samples were preserved with 0.25% trace-metal clean buffered glutaraldehyde (Twining et al., 2003) and centrifuged onto 1 x 1 mm, 200  $\mu\text{m}$  thick SiN windows. Windows were briefly rinsed with a drop of ultrapure water and dried in a Class-100 cabinet. SXRF analysis was performed using the 2-ID-E beamline at the Advanced Photon source (Argonne National Laboratory) following the protocols of Twining et al. (2011). Each cell was raster scanned with a focused 10 keV x-ray beam

with a diameter of approximately  $0.5 \mu\text{m}$ . Fluorescence spectra from the pixels covering the cell were averaged to calculate whole-cell quotas, and a fluorescence spectrum from a neighboring empty section of the grid was subtracted. Cellular Zn and  $\text{Si}_\alpha$  fluorescence intensities were fit with a modified-Gaussian model using custom software and peak areas converted to areal element concentrations using NBS-certified standard reference materials (Núñez-Milland et al., 2010; Twining et al., 2011). Spatial regions of interest representing the whole cell (including any adsorbed elements, if present) were prepared for each cell and used to calculate Zn and Si quotas. Cellular C quotas were calculated from cell biovolume using the equations of Menden-Deuer and Lessard (2000). Cell biovolume was calculated for each cell from measurements of cell diameter, length, and height using digital image processing software Image J. Shape and volume equations were taken from Hillebrand et al. (1999). In total 119 cells were analyzed, with 13–24 cells analyzed at each station.

### **3.4. Results and Discussion**

Dissolved Zn concentrations in seawater across the entire U.S. Arctic GEOTRACES GN01 section ranged 0.37–6.59 nmol/kg, averaging  $1.77 \pm 0.96$  overall ( $n = 321$ ). As can be seen in Figure 3.3, a characteristic dZn depth profile in the Western Arctic (representative Station 52) has a very different shape from those in the other major ocean basins. Instead of the classic nutrient-type profile shape of the Atlantic and Pacific, with  $\leq 0.2$  nmol/kg concentrations in the surface that increase to maximum values at depth, the Western Arctic dZn concentrations were elevated even at the surface, climbed to a maximum near 250 m depth, and had lowest concentrations below 2000 m depth (Figure 3.3b). Here, we explain

this unique profile shape as a result of water mass mixing, external dZn fluxes, and internal biological cycling alongside the macronutrient Si. We then return to a comparison to global dZn distributions.

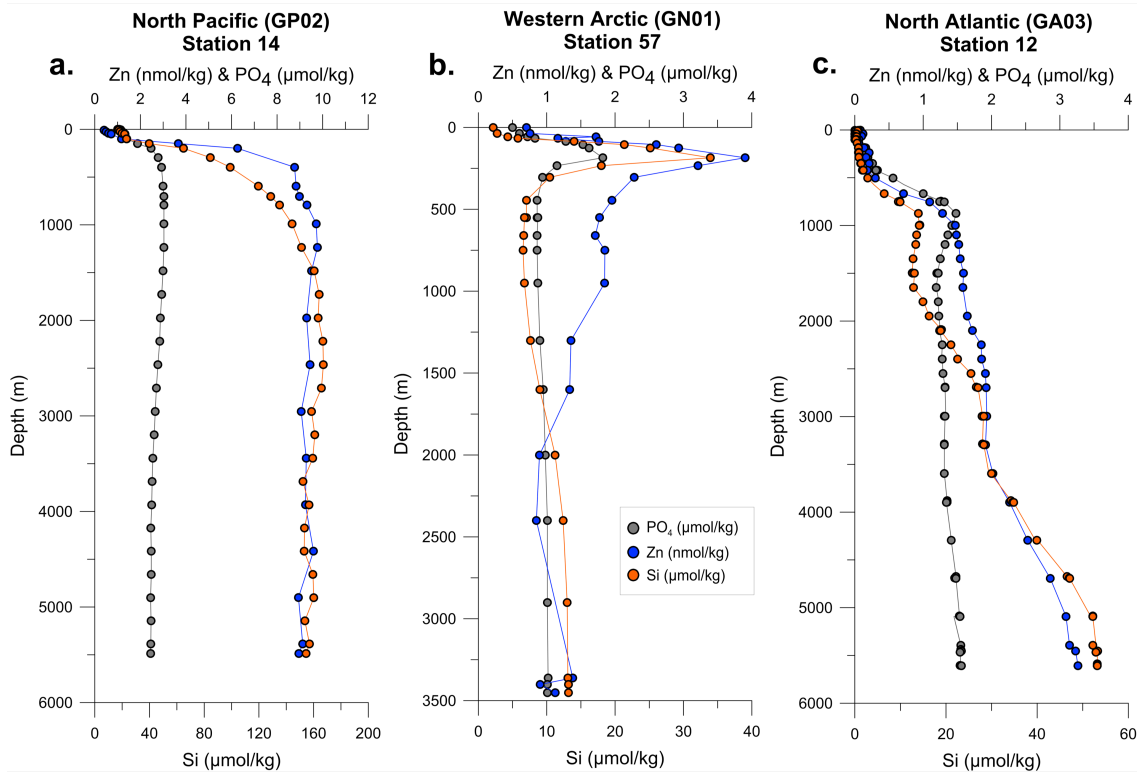


**Figure 3.3** Global comparison of P, Si, and dZn profiles in the (a) North Pacific GP02 (Station 14, 47.0°N/170.0°W), (b) Western Arctic GN01 (Station 57, this study, 73.4°N/156.5°W), and (c) North Atlantic GA03 (Station 12, 29.7°N/56.8°W; Schlitzer et al., 2018). Dissolved zinc has a uniquely different profile shape in the Arctic compared to the classic nutrient-type profiles characteristic of other ocean basins.

### 3.4.1. Hydrographic Setting

The Arctic Ocean is a semi-enclosed basin with several bathymetrically defined sub-basins. The Western Arctic, also known as the Amerasian Basin, is delineated west of the Lomonosov Ridge and contains the Canada and Makarov sub-basins, which are separated by the Alpha and Mendeleev Ridges (Figure 3.1). Station 32 of this study, located at the geographic North Pole, is the only station from GN01 located east of the Lomonosov Ridge in the Amundsen Basin, which is part of the greater Eurasian Basin. The water masses of the Western Arctic Ocean along GN01 are defined by their thermohaline and macronutrient properties (Figure 3.4). Arctic surface waters, often referred to as the Polar Mixed Layer (PML) (Rudels, 2015), in the Western Arctic originate primarily from Pacific water that is advected through the shallow Bering Strait (50 m sill). The fresh, nutrient-rich PML extends variably from ~0-50 m and has salinity (S) ranging from 22 to 31 and potential temperature ( $\theta$ ) of -1.8 to 1.8°C. Here, we define the surface PML (sPML) as 0–25 m in order to differentiate it from the deeper PML that may mix with underlying waters.

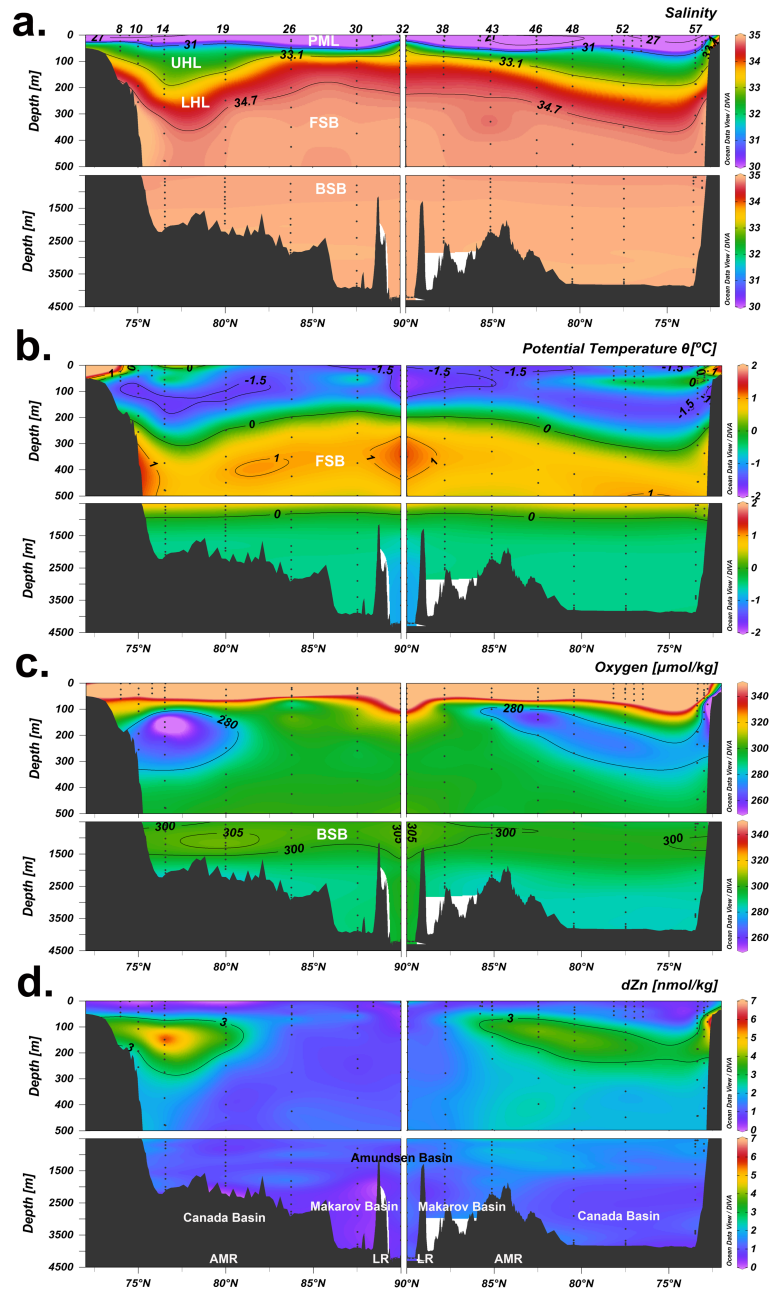


**Figure 3.4** Water mass characteristics for the northbound (left) and southbound (right) transects in the upper 500 m (top) and >500 m (bottom). (a) Salinity with contours to differentiate major water masses: Polar Mixed Layer (PML), upper halocline layer (UHL), lower halocline layer (LHL), Fram Strait branch (FSB), and Barents Sea branch (BSB) of the Atlantic layer. (b) Potential temperature with contours highlighting the temperature maximum indicative of the FSB. (c) Oxygen with contours showing the UHL oxygen minimum and the BSB maximum. (d) Dissolved zinc with a contour of 3 nmol/kg to highlight the concentration maximum within the UHL. Labels in (d) delineate the basin boundaries for the Makarov, Canada, and Amundsen Basins, as well as the Lomonosov Ridge (LR) and Alpha-Mendelev Ridge (AMR).

The deep edge of the PML is delineated by a sharp increase in salinity, leading into the water mass known as the halocline. The halocline is generated during sea ice formation from PML waters on the Arctic shelves, creating a salty, cold water mass that subducts below the fresher PML (Aagaard, 1981; Jones and Anderson, 1986). A striking feature of the Western Arctic is the diversity of halocline structures present in the Canada and Makarov basins (Figures 4, 5) described below (Bluhm et al., 2015). The Makarov Basin has a single halocline ( $\theta$  -1.5–0.7°C, S 31–34.3), primarily derived from Eurasian shelf waters and mixing from the Atlantic layer below (Rudels, 2015). Similarly, the Amundsen Basin (Station 32) has a broad, single halocline ( $\theta$  -1.8–1.6°C, S 32.7–34.7) and is also formed from the Eurasian shelves (Rudels et al., 2004). In contrast, the Canada Basin has a “double halocline” (Figures 4a and 5a,c), separated by a halostad, where the upper halocline layer (UHL:  $\theta$  -1.5– 0.4 °C, S 31–33.1) is formed primarily from Chukchi Shelf waters that have undergone brine rejection (Shimada et al., 2005; Woodgate et al., 2005). As Chukchi Shelf waters originate from incoming Pacific water, the UHL is best illustrated by a Si maximum centered on salinity 32.8 (Figure 3.5a). Here, we characterize the UHL as having a (Si) > 25  $\mu\text{mol/kg}$  (Jones and Anderson, 1986; Macdonald et al., 1989; Anderson et al., 2013), with a close correlation to dZn (Figure 3.5a,b). In contrast, the Canada Basin lower halocline layer (LHL:  $\theta$  -1.5–0.3 °C, S 33.1–34.7) is composed primarily of Atlantic-origin water that shoals and picks up brine-rejected salt on the Eurasian shelf, eventually mixing with Pacific-origin water. Following previous work (Jones and Anderson, 1986), we characterize the LHL using a

minimum in the conservative tracer NO ( $\text{NO} = [\text{O}_2] + 9[\text{NO}_3^-]$ ), indicative of a shelf origin for these waters (Figure 3.5c). It is immediately evident that while the UHL Si maximum is confined to the Canada Basin, the minimum in NO, centered at  $S = 34.6$ , is present in the Makarov and Amundsen basins as well, albeit shallower and with lower salinity around 33 (Figures 4a and 5c). This supports the idea that the LHL of the Canada, Makarov and Amundsen basins share a Eurasian shelf origin, although the exact continental shelf is likely unique in each case (Rudels et al., 1994; Rudels et al., 2004). The water mass known as the Atlantic layer, hereafter specified as Fram Strait Branch (FSB) water, lies below the halocline and originates from North Atlantic waters ( $\theta > 3^\circ\text{C}$ ) that enter the Fram Strait and split into 1) a branch that travels to the west of Svalbard island, becoming the warmer, fresher FSB, and 2) a branch that loops eastward over the Barents Sea, becoming colder and saltier from shelf convection to form the deeper Barents Sea Branch (BSB) (Woodgate et al., 2001; Schauer et al., 2002). Due to these different water mass histories, these two branches likely carry different biogeochemical signatures. The FSB mixes with the colder, less saline halocline layers above, losing temperature along the 27.9 isopycnal as it circulates counterclockwise through the Makarov and Canada basins (Rudels et al., 1994; Woodgate et al., 2001; Schauer et al., 2002). The FSB ( $\theta > 0^\circ\text{C}$ ,  $S 34.86$ ) lies within the Makarov and Canadian basins between 350 and 800 m (Figure 3.4). The underlying BSB ( $\theta > -0.15$ – $0^\circ\text{C}$ ,  $S 34.88$ ) extends to 1150m.

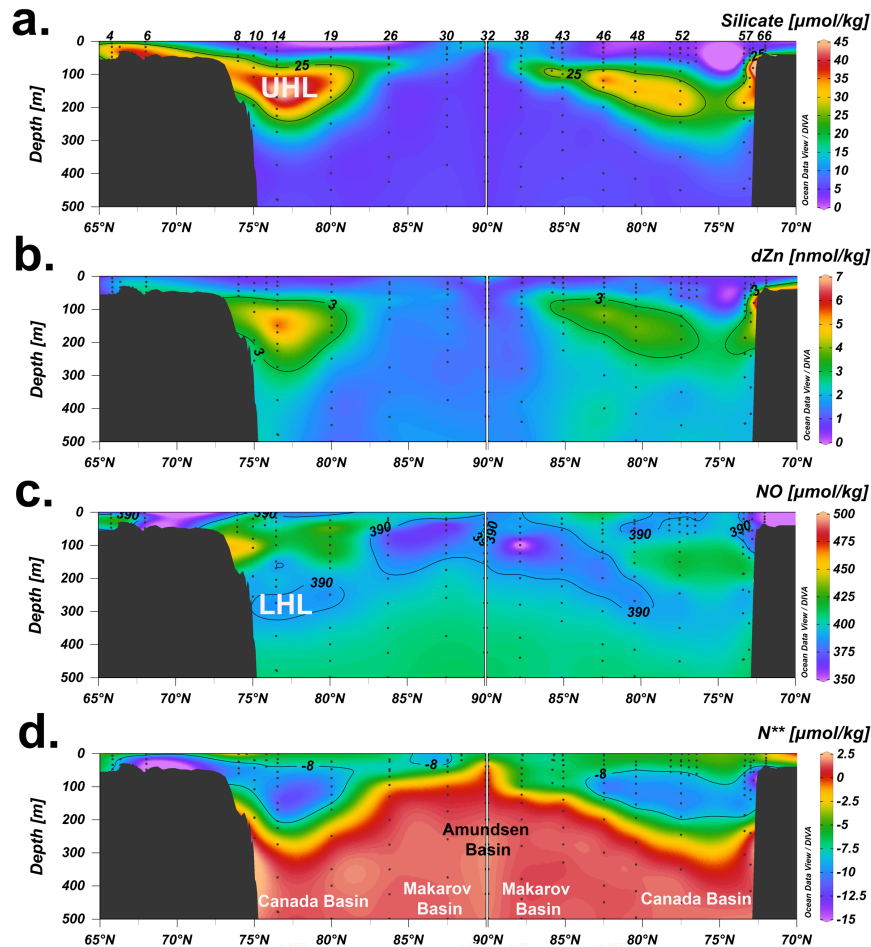


**Figure 3.5** Upper 500 m of the northbound (left) and southbound (right) transects to characterize the halocline layers. (a)  $\text{Si} > 25 \mu\text{mol/kg}$  defines the Pacific-derived upper halocline layer (UHL; Anderson et al., 2013; Jones & Anderson, 1986; Macdonald et al., 1989). (b) Dissolved zinc with a contour of 3  $\text{nmol/kg}$  to highlight the location of the UHL and tight correlation to Si. (c) The tracer NO with a contour  $< 390 \mu\text{mol/kg}$  defines the Atlantic-derived lower halocline layer (LHL). (d) The tracer  $\text{N}^{**}$  (Aguilar-Islas et al., 2013) indicative of Chukchi Shelf porewater denitrification fluxes with a contour of  $-8 \mu\text{mol/kg}$  in the UHL. Labels in (d) delineate the basin boundaries for the Makarov, Canada, and Amundsen Basins.

Arctic deep waters ( $> 1200 \text{ m}$ ) originate in the far North Atlantic (Greenland and Norwegian Seas) and both enter and exit the Arctic through the Fram Strait (2600 m sill). Radiocarbon data show Arctic deep water ages of  $\sim 250$  years in the Eurasian Basin

and ~350 years in the Amerasian Basin (Schlosser et al., 1997; Tanhua et al., 2009), with interbasin exchange restricted by the 1870 m Lomonosov Ridge sill (Björk et al., 2007). However, the Makarov and Canada basins are also separated by a 2200 m sill in the Alpha-Mendeleev Ridge, leading to a mean deep water age of ~300 years for the Makarov and ~400 years for the Canada Basin (Timmermans and Garrett, 2006; Tanhua et al., 2009). These old, deep waters in the Western Arctic are also subject to mixing and continental slope fluxes as a result of brine rejection and dense water subduction during aging (Aagaard et al., 1985).

#### **3.4.2. The sPML dZn Distribution**

In the sPML (0–25 m) along GN01, dZn ranged 0.37–3.04 nmol/kg with an average of  $1.06 \pm 0.52$  nmol/kg ( $n = 63$ ). This is significantly higher than the global surface dZn average of  $0.36 \pm 0.48$  nmol/kg ((Schlitzer et al., 2018);  $n = 187$ ). Within the North Pacific, this average increases slightly to  $0.48 \pm 0.40$  nmol/kg (Kim et al., 2017);  $n = 27$ ), but even this is less than 50 % of the mean surface dZn concentration of the Western Arctic. In addition to higher concentrations, surface dZn concentrations in the Western Arctic also show distinct spatial variations (Figure 3.6a), averaging  $1.31 \pm 0.81$  nmol/kg over the Bering Shelf/Chukchi Shelf (Stations 2–6), decreasing to  $0.84 \pm 0.25$  nmol/kg across the Chukchi Shelf break (Stations 8–14 and 5–66), and gradually increasing again to  $1.11 \pm 0.60$  nmol/kg near the North Pole (Stations 30–43), compared with only 0.51 nmol/kg at our subarctic North Pacific (Station 1) site. In order to assess how Arctic sPML dZn distributions might be altered by future modifications of riverine fluxes, sea ice melt, and Arctic circulation (Peterson et al., 2002; Overland and Wang,

2005; Markus et al., 2009; Woodgate, 2018), a quantitative assessment of dZn provenance in the surface Arctic is required.

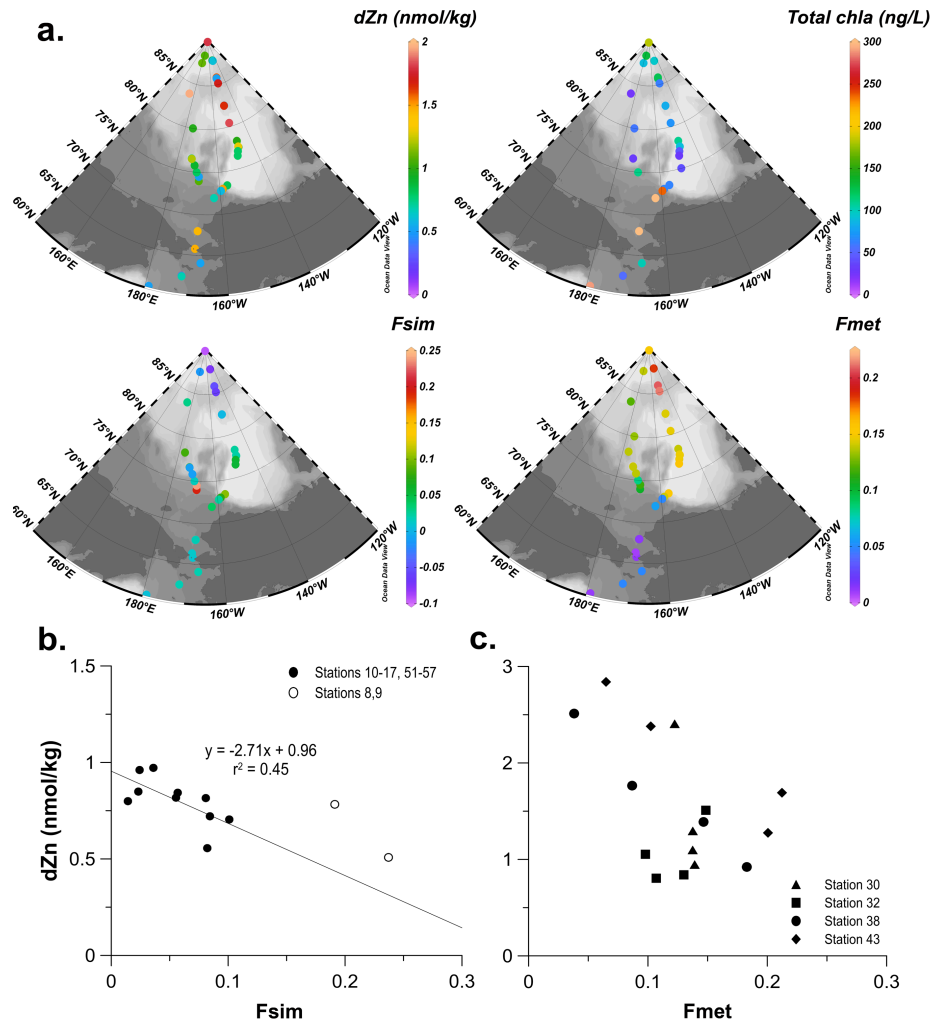


**Figure 3.6** Characterization of dissolved zinc (dZn) in the surface Polar Mixed Layer (0–25 m). Isosurface plots of dZn, total chlorophyll *a* (chl*a*), fraction of sea-ice melt (Fsim), and fraction of meteoric water (Fmet); (b) dZn versus Fsim at stations in the MIZ with an inverse correlation indicating dilution of dZn in seawater by sea-ice melt where shelf-influenced Stations 8 and 9 were removed; and (c) dZn versus Fmet in the upper 80 m at transpolar drift-influenced stations. There appears to be no clear meteoric water influence on dZn at these stations, despite the high dZn concentration in Siberian rivers (Hölemann et al., 2005).

### 3.4.2.1. Sea Ice Inputs (Marginal Ice Zone)

Sea ice is thought to be a significant source of dZn to Arctic surface waters, based on total (unfiltered) Zn concentrations averaging 450 nmol/kg (Tovar-Sánchez et al., 2010). However, the concentration of dZn in sea ice during GN01 has been recently reported as much lower ( $3.12 \pm 1.66$  nmol/kg (Marsay et al., 2018)) suggesting a less significant source of dZn to the Western Arctic sPML than first hypothesized. In the present study, the fraction of water derived from sea ice melt ( $F_{sim}$ , Figure 3.6a) at MIZ stations (Stations 8–17, 51–57) was quantified using  $\delta^{18}O$ , macronutrient, and salinity end members as well as the “Arctic N-P” tracer method described in Newton et al. (2013) for sea ice, meteoric water (river and precipitation, “Fmet”), and Atlantic and Pacific seawaters. When dZn is plotted against  $F_{sim}$ , a weak negative linear correlation ( $r^2 = 0.45$ ) is evident at the MIZ stations (Figure 3.6b; Stations 8–9 excluded because of shelf influence). This indicates that sPML dZn concentrations are either 1) diluted by sea ice melt, and/or 2) coincidentally decreased at MIZ stations because of biological uptake of dZn in the surface, which is a primary driver of low surface dZn globally (Bruland, 1980; Lohan et al., 2002; Croot et al., 2011), or 3) diluted by Beaufort Gyre water (discussed below). If the removal of Zn was primarily biological, one might expect to find a negative relationship between dZn and the pigment chlorophyll *a* (chl*a*; (Jakuba et al., 2012; Wyatt et al., 2014)) a known tracer of phytoplankton biomass. Since no such relationship was observed ( $r^2 = 0.003$  data not shown), mixing with low-dZn sea ice melt was more likely the dominant control on dZn concentrations within the MIZ.

In fact, biological uptake of dZn during GN01 was largely insignificant in the central Arctic away from the productive shelves. Isosurface views of chl $a$  (Figure 3.6a) show high values on the Chukchi Shelf (chl $a$  up to 12.8  $\mu\text{g/L}$ ) and oligotrophic conditions off-shelf (Stations 10–60 chl $a$  < 0.2  $\mu\text{g/L}$ ), indicating that offshore primary production exerts little control on sPML dZn distributions. Together, the Chukchi Shelf and Bering Strait/Shelf are the most productive in the Arctic (Sakshaug, 2004), and biological uptake of dZn likely occurs in surface waters of these shelves such that residual low surface dZn concentrations can be transported offshore to open Arctic sPML waters. In fact, the increasing sPML dZn concentrations moving from the Chukchi shelf (<1 nmol/kg) to the open Arctic (>1 nmol/kg; Figure 3.6a) suggest not only negligible biological uptake in the central Arctic but require sources of dZn to the sPML via mixing from the halocline below or via external dZn sources, as discussed next.

#### **3.4.2.2. River and Precipitation Inputs**

Rivers are known to be an important source of freshwater to the Arctic Ocean with over 3300 km<sup>3</sup> of freshwater supplied annually (Aagaard and Carmack, 1989), most of which comes from the Yukon, Mackenzie, Ob, and Yenisey Rivers (Figure 3.1. Arctic riverine flux has increased by 7% between 1936–1999 as a result of climate change (Peterson et al., 2002), leading to changes in nutrient fluxes and Arctic stratification (Macdonald et al., 1999; Macdonald et al., 2015). Along the GN01 transect, Stations 2 and 3 were chosen to characterize potential Yukon River outflow (Figure 3.1. The fraction of meteoric water (F<sub>met</sub>, Figure 3.6a), which includes a combination of riverine

and precipitation-sourced freshwaters, at the surface was elevated to 5% compared to non-riverine Stations 4–6 (< 1%), but even 5% Fmet was low compared to central Arctic stations (e.g. Stations 30–43) in the path of the Transpolar Drift (TPD), where Fmet consistently exceeded 10% in the surface. The low Fmet at Stations 2–3 likely occurs because they are located outside the path of the coastal current that carries Yukon River water northward along the Alaskan coast (Li et al., 2017). Accordingly, there was no significant correlation between Fmet and dZn at these two stations (data not shown). While the Mackenzie River outflow lies outside of our transect, it is known to contribute freshwater to the Beaufort Gyre and Canada Basin (Macdonald et al., 1999).

Offshore from the Chukchi Shelf, freshwater injections into the central Arctic are evident, particularly from a decrease in salinity and depression of isopycnals along both transects (> 75°N), likely originating in the Beaufort Gyre (Proshutinsky et al., 2002). North of 85°N, Fmet increased (13–22 %) toward the North Pole (Stations 30–43, Figure 3.6a), indicating the presence of riverine- and/or snow-sourced meteoric freshwaters derived from the well-known TPD (Rutgers van der Loeff et al., 2012; Rudels, 2015; Kadko et al., 2016). As described previously, an enrichment in sPML dZn concentration was also observed at these stations ( $1.11 \pm 0.60$  nmol/kg). However, the absence of a significant correlation between dZn and Fmet in the upper 80 m ( $r^2 = 0.20$ , Figure 3.6c) suggests that the TPD is not the source of dZn.

If not rivers, then what explains the apparent increase in dZn north of 85°N? We argue that it is 1) not actually an increase in dZn but, instead, an ‘apparent enrichment’ accentuated by the MIZ sea ice melt and Beaufort Gyre freshwater dilution of surface

dZn at 70–80°N, 2) influenced somewhat by vertical mixing with the dZn enriched, shallow Makarov Basin halocline (80–100 m depth; discussed below), and 3) at least somewhat facilitated by transport of Chukchi Shelf-derived dZn enrichments (discussed in section 3.3 below). Thus, we conclude here that rivers themselves do not appear to be a major source of dZn to the open Arctic.

#### **3.4.2.3. Continental shelf/Pacific Inputs**

Along the Bering and Chukchi shelves (Stations 2–8, 61–66), dZn concentrations in the upper 80 m were elevated, ranging between 0.37–6.49 nmol/kg with the lowest concentrations associated with PML water at the shelf break (MIZ dilution by low-dZn sea ice melt) and the highest concentrations located in near-bottom waters of the shelf (Figure 3.5b). This clearly indicates an enrichment of dZn along the Bering and Chukchi shelves. Three potential sources of dZn to the continental shelf are 1) incoming North Pacific waters, 2) authigenic dZn sources from shelf sediments, and/or 3) shelf remineralization inputs.

We note that while we have scant sample coverage of the Bering Strait and Chukchi Shelf, dZn concentrations were most elevated in bottom waters of the Chukchi Shelf (> 6 nmol/kg; Figure 3.7) where there is a known benthic source of up to 13 nmol/kg dZn in near-sediment bottom waters (Cid et al., 2012) concurrent with decreased light transmission resulting from resuspended sediments (Gardner et al., 2018). Following this, we hypothesized a sediment-derived source of dZn to these shelf waters as they enter from the North Pacific and traverse the margin, discounting the hypothesis that these dZn enrichments are Pacific-derived. In support of this, the Zn:Si

linear regression slope for the Bering Strait and Bering/Chukchi Shelves of  $0.076 \pm 0.012$  nmol/ $\mu$ mol (Figure 3.7a) is higher than that for the upper 100 m of the North Pacific (Station 1,  $0.052 \pm 0.012$  nmol/ $\mu$ mol), the regression slope for the central subarctic North Pacific ( $0.053$  nmol/ $\mu$ mol; (Kim et al., 2017)), and the global GEOTRACES data set ( $0.0596 \pm 0.0003$  nmol/ $\mu$ mol; (Schlitzer et al., 2018), suggesting Zn:Si enrichment in the Chukchi Shelf sediments.

A shelf sediment dZn flux could be derived from authigenic minerals or remineralization of biogenic particles. Dissolved Si also showed a strong maximum in bottom waters of the Bering Strait and Chukchi Shelf, reaching  $61 \mu\text{mol/kg}$  compared with  $25$  and  $14 \mu\text{mol/kg}$  north of the Chukchi Shelf along the northbound and southbound lines, respectively (Figure 3.5a), suggesting some sediment dZn source, rather than an authigenic source. Authigenic Zn sulfides can precipitate in low- $\text{O}_2$ , sulfidic porewaters, and if these Zn sulfides form in the colloidal fraction they may provide a sedimentary source of dZn (Trefry et al., 2014; Conway and John, 2015). However, we find this unlikely given that Chukchi Shelf upper sediments are rarely and only sparingly sulfidic (Gobeil et al., 2001).

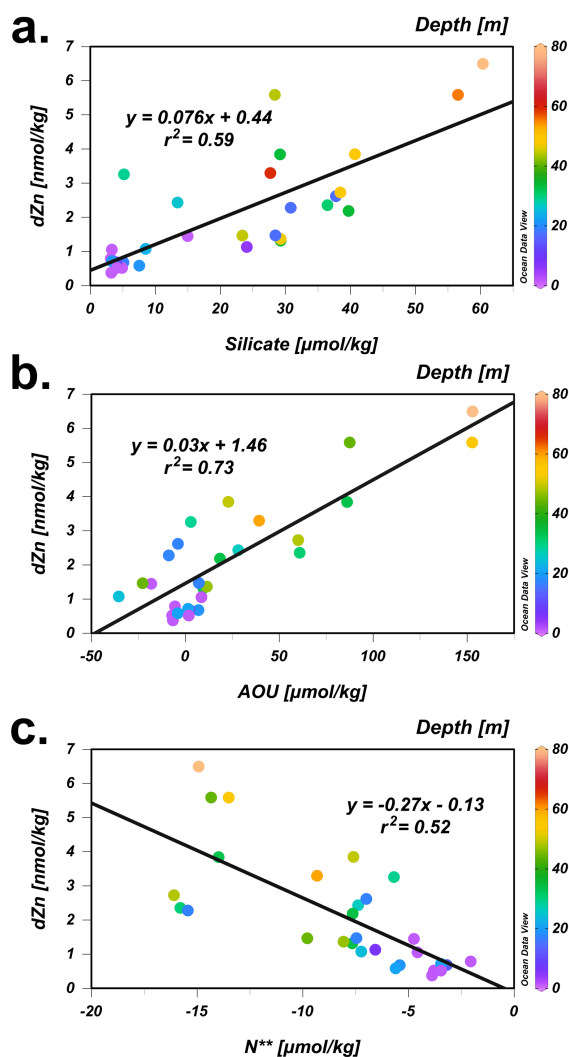


**Figure 3.7** Chukchi Shelf (Stations 2–8 and 61–66) correlation between dZn and (a) Si ( $\mu\text{mol/kg}$ ) to show a remineralized nutrient source, (b) apparent oxygen utilization (AOU) to confirm a remineralization source, and (c)  $N^{**}$  to show a remineralization source constrained to the sediments. The color bar indicates depth along the shelf (maximum 80 m), and we note that remineralization signals are greatest at deepest depths, indicating a porewater remineralization source.

Finally, we also observed a benthic maximum in apparent oxygen utilization (AOU), a tracer for biological respiration, and a positive linear regression between AOU and dZn ( $0.030 \pm 0.004 \text{ nmol}/\mu\text{mol}$ ,  $r^2 = 0.73$ ) within Chukchi Shelf waters (Figure 3.7b), further

supporting a sediment remineralization source of dZn to shelf bottom waters concurrent with opal dissolution.

Our hypothesized sediment remineralization source of dZn was reinforced by measured cellular stoichiometry in Chukchi Shelf waters, showing elevated Zn:Si and Zn:C ratios in cells compared to a global compilation of cellular data (Twining and Baines, 2013). Zn:Si within diatoms in Chukchi Shelf waters (Stations 5, 8, and 61) averaged  $4.8 \pm 3.6$  mmol/mol (geometric mean  $\pm$  SD of station geometric means), which is higher than the North Pacific (Station 1) value of  $2.0 \pm 0.7$  mmol/mol (Figure 3.8a). Zn:C within all analyzed phytoplankton cells along the same shelf stations averaged  $26.5 \pm 9.8$   $\mu$ mol/mol compared to  $11.7 \pm 9.3$   $\mu$ mol/mol off-shelf and in lower latitude oligotrophic communities (Figure 3.8b) (Twining et al., 2011; Twining et al., 2015). This suggests a clear enrichment of dZn compared to C and Si in phytoplankton cells along the Chukchi Shelf. We postulate that the elevated cellular Zn:C in Chukchi Shelf phytoplankton likely results from increased dZn availability and uptake compared with the central Arctic, as previously observed for the highly productive California Shelf region (Twining, 2018).

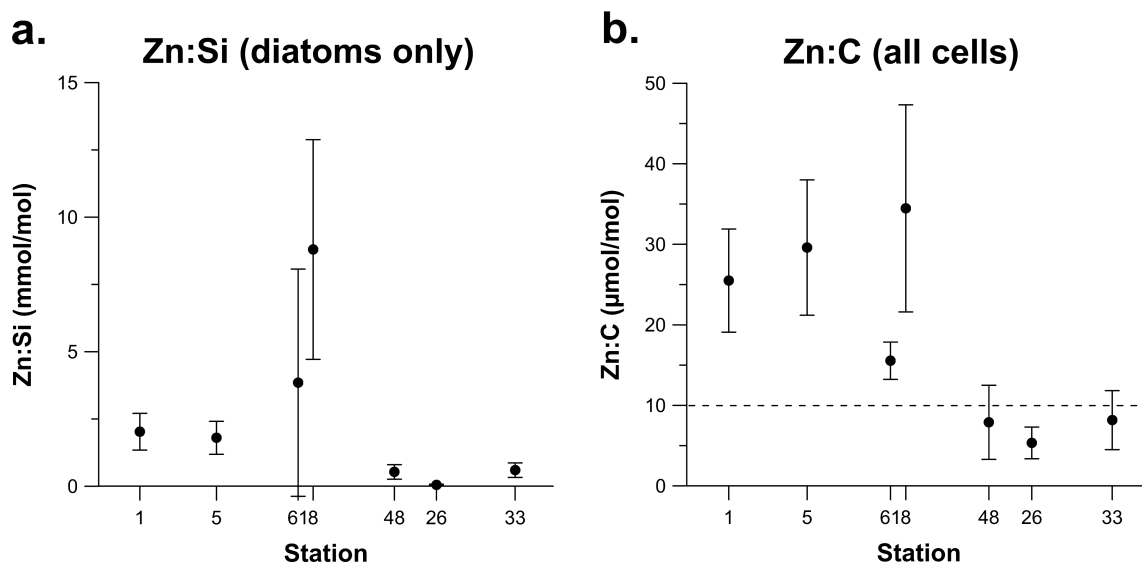


**Figure 3.8** Plots of Zn:Si and Zn:C in Arctic cells. (a) The geometric mean Zn:Si ratios determined by synchrotron X-ray fluorescence analyses in diatoms only (with associated standard error), (b) The geometric mean Zn:C ratios determined by SXRF in all cells (with associated standard error). The dotted line represents previous phytoplankton net-tow measurements compiled from (Bruland et al., 1991). Both plots include the North Pacific (Station 1), on-shelf stations (5, 8, and 61) and off-shelf stations (26, 33, and 48) plotted in order of increasing latitude. Notably, Zn:Si and Zn:C ratios are higher along the shelf compared to the off-shelf stations.

Critically for the Arctic dZn cycle, we hypothesize that once the shelf phytoplankton deposit their elevated Zn:Si and Zn:C as phytodetritus in the shallow shelf sediments, sedimentary remineralization of the organic tissue of those cells would supply a Zn-rich dissolved nutrient flux back into shelf waters, effectively increasing the Zn:macronutrient ratios observed in the water column. This sedimentary dZn flux might be accentuated compared to Si due to the preferential remineralization of “soft” tissues containing Zn and C over the “hard” Si tests, as demonstrated by decreasing cellular Zn:Si ratios with depth in the subtropics (Twining et al., 2014) and in the 1000-fold lower Zn:Si ratio of sedimentary frustules (Ellwood and Hunter, 1999; Hendry and

Rickaby, 2008; Andersen et al., 2011) compared with the water column phytoplankton in Arctic shelf waters.

To test this hypothesis, we compared our phytoplankton cellular Zn:C with estimated Zn:C derived from our water column dissolved Zn:AOU regression analyses using a Redfield O:C of 170:117 (Anderson and Sarmiento, 1994). Over the Chukchi Shelf, the Zn:AOU regression slope of  $0.030 \pm 0.004$  nmol/ $\mu$ mol yielded an estimated Zn:C of  $43 \pm 6$   $\mu$ mol/mol. This value is well within the range of median Zn:C cellular stoichiometries from the shelf stations (13-75  $\mu$ mol/mol). We note that there is significant intrapopulation variability associated with single-cell measurements (i.e., SXRF, nanoSIMS, flow cytometry), and multiple approaches can be taken to estimate average population stoichiometry. The arithmetic mean Zn:C for shelf station phytoplankton populations was 57  $\mu$ mol/mol, above the calculated Zn:C from water column remineralization.

Regardless of the metric used, Zn:C cellular stoichiometries for shelf phytoplankton (13-75  $\mu$ mol/mol) are elevated above offshore cellular Zn:C (4–6  $\mu$ mol/mol), strengthening our argument that the dZn enrichments in Chukchi Shelf bottom waters are derived from “soft” tissue remineralization of high-Zn:C phytoplankton. In addition, the geometric mean cellular Zn:Si ranged 2–9 mmol/mol along the shelf, which is two orders of magnitude higher than the dissolved water column slope of 0.076 mmol/mol. If dZn and C are preferentially remineralized over Si in the water column, this would elevate the Zn:Si of the water column through the Bering Strait and Chukchi Shelf. However, these waters are regularly resupplied by

incoming Si-rich North Pacific waters with a lower Zn:Si slope of 0.052 nmol/ $\mu$ mol, only allowing moderate elevation of Chukchi shelf Zn:Si slopes over their source ratios.

Additionally, to support our conclusion that the remineralization of these Zn-enriched phytoplankton is occurring in the upper sediment porewaters of the shelf instead of in the water column, we point to the chemical tracer  $N^{**}$  (Figure 3.5d). Negative values of this parameter, defined as  $(0.87([\text{DIN}] - 16[\text{PO}_4^{3-}] + 2.9) \mu\text{mol/kg})$ , where DIN is the sum of nitrate and nitrite, are a tracer of porewater denitrification and/or anammox in the Chukchi and Bering shelves, since water column dissolved oxygen concentrations ( $> 240 \mu\text{mol/kg}$ ) above these shelves are far too high to enable water column denitrification (Nishino et al., 2005; Aguilar-Islas et al., 2013). During GN01, over both shelves (Stations 2–8, 61–66) there was a significant negative correlation between dZn and  $N^{**}$ , indicating a similar porewater remineralization source for both variables (Figure 3.7c).

Thus, to conclude, PML surface waters of the Arctic have elevated dZn concentrations compared to other ocean global basins. The elevated dZn is primarily due to nutrient-rich incoming Pacific waters that receive further dZn-rich fluxes from the sediment porewater remineralization of deposited high Zn:C and Zn:Si phytoplankton cells over the Bering and Chukchi shelves; these high-dZn shelf bottom waters form the subsurface halocline offshore, which is discussed next. The lower-dZn sPML waters over the shelf are eventually advected offshore into the Canada Basin by local currents (Pickart et al., 2005; Corlett and Pickart, 2017), where they appear to be at least seasonally diluted by low-Zn sea ice melt at the shelf break, despite high concentrations

of total Zn in ice cores from the literature (Tovar-Sánchez et al., 2010). While Arctic rivers do contain substantial dZn (Hölemann et al., 2005), the correlations between dZn and Fmet near both the Yukon outflow and in the path of the Transpolar Drift reject the hypothesis of major riverine dZn sources to the central Arctic. Instead, elevated dZn in the open Arctic PML primarily results from mixing up of shelf-derived porewater inputs following the remineralization of Zn-rich phytoplankton, as well as limited biological uptake of dZn under the ice.

### 3.4.3. Halocline Zn Distribution

The most prominent feature of the Western Arctic dZn distribution (Figure 3.5b) is the subsurface maximum in the Canada Basin (110–200 m) with concentrations ranging from 3.62–6.59 nmol/kg (average  $4.39 \pm 0.88$  nmol/kg). The salinity range of 31–33.1 designates these waters as the UHL (Figure 3.4a). The magnitude of this UHL dZn maximum agrees well with data from prior studies near the Chukchi Shelf break (Cid et al., 2012; Kondo et al., 2016). In the Makarov Basin (Stations 26, 30 and 38), this halocline feature is also present but is shoaled to ~80 m and is lower in concentration at  $2.59 \pm 0.24$  nmol/kg. Using the  $[\text{Si}] > 25 \mu\text{mol/kg}$  tracer (Figure 3.5a) to trace this feature, we see that Si concentrations reach ~50  $\mu\text{mol/kg}$  and coincide with the dZn maximum. The Zn:Si slope in the UHL is  $0.110 \pm 0.010$  nmol/ $\mu\text{mol}$  ( $r^2 = 0.90$ ), much higher than the North Pacific Zn:Si slope of  $0.052 \pm 0.012$  nmol/ $\mu\text{mol}$  (Station 1, to 100 m), suggesting an additional source of excess dZn to the Arctic halocline beyond that advected from the North Pacific.

The Zn:Si slope increases along its transport path from  $0.052 \pm 0.012$  nmol/ $\mu$ mol in the Bering Sea (Station 1) to  $0.076 \pm 0.012$  nmol/ $\mu$ mol along the Chukchi and Bering shelves (Stations 2–3, 61–66) to  $0.110 \pm 0.010$  nmol/ $\mu$ mol in the subducted UHL. As discussed above, the increase in the Zn:Si regression slope moving from the Bering Sea over the Chukchi shelf is due to the preferential remineralization of Zn and C in “soft” tissues sourced to the incoming nutrient-rich North Pacific waters. But why do the Zn:Si regression slopes continue to increase from the shelf to the UHL? The UHL forms from the bottom-most brine-rejected waters of the shelf, which should carry elevated Zn:Si ratios due to the preferential remineralization of Zn compared to Si in sediment porewaters (see Section 3.2.3 above). This shelf porewater influence on the UHL can be seen by the correlation of dZn with the sediment-derived N\*\* minimum, which also extends offshore into the UHL (Figure 3.5d). We also observed the same Zn:AOU relationship in the UHL ( $0.029 \pm 0.003$  nmol/ $\mu$ mol,  $r^2 = 0.65$ ) as we do in the Chukchi Shelf water column ( $0.030 \pm 0.004$  nmol/ $\mu$ mol, Figure 3.7b), both leading to Zn:C ratios of 42–43  $\mu$ mol/mol that match the cellular stoichiometry of shelf phytoplankton as described above, reinforcing the dominance of “soft” tissue remineralization of dZn. In fact, given the low cellular Zn:C stoichiometries ( $< 10$   $\mu$ mol/mol) for phytoplankton in offshore stations, this Zn:AOU relationship in the UHL can only be derived from cells with higher cellular Zn:C, as on the Chukchi Shelf.

It is worth mentioning that the northbound and southbound distributions of dZn in the UHL are distinctly different (Figure 3.5b). In particular, a point source for dZn at Station 14 at 150 m can be attributed to an eastward moving eddy (ADCP data not

shown), a common mode of transport for Pacific-origin water advected rapidly off-shelf (Pickart et al., 2005). Recent findings suggest that Pacific water does not flow uniformly offshore from the Chukchi Shelf (Brugler et al., 2014; Corlett and Pickart, 2017). The eastern Chukchi Shelf Stations 57–66 are more affected by shelf break jets traveling eastward from Herald canyon, while the more western Stations 8–10 are further north and are affected by the westward Chukchi slope current.

In contrast to the UHL, the dZn concentrations of the Canada Basin LHL, as well as the haloclines of the Makarov and Amundsen Bains, were lower (2.44–4.28 nmol/kg) with lower slopes of Zn:Si ( $0.057 \pm 0.008$  nmol/ $\mu$ mol). The LHL dZn appears to be controlled by mixing between the overlying dZn-rich UHL and the underlying dZn-poor Atlantic layer (discussed below). In fact, a plot of dZn concentrations versus conservative  $\theta$  is linear between the core of the FSB Atlantic layer (at the depth of maximum  $\theta$ ) and the core of the UHL (at the depth of maximum dZn) (Figure 3.9a). While the T-S signature shows the intrusion of the slightly colder and saltier Eurasian-formed LHL waters, dZn appears to result simply from mixing, without additional Eurasian shelf supply. Thus, a critical question remains: if all Arctic halocline layers are formed from brine rejection on Arctic shelves that could produce excess dZn inputs from shelf sediments, then why is the Pacific/Chukchi UHL particularly enriched in dZn, while LHL waters formed on Eurasian shelves are not? In the case of the Barents Sea, no evidence has been found of nutrient-rich water emanating from the St Anna Trough (Anderson et al., 2013). Brine-rejected waters also contact the sediment surface of the Eurasian Shelf, but much of the Eurasian Shelf (e.g. the Barents Sea) is deeper, in which

case more of the phytoplankton would be remineralized in the water column, preventing such a significant porewater remineralization flux as observed in the shallow Chukchi Shelf.

In summary, the highest dZn concentrations along the entire GN01 transect were found in the Chukchi Shelf-derived UHL. Notably, the Canada Basin LHL (designated by a minimum in NO), and to some extent the Makarov and Amundsen haloclines, showed much lower dZn (Figure 3.9b), despite the fact that this halocline is also formed on other (Eurasian) shelves. Thus, Chukchi Shelf and slope sediments appear to be unique in delivering a dZn enrichment to its overlying PML water column and downstream UHL, through a combination of high productivity, active remineralization of high Zn:C cells in shelf sediments, and shallow Chukchi Shelf depth where brine rejected waters contact the sediments.

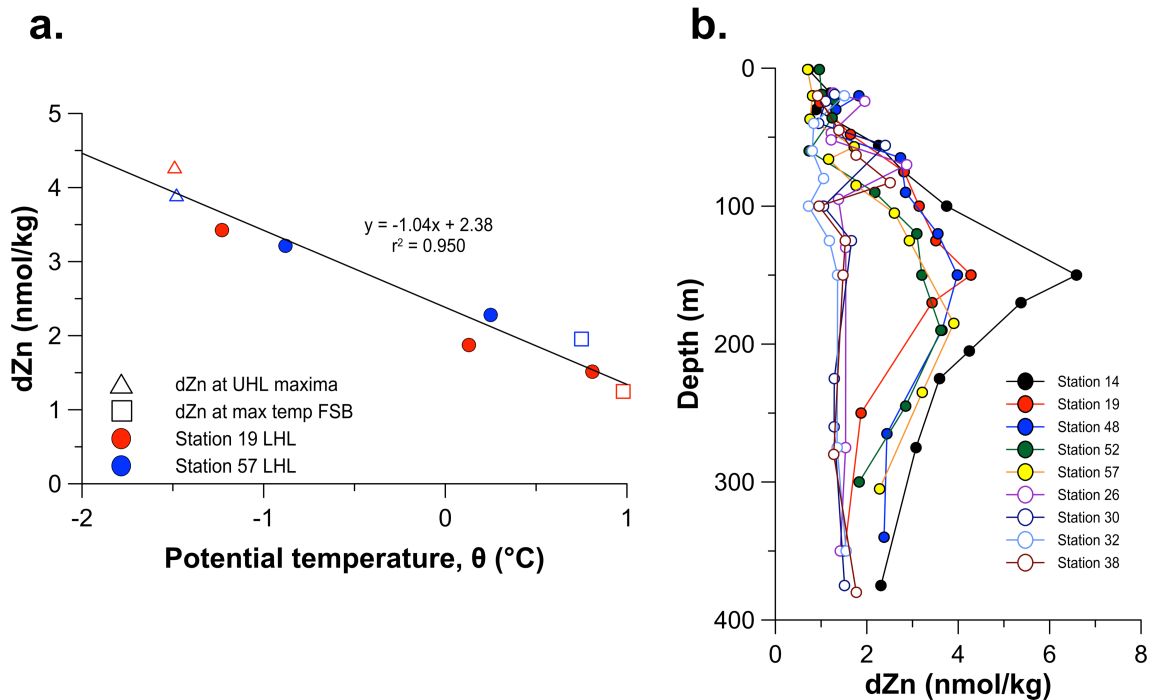


**Figure 3.9** Plots of Zn in the LHL and UHL. (a) Dissolved zinc (dZn) versus potential temperature demonstrating that the lower halocline layer (LHL) dZn concentrations (filled dots) are formed from mixing between the upper halocline layer (UHL) dZn maximum (triangles) and the Atlantic layer (Fram Strait Branch (FSB), squares) end members at two representative Canada Basin stations (19 and 57); (b) dZn depth profiles at select stations in the Makarov (26–38) and Canadian (14, 19, and 48–57) basins demonstrating a UHL dZn peak between 100 and 200 m that shoals in the Makarov to 50–80 m and is virtually absent in the Canadian LHL 250–450 m.

#### 3.4.4. Atlantic Layer: FSB

Below the Western Arctic Ocean halocline is the Atlantic layer, primarily composed of the warm ( $\theta > 0^\circ\text{C}$ ) FSB between 350–800 m (Figure 3.4b) (Timofeyev, 1962; Coachman and Barnes, 1963). The FSB waters slowly lose their heat ( $\theta$  maximum attenuated) through mixing with overlying cold halocline waters as they circulate cyclonically from the Amundsen to Makarov to Canada Basin along their known flow path (Rudels et al., 1994). Dissolved Zn in the FSB  $\theta$  maximum ranged 1.24–3.59

nmol/kg throughout the three basins sampled on GN01. This range is consistent with published dZn concentrations in the Atlantic layer of stations sampled previously off the Chukchi Shelf (Kondo et al., 2016).

In other ocean basins at these intermediate depths, we would expect to see a nutricline, representing a combination of pre-formed and *in situ* vertical remineralization inputs of nutrients including dZn. Instead, in the FSB there is a sharp decrease in dZn concentrations with depth (Figure 3.3). In the absence of significant biological production under the central Arctic ice (Arrigo et al., 2003), we hypothesized that this gradient was a product of water mass mixing between the dZn-rich halocline above and the incoming low-dZn FSB.

Maximum potential temperature ( $\theta_{\max}$ ) is a conservative tracer of the FSB, and we found a positive relationship between  $\theta_{\max}$  and dZn ( $r^2 = 0.80$ ; Figure 3.10b), which suggests that Western Arctic FSB dZn concentration gradients are derived from conservative mixing alone, while vertical regeneration inputs of dZn to FSB waters are negligible. Similarly, mixing was sufficient to predict subsurface dZn concentrations in the subtropical North Atlantic (Roshan and Wu, 2015), reinforcing the fact that mixing of dZn across water masses can be a significant driver of intermediate water dZn. To further emphasize the lack of regenerative dZn inputs to FSB waters, we also examined the respiration tracer AOU in the FSB. At the  $\theta_{\max}$  of each station, dZn and Si both show a linear relationship with AOU (data not shown), typically indicating remineralization fluxes. However, AOU and  $\theta_{\max}$  also have a linear relationship ( $r^2 =$

0.88; Figure 3.10c), indicating that even AOU is conservatively mixed in the FSB layer of the Western Arctic and as such does not trace *in situ* remineralization.

We note that Station 32 (Amundsen Basin) falls off the mixing line (Figure 3.10b,c) due to its younger age. FSB waters feeding the Western Arctic spend time along the Laptev Sea continental slope where they are cooled by mixing as compared to the FSB branch of the Amundsen Basin ((Rudels et al., 1994; Jones et al., 1998), Figure 3.10a). Additionally, Station 10 falls off the mixing line due to elevated AOU from the Chukchi Shelf. By extrapolating the  $\theta_{\max}$ -dZn linear relationship to the core  $\theta$  of FSB waters at the continental slope of the Laptev Sea,  $\sim 1^{\circ}\text{C}$ , we estimate the “pre-formed” dZn concentration that enters the Western Arctic in the intermediate FSB Atlantic layer as  $\sim 1.3$  nmol/kg. This relationship confirms that the dZn concentrations in the FSB layer arise from conservative mixing with the overlying, dZn-rich UHL during water mass aging, which raises the dZn concentrations and decreases the  $\theta$  of FSB waters in the Western Arctic.

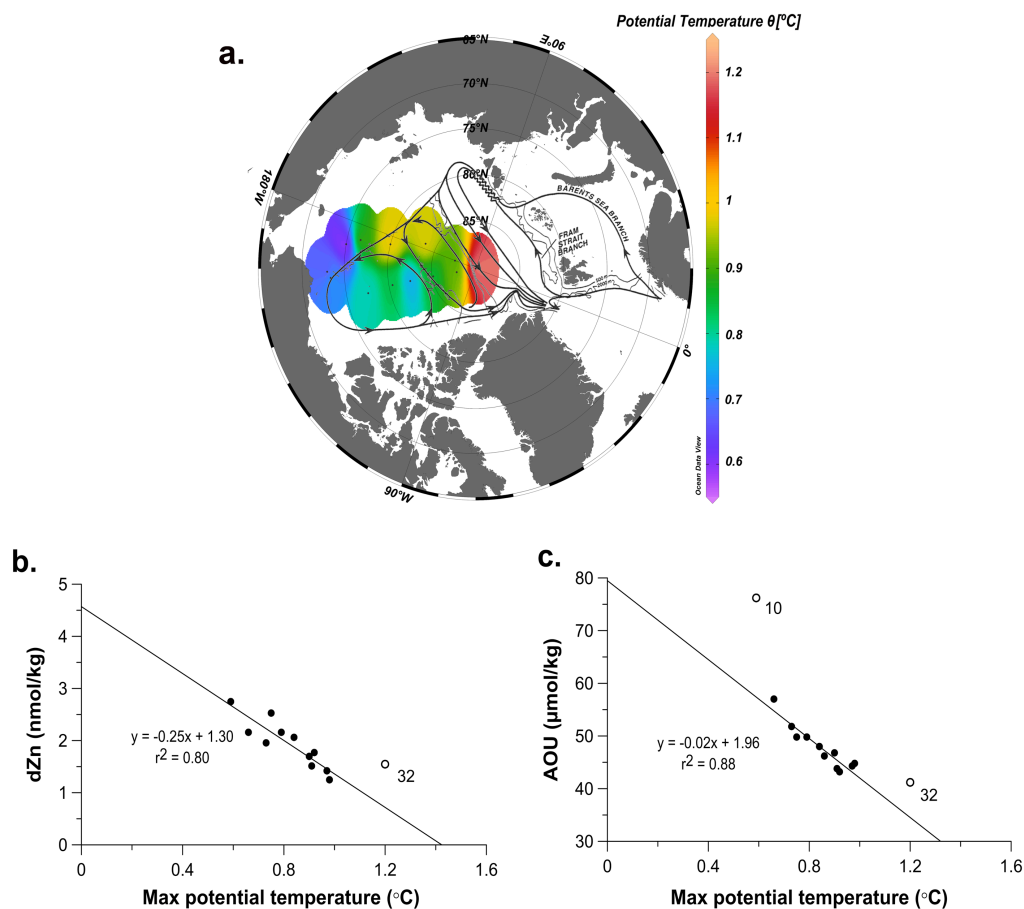


**Figure 3.10** Intermediate Atlantic layer dZn dynamics. (a) An isosurface plot of max potential temperature at every station demonstrating the conservative temperature attenuation that follows the overlaid Atlantic layer circulation (Rudels<sub>SEP</sub> et al., 1994). (b) Dissolved zinc (dZn) and (c) apparent oxygen utilization (AOU) versus the maximum potential temperature at every station, illustrating conservative mixing of dZn, instead of regenerative dZn inputs, in the Atlantic layer Fram Strait Branch. Station 32 was removed in (b) and (c) as an outlier for temperature due to its location in the Eurasian Basin, while Station 10 was removed in (c) given its close proximity to the Chukchi Shelf.

### 3.4.5. Arctic Deep Water

Below 1000 m, dZn had uniformly low concentrations ( $1.27 \pm 0.29$  nmol/kg; Figure 3.11) compared to global deep water data from the North Atlantic ( $1.78 \pm 0.44$  nmol/kg) and North Pacific ( $9.82 \pm 0.65$  nmol/kg) (Figure 3.3, (Schlitzer et al., 2018)).

We explore two potential sources/sinks of dZn to/from deep waters (hydrothermal vents and bottom suspended particle nepheloid layers) and then investigate the cause for the low deep water dZn concentrations in the Arctic by comparing dZn across the Arctic basins sampled during GN01.

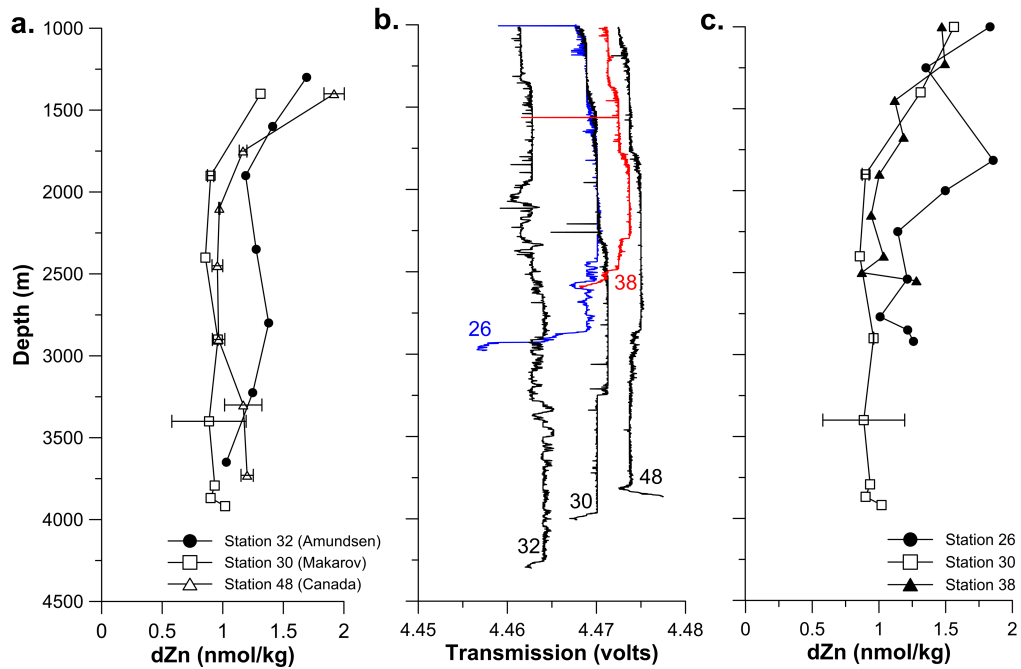


**Figure 3.11** Arctic deepwater dZn. (a) Dissolved zinc (dZn) below 1,000 m where Station 32 (Amundsen Basin) shows a slight peak at 2,800 m compared to Stations 30 (Makarov Basin) and 48 (Canada Basin), which may be derived from hydrothermal fluxes; (b) light transmission data from the GEOTRACES carousel CTD transmissometer, showing potential benthic nepheloid layer particles causing light attenuation at Stations 26, 30, and 38 (color to differentiate) and potential hydrothermal particles 2,000- to 2,500-m depth at Station 32 as well as a lack of hydrothermal particles at Station 48; (c) dZn below 1,000 m at stations where there was a benthic source of dZn coincident with low transmissometry. Error bars are included on plots where replicate analyses were available.

### **3.4.5.1. Hydrothermal Vents**

Recent literature suggests that hydrothermal vents may supply dZn to deep waters of the South Pacific (Roshan et al., 2016). The Gakkel Ridge (Figure 3.1 is a known location of hydrothermal activity in the Arctic Ocean (Edmonds et al., 2003), and there is evidence that hydrothermally-influenced waters can be traced toward the Western Arctic using dFe and dMn distributions, even reaching the Amundsen Basin (Middag et al., 2011; Klunder et al., 2012). Along GN01, Station 32 in the Amundsen Basin is the easternmost station, and thus we have no samples from near the Gakkel Ridge to prove or disprove a hydrothermal source of Zn in the Arctic. Most water in the Amundsen Basin is of Atlantic origin, with potential inputs from brine rejection on the Barents Shelf (Jones, 2001). However, Station 32 shows a slight increase in dZn at depths 2000–3700 m with a broad maximum centered at 2800 m (Figure 3.11a). Beam transmission at these depths do not confirm or deny a distal hydrothermal signal (Figure 3.11b). This 2800 m dZn maximum at the North Pole is only slightly deeper than the 2500 m hydrothermal peak observed for dFe in the Amundsen Basin by Klunder et al. (2012) and is unique to the Amundsen Basin, as profiles from the Makarov (Station 30) and Canada (Station 48) basins do not show deep water dZn maxima (Figure 3.11a). Further confirmation of hydrothermal influence awaits measurement of conservative hydrothermal tracers, namely  $^3\text{He}$ , from GN01.

### **3.4.5.2. BNLs**

Suspended particle benthic nepheloid layers (BNLs), typically identified by a reduction in light transmission from the CTD transmissometer (Gardner et al., 2018), are

known to variably supply and/or remove dissolved trace elements and isotopes such as Fe, Al, Ti, Th, Pb, Nd, Ni and Co from the water column (Rutgers van der Loeff et al., 2002; Fitzsimmons et al., 2015; Middag et al., 2015; Ohnemus and Lam, 2015; Noble et al., 2017). Recent analyses of transmissometry data (Gardner et al., 2018) suggest that along GN01, BNLs were present in the Western Arctic but dropped off substantially in thickness and particle concentration seaward of the Chukchi Shelf. At Stations 26, 30, and 38 in the Makarov Basin, we see small elevations in dZn at bottom depths (Figure 3.11c) where the light transmission is also reduced (Figure 3.11b). This suggests a small source of dZn ( $\leq 0.3$  nmol/kg) associated with resuspended material in the deep waters of the Makarov Basin. While Stations 48 and 57 within the Canada Basin also show slight enrichments in dZn in the bottom waters, they are not concurrent with decreased light transmission. Overall, while these data may reflect BNL sources, we emphasize that this dZn source is much smaller in magnitude than the dZn enrichments of the shelf-derived halocline.

#### **3.4.5.3. Interbasin Differences**

Nutrient-type metal concentrations in deep waters of the global ocean are usually sourced by the remineralization of vertically settling phytoplankton debris. Thus, we attributed the remarkably low and consistent Western Arctic deep water dZn concentrations to a negligible regenerative dZn supply from the low-productivity surface Arctic, and instead, to a simple advective supply of low dZn from the North Atlantic and Eurasian basins.

However, the Western Arctic's Amerasian Basin is isolated from the Eastern Arctic's Eurasian Basin by the Lomonosov Ridge (1870 m sill) (Timmermans et al., 2003; Timmermans and Garrett, 2006; Rudels, 2015). Above the sill, Arctic dZn concentrations at 1000–1800 m depth in the Amerasian's Makarov Basin ( $1.44 \pm 0.18$  nmol/kg at Stations 30 and 38 closest to the Lomonosov Ridge) were identical to the Eurasian's Amundsen Basin dZn ( $1.46 \pm 0.21$  nmol/kg, 1000–1800 m, Station 32). This is consistent with active exchange between the basins above the sill and no significant inputs (including remineralization) to or scavenging removal from this layer. Amundsen-Makarov exchange below the ~1870 m sill is likely intermittent, with the flow direction dependent on the pressure gradient at the sill, which varies over time (Björk et al., 2007; Rudels, 2015). Below 1800 m, dZn in the two Makarov Basin stations decreased to a low and homogenous  $0.97 \pm 0.10$  nmol/kg compared with the Amundsen Basin dZn of  $1.22 \pm 0.14$  nmol/kg from which they are thought to derive. In contrast to dZn, the Si concentrations increased from the Amundsen to the Makarov stations between 1000–2000 m ( $6.7 \pm 0.6$  to  $12.1 \pm 0.7$   $\mu\text{mol/kg}$ ) and again below 2000 m ( $12.6 \pm 0.9$   $\mu\text{mol/kg}$ ). Thus, dZn and Si are each homogenous below ~2000 m, but are decoupled (Figure 3.12, discussed next in Section 3.4.6).

The Western Arctic's Makarov and Canada sub-basins are separated by the ~2200 m Alpha and Mendeleev Ridges (Figure 3.1, which contain a deep gap (~2400 m) where deep water exchange between the two basins is possible. While the ventilation timescale is perhaps too long to capture significant changes in dZn at these depths, dissolved Si and Al concentrations indicate water flow from the Canada to the Makarov

Basin via the Mendeleev Ridge near ~2500m (Swift et al., 1997; Middag et al., 2009). During GN01, we observed no significant difference between dZn in deep waters (> 2000 m) of the Canada Basin ( $1.17 \pm 0.30$  nmol/kg) compared with the Makarov Basin ( $1.09 \pm 0.20$  nmol/kg), despite their ~100 year estimated age difference (Tanhua et al., 2009). This is consistent with (1) the hypothesized Canada-Makarov sub-basin exchange, (2) a lack of vertically remineralized dZn inputs to depth due to low biological production below the surface sea ice, as above, and (3) a lack of reversible scavenging suggested by Weber et al. (2018).

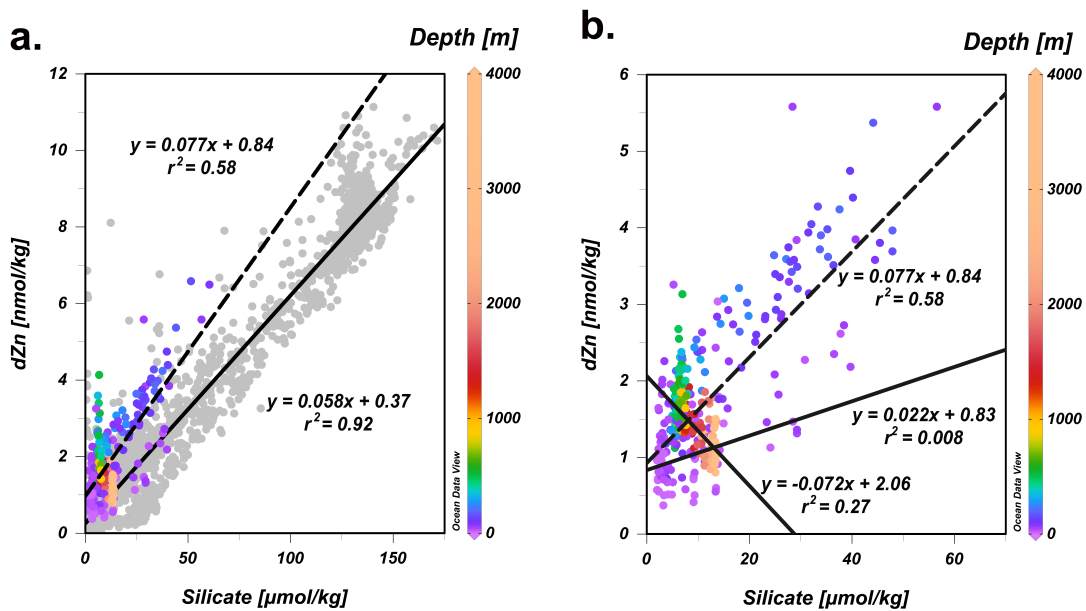


**Figure 3.12** Relationships between dissolved Zn and Si. (a) Zn:Si in the Arctic versus depth (in color), overlaid on top of global Zn:Si from the 2017 GEOTRACES IDP (Schlitzer et al., 2018; in gray). While halocline values (dashed line) fall above the average global Zn:Si slope (solid line), intermediate and deep waters fit more closely in the spread of Zn:Si. (b) Zn:Si in the Arctic with depth (in color) showing full water column slope (dotted line), >1,000 m (negative slope), and >2,000 m (positive slope and solid). This demonstrates the decoupling of dissolved zinc (dZn) and Si in Arctic deep waters.

### 3.4.6. Zn:Si Global Comparison

The oceanic relationship between dZn and Si is tied to the biological pump and global thermohaline circulation (Bruland et al., 1978; Vance et al., 2017; Weber et al., 2018). However, along GN01, nutrients and nutrient-type metals such as dZn do not exhibit *in situ* deep water regeneration. Consequently, across the entire GN01 Arctic transect (excluding Pacific Station 1), the Zn:Si slope ( $0.077 \pm 0.004$  nmol/ $\mu$ mol,  $r^2 = 0.58$ ) is higher and weaker than the global average ( $0.060 \pm 0.0003$  nmol/ $\mu$ mol,  $r^2 = 0.95$ , (Schlitzer et al., 2018)), the eastern and western North Pacific ( $0.054$  nmol/ $\mu$ mol,  $r^2 = 0.99$  and  $0.059$  nmol/ $\mu$ mol,  $r^2 = 0.99$  respectively; (Bruland, 1980; Kim et al., 2015)), and the central North Atlantic ( $0.058$  nmol/ $\mu$ mol;  $r^2 = 0.76$  (Roshan and Wu, 2015)), but it is lower than the oxygenated waters of the HNLC subarctic northeast Pacific ( $0.102$  nmol/ $\mu$ mol;  $r^2 = 0.92$  (Janssen and Cullen, 2015)). The high Arctic Zn:Si slope is driven by the higher Zn:Si regression in the shelf bottom waters and in the halocline downstream, but the overall more scattered (lower  $r^2$ ) Zn:Si relationship is due to Arctic deep waters, where dZn and Si are decoupled (Figure 3.12a, 13).

The North Pacific end member Zn:Si regression at GN01 Station 1 in the Bering Sea ( $0.052 \pm 0.010$  nmol/ $\mu$ mol, upper 100 m) is oceanographically consistent with the global average. Along the Bering and Chukchi shelves, this Zn:Si slope increases ( $0.076 \pm 0.012$  nmol/ $\mu$ mol, Stations 2–8, 61–66) due to “soft-tissue” sediment porewater remineralization inputs richer in dZn than in Si (see 3.2–3.3 above), and becomes even higher within the Canada Basin UHL ( $0.11 \pm 0.01$  nmol/ $\mu$ mol), which is formed from the bottom-most (brine-rich) waters of the Chukchi shelf. In Arctic intermediate and

deep waters, Zn:Si shifts to negative slopes (Figure 3.12b) because dZn concentrations decrease from  $1.76 \pm 0.29$  nmol/kg between 300–500 m to  $1.03 \pm 0.18$  nmol/kg below 3650 m in Arctic deep water, while Si concentrations increase from  $6.81 \pm 0.97$   $\mu$ mol/kg to  $12.71 \pm 0.84$   $\mu$ mol/kg over the same depths (Figure 3.3). This decoupling of Zn:Si lies in contrast to our global view of coupled Zn:Si driven by deep water remineralization (Figure 3.12a, (Bruland et al., 1978; Lohan et al., 2002)). More recent work suggests that Zn:Si ratios are driven by interactions between biogeochemistry and physical processes occurring in the Southern Ocean, leading to water mass mixing of these preformed ratios in addition to scavenging and remineralization (Vance et al., 2017; Weber et al., 2018). We hypothesize three potential causes of this Arctic deep water Zn:Si decoupling: scavenging removal of dZn at depth, a source of Si from deep Arctic sediments, or deep water ventilation from waters containing a different Zn:Si ratio.

Pacific Ocean results from Janssen and Cullen (2015) show preferential removal of dZn relative to Si, resulting in low Zn:Si slopes in low-oxygen environments due to hypothesized precipitation of Zn sulfides. However, we see well-oxygenated waters ( $> 200$   $\mu$ mol/kg) throughout deep waters of the Arctic, making Zn sulfide precipitation unlikely. It has been hypothesized that up to 1% of the dZn pool is subject to scavenging (John and Conway, 2014), which could explain the deep Si enrichment compared to dZn, though these studies have focused on upper ocean dZn scavenging onto organic particles, concentrations of which are negligible in Arctic deep waters. In contrast, recent work demonstrates that a reversibly scavenged pool of dZn may account for a significant portion of deep water column dZn (Weber et al., 2018), likely resulting in dZn

accumulation with age. However, we observe statistically insignificant differences in deep water dZn between the Canada, Makarov, and Amundsen basins, despite > 100 year age differences between each, which is at odds with any scavenging or addition upon aging. In short, the entire Arctic appears to have homogeneously low Zn:Si compared to surface waters, despite century-scale aging of deep waters.

One might also hypothesize that Si fluxes from deep Arctic sediments in a relatively isothermal, isohaline water column could cause an increase in Si without a concomitant release of dZn, given the 1000 fold lower Zn:Si ratios in diatomaceous frustules compared to water column phytoplankton in this study (Ellwood and Hunter, 1999; Hendry and Rickaby, 2008; Andersen et al., 2011). However, benthic Si fluxes were found to be quite low throughout the Arctic, likely due to low export of biogenic opal (März et al., 2015). If we assume that the long deep water residence times in the Canada and Makarov basins are due to slow ventilation, we can estimate an accumulation of Si coming from this benthic flux in the deep water, in addition to the pre-formed Atlantic signature. The total off-shelf area in the Canada and Makarov basins is  $2.1 \times 10^6 \text{ km}^2$  (Jakobsson et al., 2004) with an average depth of 3400 m based on this transect. Given that the Si maximum extends from 2000 m to the bottom, we estimate that the total deep water volume is  $3.3 \times 10^9 \text{ km}^3$  below 2000 m depth in the Makarov and Canada basins. The extrapolated total dSi flux from off-shelf sediments thus ranges from  $4.5\text{--}68 \times 10^9 \text{ mol/year}$  (März et al., 2015), resulting in  $0.40\text{--}6.03 \mu\text{mol/kg}$  of additional or sediment-derived Si supplied to the Canada and Makarov basin over 300 years (a median estimate of the deep water age in the Makarov and Canada basins

(Tanhua et al., 2009)). The “background” dSi in the Atlantic layer is  $6.24 \pm 0.60$   $\mu\text{mol}/\text{kg}$  while the deep water is  $12.58 \pm 0.85$   $\mu\text{mol}/\text{kg}$ , giving an average excess dSi of  $6.34 \pm 1.04$   $\mu\text{mol}/\text{kg}$ . Thus, only the upper end of the estimate proffered in März et al. (2015) is nearly equivalent to the average excess of dSi in the deep Western Arctic waters. Thus, only if dSi were sourced from deep Arctic porewaters at the highest measured rates across the entire open Arctic could a sedimentary Si source explain the Zn:Si decoupling, and this all must occur without any porewater dZn inputs; this seems unlikely to be the complete explanation.

We observed negative Zn:Si slopes below 1000 m ( $-0.072 \pm 0.010$   $\text{nmol}/\mu\text{mol}$ ,  $r^2 = 0.27$ , Figure 3.12b), and the Zn:Si relationship fell apart completely below 2000 m ( $0.022 \pm 0.04$   $\text{nmol}/\mu\text{mol}$ ,  $r^2 = 0.008$ , Figure 3.12b). It appears that the Zn:Si slopes in the BSB layer (~1000–2000 m) of the Atlantic Water and Zn:Si slopes in the Arctic deep waters are each homogenous but distinct from each other (Figure 3.12b). This important clue leads us to a water mass explanation. We posit that the homogeneity of the deep layer likely represents deep water renewal from nearly 500 years ago (Timmermans et al., 2003), dating back to the Little Ice Age (Paasche and Bakke, 2010). Lower productivity (Chan et al., 2017), as well as circulation changes driven by the greater ice coverage and lower temperature (Aagaard and Carmack, 1989), could have resulted in different community composition and thus different Zn:Si ratios compared to what we currently observe in the surface and shelves. In a basin marked by low productivity and advective water mass movement, differences in the nutrient stoichiometry in these deepest water layers is unsurprising.

### 3.5. Conclusions

Dissolved Zn distributions in the Western Arctic Ocean represent a departure from the classic, “nutrient-type” profile that is prevalent in the global ocean. Rather than being influenced primarily by the biological pump, resulting in low surface concentrations and regeneration with depth, the Arctic dZn biogeochemistry is governed by a combination of 1) dZn-rich benthic shelf remineralization inputs that are advected into the subsurface western basins, and 2) mixing of pre-formed dZn concentrations from the Atlantic and past ventilation events. Over the shelf, biological processing of dZn is significant, but moving offshore in the surface PML, effects of biological uptake are small, and sea ice melt dilutes dZn in this study, despite previous reports of high dZn concentrations within Arctic sea ice (Tovar-Sánchez et al., 2010). Likewise, no clear riverine source was observed despite elevated dZn concentrations in Arctic rivers (Hölemann et al., 2005). Surface concentrations are primarily determined by incoming Pacific water through the Bering Strait modified by shelf sediment fluxes following the porewater remineralization of high Zn:C and Zn:Si phytoplankton cells.

This high-Zn signature is preserved in the shelf-derived UHL of the Canada Basin, where a maximum in macronutrients and dZn was observed at every station. The dZn-enriched UHL feature dominates the Arctic profile and remains distinctly similar to the shelf in both concentration range and stoichiometry of Zn:Si and Zn:C regression slopes (Figure 3.13), which compare well with cellular stoichiometries of phytoplankton on the Chukchi Shelf, not from open Arctic cells. The Chukchi Shelf seems uniquely suited to provide this signal due to its high seasonal productivity within a shallow water

column, leading to efficient export of organic matter to the sediments and allowing brine-rejected waters to contact the sediment surface, from which nutrients are remineralized. This is in contrast to the Canada Basin LHL, which is Eurasian shelf-derived, and exhibits relatively low dZn concentrations that appear to represent a mixture between the overlying UHL and the underlying Atlantic layer. While brine-rejected waters also contact the sediment surface on the Eurasian Shelf, we argue that the lower dZn in Eurasian-derived halocline layers (such as the LHL) occurs because of the deeper Eurasian shelf water column depths, in which more dZn can be remineralized in the water column, preventing the significant porewater remineralization nutrient fluxes observed in the shallower Chukchi Shelf.

The warm Atlantic layer is an easily traceable water mass that serves as an excellent illustration of the effects of mixing on dZn distribution in the Arctic. With potential temperatures  $> 0^{\circ}\text{C}$ , this layer originates from the warmer, low-nutrient, low-dZn North Atlantic. As it circulates through the Arctic, it loses heat through conservative mixing with the halocline above. We observe that dZn has a linear relationship with potential temperature in this layer, suggesting that the dZn derives entirely from conservative mixing with the overlying dZn-rich halocline layers. This illustrates how mixing controls intermediate dZn concentrations, not *in situ* remineralization as might be expected for a nutrient-type element.

Overall, in deep waters we find that while dZn fluxes to the Amundsen Basin from hydrothermal sources and to the Makarov Basin from BNL sources may be present, they are small ( $\leq 0.3$  nmol/kg). With little regenerative inputs to depth, dZn

concentrations in Western Arctic deep water are consistently low and are decoupled from the macronutrient Si, likely because of changes in source water stoichiometry over ventilation timescales and/or from low but steady sediment porewater Si fluxes over the long lifetimes of Arctic deep waters.

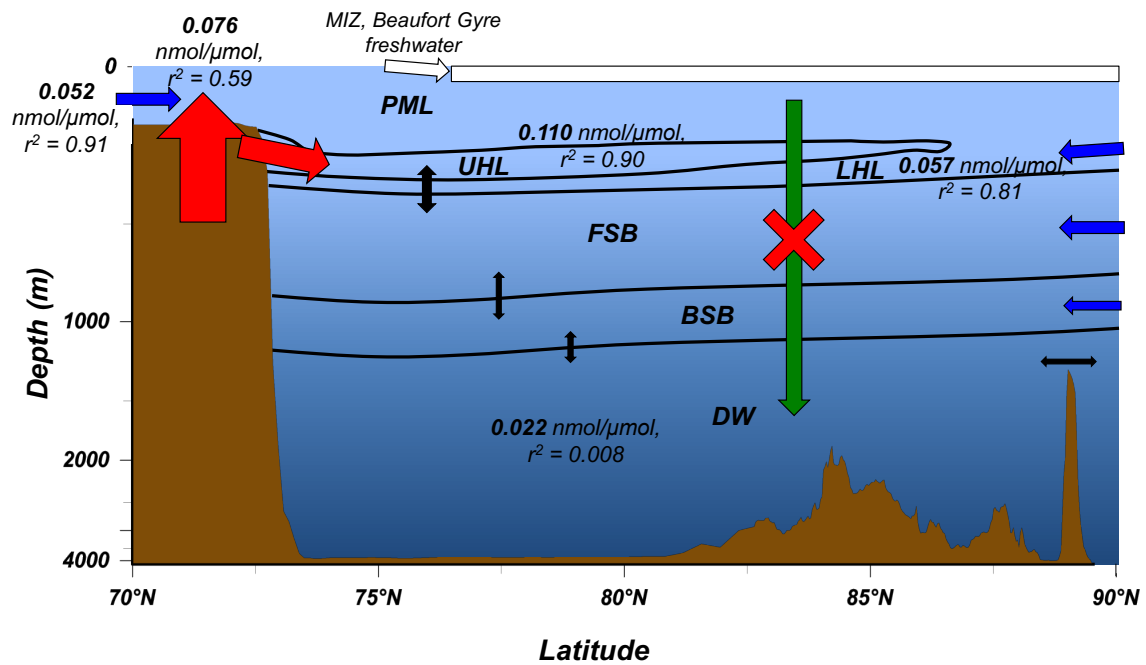


**Figure 3.13** Summary schematic of the major sources of dissolved zinc to the Western Arctic, where relative arrow size reflects the magnitude of the source. (red) Major inputs such as the Chukchi Shelf and halocline. (blue) External water masses such as the Atlantic and Pacific Oceans. (white) Freshwater inputs from the MIZ and riverine sources. (black) The influence of mixing on deep waters below the halocline. (green) Indicates the lack of observed vertical biological regeneration that we would expect to influence deep water dZn distributions. Zn:Si water column regression slopes are also shown for the shelf, halocline, and deep water (>2,000 m), highlighting the evolution of this stoichiometry.

### 3.6. References

- Aagaard, K. 1981. "On the deep circulation in the Arctic Ocean." *Deep Sea Research Part A. Oceanographic Research Papers* 28 (3):251-268. doi: [http://dx.doi.org/10.1016/0198-0149\(81\)90066-2](http://dx.doi.org/10.1016/0198-0149(81)90066-2).
- Aagaard, K., and Ee C Carmack. 1989. "The role of sea ice and other fresh water in the Arctic circulation." *Journal of Geophysical Research: Oceans* 94 (C10):14485-14498.
- Aagaard, K., J. H. Swift, and E. C. Carmack. 1985. "Thermohaline circulation in the Arctic Mediterranean Seas." *Journal of Geophysical Research: Oceans* 90 (C3):4833-4846. doi: 10.1029/JC090iC03p04833.
- Aguilar-Islas, Ana M., Robert Rember, Shigeto Nishino, Takashi Kikuchi, and Motoyo Itoh. 2013. "Partitioning and lateral transport of iron to the Canada Basin." *Polar Science* 7 (2):82-99. doi: <http://dx.doi.org/10.1016/j.polar.2012.11.001>.
- Andersen, M. B., D. Vance, C. Archer, R. F. Anderson, M. J. Ellwood, and C. S. Allen. 2011. "The Zn abundance and isotopic composition of diatom frustules, a proxy for Zn availability in ocean surface seawater." *Earth and Planetary Science Letters* 301:137-145. doi: 10.1016/j.epsl.2010.10.032.
- Anderson, L. G., Per S Andersson, Göran Björk, E Peter Jones, Sara Jutterström, and Iréne Wåhlström. 2013. "Source and formation of the upper halocline of the Arctic Ocean." *Journal of Geophysical Research: Oceans* 118 (1):410-421.
- Arrigo, K. R., T Mock, and MP Lizotte. 2003. "Primary production in sea ice." *Sea ice: an introduction to its physics, chemistry, biology and geology*:143-183.

- Björk, Göran, Martin Jakobsson, Bert Rudels, James H Swift, Leif Anderson, Dennis A Darby, Jan Backman, Bernard Coakley, Peter Winsor, and Leonid Polyak. 2007. "Bathymetry and deep-water exchange across the central Lomonosov Ridge at 88–89 N." *Deep Sea Research Part I: Oceanographic Research Papers* 54 (8):1197-1208.
- Bluhm, B. A., K. N. Kosobokova, and E. C. Carmack. 2015. "A tale of two basins: An integrated physical and biological perspective of the deep Arctic Ocean." *Progress in Oceanography* 139 (Supplement C):89-121. doi: <https://doi.org/10.1016/j.pocean.2015.07.011>.
- Boyd, Philip W., Michael J. Ellwood, Alessandro Tagliabue, and Benjamin S. Twining. 2017. "Biotic and abiotic retention, recycling and remineralization of metals in the ocean." *Nature Geoscience* 10:167. doi: 10.1038/ngeo2876 <https://www.nature.com/articles/ngeo2876#supplementary-information>.
- Brugler, Eric T, Robert S Pickart, GWK Moore, Steven Roberts, Thomas J Weingartner, and Hank Statscewich. 2014. "Seasonal to interannual variability of the Pacific water boundary current in the Beaufort Sea." *Progress in Oceanography* 127:1-20.
- Bruland, K. W. 1980. "Oceanographic distributions of cadmium, zinc, nickel, and copper in the North Pacific." *Earth and Planetary Science Letters* 47 (2):176-198.

- Bruland, K. W. 1989. "Complexation of zinc by natural organic ligands in the central North Pacific." *Limnology and Oceanography* 34 (2):269-285. doi: 10.4319/lo.1989.34.2.0269.
- Bruland, K. W., John R. Donat, and David A. Hutchins. 1991. "Interactive influences of bioactive trace metals on biological production in oceanic waters." *Limnology and Oceanography* 36 (8):1555-1577. doi: doi:10.4319/lo.1991.36.8.1555.
- Bruland, K. W., G. A. Knauer, and J. H. Martin. 1978. "Zinc in north-east Pacific water." *Nature* 271 (5647):741-743.
- Cai, M. H., J. Lin, Q. Q. Hong, Y. Wang, and M. G. Cai. 2011. "Content and distribution of trace metals in surface sediments from the northern Bering Sea, Chukchi Sea and adjacent Arctic areas." *Marine Pollution Bulletin* 63 (5):523-527. doi: <https://doi.org/10.1016/j.marpolbul.2011.02.007>.
- Carpenter, James H. 1965. "The Chesapeake Bay Institute technique for the Winkler dissolved oxygen method." *Limnology and Oceanography* 10 (1):141-143.
- Chan, P., J. Halfar, W. Adey, S. Hetzinger, T. Zack, G. W. K. Moore, U. G. Wortmann, B. Williams, and A. Hou. 2017. "Multicentennial record of Labrador Sea primary productivity and sea-ice variability archived in coralline algal barium." *Nature Communications* 8:15543. doi: 10.1038/ncomms15543  
<https://www.nature.com/articles/ncomms15543#supplementary-information>.
- Chang, Bonnie X, and Allan H Devol. 2009. "Seasonal and spatial patterns of sedimentary denitrification rates in the Chukchi Sea." *Deep Sea Research Part II: Topical Studies in Oceanography* 56 (17):1339-1350.

- Cid, Abigail Parcasio, Seiji Nakatsuka, and Yoshiki Sohrin. 2012. "Stoichiometry among bioactive trace metals in the Chukchi and Beaufort Seas." *Journal of oceanography* 68 (6):985-1001.
- Coachman, L. K., and C. A. Barnes. 1963. "The Movement of Atlantic Water in the Arctic Ocean." *ARCTIC; Vol 16, No 1 (1963): March: 1–80*. doi: 10.14430/arctic3517.
- Conway, T. M., and Seth G. John. 2014. "The biogeochemical cycling of zinc and zinc isotopes in the North Atlantic Ocean." *Global Biogeochemical Cycles* 28 (10):1111-1128. doi: 10.1002/2014GB004862.
- Conway, T. M., and Seth G. John. 2015. "The cycling of iron, zinc and cadmium in the North East Pacific Ocean—Insights from stable isotopes." *Geochimica et Cosmochimica Acta* 164:262-283.
- Corlett, W. Bryce, and Robert S. Pickart. 2017. "The Chukchi slope current." *Progress in Oceanography* 153:50-65.
- Cox, Alysia D., and Mak A. Saito. 2013. "Proteomic responses of oceanic *Synechococcus* WH8102 to phosphate and zinc scarcity and cadmium additions." *Frontiers in microbiology* 4.
- Croot, Peter L., Oliver Baars, and Peter Streu. 2011. "The distribution of dissolved zinc in the Atlantic sector of the Southern Ocean." *Deep Sea Research Part II: Topical Studies in Oceanography* 58 (25–26):2707-2719. doi: <https://doi.org/10.1016/j.dsr2.2010.10.041>.

- Culberson, Charles H, George P Knapp, Marvel C Stalcup, Robert T Williams, and Frank Zemlyak. 1991. "A comparison of methods for the determination of dissolved oxygen in seawater."
- Cutter, G, P Andersson, Lou Codispoti, P Croot, R Francois, MC Lohan, H Obata, and Michiel Rutgers vd Loeff. 2010. Sampling and sample-handling protocols for GEOTRACES cruises. GEOTRACES.
- Danielsson, Lars-Göran, and Stig Westerlund. 1983. "Trace Metals in the Arctic Ocean." In *Trace Metals in Sea Water*, edited by C. S. Wong, Edward Boyle, Kenneth W. Bruland, J. D. Burton and Edward D. Goldberg, 85-95. Boston, MA: Springer US.
- Edmonds, H. N., P. J. Michael, E. T. Baker, D. P. Connelly, J. E. Snow, C. H. Langmuir, H. J. B. Dick, R. Mühe, C. R. German, and D. W. Graham. 2003. "Discovery of abundant hydrothermal venting on the ultraslow-spreading Gakkel ridge in the Arctic Ocean." *Nature* 421:252. doi: 10.1038/nature01351 <https://www.nature.com/articles/nature01351#supplementary-information>.
- Ellwood, M.J. 2008. "Wintertime trace metal (Zn, Cu, Ni, Cd, Pb and Co) and nutrient distributions in the Subantarctic Zone between 40–52 S; 155–160 E." *Marine Chemistry* 112 (1-2):107-117.
- Ellwood, M.J., and Keith Hunter. 1999. *Determination of the Zn/Si ratio in diatom opal: A method for the separation, cleaning and dissolution of diatoms*. Vol. 66.

- Ellwood, M.J., and Keith A. Hunter. 2000. "The incorporation of zinc and iron into the frustule of the marine diatom *Thalassiosira pseudonana*." *Limnology and Oceanography* 45 (7):1517-1524. doi: 10.4319/lo.2000.45.7.1517.
- Ellwood, M.J., and Constant MG Van den Berg. 2000. "Zinc speciation in the northeastern Atlantic Ocean." *Marine Chemistry* 68 (4):295-306.
- Fitzsimmons, Jessica N., and Edward A. Boyle. 2012. "An intercalibration between the GEOTRACES GO-FLO and the MITESS/Vanes sampling systems for dissolved iron concentration analyses (and a closer look at adsorption effects)." *Limnology and Oceanography: Methods* 10 (6):437-450. doi: 10.4319/lom.2012.10.437.
- Fitzsimmons, Jessica N., G. G. Carrasco, J. Wu, S. Roshan, M. Hatta, C. I. Measures, T. M. Conway, S. G. John, and E. A. Boyle. 2015. "Partitioning of dissolved iron and iron isotopes into soluble and colloidal phases along the GA03 GEOTRACES North Atlantic Transect." *Deep-Sea Research Part II: Topical Studies in Oceanography* 116:130-151. doi: 10.1016/j.dsr2.2014.11.014.
- Franck, Valerie M, Kenneth W Bruland, David A Hutchins, and Mark A Brzezinski. 2003. "Iron and zinc effects on silicic acid and nitrate uptake kinetics in three high-nutrient, low-chlorophyll (HNLC) regions." *Marine Ecology Progress Series* 252:15-33.
- Gardner, Wilford D., Mary Jo Richardson, and Alexey V. Mishonov. 2018. "Global assessment of benthic nepheloid layers and linkage with upper ocean

- dynamics." *Earth and Planetary Science Letters* 482 (Supplement C):126-134.  
doi: <https://doi.org/10.1016/j.epsl.2017.11.008>.
- Gobeil, C, B Sundby, RW Macdonald, and JN Smith. 2001. "Recent change in organic carbon flux to Arctic Ocean deep basins: evidence from acid volatile sulfide, manganese and rhenium discord in sediments." *Geophysical Research Letters* 28 (9):1743-1746.
- Gosnell, Kathleen J, William M Landing, and Angela Milne. 2012. "Fluorometric detection of total dissolved zinc in the southern Indian Ocean." *Marine Chemistry* 132:68-76.
- Hendry, Katharine R., and Rosalind E. M. Rickaby. 2008. "Opal (Zn/Si) ratios as a nearshore geochemical proxy in coastal Antarctica." *Paleoceanography* 23 (2).  
doi: [doi:10.1029/2007PA001576](https://doi.org/10.1029/2007PA001576).
- Hillebrand, Helmut, Claus-Dieter Dürselen, David Kirschtel, Utsa Pollinger, and Tamar Zohary. 1999. "Biovolume calculation for pelagic and benthic microalgae." *Journal of phycology* 35 (2):403-424.
- Hioki, Nanako, Kenshi Kuma, Yuichirou Morita, Ryouhei Sasayama, Atsushi Ooki, Yoshiko Kondo, Hajime Obata, Jun Nishioka, Youhei Yamashita, and Shigeto Nishino. 2014. "Laterally spreading iron, humic-like dissolved organic matter and nutrients in cold, dense subsurface water of the Arctic Ocean." *Scientific reports* 4.
- Hölemann, J. A., M. Schirmacher, and A. Prange. 2005. "Seasonal variability of trace metals in the Lena River and the southeastern Laptev Sea: Impact of the spring

- freshet." *Global and Planetary Change* 48 (1–3):112-125. doi:  
<http://dx.doi.org/10.1016/j.gloplacha.2004.12.008>.
- Hydes, D, M Aoyama, Alain Aminot, K Bakker, S Becker, S Coverly, Anne Daniel, A Dickson, O Grosso, and Roger Kerouel. 2010. "Determination of dissolved nutrients (N, P, Si) in seawater with high precision and inter-comparability using gas-segmented continuous flow analysers."
- Jaccard, Thomas, Daniel Ariztegui, and Kevin J. Wilkinson. 2009. "Incorporation of zinc into the frustule of the freshwater diatom *Stephanodiscus hantzschii*." *Chemical Geology* 265 (3):381-386. doi:  
<https://doi.org/10.1016/j.chemgeo.2009.04.016>.
- Jakobsson, M, A Grantz, Y Kristoffersen, R Macnab, RW MacDonald, E Sakshaug, R Stein, and W Jokat. 2004. "The Arctic Ocean: Boundary conditions and background information." In *The organic carbon cycle in the Arctic Ocean*, 1-32. Springer.
- Jakuba, Rachel Wisniewski, Mak A Saito, James W Moffett, and Yan Xu. 2012. "Dissolved zinc in the subarctic North Pacific and Bering Sea: its distribution, speciation, and importance to primary producers." *Global Biogeochemical Cycles* 26 (2).
- Janssen, David J., and Jay T. Cullen. 2015. "Decoupling of zinc and silicic acid in the subarctic northeast Pacific interior." *Marine Chemistry* 177:124-133. doi:  
<http://dx.doi.org/10.1016/j.marchem.2015.03.014>.

- John, Seth, and T.M. Conway. 2014. *A role for scavenging in the marine biogeochemical cycling of zinc and zinc isotopes*. Vol. 394.
- Jones, E.P. 2001. "Circulation in the Arctic Ocean." *Polar Research* 20 (2):139-146.  
doi: 10.1111/j.1751-8369.2001.tb00049.x.
- Jones, E.P., and L. G. Anderson. 1986. "On the origin of the chemical properties of the Arctic Ocean halocline." *Journal of Geophysical Research: Oceans* 91 (C9):10759-10767. doi: 10.1029/JC091iC09p10759.
- Jones, E.P., L. G. Anderson, and James H. Swift. 1998. "Distribution of Atlantic and Pacific waters in the upper Arctic Ocean: Implications for circulation." *Geophysical Research Letters* 25 (6):765-768. doi: 10.1029/98GL00464.
- Kadko, David, Ben Galfond, William M. Landing, and Rachel U. Shelley. 2016. "Determining the pathways, fate, and flux of atmospherically derived trace elements in the Arctic ocean/ice system." *Marine Chemistry* 182 (Supplement C):38-50. doi: <https://doi.org/10.1016/j.marchem.2016.04.006>.
- Kim, Taejin, Hajime Obata, Yoshiko Kondo, Hiroshi Ogawa, and Toshitaka Gamo. 2015. "Distribution and speciation of dissolved zinc in the western North Pacific and its adjacent seas." *Marine Chemistry* 173:330-341.
- Kim, Taejin, Hajime Obata, Jun Nishioka, and Toshitaka Gamo. 2017. "Distribution of Dissolved Zinc in the Western and Central Subarctic North Pacific." *Global Biogeochemical Cycles* 31 (9):1454-1468. doi: 10.1002/2017GB005711.
- Klunder, M. B., P. Laan, R. Middag, H. J. W. de Baar, and K. Bakker. 2012. "Dissolved iron in the Arctic Ocean: Important role of hydrothermal sources,

shelf input and scavenging removal." *Journal of Geophysical Research: Oceans* 117 (C4):n/a-n/a. doi: 10.1029/2011JC007135.

Kondo, Yoshiko, Hajime Obata, Nanako Hioki, Atsushi Ooki, Shigeto Nishino, Takashi Kikuchi, and Kenshi Kuma. 2016. "Transport of trace metals (Mn, Fe, Ni, Zn and Cd) in the western Arctic Ocean (Chukchi Sea and Canada Basin) in late summer 2012." *Deep Sea Research Part I: Oceanographic Research Papers* 116:236-252. doi: <http://dx.doi.org/10.1016/j.dsr.2016.08.010>.

Lagerström, M. E., M. P. Field, M. Séguret, L. Fischer, S. Hann, and R. M. Sherrell. 2013. "Automated on-line flow-injection ICP-MS determination of trace metals (Mn, Fe, Co, Ni, Cu and Zn) in open ocean seawater: Application to the GEOTRACES program." *Marine Chemistry* 155 (0):71-80. doi: <http://dx.doi.org/10.1016/j.marchem.2013.06.001>.

Li, Qi, Min Chen, Renming Jia, Jian Zeng, Hui Lin, Minfang Zheng, and Yusheng Qiu. 2017. "Transit time of river water in the Bering and Chukchi Seas estimated from  $\delta^{18}\text{O}$  and radium isotopes." *Progress in Oceanography* 159 (Supplement C):115-129. doi: <https://doi.org/10.1016/j.pocean.2017.08.004>.

Little, S.H., Derek Vance, James McManus, and Silke Severmann. 2016. "Key role of continental margin sediments in the oceanic mass balance of Zn and Zn isotopes." *Geology* 44 (3):207-210.

Little, S.H., D Vance, C Walker-Brown, and WM Landing. 2014. "The oceanic mass balance of copper and zinc isotopes, investigated by analysis of their inputs, and

outputs to ferromanganese oxide sediments." *Geochimica et Cosmochimica Acta* 125:673-693.

Lohan, Maeve C., Peter J. Statham, and David W. Crawford. 2002. "Total dissolved zinc in the upper water column of the subarctic North East Pacific." *Deep Sea Research Part II: Topical Studies in Oceanography* 49 (24):5793-5808. doi: [https://doi.org/10.1016/S0967-0645\(02\)00215-1](https://doi.org/10.1016/S0967-0645(02)00215-1).

Macdonald, R.W., EC Carmack, FA McLaughlin, KK Falkner, and JH Swift. 1999. "Connections among ice, runoff and atmospheric forcing in the Beaufort Gyre." *Geophysical Research Letters* 26 (15):2223-2226.

Macdonald, R.W., E. C. Carmack, F. A. McLaughlin, K. Iseki, D. M. Macdonald, and M. C. O'Brien. 1989. "Composition and modification of water masses in the Mackenzie shelf estuary." *Journal of Geophysical Research: Oceans* 94 (C12):18057-18070. doi: 10.1029/JC094iC12p18057.

Macdonald, R.W., Z. A. Kuzyk, and S. C. Johannessen. 2015. "It is not just about the ice: a geochemical perspective on the changing Arctic Ocean." *Journal of Environmental Studies and Sciences* 5 (3):288-301. doi: 10.1007/s13412-015-0302-4.

Mahaffey, Claire, Sarah Reynolds, Clare E Davis, and Maeve C Lohan. 2014. "Alkaline phosphatase activity in the subtropical ocean: insights from nutrient, dust and trace metal addition experiments." *Frontiers in Marine Science* 1:73.

- Markus, Thorsten, Julienne C. Stroeve, and Jeffrey Miller. 2009. "Recent changes in Arctic sea ice melt onset, freezeup, and melt season length." *Journal of Geophysical Research: Oceans* 114 (C12). doi: doi:10.1029/2009JC005436.
- Marsay, Chris M, Ana Aguilar-Islas, Jessica N Fitzsimmons, Mariko Hatta, Laramie T Jensen, Seth G John, David Kadko, William M Landing, Nathan T Lanning, and Peter L Morton. 2018. "Dissolved and particulate trace elements in late summer Arctic melt ponds." *Marine Chemistry*.
- März, C, A-K Meinhardt, B Schnetger, and H-J Brumsack. 2015. "Silica diagenesis and benthic fluxes in the Arctic Ocean." *Marine Chemistry* 171:1-9.
- Mawji, Edward, Reiner Schlitzer, and Elena Dodas. 2015. "The GEOTRACES Intermediate Data Product 2014." *Marine Chemistry* 177:1-8. doi: <https://doi.org/10.1016/j.marchem.2015.04.005>.
- Menden-Deuer, Susanne, and Evelyn J Lessard. 2000. "Carbon to volume relationships for dinoflagellates, diatoms, and other protist plankton." *Limnology and oceanography* 45 (3):569-579.
- Middag, R., H. J. W. de Baar, P. Laan, and M. B. Klunder. 2011. "Fluvial and hydrothermal input of manganese into the Arctic Ocean." *Geochimica et Cosmochimica Acta* 75 (9):2393-2408. doi: <http://dx.doi.org/10.1016/j.gca.2011.02.011>.
- Middag, R., R. Séférian, T. M. Conway, S. G. John, K. W. Bruland, and H. J. W. de Baar. 2015. "Intercomparison of Dissolved Trace Elements at the Bermuda

- Atlantic Time Series Station." *Marine Chemistry* (0). doi:  
<http://dx.doi.org/10.1016/j.marchem.2015.06.014>.
- Moore, R. M. 1981. "Oceanographic distributions of zinc, cadmium, copper and aluminium in waters of the central arctic." *Geochimica et Cosmochimica Acta* 45 (12):2475-2482. doi: [http://dx.doi.org/10.1016/0016-7037\(81\)90099-5](http://dx.doi.org/10.1016/0016-7037(81)90099-5).
- Morel, F. M. M. 2008. "The co-evolution of phytoplankton and trace element cycles in the oceans." *Geobiology* 6 (3):318-324. doi: [doi:10.1111/j.1472-4669.2008.00144.x](https://doi.org/10.1111/j.1472-4669.2008.00144.x).
- Newton, Robert, Peter Schlosser, Richard Mortlock, James Swift, and Robie MacDonald. 2013. "Canadian Basin freshwater sources and changes: Results from the 2005 Arctic Ocean Section." *Journal of Geophysical Research: Oceans* 118 (4):2133-2154. doi: [doi:10.1002/jgrc.20101](https://doi.org/10.1002/jgrc.20101).
- Nishino, Shigeto, Koji Shimada, and Motoyo Itoh. 2005. "Use of ammonium and other nitrogen tracers to investigate the spreading of shelf waters in the western Arctic halocline." *Journal of Geophysical Research: Oceans* 110 (C10):n/a-n/a. doi: [10.1029/2003JC002118](https://doi.org/10.1029/2003JC002118).
- Noble, A. E., D. C. Ohnemus, N. J. Hawco, P. J. Lam, and M. A. Saito. 2017. "Coastal sources, sinks and strong organic complexation of dissolved cobalt within the US North Atlantic GEOTRACES transect GA03." *Biogeosciences* 14 (11):2715-2739. doi: [10.5194/bg-14-2715-2017](https://doi.org/10.5194/bg-14-2715-2017).

- Nowicki, Jocelyn L, Kenneth S Johnson, Kenneth H Coale, Virginia A Elrod, and Steve H Lieberman. 1994. "Determination of zinc in seawater using flow injection analysis with fluorometric detection." *Analytical Chemistry* 66 (17):2732-2738.
- Núñez-Milland, Daliángelis R, Stephen B Baines, Stefan Vogt, and Benjamin S Twining. 2010. "Quantification of phosphorus in single cells using synchrotron X-ray fluorescence." *Journal of synchrotron radiation* 17 (4):560-566.
- Ohnemus, Daniel C., and Phoebe J. Lam. 2015. "Cycling of lithogenic marine particles in the US GEOTRACES North Atlantic transect." *Deep Sea Research Part II: Topical Studies in Oceanography* 116:283-302. doi:  
<https://doi.org/10.1016/j.dsr2.2014.11.019>.
- Overland, J. E., and M. Wang. 2005. "The Arctic climate paradox: The recent decrease of the Arctic Oscillation." *Geophysical Research Letters* 32 (6). doi:  
doi:10.1029/2004GL021752.
- Paasche, Øyvind, and Jostein Bakke. 2010. "Defining the Little Ice Age." *Climate of the Past Discussions* 6 (5):2159-2175.
- Peterson, Bruce J., Robert M. Holmes, James W. McClelland, Charles J. Vörösmarty, Richard B. Lammers, Alexander I. Shiklomanov, Igor A. Shiklomanov, and Stefan Rahmstorf. 2002. "Increasing River Discharge to the Arctic Ocean." *Science* 298 (5601):2171-2173. doi: 10.1126/science.1077445.
- Pickart, Robert S, Thomas J Weingartner, Lawrence J Pratt, Sarah Zimmermann, and Daniel J Torres. 2005. "Flow of winter-transformed Pacific water into the

- Western Arctic." *Deep Sea Research Part II: Topical Studies in Oceanography* 52 (24):3175-3198.
- Proshutinsky, A., R. H. Bourke, and F. A. McLaughlin. 2002. "The role of the Beaufort Gyre in Arctic climate variability: Seasonal to decadal climate scales." *Geophysical Research Letters* 29 (23):15-1-15-4. doi: doi:10.1029/2002GL015847.
- Roshan, Saeed, and Jingfeng Wu. 2015. "Water mass mixing: The dominant control on the zinc distribution in the North Atlantic Ocean." *Global Biogeochemical Cycles* 29 (7):1060-1074. doi: 10.1002/2014GB005026.
- Roshan, Saeed, Jingfeng Wu, and William J Jenkins. 2016. "Long-range transport of hydrothermal dissolved Zn in the tropical South Pacific." *Marine Chemistry* 183:25-32.
- Rudels, B. 2015. "Arctic Ocean circulation, processes and water masses: A description of observations and ideas with focus on the period prior to the International Polar Year 2007–2009." *Progress in Oceanography* 132:22-67. doi: <http://dx.doi.org/10.1016/j.pocean.2013.11.006>.
- Rudels, B., E. P. Jones, L. G. Anderson, and G. Kattner. 1994. "On the Intermediate Depth Waters of the Arctic Ocean." In *The Polar Oceans and Their Role in Shaping the Global Environment*, 33-46. Washington, D.C.: American Geophysical Union.

- Rudels, B., E. Peter Jones, Ursula Schauer, and Patrick Eriksson. 2004. "Atlantic sources of the Arctic Ocean surface and halocline waters." *Polar Research* 23 (2):181-208. doi: 10.1111/j.1751-8369.2004.tb00007.x.
- Rutgers van der Loeff, M., P. Cai, I. Stimac, D. Bauch, C. Hanfland, T. Roeske, and S. B. Moran. 2012. "Shelf-basin exchange times of Arctic surface waters estimated from <sup>228</sup>Th/<sup>228</sup>Ra disequilibrium." *Journal of Geophysical Research: Oceans* 117 (C3):n/a-n/a. doi: 10.1029/2011JC007478.
- Rutgers van der Loeff, M., R. Meyer, B. Rudels, and E. Rachor. 2002. "Resuspension and particle transport in the benthic nepheloid layer in and near Fram Strait in relation to faunal abundances and <sup>234</sup>Th depletion." *Deep Sea Research Part I: Oceanographic Research Papers* 49 (11):1941-1958. doi: [https://doi.org/10.1016/S0967-0637\(02\)00113-9](https://doi.org/10.1016/S0967-0637(02)00113-9).
- Sakshaug, E. 2004. "Primary and secondary production in the Arctic Seas." In *The organic carbon cycle in the Arctic Ocean*, 57-81. Springer.
- Schauer, Ursula, B Rudels, EP Jones, LG Anderson, RD Muench, G Björk, JH Swift, V Ivanov, and A-M Larsson. 2002. "Confluence and redistribution of Atlantic water in the Nansen, Amundsen and Makarov basins." *Annales Geophysicae*.
- Schlitzer, Reiner, Robert F. Anderson, Elena Masferrer Dodas, Maeve Lohan, Walter Geibert, Alessandro Tagliabue, Andrew Bowie, Catherine Jeandel, Maria T. Maldonado, William M. Landing, Donna Cockwell, Cyril Abadie, Wafa Abouchami, Eric P. Achterberg, Alison Agather, Ana Aguliar-Islas, Hendrik M. van Aken, Morten Andersen, Corey Archer, Maureen Auro, Hein J. de Baar,

Oliver Baars, Alex R. Baker, Karel Bakker, Chandranath Basak, Mark Baskaran, Nicholas R. Bates, Dorothea Bauch, Pieter van Beek, Melanie K. Behrens, Erin Black, Katrin Bluhm, Laurent Bopp, Heather Bouman, Katlin Bowman, Johann Bown, Philip Boyd, Marie Boye, Edward A. Boyle, Pierre Branellec, Luke Bridgestock, Guillaume Brissebrat, Thomas Browning, Kenneth W. Bruland, Hans-Jürgen Brumsack, Mark Brzezinski, Clifton S. Buck, Kristen N. Buck, Ken Buesseler, Abby Bull, Edward Butler, Pinghe Cai, Patricia Cámara Mor, Damien Cardinal, Craig Carlson, Gonzalo Carrasco, Núria Casacuberta, Karen L. Casciotti, Maxi Castrillejo, Elena Chamizo, Rosie Chance, Matthew A. Charette, Joaquin E. Chaves, Hai Cheng, Fanny Chever, Marcus Christl, Thomas M. Church, Ivya Closset, Albert Colman, Tim M. Conway, Daniel Cossa, Peter Croot, Jay T. Cullen, Gregory A. Cutter, Chris Daniels, Frank Dehairs, Feifei Deng, Huong Thi Dieu, Brian Duggan, Gabriel Dulaquais, Cynthia Dumousseaud, Yolanda Echevoyen-Sanz, R. Lawrence Edwards, Michael Ellwood, Eberhard Fahrback, Jessica N. Fitzsimmons, A. Russell Flegal, Martin Q. Fleisher, Tina van de Flierdt, Martin Frank, Jana Friedrich, Francois Fripiat, Henning Fröllje, Stephen J. G. Galer, Toshitaka Gamo, Raja S. Ganeshram, Jordi Garcia-Orellana, Ester Garcia-Solsona, Melanie Gault-Ringold, Ejin George, Loes J. A. Gerringa, Melissa Gilbert, Jose M. Godoy, Steven L. Goldstein, Santiago R. Gonzalez, Karen Grissom, Chad Hammerschmidt, Alison Hartman, Christel S. Hassler, Ed C. Hathorne, Mariko Hatta, Nicholas Hawco, Christopher T. Hayes, Lars-Eric Heimbürger, Josh

Helgoe, Maija Heller, Gideon M. Henderson, Paul B. Henderson, Steven van Heuven, Peng Ho, Tristan J. Horner, Yu-Te Hsieh, Kuo-Fang Huang, Matthew P. Humphreys, Kenji Isshiki, Jeremy E. Jacquot, David J. Janssen, William J. Jenkins, Seth John, Elizabeth M. Jones, Janice L. Jones, David C. Kadko, Rick Kayser, Timothy C. Kenna, Roulin Khondoker, Taejin Kim, Lauren Kipp, Jessica K. Klar, Maarten Klunder, Sven Kretschmer, Yuichiro Kumamoto, Patrick Laan, Marie Labatut, Francois Lacan, Phoebe J. Lam, Myriam Lambelet, Carl H. Lamborg, Frédéric A. C. Le Moigne, Emilie Le Roy, Oliver J. Lechtenfeld, Jong-Mi Lee, Pascale Lherminier, Susan Little, Mercedes López-Lora, Yanbin Lu, Pere Masque, Edward Mawji, Charles R. McClain, Christopher Measures, Sanjin Mehic, Jan-Lukas Menzel Barraqueta, Pier van der Merwe, Rob Middag, Sebastian Mieruch, Angela Milne, Tomoharu Minami, James W. Moffett, Gwenaelle Moncoiffe, Willard S. Moore, Paul J. Morris, Peter L. Morton, Yuzuru Nakaguchi, Noriko Nakayama, John Niedermiller, Jun Nishioka, Akira Nishiuchi, Abigail Noble, Hajime Obata, Sven Ober, Daniel C. Ohnemus, Jan van Ooijen, Jeanette O'Sullivan, Stephanie Owens, Katharina Pahnke, Maxence Paul, Frank Pavia, Leopoldo D. Pena, Brian Peters, Frederic Planchon, Helene Planquette, Catherine Pradoux, Viena Puigcorbé, Paul Quay, Fabien Queroue, Amandine Radic, S. Rauschenberg, Mark Rehkämper, Robert Rember, Tomas Remenyi, Joseph A. Resing, Joerg Rickli, Sylvain Rigaud, Micha J. A. Rijkenberg, Stephen Rintoul, Laura F. Robinson, Montserrat Roca-Martí, Valenti Rodellas, Tobias Roeske, John M. Rolison, Mark Rosenberg,

Saeed Roshan, Michiel M. Rutgers van der Loeff, Evgenia Ryabenko, Mak A. Saito, Lesley A. Salt, Virginie Sanial, Geraldine Sarthou, Christina Schallenberg, Ursula Schauer, Howie Scher, Christian Schlosser, Bernhard Schnetger, Peter Scott, Peter N. Sedwick, Igor Semiletov, Rachel Shelley, Robert M. Sherrell, Alan M. Shiller, Daniel M. Sigman, Sunil Kumar Singh, Hans A. Slagter, Emma Slater, William M. Smethie, Helen Snaith, Yoshiki Sohrin, Bettina Sohst, Jeroen E. Sonke, Sabrina Speich, Reiner Steinfeldt, Gillian Stewart, Torben Stichel, Claudine H. Stirling, Johnny Stutsman, Gretchen J. Swarr, James H. Swift, Alexander Thomas, Kay Thorne, Claire P. Till, Ralph Till, Ashley T. Townsend, Emily Townsend, Robyn Tuerena, Benjamin S. Twining, Derek Vance, Sue Velazquez, Celia Venchiarutti, Maria Villa-Alfageme, Sebastian M. Vivancos, Antje H. L. Voelker, Bronwyn Wake, Mark J. Warner, Ros Watson, Evaline van Weerlee, M. Alexandra Weigand, Yishai Weinstein, Dominik Weiss, Andreas Wisotzki, E. Malcolm S. Woodward, Jingfeng Wu, Yingzhe Wu, Kathrin Wuttig, Neil Wyatt, Yang Xiang, Ruifang C. Xie, Zichen Xue, Hisayuki Yoshikawa, Jing Zhang, Pu Zhang, Ye Zhao, Linjie Zheng, Xin-Yuan Zheng, Moritz Zieringer, Louise A. Zimmer, Patrizia Ziveri, Patricia Zunino, and Cheryl Zurbrick. 2018. "The GEOTRACES Intermediate Data Product 2017." *Chemical Geology* 493:210-223. doi: <https://doi.org/10.1016/j.chemgeo.2018.05.040>.

Schlosser, Peter, Bernd Kromer, Brenda Ekwurzel, Gerhard Bönisch, Ann McNichol, Robert Schneider, Karl von Reden, HG Östlund, and JH Swift. 1997. "The first

trans-Arctic 14C section: comparison of the mean ages of the deep waters in the Eurasian and Canadian basins of the Arctic Ocean." *Nuclear Instruments and Methods in Physics Research Section B: Beam Interactions with Materials and Atoms* 123 (1-4):431-437.

Shimada, Koji, Motoyo Itoh, Shigeto Nishino, Fiona McLaughlin, Eddy Carmack, and Andrey Proshutinsky. 2005. "Halocline structure in the Canada Basin of the Arctic Ocean." *Geophysical Research Letters* 32 (3):n/a-n/a. doi: 10.1029/2004GL021358.

Sohrin, Yoshiki, Shouhei Urushihara, Seiji Nakatsuka, Tomohiro Kono, Eri Higo, Tomoharu Minami, Kazuhiro Norisuye, and Shigeo Umetani. 2008. "Multielemental Determination of GEOTRACES Key Trace Metals in Seawater by ICPMS after Preconcentration Using an Ethylenediaminetriacetic Acid Chelating Resin." *Analytical Chemistry* 80 (16):6267-6273. doi: 10.1021/ac800500f.

Sunda, William G., and Susan A. Huntsman. 1995. "Cobalt and zinc interreplacement in marine phytoplankton: Biological and geochemical implications." *Limnology and Oceanography* 40 (8):1404-1417. doi: doi:10.4319/lo.1995.40.8.1404.

Swift, JH, EP Jones, K Aagaard, EC Carmack, M Hingston, RW Macdonald, FA McLaughlin, and RG Perkin. 1997. "Waters of the Makarov and Canada basins." *Deep Sea Research Part II: Topical Studies in Oceanography* 44 (8):1503-1529.

- Tanhua, Toste, E. Peter Jones, Emil Jeansson, Sara Jutterström, William M. Smethie, Douglas W. R. Wallace, and Leif G. Anderson. 2009. "Ventilation of the Arctic Ocean: Mean ages and inventories of anthropogenic CO<sub>2</sub> and CFC-11." *Journal of Geophysical Research: Oceans* 114 (C1):n/a-n/a. doi: 10.1029/2008JC004868.
- Timmermans, M-L., and Chris Garrett. 2006. "Evolution of the Deep Water in the Canadian Basin in the Arctic Ocean." *Journal of Physical Oceanography* 36 (5):866-874. doi: 10.1175/jpo2906.1.
- Timmermans, M-L., Chris Garrett, and Eddy Carmack. 2003. "The thermohaline structure and evolution of the deep waters in the Canada Basin, Arctic Ocean." *Deep Sea Research Part I: Oceanographic Research Papers* 50 (10):1305-1321. doi: [https://doi.org/10.1016/S0967-0637\(03\)00125-0](https://doi.org/10.1016/S0967-0637(03)00125-0).
- Timofeyev, V. T. 1962. "The movement of atlantic water and heat into the arctic basin." *Deep Sea Research and Oceanographic Abstracts* 9 (7):358-361. doi: [https://doi.org/10.1016/0011-7471\(62\)90016-5](https://doi.org/10.1016/0011-7471(62)90016-5).
- Tovar-Sánchez, Antonio, Carlos M. Duarte, Juan C. Alonso, Silvia Lacorte, Romà Tauler, and Cristobal Galbán-Malagón. 2010. "Impacts of metals and nutrients released from melting multiyear Arctic sea ice." *Journal of Geophysical Research: Oceans* 115 (C7):n/a-n/a. doi: 10.1029/2009JC005685.
- Trefry, John H, Robert P Trocine, Lee W Cooper, and Kenneth H Dunton. 2014. "Trace metals and organic carbon in sediments of the northeastern Chukchi Sea." *Deep Sea Research Part II: Topical Studies in Oceanography* 102:18-31.

- Twining, B. S. 2018. "Contrasts in trace element content of marine phytoplankton from different ocean basins." Ocean Sciences Meeting, Portland, OR.
- Twining, B. S., and Stephen B Baines. 2013. "The trace metal composition of marine phytoplankton." *Annual review of marine science* 5:191-215.
- Twining, B. S., Stephen B Baines, James B Bozard, Stefan Vogt, Elyse A Walker, and David M Nelson. 2011. "Metal quotas of plankton in the equatorial Pacific Ocean." *Deep Sea Research Part II: Topical Studies in Oceanography* 58 (3-4):325-341.
- Twining, B. S., Stephen B Baines, and Nicholas S Fisher. 2004. "Element stoichiometries of individual plankton cells collected during the Southern Ocean Iron Experiment (SOFeX)." *Limnology and oceanography* 49 (6):2115-2128.
- Twining, B. S., Stephen B Baines, Nicholas S Fisher, Jörg Maser, Stefan Vogt, Chris Jacobsen, Antonio Tovar-Sanchez, and Sergio A Sañudo-Wilhelmy. 2003. "Quantifying trace elements in individual aquatic protist cells with a synchrotron X-ray fluorescence microprobe." *Analytical chemistry* 75 (15):3806-3816.
- Twining, B. S., Scott D Nodder, Andrew L King, David A Hutchins, Gary R LeClerc, Jennifer M DeBruyn, Elizabeth W Maas, Stefan Vogt, Steven W Wilhelm, and Philip W Boyd. 2014. "Differential remineralization of major and trace elements in sinking diatoms." *Limnology and Oceanography* 59 (3):689-704.
- Twining, B. S., Sara Rauschenberg, Peter L. Morton, and Stefan Vogt. 2015. "Metal contents of phytoplankton and labile particulate material in the North Atlantic

Ocean." *Progress in Oceanography* 137 (Part A):261-283. doi:

<https://doi.org/10.1016/j.pocean.2015.07.001>.

Vance, D., Susan H. Little, Gregory F. de Souza, Samar Khatiwala, Maeve C. Lohan, and Rob Middag. 2017. "Silicon and zinc biogeochemical cycles coupled

through the Southern Ocean." *Nature Geosci* 10 (3):202-206. doi:

10.1038/ngeo2890

<http://www.nature.com/ngeo/journal/v10/n3/abs/ngeo2890.html#supplementary-information>.

Weber, Thomas, Seth John, Alessandro Tagliabue, and Tim DeVries. 2018. "Biological uptake and reversible scavenging of zinc in the global ocean." *Science* 361

(6397):72-76. doi: 10.1126/science.aap8532.

Woodgate, Rebecca A. 2018. "Increases in the Pacific inflow to the Arctic from 1990 to 2015, and insights into seasonal trends and driving mechanisms from year-

round Bering Strait mooring data." *Progress in Oceanography* 160:124-154.

doi: <https://doi.org/10.1016/j.pocean.2017.12.007>.

Woodgate, Rebecca A., Knut Aagaard, Robin D. Muench, John Gunn, Göran Björk,

Bert Rudels, A. T. Roach, and Ursula Schauer. 2001. "The Arctic Ocean

Boundary Current along the Eurasian slope and the adjacent Lomonosov Ridge:

Water mass properties, transports and transformations from moored

instruments." *Deep Sea Research Part I: Oceanographic Research Papers* 48

(8):1757-1792. doi: [https://doi.org/10.1016/S0967-0637\(00\)00091-1](https://doi.org/10.1016/S0967-0637(00)00091-1).

- Woodgate, Rebecca A., Knut Aagaard, James H. Swift, Kelly K. Falkner, and William M. Smethie. 2005. "Pacific ventilation of the Arctic Ocean's lower halocline by upwelling and diapycnal mixing over the continental margin." *Geophysical Research Letters* 32 (18):n/a-n/a. doi: 10.1029/2005GL023999.
- Wyatt, N. J., A. Milne, E. M. S. Woodward, A. P. Rees, T. J. Browning, H. A. Bouman, P. J. Worsfold, and M. C. Lohan. 2014. "Biogeochemical cycling of dissolved zinc along the GEOTRACES South Atlantic transect GA10 at 40°S." *Global Biogeochemical Cycles* 28 (1):44-56. doi: 10.1002/2013GB004637.
- Yeats, Philip A. 1988. "Manganese, nickel, zinc and cadmium distributions at the Fram-3 and Cesar Ice Camps in the Arctic Ocean." *Oceanologica acta* 11 (4):383-388.
- Yeats, Philip A., and Stig Westerlund. 1991. "Trace metal distributions at an Arctic Ocean ice island." *Marine Chemistry* 33 (3):261-277. doi: [http://dx.doi.org/10.1016/0304-4203\(91\)90071-4](http://dx.doi.org/10.1016/0304-4203(91)90071-4).
- Zhao, Y, Derek Vance, Wafa Abouchami, and Hein JW de Baar. 2014. "Biogeochemical cycling of zinc and its isotopes in the Southern Ocean." *Geochimica et Cosmochimica Acta* 125:653-672.

## 4. A COMPARISON OF MARINE FE AND MN CYCLING: U.S. ARCTIC GEOTRACES GN01 WESTERN ARCTIC CASE STUDY\*

### 4.1. Overview

Dissolved iron (Fe) and manganese (Mn) share common sources and sinks in the global ocean, leading to similar distributions, such that observations about the processes affecting one element are often used to better understand the cycling of the other. However, Fe and Mn also have different redox reactivity and speciation that can cause their distributions to become decoupled. The Arctic Ocean provides a unique opportunity to juxtapose Fe and Mn cycling because the wide Arctic continental shelves provide significant margin fluxes of both elements, yet in situ vertical regeneration processes that can complicate scavenging calculations are negligible under the ice of the Arctic Ocean, making it easier to interpret metal fate along horizontal gradients. We present here a large-scale case study demonstrating a three-step mechanism for Fe and Mn decoupling in the upper 400 m of the Western Arctic Ocean. Both Fe and Mn are released during diagenesis in porewaters of the Chukchi Shelf, but they become immediately decoupled when Fe is much more rapidly oxidized and re-precipitated than Mn in the oxic Chukchi Shelf water column, leading to Fe being primarily particulate and Mn primarily dissolved. However, as these shelf fluxes are transported toward the shelf break and subducted into the subsurface halocline water mass, the loss rates of all

---

\* In review at *Geochimica et Cosmochimica Acta*, April 2020

species change significantly, causing further Fe and Mn decoupling. In the second decoupling step in the particle-rich shelf break region, the dominant shelf species are removed rapidly via particle scavenging, with smallest soluble Fe ( $s\text{Fe} < 0.02 \mu\text{m}$ ) being least subject to loss, while colloidal Fe ( $0.02 \mu\text{m} < c\text{Fe} < 0.2 \mu\text{m}$ ), dissolved Mn ( $d\text{Mn}$ ), and excess particulate Fe ( $p\text{Fexs}$ ) are all lost at similar, rapid rates. In the third decoupling step, once these species are swept beyond the shelf break into the low-particle waters of the open Arctic,  $c\text{Fe}$  and  $d\text{Mn}$  appear conserved, while  $p\text{Fexs}$ ,  $d\text{Fe}$ , and  $s\text{Fe}$  are very slowly removed with variable log-scale distances of transport:  $p\text{Fexs} \ll d\text{Fe} < s\text{Fe}$ . To assess the role of physicochemical speciation on these trends, we observed that Fe(II) was a small ( $\sim 7\%$ ) fraction of total  $d\text{Fe}$  in the upper 400 m, even over the shelf (up to 2%). Also, colloidal contribution to  $d\text{Fe}$  was very low ( $\sim 20\%$ ) in the open Arctic, in contrast to  $d\text{Fe}$  in the North Atlantic, which comprises a much higher fraction in the colloidal size range ( $\geq 50\%$ ). Throughout the Western Arctic Ocean, Fe and Mn are thus decoupled as a result of distinct oxidation kinetics and different scavenging rates within high- and low-particle regimes. As the "scavengers of the sea", the relative distribution of particulate Fe and Mn phases across the Arctic Ocean shelf and slope, respectively, will play an important role in determining the distribution and ultimate sediment burial site for other scavenging-prone trace elements. Additionally, we suggest that the future effects of climate change, including loss of sea ice that could impact the formation of the halocline, will likely change Fe and Mn distributions in the future Arctic.

## 4.2. Introduction

Iron (Fe) and manganese (Mn) are both essential micronutrients for marine phytoplankton as well as important tracers of redox processes in the global ocean. These metals share common sources (Figure 4.1), including diagenetic release from sediments (Froelich et al., 1979), hydrothermal vent fluxes (German et al., 2016), and dust input (Arimoto et al., 1985; Shiller, 1997; Boyle et al., 2005). They also are subject to similar removal processes such as biological uptake (Sunda and Huntsman, 1995; 1998; Sunda, 2012), oxidative precipitation (Bruland and Lohan, 2003), flocculation in estuaries as freshwaters with high Fe and Mn concentrations mix with higher-salinity seawater (Sholkovitz et al., 1978; Sholkovitz, 1978), and scavenging (Balistrieri et al., 1981; Martin and Knauer, 1985). Both Fe and Mn have a significant particulate fraction due to a combination of their high concentrations in lithogenic particles, their propensity towards oxidative precipitation, and their abundance within cells in the surface ocean, leading to subsurface remineralization during the decay of organic matter. These commonalities often lead to studies comparing dissolved Fe and Mn distributions, particularly in hydrothermal and margin environments where their coupled enrichments can be used as indicators of a common source flux, often margin sediment- or hydrothermal-derived (Cowen and Bruland, 1985; Landing and Bruland, 1987; Saager et al., 1989; Lewis and Landing, 1991; Sedwick et al., 1997; Sedwick et al., 2000; Bucciarelli et al., 2001; Boyle et al., 2005; Chase et al., 2005; Lam and Bishop, 2008; Noble et al., 2012; Fitzsimmons et al., 2014; Hatta et al., 2015; Fitzsimmons et al., 2017; Sanial et al., 2017; Sherrell et al., 2018). Seminal studies comparing the marine geochemical behavior of these two elements, such as Landing and Bruland (1987), have

set the stage for examining Fe and Mn cycling and transformations in complex and coastal environments.

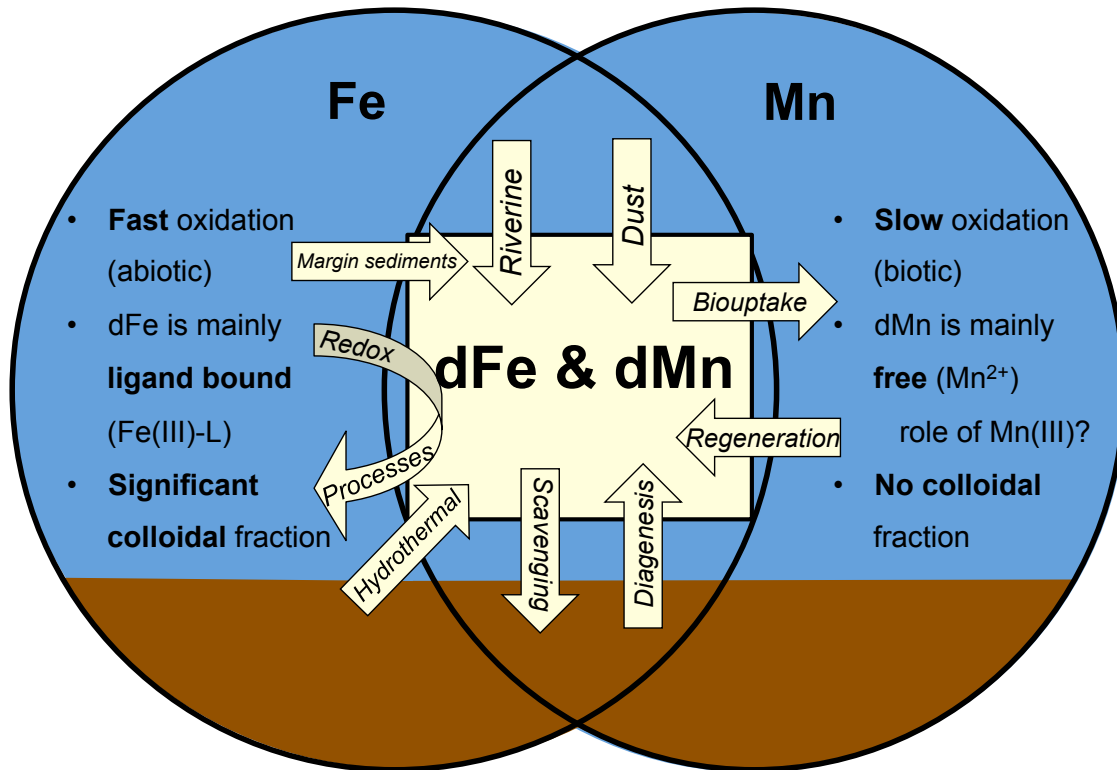


**Figure 4.1** Schematic of the similarities and differences between Fe and Mn highlighted in this study. The two elements share similar sources and sinks but differing chemistries. Blue represents water and brown represents the sediments.

However, despite similarities in their distributions resulting from their shared source fluxes, Fe and Mn do have disparate speciation and reactivity that can cause them to be decoupled in the ocean (Figure 4.1). The best example of this is their oxidation kinetics. While both Fe(II) and Mn(II) are produced during sediment diagenesis (Froelich et al., 1979), Fe(II) oxidizes rapidly and abiotically to Fe(III) oxides in the presence of oxygen, often within minutes in fully oxygenated seawater (Millero et al.,

1987), while Mn(II) oxidizes more slowly to Mn(III)/Mn(IV), and this process often requires microbial mediation (Stumm and Morgan, 1981; Tebo et al., 2004). This plays out as a critical decoupling in surface waters, where dissolved Mn<sup>2+</sup> can be produced by photochemical reduction of MnO<sub>2</sub>(s), and the slow reoxidation kinetics allow dissolved Mn to be retained in the surface ocean to a much more significant extent (Sunda et al., 1983b; Sunda and Huntsman, 1994); in contrast, any photochemical reduction of analogous solid Fe(III) oxyhydroxides would be quickly reversed by reoxidation, preventing surface accumulation of dFe species (Barbeau et al., 2001). Additionally, while both Fe(III) and Mn(IV) are insoluble under seawater conditions (Sunda et al., 1983b; Kuma et al., 1996; Liu and Millero, 2002), only Fe(III) is appreciably stabilized by organic ligands in the water column (Bruland and Lohan, 2003; Gledhill and Buck, 2012). While Mn(III) bound to organic ligands has been found to have a variable contribution to total dissolved Mn in coastal areas, continental margin, and hydrothermal sites (Madison et al., 2013; Oldham et al., 2015; Oldham et al., 2017; Chen et al., 2019), most dissolved Mn in the open ocean is thought to exist in the free Mn<sup>2+</sup> form (Byrne, 2002). Together, these differences in oxidation pathways and speciation can lead to different trajectories and residence times of Fe and Mn in the ocean, including shorter dFe residence times in the upper water column, and longer dFe residence times in the deep water (Landing and Bruland, 1987; Bruland et al., 1994).

While some prior studies have compared the distributions and cycling of the Fe and Mn (Landing and Bruland, 1987; Lewis and Landing, 1991; Chase et al., 2005; Noble et al., 2008; Noble et al., 2012; Hatta et al., 2015; Fitzsimmons et al., 2017;

Cheize et al., 2019), this has not been done in the Arctic Ocean, nor by directly juxtaposing Fe and Mn distributions. The Arctic Ocean is unique compared to these previously studied sites because it is dominated by shallow continental shelves (>50% by area (Jakobsson et al., 2004; Talley et al., 2011)) and is largely isolated because of limited exchange with the Atlantic and Pacific Oceans (Talley et al., 2011). The waters of the Arctic's highly productive Chukchi Shelf, which receives nutrient-rich inputs through the Bering Strait (Jones and Anderson, 1986; Anderson et al., 2013), are carried offshore into the open Western Arctic within the halocline, a high-salinity water mass that forms during sea ice formation from brine rejection of Arctic shelf waters. Arctic shelf waters are in contact with shelf sediments over the shallow Chukchi Shelf, such that the Western Arctic halocline uniquely carries a large sedimentary flux of redox-active metals far into the Canada Basin of the Western Arctic (Nakayama et al., 2011; Cid et al., 2012; Nishimura et al., 2012; Aguilar-Islas et al., 2013; Kondo et al., 2016). The Western Arctic's halocline is also special because, although some algae do grow directly under the sea ice in this region (Sakshaug, 2004; Arrigo et al., 2012), *in situ* vertical remineralization fluxes through the halocline are very limited for metal micronutrients and macronutrients, especially farther away from the shelves where few sinking cells grow under the ice (Middag et al., 2011; Klunder et al., 2012b; Klunder et al., 2012a; Kondo et al., 2016; Jensen et al., 2019). Thus, the Western Arctic's shelf signal remains relatively undisturbed by vertical remineralization inputs from biogenic particles sinking into the central Arctic and can be used to trace the effects of aging shelf fluxes to the open ocean with little correction for other processes.

For these reasons, the Arctic Ocean provides an ideal location in which to examine the contrasting chemistry of Fe and Mn. Here, we present Fe and Mn data from the U.S. Arctic GEOTRACES GN01 transect to examine the effects of long-range transport of Fe and Mn from shelf sources as well as surface oxidation rates. The large spatial scale of our GN01 Western Arctic study provides a critical link between high productivity shelf regimes with open ocean circulation in a rapidly changing environment. Our results show that Fe and Mn have decoupled cycles in the Western Arctic with a distinct three-step pattern of differentiation. We find 1) rapid Fe oxidation to the particulate phase over the Chukchi Shelf compared to Mn due to a difference in oxidation kinetics, 2) rapid removal of both dFe and dMn resulting from interaction with the high particle concentrations over the outer shelf and shelf break, followed by 3) slower scavenging of dFe away from the shelf while dMn remains conserved. This is in line with a common diagenetic source of Fe and Mn that is not equally preserved due to differences in oxidation kinetics and proclivity to scavenging. While these processes have been identified previously, the Western Arctic provides a rare showcase of the stark differences in the geochemical cycling of these two important metals.

### **4.3. Sample Collection and Analysis Methods**

Seawater samples for this study were collected during the 2015 U.S. Arctic GEOTRACES cruise (GN01), which departed from Dutch Harbor, AK aboard the USCGC *Healy* (HLY1502) and continued from 9 August 2015 to 12 October 2015. The cruise track (Figure 4.2) originated in the North Pacific in the Bering Sea and transited north, entering the Arctic Ocean through the Bering Strait and continuing to the North

Pole (“northbound”) along ~170-180°W before returning along 150°W (“southbound”) and terminating on the Chukchi Shelf. Samples were taken in the Canada, Makarov, and Amundsen basins in the Western Arctic along the shelf, within the marginal ice zone, and at shallow-depth ice hole stations. While many stations were full-depth (0-4000 m), only data from the upper 400 m are reported in this study.

Dissolved and particulate trace metal sample collection followed established GEOTRACES protocols (Cutter et al., 2010). Seawater was first collected using a trace metal-clean carousel/CTD (Seabird) with a conductive Vectran-coated cable and 24 x 12 L GO-Flo bottles. Two GO-Flo bottles were tripped per sampling depth on ascent at ~3 m/min and pressurized (~0.5 atm) with HEPA-filtered air upon recovery. One of the two GO-Flo bottles was fitted with a 0.2 µm AcroPak-200 polyethersulfone filter capsule (Pall), and seawater was subsequently filtered into 250 mL acid pre-cleaned low density polyethylene (LDPE) Nalgene bottles following three 10% volume sample rinses of the bottle, cap, and threads. Samples were promptly acidified to pH<2 (0.012 M HCl, Optima, Fisher Scientific) (Fitzsimmons and Boyle, 2012)).

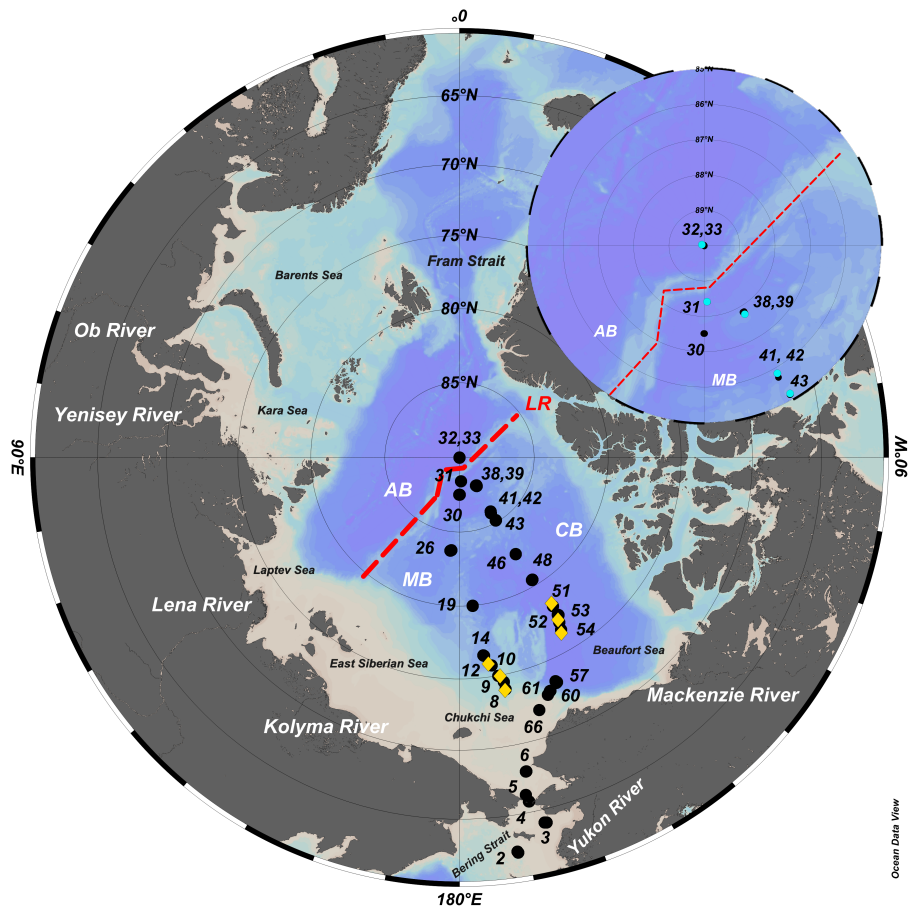


**Figure 4.2** U.S. GEOTRACES Arctic GN01 transect with relevant stations, rivers, seas, and bathymetric features identified. Blue dots = ice Stations 31, 33, 39, 42, 43, gold diamonds = MIZ Stations 8, 9, 10, 12, 52, 53, 54, black dots = full depth stations. AB = Amundsen Basin, MB = Makarov Basin, CB = Canada Basin, GR = Gakkel Ridge, LR = Lomonosov Ridge. Stations 2-5 are considered “Bering Strait” while stations 6-8, 66-61 are “Chukchi Shelf.” Stations 8-31 are “northbound” transect, Station 32 is the North Pole, and Stations 38-66 are “southbound” transect. More detail can be found in Jensen et al. (2019), Figure 1.

The second GO-Flo bottle was used to collect particle samples, following the techniques of Planquette and Sherrell (2012). Immediately before sampling, each GO-Flo was gently inverted to homogenize the particle distribution and then fitted with a 0.45  $\mu\text{m}$  polypropylene Supor filter in a Swinnex filter holder. Process blanks were

generated by passing filtered seawater ( $<0.2 \mu\text{m}$  AcroPak filtered) through the same Supor-substrate filters used for samples.

Surface and near-surface ice hole samples (Stations 31, 33, 39, 43) were collected by small boat or through holes in the sea ice at 1, 5, and 20 m using a polypropylene high-head battery-powered motor diaphragm pump with  $\frac{1}{2}$ -inch FEP-lined Tygon tubing (Cole Parmer) fitted with a pre-cleaned  $0.2 \mu\text{m}$  AcroPak filter. Samples were filtered on the ice into a 25 L acid-cleaned LDPE carboy and immediately subsampled into clean LDPE bottles on the ship.

#### **4.3.1. Ultrafiltration**

Following collection, filtered ( $0.2 \mu\text{m}$ ) seawater was immediately brought to a shipboard clean lab (plastic “bubble” under positive pressure via HEPA-filtered air) for further ultrafiltration into soluble size fractions. Ultrafiltration using Anopore filters was carried out at all stations and depths where dissolved samples were collected, completing ultrafiltration within 3 hours of collection to prevent bottle effects (Jensen et al., 2020). This direct ultrafiltration system employed the use of custom-made filtration rigs and vacuum filtration ( $<0.5 \text{ atm}$ ) and used  $0.02 \mu\text{m}$  Anodisc filters (47 mm Anopore membranes, Whatman) that were cleaned on the rig with  $\sim 50 \text{ mL}$  dilute HCl ( $\sim 0.005 \text{ M}$ , pH  $<2$ , Optima) followed by  $\sim 50 \text{ mL}$  ultrapure MQ water, and finally conditioned with  $\sim 50 \text{ mL}$  of the seawater sample, all immediately before filtering the sample (Fitzsimmons and Boyle). Seawater ( $<0.2 \mu\text{m}$ ) was poured onto the filtration rig under vacuum ( $<0.5 \text{ atm}$ ) until each LDPE (Nalgene) 60 mL bottle was filled following a 10% rinse of the bottle, cap, and threads. All samples were promptly acidified to pH  $<2$

(0.012 M HCl, Optima, Fisher Scientific) (Fitzsimmons and Boyle, 2012)). Colloidal concentrations ( $cFe$ ) were calculated by subtracting the soluble Fe concentration ( $sFe$ , permeate) from the dissolved concentration, i.e.  $cFe = dFe - sFe$ .

#### 4.3.2. Dissolved analyses

Acidified samples were allowed to sit for at least 9 months following acidification, allowing adequate time for complete desorption of metals from bottle walls (Jensen et al.). Following this period, samples were pre-concentrated for dissolved Fe and Mn using a SeaFAST-pico system (ESI, Omaha, NE) at Texas A&M University using an isotope dilution and standard curve method modified from Lagerström et al. (2013) and described in (Jensen et al., 2020). Other elements concurrently analyzed were Zn and Cd, already published (Jensen et al., 2019; Zhang et al., 2019), and Ni, Cu, and Pb, which will be published elsewhere. For each sample, a 10 mL aliquot of seawater was weighed and spiked with a known isotopic composition of  $^{57}Fe$  and loaded into the SeaFAST system. Manganese is a monoisotopic element, and so instead of isotope dilution, Mn was quantified using a six-point Mn standard curve spanning 0 to 10 nmol/kg (and further up to 80 nmol/kg for shelf stations) made in matrix-matched, low-metal seawater and also processed through the SeaFAST system. Once loaded onto the SeaFAST, all samples were buffered in-line to pH ~6.3 with an ammonium acetate buffer (Optima, Fisher Scientific) and loaded onto a column fitted with Nobias-chelate PA1 resin and rinsed with buffered ultrapure water to remove any salts. Following metal extraction onto the resin, samples were back eluted with 10% (v/v) nitric acid ( $HNO_3$ , Optima) into 400  $\mu$ L of eluent (25x pre-concentration factor) for analysis. Pre-

concentrated eluents were subsequently analyzed in medium resolution for Fe and Mn on a Thermo Element XR high-resolution inter-coupled plasma mass spectrometer (HR-ICP-MS) housed at the R. Ken Williams Radiogenic laboratory at Texas A&M University. Accuracy, precision and limits of detection of these measurements are summarized in Table 4.1.

**Table 4.1** Reported certified SAFe D1, D2, and S values as well as blanks and detection limits for dissolved Fe and Mn. Reported certified and consensus values as well as blanks and detection limits for Total and Labile particulate Fe and Mn. \*value for dMn from SAFe D2 consensus (May 2013).\*\*Informational, non-certified value reported by CRM distributor.

Sample	(nmol/kg)			Sample	(µg/g)		
	n	Fe	Mn		n	Total Fe	Total Mn
<b>SAFe D1</b>	35	0.602	0.395	<b>BCR-414</b>	5	<b>1737</b>	<b>253</b>
<b>1SD</b>		0.059	0.02	<b>1SD</b>		<b>41</b>	<b>10</b>
Consensus (May 2013)*			0.35				299
<b>1SD</b>		0.67	0.05	Certified		1850**	
		0.04		<b>1SD</b>		190	12
<b>SAFe S</b>	4	0.085	0.869	<b>NRC</b>	5	<b>41800</b>	<b>322</b>
<b>1SD</b>		0.038	0.011	<b>MESS-3</b>		<b>1SD</b>	<b>1700</b>
Consensus (May 2013)		0.093	0.79			43400	324
<b>1SD</b>		0.008	0.06	Certified		1100	12
<b>GSP</b>	12	0.159	0.757	<b>NRC</b>	4	<b>41300</b>	<b>1070</b>
<b>1SD</b>		0.03	0.025	<b>PACS-2</b>		<b>1SD</b>	<b>300</b>
Consensus (2019)		0.155	0.778			40900	960
<b>1SD</b>		0.045	0.034	Certified		600	40
<b>GSC</b>	12	1.65	2.109				
<b>1SD</b>		0.062	0.11				
Consensus (2019)		1.535	2.18				
<b>1SD</b>		0.115	0.075				

**Table 4.1** Continued.

Sample	n	(nmol/kg)		n	(nmol/kg)	
		Fe	Mn		Total Fe	Total Mn
Average blank	31	0.0635	0.000478	21	0.044	0.0033
Detection limit (3 x 1SD of blank)	29	0.0174	0.000135	21	0.094	0.0073

### 4.3.3. Particulate analyses

All filters for particle analyses were stored frozen until they were digested in acid-cleaned perfluoroalkoxy alkane (PFA) vials (Savillex) by adding 2 mL of a mixture of 4 M HCl, 4 M HNO<sub>3</sub>, and 4 M hydrofluoric acid (Optima, Fisher Scientific) and heated at 110°C for four hours (Ohnemus and Lam, 2015; Twining et al., 2015). The digest solution was carefully poured into a second Savillex vial without transferring the Supor filter itself, and 60 µL of concentrated H<sub>2</sub>SO<sub>4</sub> (18.4 M; Fisher Optima grade) and 20 µL of H<sub>2</sub>O<sub>2</sub> (9.8 M; Fisher Optima grade) were added to the solution to break down any Supor filter fragments. The solution was taken to dryness and the residue re-dissolved with 0.32 M HNO<sub>3</sub> (Fisher Optima or double-distilled grade) containing 10 ppb In to correct for matrix effects and instrumental drift. The analytical assessments including blanks and reference material recoveries are shown in Table 4.1. All particulate values reported here are the non-lithogenic or “excess” fraction (shown here as p[Metal]<sub>xs</sub>), determined by applying the metal/Al crustal abundance ratio from Table 4.1 of Rudnick and Gao (2003) and then multiplying by the pAl concentration, assuming

all pAl is lithogenic, and subtracting this lithogenic term from the overall particulate metal concentration (ex.  $pFe_{xs} = [pFe] - (Fe/Al)_{crustal} \times [pAl]$ ). This lithogenic correction was an average of  $7 \pm 3\%$  and  $7 \pm 13\%$  of the total particulate phase for both particulate Fe and Mn, respectively, across the shelf and offshore waters.

#### **4.3.4. Intercalibration of dissolved Fe and Mn datasets**

The U.S. GEOTRACES GN01 effort to measure dissolved metals comprised multiple laboratories, methods, and analyses. Dissolved Fe and Mn analyses took place at Texas A&M University, the University of Southern California, and shipboard by the team from the University of Hawaii (methods described in the Supplementary Information). The three dissolved metal datasets agreed well at the subset of stations where they were intercalibrated (Figure 4.3), and the Texas A&M University dataset is reported in this manuscript for convenience.

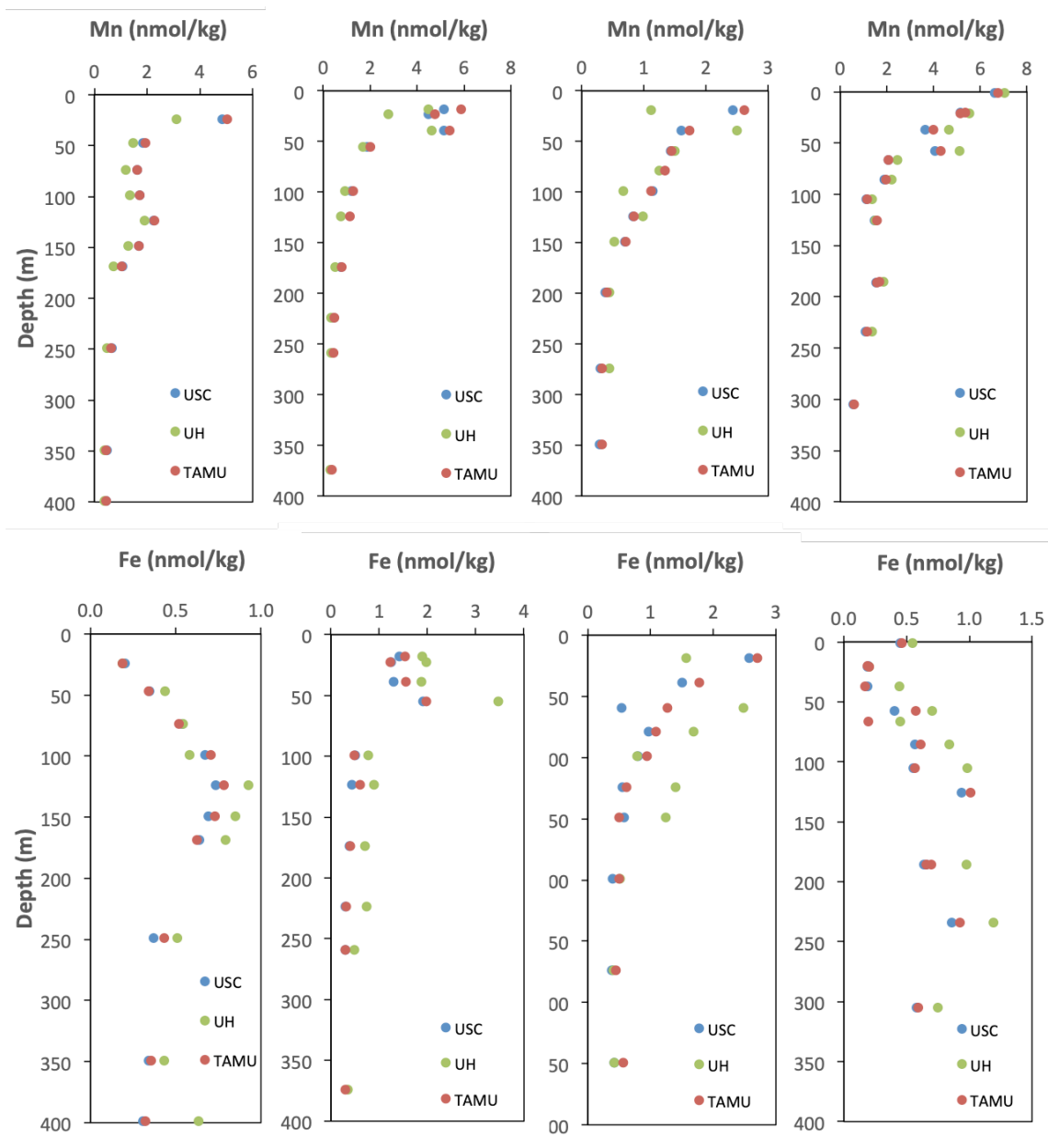


**Figure 4.3** Intercalibration across GN01. Stations 19, 30, 32, 57 (left to right, upper 400m) showing overlap among TAMU (red), USC (blue) and UH (green) labs for Mn (top panels) and Fe (bottom panels). TAMU data generally agreed best with USC data and fell between USC and UH data, lending these data to be used for this manuscript. A brief description of the methods used in each laboratory is found below and in the Methods section of the main manuscript.

#### **4.3.5. Hydrographic analyses**

Salinity, macronutrients and other hydrographic variables were determined shipboard by the Scripps Institute of Oceanography Ocean Data Facility (SIO ODF) team. Temperature and pressure for all samples were taken directly from the trace metal CTD (Seabird 911+) sensors. Bottle salinity, collected from the same GO-Flos used for metal analyses, was measured unfiltered at room temperature on a shipboard Guideline Autosal 8400B salinometer. Dissolved macronutrients nitrate, phosphate, and silicate were analyzed shipboard at room temperature on a Seal Analytical continuous-flow AutoAnalyzer 3 (Hydes et al., 2010). Depth-matched dissolved oxygen samples were collected using a 36-place, ~10 liter Niskin bottle rosette equipped with a Seabird SBE9+ CTD and other sensors operated by the SIO ODF team and analyzed shipboard using a Winkler titration method (Carpenter, 1965; Culberson et al., 1991). All surface and contoured sections in this paper were made using Ocean Data View software (Schlitzer, 2016).

### **4.4. Results**

#### **4.4.1. Hydrography**

The hydrography of the upper 400 m of the Western Arctic is defined by water masses with unique thermohaline and macronutrient structure (Aagaard et al., 1985; Rudels, 2015). Briefly, along the GN01 section, four major water masses were observed (Jensen et al., 2019): 1) the surface polar mixed layer (sPML) extending 0-25 m (salinity, S of 25-31), 2) the upper halocline layer (UHL), extending ~50-150 m (S of 31-33.1), 3) the lower halocline layer (LHL) waters extending ~150-400 m (S of 33.1-34.7),

and 4) the Makarov/Amundsen basins' single halocline, extending from ~50-300 m (S of 31-34.3). Importantly, the UHL and LHL were observed only in the Canada Basin (GN01 Stations 10-19, 46-60). The UHL results from nutrient-rich Pacific waters entering through the shallow Bering Strait and becoming entrained via brine rejection into this subsurface water mass (Shimada et al., 2005; Woodgate et al., 2005); as such, we define the UHL as having  $[\text{Si}] > 25 \mu\text{mol/kg}$  (Jones and Anderson, 1986; Macdonald et al., 1989; Anderson et al., 2013) and centering on S of 32.8 (Figure 4.4). In contrast, the LHL originates in the Eastern Arctic on the Eurasian shelves and can be traced using a minimum in the conservative tracer NO ( $\text{NO} = [\text{O}_2] + 9[\text{NO}_3^-]$ ), following the work of Jones and Anderson (1986). Along GN01, the LHL has depths 150-400 m under the UHL near the shelf and shoals to depths of 100-200 m further offshore. Similarly, the single halocline was found only in the Makarov and Amundsen basins (Stations 26-43), and was also formed on Eurasian shelves and advected into both the Amundsen and then the Makarov across the Lomonosov Ridge (Rudels, 2015).

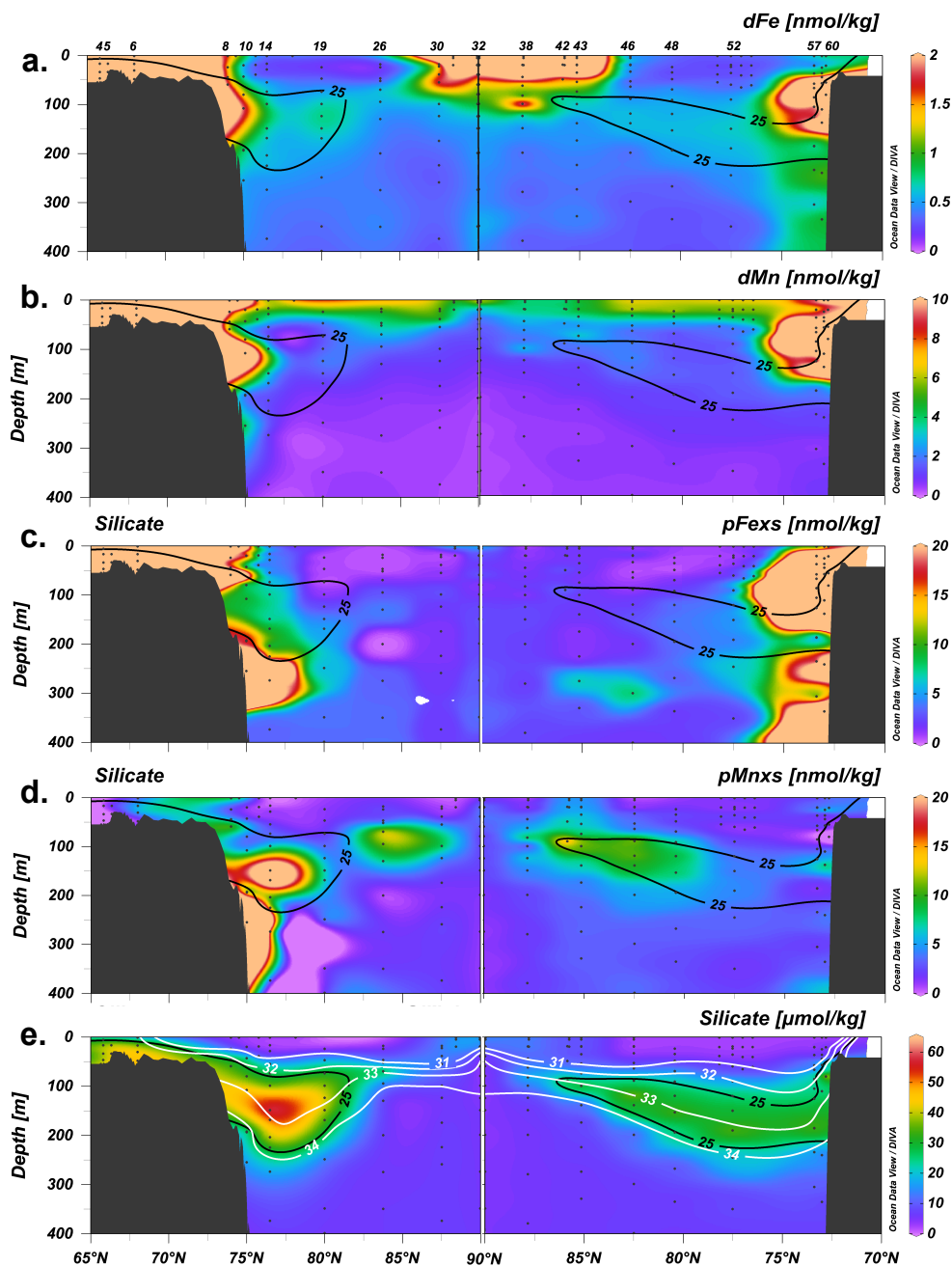


**Figure 4.4** Sectional plots of a)  $d\text{Fe}$ , b)  $d\text{Mn}$ , c)  $p\text{Fe}_{\text{XS}}$  (particulate Fe excess), d)  $p\text{Mn}_{\text{XS}}$  (particulate Mn excess), e) salinity in the upper 400m. Silicate contour line for  $[\text{Si}] = 25 \mu\text{mol/kg}$  is overlaid in black to denote the bounds of the Upper Halocline layer (UHL; see text) and in e) the salinity contour is shown in white. Transect progressed northbound from Station 4 to Station 30 (left) and then southbound from the North Pole (Station 32) to the shelf break (Station 60, right).

#### 4.4.2. Overview of Fe and Mn observations

Dissolved and excess particulate Fe and Mn concentrations (shown as dFe, pFe<sub>xs</sub>, dMn, pMn<sub>xs</sub>) varied by orders of magnitude in the upper 400 m of the Western Arctic, demonstrating the inherent diversity in source and evolution of these redox-sensitive metals (Figure 4.4). Nonetheless, the concentrations reported here compare well with previous reports of the geochemistry of the Canada Basin (Cid et al., 2012; Aguilar-Islas et al., 2013; Kondo et al., 2016), as well as in the Makarov and Amundsen basins (Middag et al., 2011; Klunder et al., 2012b).

The widest concentration range was found along the dynamic Chukchi Shelf and Bering Strait (Stations 2-8, 61-66, depth 0 to 80m), where dFe ranged from 0.24 to 19.6 nmol/kg, dMn from 3.81 to 197 nmol/kg, non-lithogenic pFe<sub>xs</sub> from 0 to 2130 nmol/kg, and pMn<sub>xs</sub> from 0 to 17.4 nmol/kg. Within surface waters (Figure 4.5), dFe decreased rapidly from a broad average of  $3.19 \pm 2.65$  nmol/kg over the shelf/strait stations to  $0.521 \pm 0.100$  nmol/kg off shelf (Stations 10-12, 57-60), with an increase again at the North Pole due to the Transpolar Drift current, which is the subject of another paper (Charette et al., 2020). In contrast, dMn remained more consistently elevated, decreasing progressively from  $23.6 \pm 10.8$  nmol/kg over the shelf/strait to 2.61 nmol/kg at the North Pole. In the particulate fraction, surface pFe<sub>xs</sub> was high over the shelf (as high as 346 nmol/kg at Station 5) and decreased dramatically off-shelf, to a minimum of 0.33 nmol/kg (Station 31), while surface pMn<sub>xs</sub> was quite low and inconsistently distributed, roughly decreasing from 10.0 nmol/kg along the shelf to negligible concentrations in the

central Arctic (Figures 4c,d). Thus, overall surface Fe was dominated by particles, while surface Mn was dominated by dissolved species (Figure 4.5b).

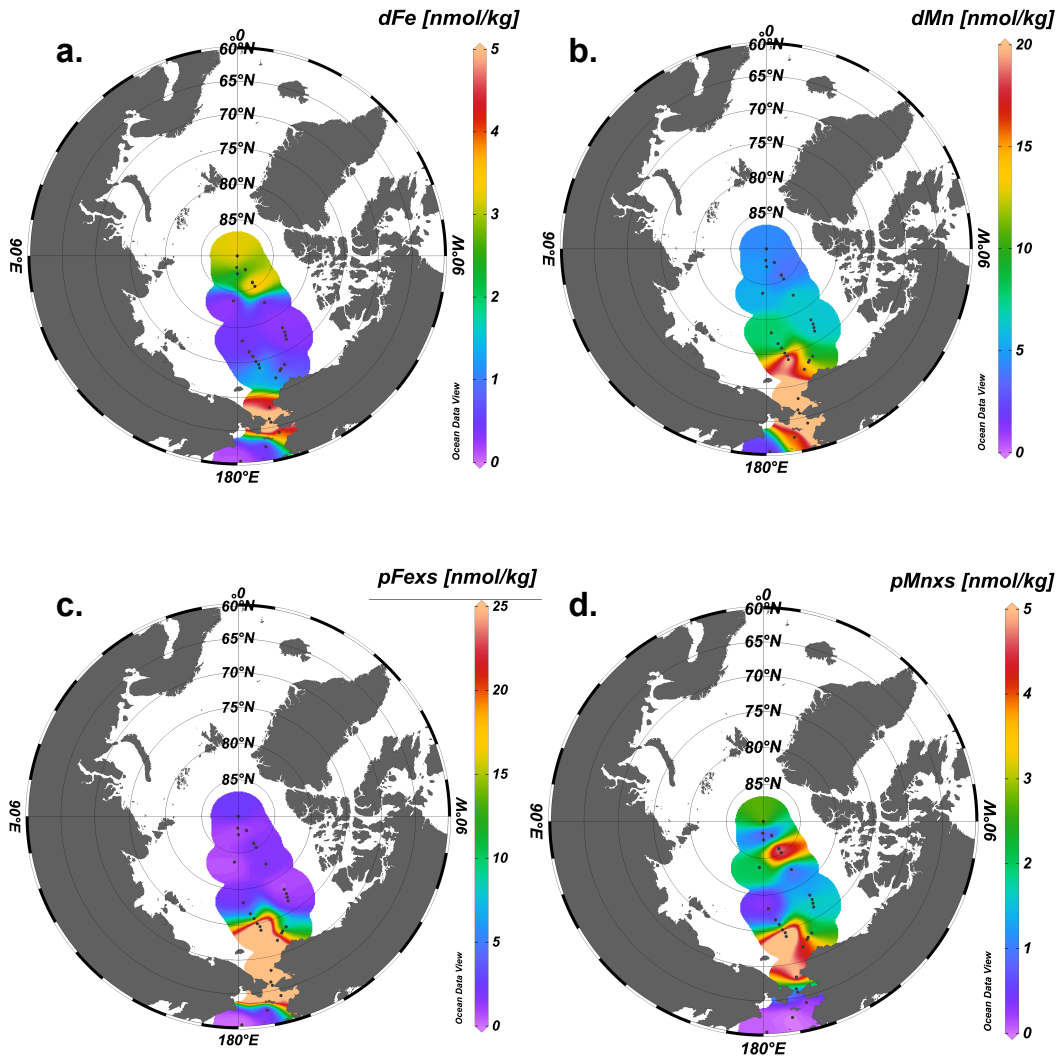


**Figure 4.5** Surface (0-20m) plots of a) dFe, b) dMn, c) pFexs, d) pMnxs. All scale bars are in nmol/kg. Stations are highlighted by black dots.

Within the Canada Basin UHL ( $[\text{Si}] > 25 \mu\text{mol/kg}$ , Stations 8-19, 46-60), dFe and dMn showed local maxima (Figure 4.4). In the UHL, dFe ranged from 0.45 nmol/kg

to 3.82 nmol/kg (average  $0.96 \pm 0.73$  nmol/kg), and the contribution of dFe to the “total” Fe phase (dFe + pFe<sub>xs</sub>) phase changed with distance from the shelf break (Figure 4.6). The dFe fraction composed <20% of total Fe at stations within 900 km of the shelf break (Stations 8, 10, 14, 48, 52, 57, 60) and increased to 15-63% of total Fe at distances greater than 900 km (Stations 19, 46). Likewise, dMn ranged from 1.19 to 25.1 nmol/kg (average  $4.38 \pm 5.98$  nmol/kg) comprising 20-85% of total dMn (Figure 4.6b) within 900 km of the shelf break and a smaller 20-50% at distances greater than 900 km. Particulate Fe ranged from 0.311 to 142 nmol/kg (average  $15.77 \pm 31.60$  nmol/kg) and pMn<sub>xs</sub> from 1.71 to 37.0 nmol/kg (average  $8.51 \pm 8.56$  nmol/kg).

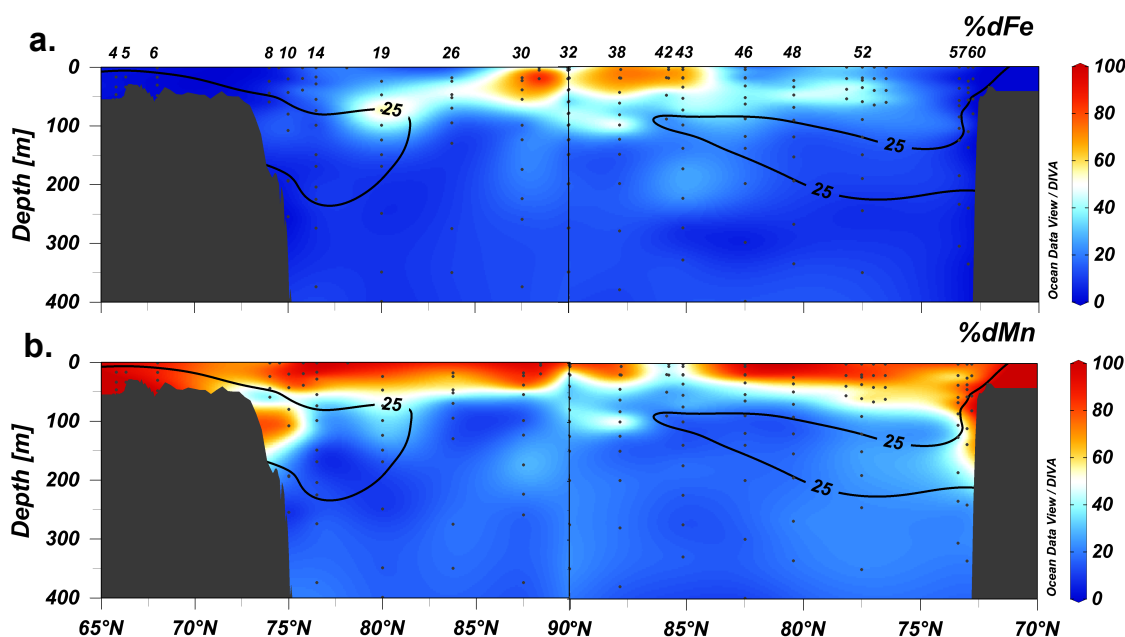


**Figure 4.6** Plots of a)  $\%dFe = dFexs/(dFe + pFexs)$  and b)  $\%dMn = dMnxs/(dMn + pMnxs)$  across the upper 400m of the transect moving northbound (left panel) to the North Pole and then southbound (right panel). All percentage values range 0 to 100% to show the influence of the dissolved phase on the total (dissolved and particulate) metal content. Silicate contours in black ( $[Si] = 25 \mu\text{mol/kg}$ ) denote the bounds of the UHL.

In the deeper Canada Basin LHL (150-400 m), concentrations for all species were, on average, lower than in the UHL. Dissolved Fe averaged  $0.611 \pm 0.246$  nmol/kg, dMn at  $1.10 \pm 0.39$  nmol/kg, pFe<sub>xs</sub> at  $10.0 \pm 10.6$  nmol/kg, and pMn<sub>xs</sub> at  $4.88 \pm 2.35$  nmol/kg. Within the Eurasian shelf-influenced Makarov/Amundsen halocline (Stations 26, 30, 32, 38, 43), we eliminated any depths with clear transpolar drift (TPD) influence; this surface current dominated dFe and dMn patterns in the upper 80 m of the water column (Charette et al.). For reference, at the TPD influenced depths, dFe averaged  $0.54 \pm 0.09$  nmol/kg, dMn  $1.71 \pm 0.85$  nmol/kg, pFe<sub>xs</sub>  $2.43 \pm 1.01$  nmol/kg, and pMn<sub>xs</sub>  $8.97 \pm 4.61$  nmol/kg.

#### **4.4.2.1. Marginal Ice Zone (MIZ)**

Sea ice can be an important source of dissolved and particulate Fe and Mn in the Arctic and other polar regions. Previous studies have shown elevated dFe in sediment-laden Arctic sea ice (up to  $\sim 3600$  nmol/kg, (Tovar-Sánchez et al., 2010)) and point to sea ice melting as a potentially significant dFe and pFe source (Measures, 1999; Aguilar-Islas et al., 2008; Tovar-Sánchez et al., 2010; Kanna et al., 2014). During GN01, reported dFe concentrations in sea ice ( $1.1 \pm 1.0$  nmol/kg (Marsay et al., 2018)) were very low, likely due to desalination of first-year ice so late in the summer season (Nakawo and Sinha, 1981; Vancoppenolle et al., 2006). In contrast to Fe, little is known about Mn in Arctic sea ice, though both dMn and pMn are known to be quite low in Antarctic sea ice (less than 1.5 and 5 nmol/kg, respectively (Lannuzel et al., 2011)). Dissolved Mn was more elevated in sea ice from the central Arctic during GN01 ( $6.0 \pm 4.2$  nmol/kg (Marsay et al., 2018)), despite desalination.

During GN01, sea ice met open ocean water near the Chukchi Shelf break at what is termed the Marginal Ice Zone (MIZ). The fraction of each water sample that derives from melted sea ice was mapped in the MIZ using oxygen isotopes (Newton et al., 2013), here referred to as fractional ice melt (“fim”). Fractional ice melt was highest across stations 8-17 (northbound) and 51-57 (southbound), showing a 1.5 – 23% contribution from sea ice melt to total water budgets at these stations. At all ice-influenced stations, we assessed the relationship between dFe, dMn, pFe<sub>xs</sub>, and pMn<sub>xs</sub> with fim in the upper 1-10 m (Figure 4.7) to determine whether ice was a source or diluent of each metal and whether surface metals reflected conservative mixing between surface seawater and ice melt (e.g. straight line) or whether there was non-conservative metal addition from sea ice sediments or removal via biological uptake in the MIZ (e.g. curved lines). One caveat is that shallow Shelf Stations 8-10 (shown as open circles in Figure 4.7) were still likely influenced by shelf inputs of dFe, dMn, and pFe<sub>xs</sub>, and thus the metal concentrations may not be attributable solely to sea ice fluxes; thus, we have removed those stations from our sea ice melt analysis.

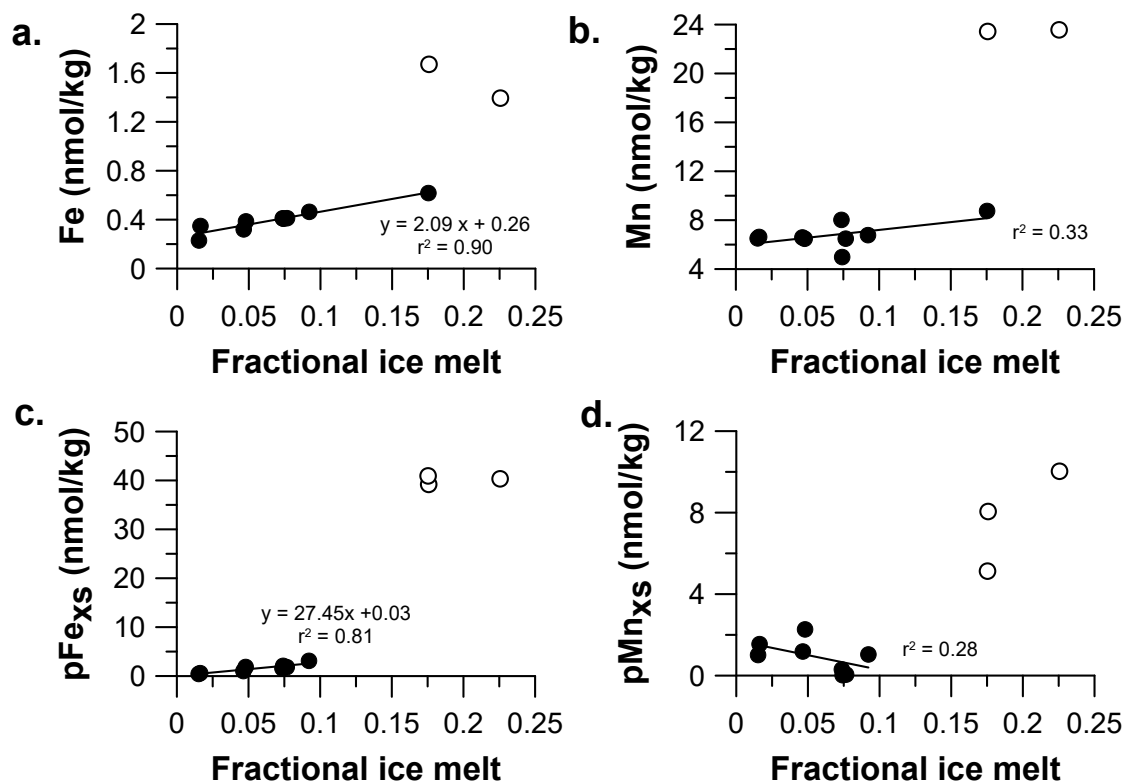


**Figure 4.7** Plots of a) dissolved Fe, b) dissolved Mn, c) particulate Fe excess, and d) particulate Mn excess in the surface at MIZ stations (8-17, 51-57) against fractional ice melt (fim = melted sea ice water/total water present from all sources). Stations 8-9 (Fe, Mn) or 8-10 (pFe<sub>xs</sub>, pMn<sub>xs</sub>) (open circles) have high shelf influence and values that fall outside the range of the other stations (12-17, 51-57, closed circles) and were therefore omitted from the regression.

Dissolved Fe and pFe<sub>xs</sub> showed positive linear relationships with fim (Figure 4.7 a, c with shelf stations excluded), indicating a clear flux from sea ice melt. However, the derived pure sea ice (fim=1.0) end-member of these relationships of 2.35 nmol/kg for dFe and 27.5 nmol/kg for pFe<sub>xs</sub> were on the low end of published sea ice estimates for Fe, which for Bering Shelf sea ice is 3-376 nmol/kg for dFe and 75-7,500 nmol/kg for total pFe (Aguilar-Islas et al., 2008). However, the dFe sea ice end-members is above the dFe range for GN01 central Arctic sea ice reported by Marsay et al. 2018 for GN01 (1.1 ± 1.0 nmol/kg; (Marsay et al., 2018)). Note that during the GN01 cruise, we did not see

any visual evidence of “dirty ice”, which might account for our low sea ice dFe values, relative to those in previous studies.

This highlights the fact that while there is a sea ice source inferred for dFe and pFe on the basis of their linear relationships with fim, the fluxes from sea ice were small, especially in contrast to the large fluxes from the continental shelf nearby (Figure 4.7, open symbols). We also note that while the mostly linear relationships ( $r^2 = 0.90$  and  $0.81$  for dFe and pFe<sub>xs</sub>, respectively) between Fe phases and fim indicate a relatively conserved source from sea ice, our narrow observed fim range of 2.5-17.5% ice melt cannot rule out curvature in these trends over a wider fim range, which might result from biological uptake, scavenging of the dFe, or aggregative sinking losses of the pFe. In contrast to Fe, dMn and pMn<sub>xs</sub> did not have linear correlations with fim (Figure 4.7b,d;  $r^2 = 0.33$  and  $0.28$ , respectively) likely due to high inputs of both on the shelf, unrelated to sea ice melting. Thus, it appears that dissolved and excess particulate Fe were sourced from sea ice to the MIZ during GN01, based on this correlation, while dMn and pMn<sub>xs</sub> had high shelf fluxes that overwhelmed any potential Mn supply to MIZ waters from sea ice.

#### **4.4.2.2. Relationship to nutrients and other metals**

Since dissolved Fe is an essential micronutrient for phytoplankton (Bruland and Lohan, 2003), we might expect that dFe would exhibit some correlation with other nutrients, particularly in the upper 400 m where biological cycling may have an influence. This is true on the shelf where there is a correlation between silicate and dFe ( $r^2 = 0.51$ , yellow circles, Fig. S2a). Likewise, dMn and dFe were strongly correlated ( $r^2$

= 0.88) over the shelf (yellow circles, Figure 4.8c) highlighting a common source that appears to overwhelm any biological processes on the shelf. Dissolved Fe and  $pFe_{xs}$  were also well correlated along the shelf ( $r^2 = 0.74$ , Figure 4.8d) and within the UHL ( $r^2 = 0.95$ , Figure 4.8d), although  $dMn$  and  $pMn_{xs}$  are not (Figure 4.8e).

However, within the UHL,  $dFe$  showed a very low ( $r^2 < 0.10$ ) correlation to any of the major macronutrients (Figure 4.9). Even silicate, a well-known tracer of UHL waters (Anderson et al., 2013) where  $dFe$  is also elevated (Figure 4.4), showed no strong correlation to Fe within the UHL (red circles in Figure 4.8 a). Away from the shelf in the UHL, we found that neither Fe nor Mn correlated with any major macronutrient in this study (Figure 4.9), though they continued to be correlated with each other throughout the UHL ( $r^2 = 0.85$ ), indicating their common shelf source.

Given this low correlation to biologically-cycled macronutrients, there is little evidence of *in situ* remineralization fluxes of  $dFe$  and  $dMn$  to offshore GN01 sites, likely resulting from low primary production under the sea ice at this time of year. This inference of low remineralization supply is also supported by the fact that profile shapes for many metals and macronutrients (reported for dissolved zinc in Jensen et al. (2019)) do not match the classic “nutrient-type” curves (Figure 4.4; Jensen et al. (2019)). Instead, the Arctic appears to be dominated by large lateral fluxes of metals from the wide Arctic shelves. This confirms that the Western Arctic behaves as a useful template with which to examine  $dFe$  and  $dMn$  redox and transport behaviors, without overprinting by significant vertical biological fluxes.

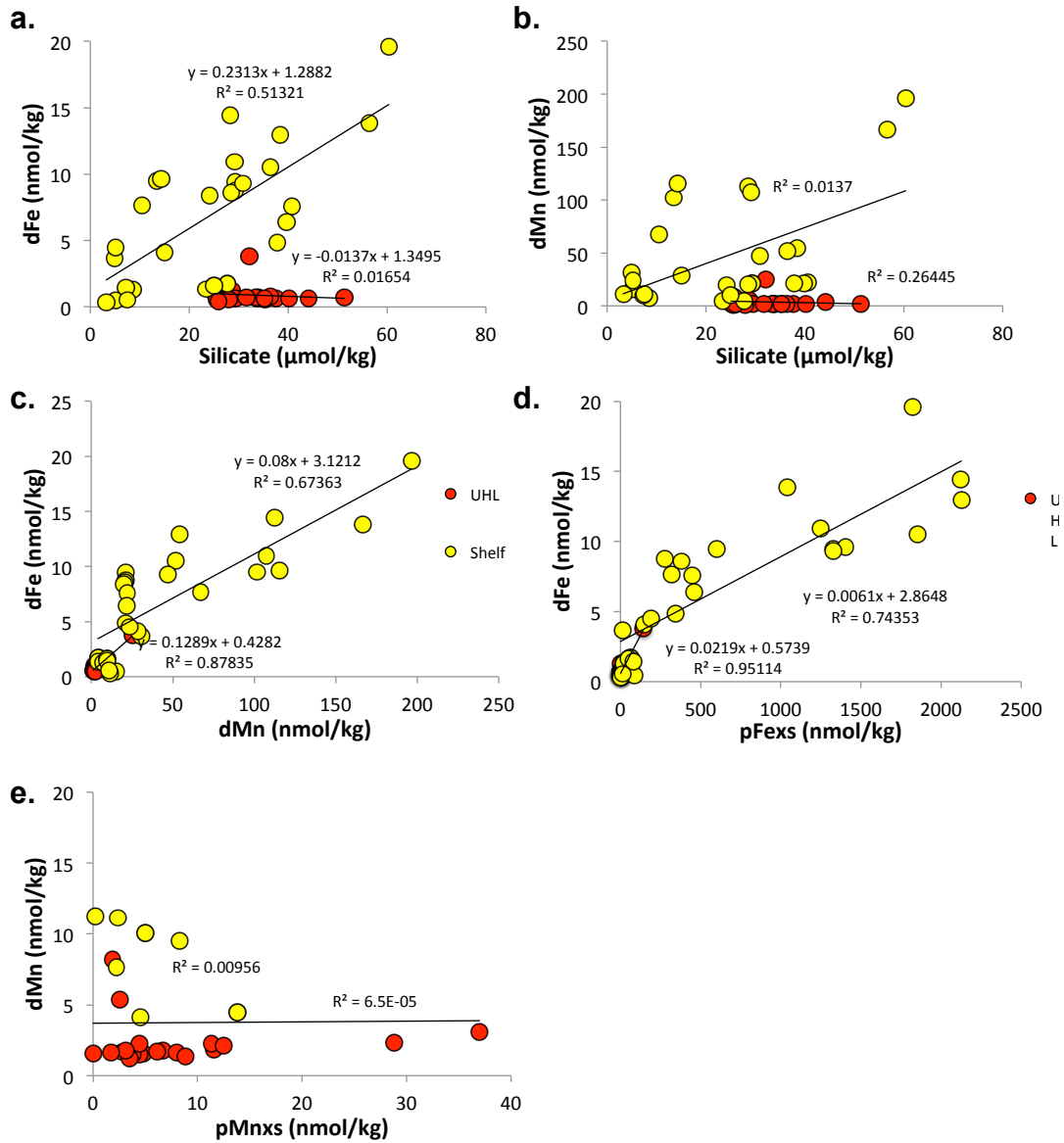


**Figure 4.8** Major elements along the shelf and UHL. a) dFe and b) dMn vs. silicate along the shelf and within the UHL, c) dFe vs dMn, d) dFe vs pFexs, e) dMn vs pMnxs along the shelf (yellow) and within the UHL (red). If the relationship is significant ( $r^2 > 0.5$ ), the linear regression is included. If the relationship is not significant, the accompanying  $r^2$  is noted.

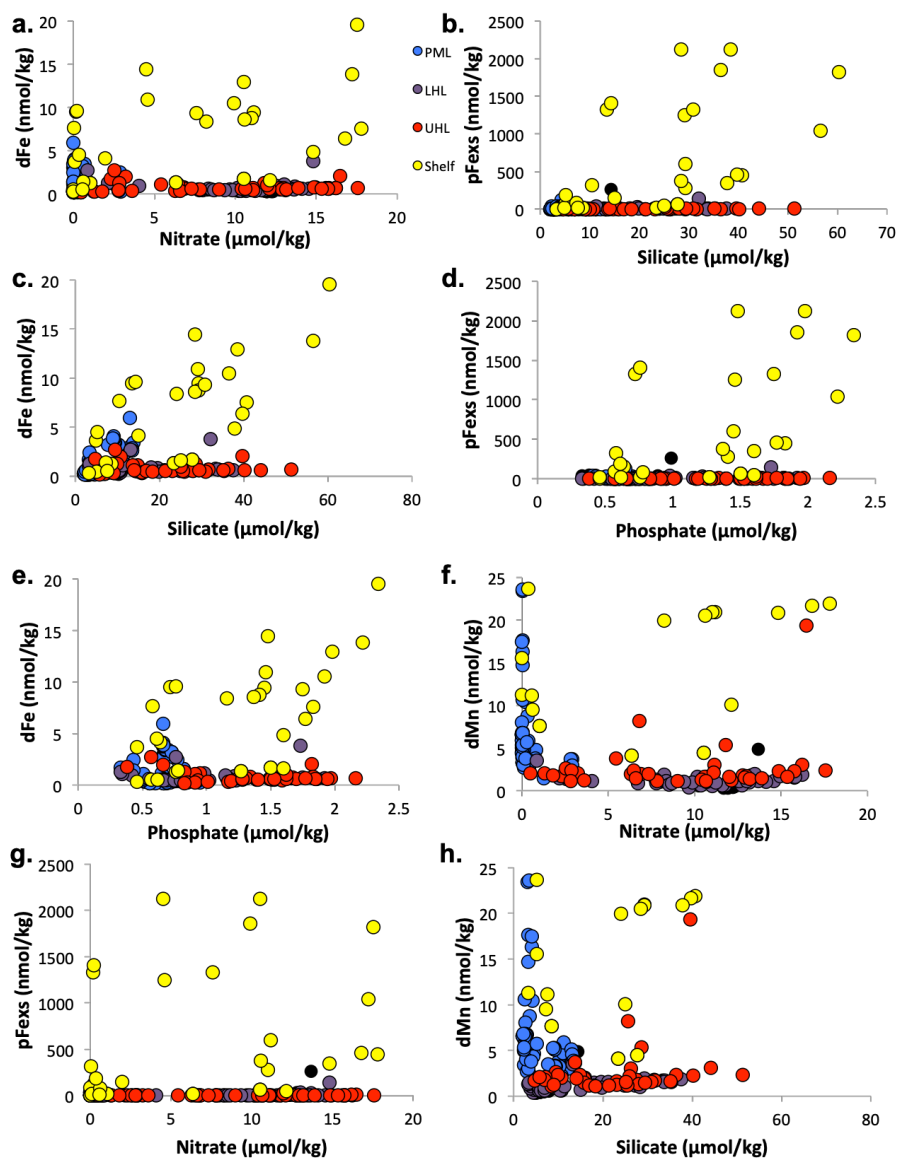


**Figure 4.9** Plots in the upper 400 m of GN01 of Fe, Mn against macronutrients. dFe vs. a) nitrate, b) silicate, c) phosphate, pFexs vs. d) nitrate, e) silicate, f) phosphate, and dMn vs. g) nitrate, h) silicate, i) phosphate and pMnxs vs. j) nitrate, k) silicate, l) phosphate. Data are grouped by the major water masses in upper 400m, PML (polar mixed layer) = blue, LHL (lower halocline layer) = purple, UHL (upper halocline layer) = red, shelf = yellow.

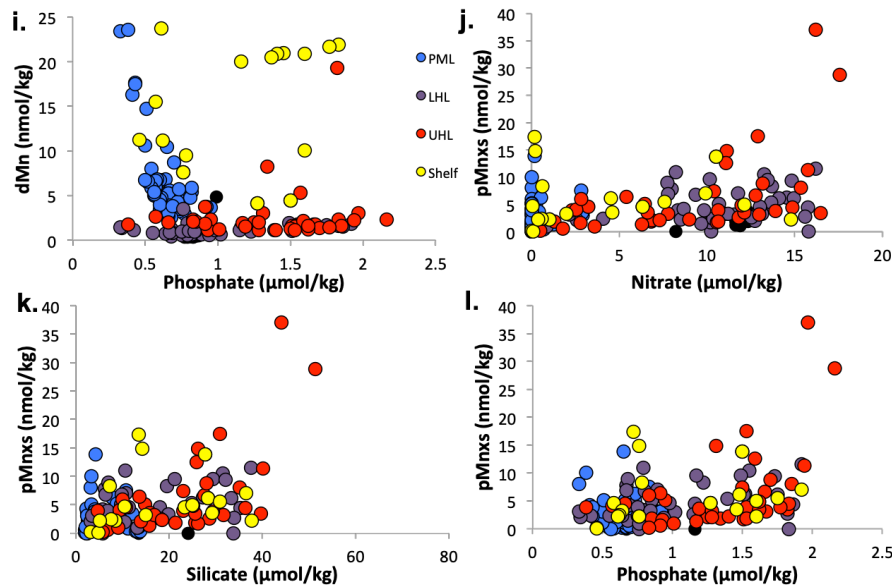


Figure 4.9 Continued.

In fact, the low chlorophyll observed along GN01 basin stations (Whitmore et al., 2019) coupled with low surface dFe offshore in the central Canadian and Makarov basins could be indicative of Fe limitation of surface primary producers. Recent work in the Eastern Arctic demonstrated the potential for Fe limitation in the Nansen Basin where surface dFe concentrations are very low (Rijkenberg et al., 2018). Rijkenberg et al. (2018) used the tracer  $Fe^*$  ( $Fe^* = [dFe] - (Fe:N) \times [N]$ ) to evaluate the potential for Fe limitation, where  $Fe^* < 0$  suggests possible Fe limitation and Fe:N is the biological uptake ratio of Fe to nitrate ( $N = [NO_3^-]$ ). They defined two scenarios using cellular ratios of Fe:P measured in Southern Ocean phytoplankton under Fe stress conditions and converted these to Fe:N using the N:P ratio from the water column in their study sites. Following this same procedure within their two extreme scenarios of Fe stress/limitation, we conclude that there is no potential Fe limitation along GN01 in the Canada and

Makarov basins (Figure 4.10). This is supported by relatively high Fe:P ratios measured in cells along GN01, suggesting that Fe uptake by phytoplankton cells is not restricted, as would be expected under Fe stress (Twining et al., 2017).

#### **4.4.3. Oxidation differences between Fe and Mn along the Bering and Chukchi shelves**

The Chukchi Shelf and its influence on the UHL is the most obvious dissolved metal feature in the Western Arctic Ocean, particularly within the Canada Basin (Cid et al., 2012; Nishimura et al., 2012; Aguilar-Islas et al., 2013; Kondo et al., 2016; Colombo et al., 2019; Jensen et al., 2019). The highest concentrations of dFe, pFe<sub>xs</sub> and dMn in this study were found in the bottom waters along the Shelf and Strait stations (stations 61-66 and 2-8, respectively, Figure 4.11), indicating a source from the sediments. This could occur from resuspension of sediments themselves (Vieira et al., 2019) or from authigenic reactions related to the biogeochemistry of porewater diagenesis (Froelich et al., 1979; Burdige, 2006). The Chukchi Shelf not only receives nutrient-rich inflow from the North Pacific via the Bering Strait (Aagaard et al., 1981), but it is also highly productive (Sakshaug, 2004). In fact, the production of both soluble Fe(II) and Mn(II) in porewaters of the Chukchi Shelf has been documented (Vandieken et al., 2006).

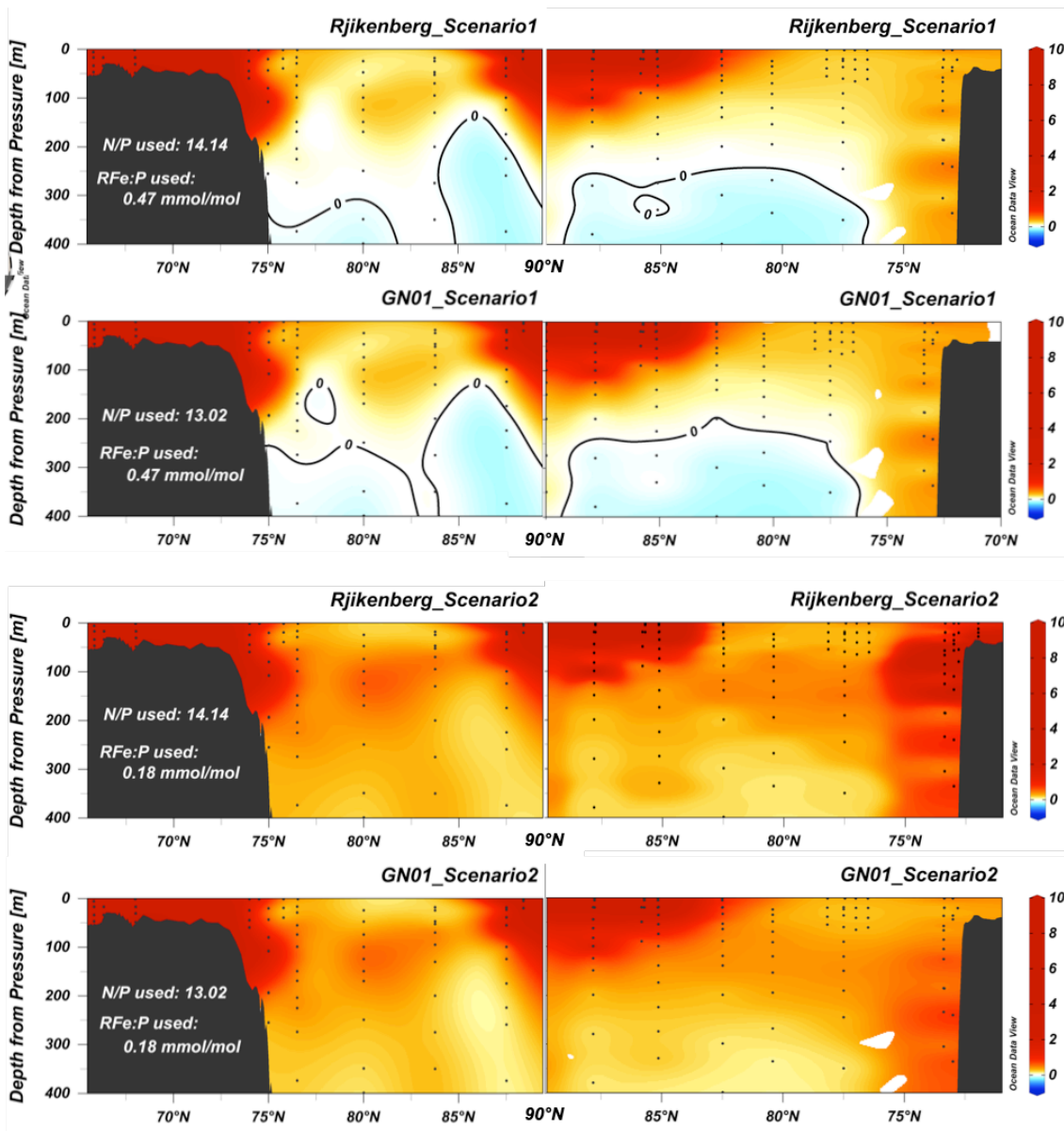


**Figure 4.10** Following the work of Rijkenberg et al. (2018) we calculated various Fe limitation scenarios along the GN01 transect in the upper 400m. In each scenario a Southern Ocean Fe-limited Fe to P ratio is used where Scenario 1 = 0.47 mmol/mol (top two panels) and Scenario 2 = 0.18 mmol/mol (bottom two panels). The slope of N/P is calculated below 100m in the water column in the Rijkenberg paper as 14.14 and below the halocline along GN01 as 13.02. A value below 0 (black contours) suggests limitation and none was found in either scenario along GN01.

In order to distinguish sediment resuspension from porewater diagenetic fluxes, we employed the porewater tracer  $N^{**}$ , as used in a previous study of dissolved Zn in these same GN01 samples, where a large dZn source from Chukchi Shelf porewaters was similarly entrained within the UHL (Jensen et al., 2019). In that study,  $N^{**}$  ( $N^{**} = (0.87[\text{DIN}] - 16[\text{PO}_4^{3-}] + 2.9) \mu\text{mol/kg}$ ) was employed as an idealized tracer of porewater diagenesis because it indicates the presence of denitrification, and water column

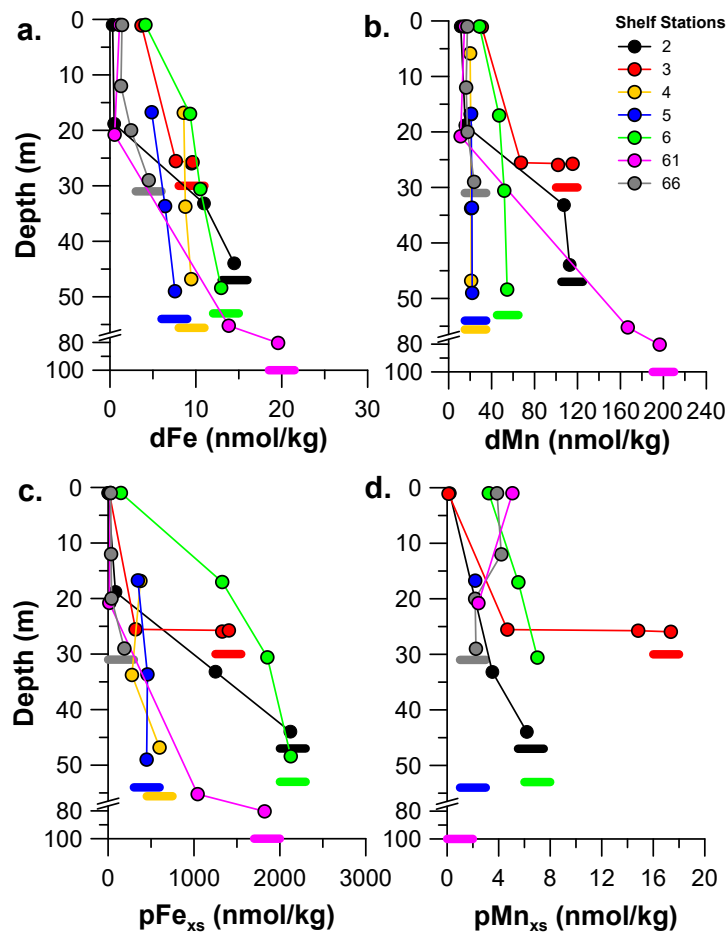


**Figure 4.11** Bering Strait/Chukchi Shelf station profiles of a) dFe b) dMn, c) pFe<sub>xs</sub>, d) pMn<sub>xs</sub> to show full range of elements at these important stations. The bottom depth for each station is shown as a solid bar below the plot to illustrate how close sampling depth was to “true bottom” along the Chukchi Shelf.

denitrification over the Chukchi Shelf is unlikely given high oxygen concentrations (Nishino et al., 2005; Aguilar-Islas et al., 2013; Granger et al., 2018); thus, the low  $N^{**}$  can only be produced in the porewaters. The negative correlation between  $N^{**}$  and  $dFe$ ,  $dMn$ , and  $pFe_{xs}$  along the shelf (Figure 4.12) confirmed a common authigenic porewater source for these metals, manifested as concentration maxima at the deepest sampled depths of the Chukchi Shelf stations (Figure 4.11).

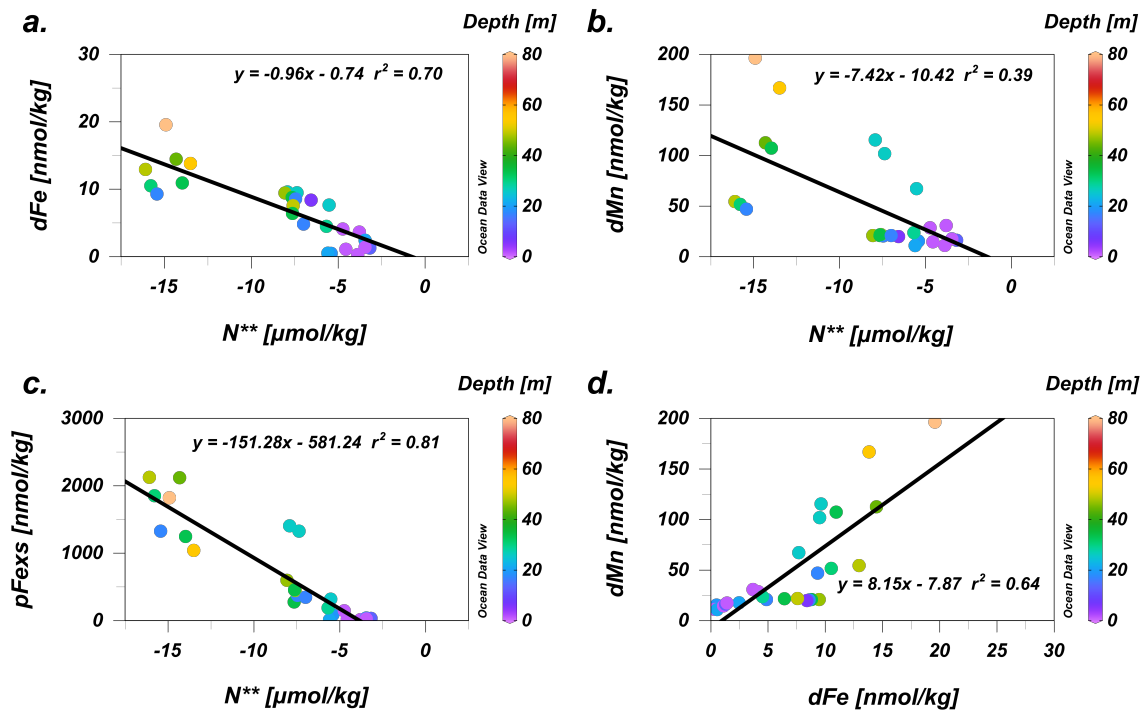


**Figure 4.12** Benthic sources along the shelf of Fe and Mn. a)  $dFe$ , b)  $dMn$ , c)  $pFexs$ , along the shelf and strait (Stations 2-6, 61, 66) vs. the tracer of porewater denitrification  $N^{**}$ . Panel d) shows  $dFe$  vs  $dMn$  along the same stations demonstrating strong correlation. Depths of samples (0-80m) are displayed in color showing that in most cases, the relationship is driven by benthic processes.

In contrast,  $pMn_{xs}$  remained low over the Chukchi Shelf and lacked a correlation to  $dFe$ ,  $pFe_{xs}$ , or even  $dMn$ , which highlights our first major divergence in Fe and Mn distributions, specifically that Chukchi Shelf  $dMn$  concentrations were much higher than  $dFe$  ( $dMn \gg dFe$ ) but particulate excess Fe concentrations were much higher than particulate excess Mn ( $pFe_{xs} \gg pMn_{xs}$ ) (Figure 4.13). Studies in Arctic sediments in the Barents Sea, known to be second in primary production only to the Chukchi Sea (Sakshaug, 2004), have demonstrated that reduction of Fe(III) and Mn(IV) account for greater than 90% of the organic carbon oxidation (Vandieken et al., 2006). Thus, our first-order hypothesis would be a large, concurrent Fe and Mn diagenetic flux from Chukchi Shelf porewaters, up to  $2.5 \mu\text{mol}/\text{m}^2/\text{day}$  for  $dFe$  and  $8.0 \mu\text{mol}/\text{m}^2/\text{day}$  for  $dMn$  (Vieira et al., 2019), which is also supported by large Fe and Mn oxide abundances in the shelf and slope sediments (Trefry et al., 2014; Hein et al., 2017).

We observed that  $dFe$  and  $dMn$  were both enriched in near-bottom waters of the Chukchi Shelf (Figure 4.11, Figure 4.13), but  $dMn$  values were significantly higher ( $dFe \ll dMn$ ). While thermodynamics might favor the production of both within sediment porewaters, kinetics favors the rapid oxidation of Fe(II)/Fe(III) back to particulate Fe(III) in the presence of oxygen. This oxidation is known to be rapid, with a half-life on the order of minutes for typical seawater (Millero et al., 1987), but can be hindered by organic ligand complexation (Rue and Bruland, 1995). In contrast, Mn(II)/Mn(III) oxidizes much more slowly in the presence of oxygen (Yeats and Strain, 1990; von Langen et al., 1997), and its oxidation is often microbially-mediated (Nealson

et al., 1988; Tebo et al., 2004), leading to a half-life on the order of days to weeks under typical seawater conditions (Stumm and Morgan, 1981).

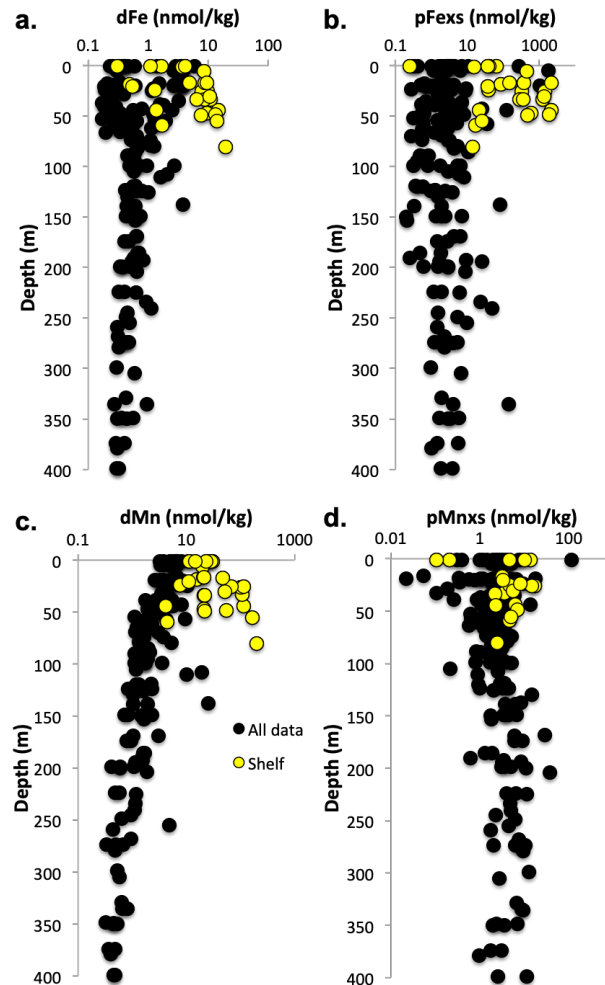


**Figure 4.13** Log-scale profiles of a) dFe, b) pFexs, c) dMn, d) pMnxs. Log-scale concentrations are used to highlight the high values found along the shelf stations (yellow) for dFe, pFexs and dMn, in particular.

We use the parameterization laid out in Millero et al. (1987) to calculate the half-life of Fe(II) along the Chukchi Shelf, where oxygen is variable (214-390  $\mu\text{mol/kg}$ ) as well as pH (7.21-7.92, (Kadko et al., 2016)), yielding a range of 12 to 700 minutes

(Figure 4.14). Assuming a bottom water transport of 15-100 cm/s (Aagaard and Roach, 1990; Münchow and Carmack, 1997), we can estimate that the highly soluble Fe(II) could be transported 112 m to 42 km from its source before being diminished to half its original concentration. In fact, Fe (II) concentrations on the shelf were generally quite low (<15 pmol/kg), composing at most 2.5% of the overall dissolved phase (Figure 4.15). This suggests that most of the dFe is Fe(III), in the form of either Fe oxyhydroxide nanoparticles or Fe(III)-organic ligand complexes. In contrast, the half-life of Mn(II) oxidation, calculated following Yeats & Strain (1990) as a product of pH, oxygen, and particulate Mn concentration, ranges 120 minutes to 2.6 days and can be transported between 1 and 230 km away from its source before significant oxidation and removal. Thus, any Fe(II) released during porewater diagenetic reactions was more rapidly oxidized to nanoparticulate and especially particulate phase (Fe(III)), while Mn(II) remained in the dissolved phase much longer along the Chukchi Shelf.

#### **4.4.3.1. Offshore transport of Fe and Mn in the UHL**

The elevated concentrations of dFe,  $pFe_{xs}$ , and dMn on the Chukchi shelves were also maintained within the UHL (Figures 4.3 and 4.4). During brine rejection on the Chukchi Shelf, nutrient- and metal-rich waters are subducted and transported offshore, creating a highly traceable water mass characterized by elevated Si concentrations ( $[Si] > 25 \mu\text{mol/kg}$ , (Anderson et al., 2013))(Figure 4.4). While dMn remained elevated in surface waters (Figure 4.5), likely due to a slow oxidation timescale after advection from the continental shelves and/or surface photoreduction of Mn oxide particles into dissolved Mn(II) (Sunda et al., 1983a; Sunda and Huntsman, 1994) away from sea ice

coverage, dissolved Fe and Mn both had their local maxima in offshore waters within the UHL (Figure 4.4). Maxima in dFe, dMn, and Si were all maintained throughout the Canada Basin UHL (Stations 8-19, 46-60), extending hundreds of kilometers away from the Chukchi Shelf. While UHL waters were not circulated directly northward along our cruise transect and instead can be entrained within cyclonic circulation along coastal currents at certain latitudes (Rudels, 2015), it is useful to consider mechanisms affecting this long-range transport of shelf-derived Fe and Mn offshore and compare to other studies that have considered Fe and Mn transport length scales.

How long might we expect various Fe and Mn species to persist over distance, based on prior studies? As calculated above, we know that the reduced forms of dissolved Fe and Mn are oxidized on different timescales, and that the oxidized species are nearly quantitatively removed back into the more slowly reacting particulate phase, effectively removing them from the water column.

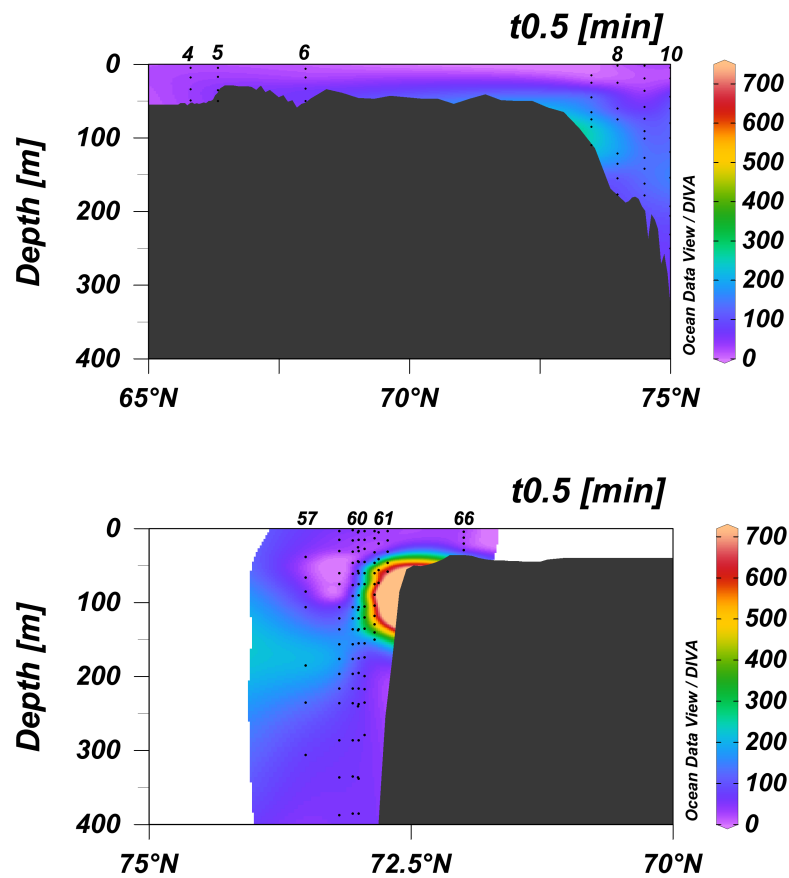


**Figure 4.14** Fe(II) oxidation half lives across the shelf and slope stations for the northbound (top panel, Stations 4-10) and southbound (bottom panel, Stations 57-66) transects. The half lives ( $t_{0.5}$ ) are expressed in minutes (color bar) and calculated following the methods of Millero et al. (1987) as summarized in the text. Values used include pH, oxygen, potential temperature, and salinity. Notice that the highest values ( $t_{0.5} \sim 700$  minutes) are on the shelf/slope at stations 66 and 61 where low oxygen was observed. Station numbers are included at the top of each panel.

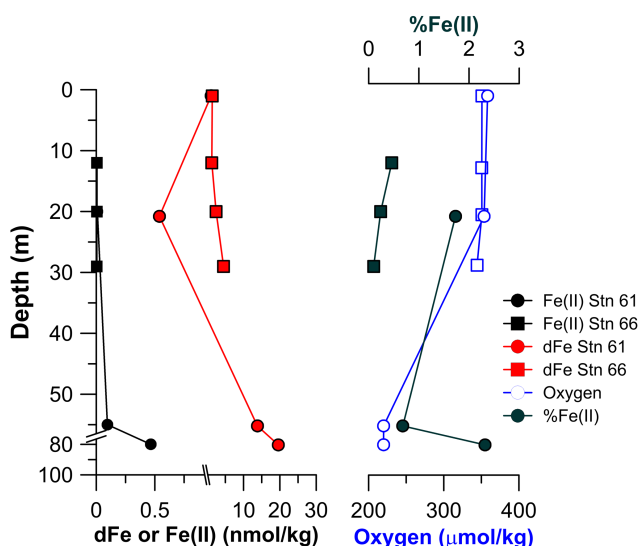


**Figure 4.15** Dissolved Fe(II) measurements taken at Stations 61 (circles) and 66 (squares) are shown in black alongside overall dissolved Fe (all species, red). To the right are the accompanying oxygen profiles (blue) and  $\%Fe(II) = [Fe(II)] / ([dFe] + [Fe(II)])$ . Overall, the contribution of Fe(II) corresponded to the area with lowest oxygen concentrations and highest dFe (bottom Station 61). Methods for Fe(II) determination can be found in Heller, M. I., P. J. Lam, J. W. Moffett, C. P. Till, J.-M. Lee, B. M. Toner, and M. A. Marcus (2017), Accumulation of Fe oxyhydroxides in the Peruvian oxygen deficient zone implies non-oxygen dependent Fe oxidation, *Geochimica et Cosmochimica Acta*, 211, 174-193. Fe(II) data courtesy of Dr. Maija Heller.

However, dissolved Fe(III), the thermodynamically stable form of dissolved Fe in oxygenated waters (Kuma et al., 1996), is highly complexed by organic ligands in all oceanic waters (>99%, (Gledhill and Buck, 2012)). In contrast, Mn(II) generally remains as the ionic dissolved  $Mn^{2+}$  species (Tebo, 1991), though any some contribution by dissolved Mn(III) phases, which can be complexed organically, is possible (Luther et al., 2015; Oldham et al., 2017), though unstudied in the Arctic. We can therefore hypothesize that organic ligands, likely in the form of DOM and humic acids (Hioki et al., 2014; Slagter et al., 2017; Slagter et al., 2019; Yamashita et al., 2020), are binding and stabilizing dFe in the halocline, making it less susceptible to adsorptive scavenging

following oxidation (Gledhill and Buck, 2012; Tagliabue et al., 2017), while dMn is mostly present as free, ionic  $\text{Mn}^{2+}$ , or is at most partially stabilized by organic ligands as Mn(III). Thus we might hypothesize that ligand stabilization could increase the longevity of dFe transport offshore relative to dMn, despite faster oxidation kinetics of the initial Fe(II) diagenetic flux.

One metric used to assess the lifetime of a margin-derived element is the natural log-scale transport (here defined as  $d_{1/e}$ ) of a species away from the continental shelf, which is the distance traveled offshore from the continental shelf before the element's concentration is reduced by 1/e of the original shelf concentration (Johnson et al., 1997). In the Arctic, this was first used in a study comparing the longevity of pFe and dFe from the Chukchi Shelf (Aguilar-Islas et al., 2013), demonstrating that within the Canada Basin UHL pFe was removed more quickly (over shorter distances) than dFe (260 km compared to 380 km). Concentrations appeared to decrease exponentially offshore, leading to a simple linearization of the natural log of concentration versus distance from the shelf-break. We applied the same equation used in Aguilar-Islas et al. (2013) to all GN01 data that fall within the bounds of the UHL ( $S \sim 31-33.1$ ,  $[\text{Si}] > 25 \mu\text{mol/kg}$ ), representing a longer total distance (0-1200 km) from the shelf break, defined here as the 100 m isobath along the Chukchi Shelf, north of the shelf-break and slope currents (Corlett and Pickart, 2017).

We would expect that if chemical species were conserved in the UHL that a plot of natural log vs. distance from the shelf break would show a flat horizontal line. For example,  $\ln(\text{Si})$  vs. distance yields a horizontal line (Figure 4.16g), suggesting that Si

concentrations barely change in the halocline with distance from the shelf. Thus, a conserved element like Si is not being supplied significantly to the UHL by *in situ* regeneration nor significantly diluted by mixing with non-halocline waters (which have lower Si concentrations). This supports our case that the UHL is a useful layer in which to quantify scavenging length scales in the absence of overprinting by other oceanographic processes.

In contrast to Si,  $\ln(d\text{Fe})$  vs. distance had a non-horizontal linear decrease moving offshore (Figure 4.16a), pointing to removal of Fe away from its shelf source. Similarly, we found linear relationships for  $\ln(d\text{Mn})$  and  $\ln(p\text{Fe}_{\text{xs}})$  vs. distance, also indicative of removal within the halocline (summarized in Table 4.2, Figure 4.16). However, in contrast to the Aguilar-Islas (2013) conclusions, we noticed two distinct slopes across 1200 km of transport: a rapid attenuation of  $d\text{Fe}$ ,  $d\text{Mn}$ , and  $p\text{Fe}_{\text{xs}}$  within 150 km of the shelf break, followed by slow removal of  $d\text{Fe}$  and  $p\text{Fe}_{\text{xs}}$  and conservation of  $d\text{Mn}$  between 150 and 1200 km.

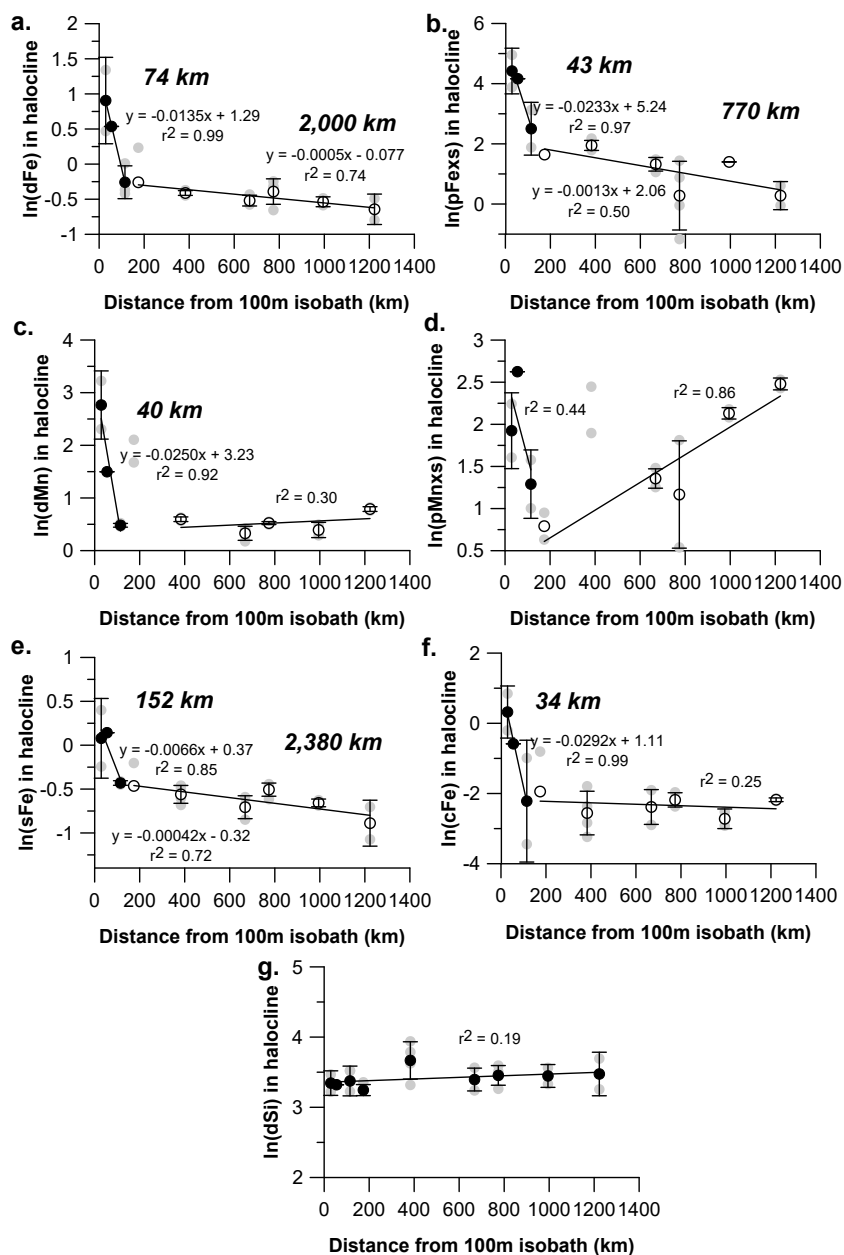


**Figure 4.16** Log-scale transport plots of  $\ln([metal])$  vs. distance from the 100 m isobath along the Chukchi Shelf for Stations 8, 10, 14, 19, 46, 48, 52, 57, and 60 in the Canada Basin. All data (grey circles) are taken within the bounds of the upper halocline as defined by silicate concentration ( $[Si] = 25 \mu\text{mol/kg}$ ) and salinity 31.0-33.1. Averages for each station are represented by filled circles (close to shore, Stations 8, 57, 60) or open circles (further from shore, Stations 10, 14, 19, 52, 46, 48) to show the general trend with accompanying error bars. Linear regression equations shown for significant relationships. The  $d_{in}$  values ( $1/\text{slope}$ , distance over which variable decreases by  $1/e$ ) are shown in bold italics where relationship is statistically significant ( $r^2 > 0.5$ ) and mentioned in the text. a) dFe, b) pFexs, c) dMn, d) pMnxs, e) sFe, f) cFe, g) silicate.

Within 150 km of the shelf break,  $d_{in}$  was only  $74 \pm 1$  km for dFe, which is a much shorter scavenging removal distance than the Aguilar-Islas estimate of 380 km (Table 4.2). Dissolved Mn and  $pFe_{xs}$  were removed even faster, with a  $d_{in}$  of approximately 40 km (Table 4.2). Farther offshore at 150-1200 km from the shelf break,  $d_{in}$  for dFe increased to  $2,051 \pm 613$  km, indicating much slower scavenging, and  $pFe_{xs}$  had a  $d_{in}$  of  $770 \pm 384$  km, again persisting much farther, while the natural log of dMn shared no statistically significant relationship ( $r^2 < 0.2$ ) with distance from the shelf break (Figure 4.16). We compared the initial  $d_{in}$  distances for dFe and  $pFe_{xs}$ , which were shorter than those found previously in the Arctic and shorter than most other reported values (Table 4.2), and noted two major conclusions. First, this two-step removal process was not reported in prior similar studies, even in the Arctic. Second, dFe was stabilized farther than dMn at first, but dFe was subject to slow removal across the longer 1200 km offshore spatial scale, whereas dMn was conserved after initial scavenging losses near the shelf break.

**Table 4.2** Summary of log scale transport distance ( $d_{in}$  in km) values for this study (red) compared to literature values, primarily for Fe species. Studies are generally listed in increasing order of  $d_{in}$  value with location and depth noted where possible. The split box indicates that two distinct linear relationships were found leading to two  $d_{in}$  values. Associated errors in  $d_{in}$  (1SD, derived from the linear regression) are reported for this study only.

Reference	Location	Depth	dFe		pFexs		sFe		cFe		dMn	
Johnson et al. (1997)	Monterey Bay	surface	16		-		-		-		-	
<b>This study</b>	<b>Canada basin</b>	<b>100-200</b>	<b>74</b> <b>±1</b>	<b>2051</b> <b>±613</b>	<b>43</b> <b>±8</b>	<b>770</b> <b>±384</b>	<b>152</b> <b>±64</b>	<b>2400</b> <b>±742</b>	<b>34</b> <b>±2</b>	-	<b>40</b> <b>±12</b>	-
Wu and Luther (1996)	Delaware Bay	-	101		-		-		-		-	
Gordon et al. 1998	Galapagos	-	103		-		-		-		-	
Bacciarelli et al. (2001)	Kerguelen	surface	151		-		-		-		-	
Klunder et al. (2012)	Nansen basin	750	260		-		-		-		-	
Aguilar-Islas et al. (2013)	Canada Basin	200-250	380		260		-		-		-	
Johnson et al. (1997)	Coastal CA	1000	5000		-		-		-		-	

Dissolved Fe, as previously mentioned, can be highly organically complexed in marine waters, which is thought to protect Fe from being scavenged to the particulate phase (Rue and Bruland, 1995; Gledhill and Buck, 2012). Particulate Fe (pFexs in this study) was more rapidly diminished, likely falling out of the water column due to aggregation. Likewise, dMn was eventually oxidized to pMn<sub>xs</sub>, which appears to “grow in” within the halocline offshore despite dMn being conserved (Figure 4.4d and 4.16d), thus requiring some pMn<sub>xs</sub> lateral source that might be supplied by the cyclonic circulation of this region. Importantly, Fe and Mn have very different spatial scales of

removal, demonstrating the stabilizing effect of ligands on dFe. Despite these ligands, however, dFe still appeared to be removed over a long distance, while dMn was eventually conserved offshore. To further investigate the speciation of dFe and dMn that might cause these patterns, in the absence of ligand measurements, we examined the colloidal size distribution of dFe.

Colloidal Fe, an intermediate size fraction between truly soluble and larger particulate phases (Wells, 2002), is gaining increased attention as a size class of Fe that can drive enrichments of dFe close to continental sources (Bergquist et al., 2007; Fitzsimmons and Boyle, 2014b; Fitzsimmons et al., 2015). This study represents the first basin-scale section of size-fractionated dFe in the Arctic. Compared to the well-studied North Atlantic, where soluble Fe concentrations (sFe <0.02 $\mu$ m) matched colloidal Fe (cFe) concentrations (~50% sFe or cFe) except at margin- and hydrothermal-influenced depths where colloids dominated (cFe>50%) (Fitzsimmons et al., 2015), the Arctic was instead dominated by small soluble Fe species (only 25 $\pm$ 16% cFe; Figure 4.17), despite similar dFe concentrations as the North Atlantic. This was surprising, given the significant margin-influence on the Arctic Ocean and the high particulate Fe concentrations, which might be expected to correspond to high nanoparticulate concentrations that are often observed in the colloidal size fraction. However, even within the halocline close to the shelf, %cFe was only 21  $\pm$  15%. Extending our previous log-scale transport calculations to these size-fractionated dFe species, the  $d_{in}$  for sFe was 152 $\pm$ 64 km (Figure 4.16e, Table 4.2), while colloidal Fe (cFe) had a much shorter  $d_{in}$  of 34 $\pm$ 2 km (Figure 4.16f). This suggests that cFe was scavenged nearly 5x as rapidly as

sFe close to the shelf. In the second, longer-distance scavenging regime, sFe had a log scale transport of  $2400 \pm 742$  km, and cFe surprisingly appeared conserved. Dissolved Mn was entirely soluble-sized in the Arctic, with  $0 \pm 7\%$  of dMn falling into the colloidal size fraction.

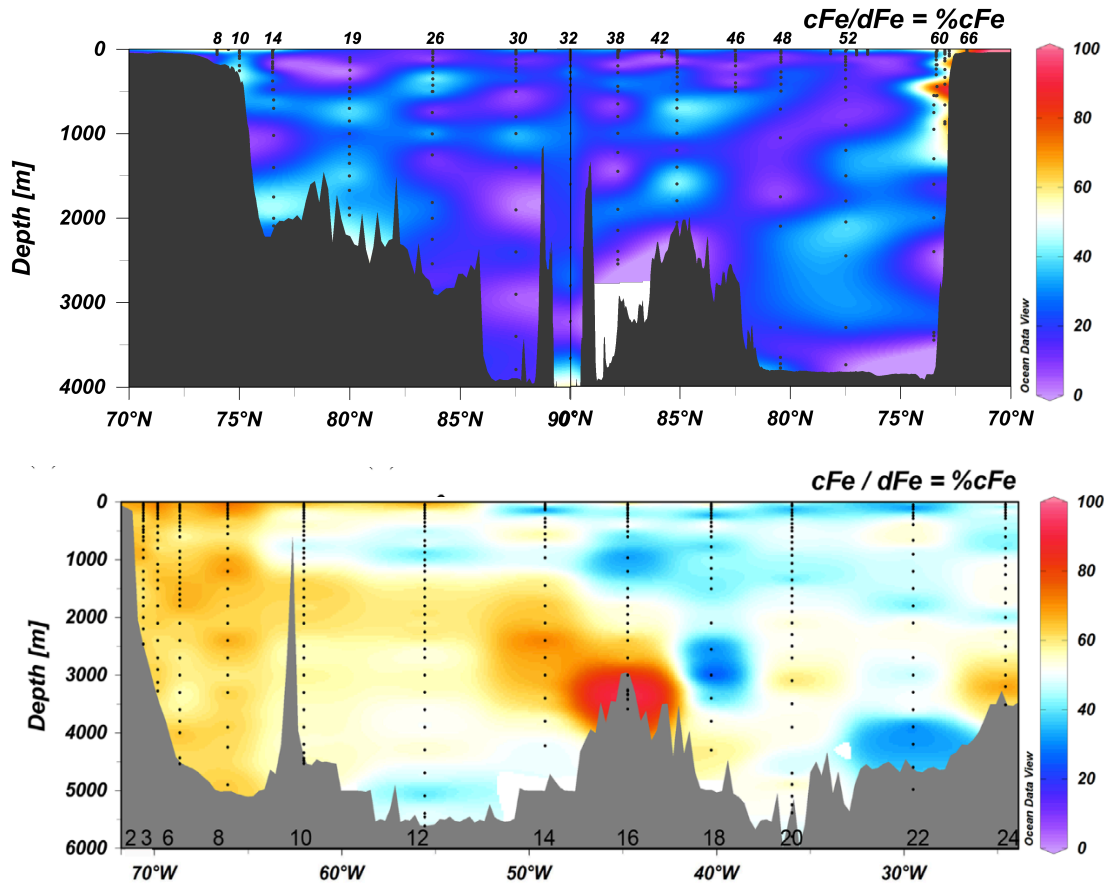


**Figure 4.17** Comparison of the Arctic Ocean (top, this study) with the North Atlantic (bottom, Fitzsimmons et al. 2015). The color bar represents the %cFe or  $cFe/dFe \times 100\%$ . Notably, the Arctic Ocean overall contains a very low colloidal contribution (average %cFe =  $25 \pm 16\%$ , 1SD) to the dissolved phase compared to the only other ocean basin section for which this quantity has been measured. Stations for this study only are shown at the top of the panel.

Size partitioning of dFe phases does not reveal anything about the chemical composition of dFe, as both ligand-bound Fe and inorganic Fe nanoparticles can be

observed in both the soluble and colloidal size fractions. However, the soluble-colloidal log-scale transport pattern could be interpreted to suggest a greater presence of stable Fe bound by organic ligands within the soluble size fraction near the shelf, with actively aggregating nanoparticles contributing more to the shorter lived colloidal size fraction. Overall, the starkly lower concentration of colloids across the entire Western Arctic transect compared to the Atlantic marks a major change in the speciation of dFe in these two ocean basins. In the absence of other Fe speciation data, we can only speculate on the cause of this difference, which may be related to lower dust inputs to the Arctic providing fewer Fe colloids, or less biological productivity in overlying waters that would otherwise promote dFe transfer to the colloidal phase. Perhaps most compelling is the role of greater particle loads and more metal-rich particles in the Arctic, particularly on the shelf where Fe colloids were elevated ( $\%cFe = 65 \pm 22\%$ ), which could remove colloids faster in the Arctic than in other ocean basins.

#### **4.5. Discussion and Implications**

The Arctic Ocean provides an excellent template with which to compare and contrast Fe and Mn chemistry. Despite a geochemical tendency to consider Fe and Mn as cycling together or as tracers of each other because of broadly common sources and sinks (Figure 4.1), their chemical compositions and thus reactivity are different and lead to decoupled distributions within the upper 400 m of the Western Arctic Ocean. In the relative absence of overprinting from external fluxes or biological transformations, we present a relatively simple demonstration of the contrasting oxidation rates and scavenging of Fe and Mn within the water column.

Our results show a three-step differentiation of the Fe and Mn distributions in the Arctic. First, there is a large, diagenetic porewater flux that releases both dFe and dMn via reductive dissolution of Fe and Mn oxides in Chukchi Shelf sediments. However, the two metals are immediately decoupled at their source, when faster oxidation kinetics of Fe(II) in the presence of oxygen creates high  $p\text{Fe}_{\text{xs}}$  (up to 2100 nmol/kg) compared to dFe (up to 19.6 nmol/kg), and slower oxidation of Mn(II) allows for high dMn (up to 196 nmol/kg) and lower  $p\text{Mn}_{\text{xs}}$  (up to 17 nmol/kg). These patterns confirm rapid Fe oxidation and slower (kinetically inhibited) oxidation of Mn (Stumm and Morgan, 1981; Yeats and Strain, 1990; von Langen et al., 1997). We might expect that this Fe:Mn pattern would persist moving offshore into the shelf-influenced UHL. However, the second step of Fe and Mn differentiation occurs within the UHL <150 km from the shelf, where there is rapid removal of both dFe and dMn (Figure 4.16). Then, in the third step of differentiation even farther offshore >150 km from shelf break), dFe persists with very slow scavenging, likely due to the presence of soluble-sized organic ligands that allow soluble Fe to have a longer  $d_{\text{in}}$  than any other species. In contrast, dMn is more rapidly removed to the particulate phase in the near-shelf scavenging regime, in line with previous work along the Chukchi slope and basin (Macdonald and Gobeil, 2012), but remained conserved through the next 1000 km away from the shelf.

This three-step Fe and Mn differentiation explains the overall balance of the dissolved and particulate phases of Fe and Mn. Much of the dissolved Fe is converted to particulate Fe immediately over the shelf, and some of this particulate Fe persists offshore. In contrast, dissolved Mn persists over the shelf without precipitating, but is

eventually transformed to pMn within the halocline (Figure 4.4d, 4.16d). The particulate phase eventually dominates for both metals below 100 m, which isn't necessarily true in the rest of the global ocean where dMn often dominates pMn and  $dFe \approx pFe$  at depth, e.g. (Noble et al., 2012), but it is consistent with other studies in the Canada Basin and along the Bering and Chukchi shelves (Aguilar-Islas et al., 2013). The differentiation between the second and third steps can thus be ascribed to a zone of higher scavenging on/near the shelf due to scavenging onto higher particle abundances and then a zone of lower scavenging offshore where Fe scavenging is mostly complete but some pMn formation or advection is still occurring (Figure 4.18).

This decoupling of Fe and Mn has been observed in prior studies from various oceanic regimes (Landing and Bruland, 1987; Noble et al., 2012; Hatta et al., 2013; Hatta et al., 2015; Fitzsimmons et al., 2017).

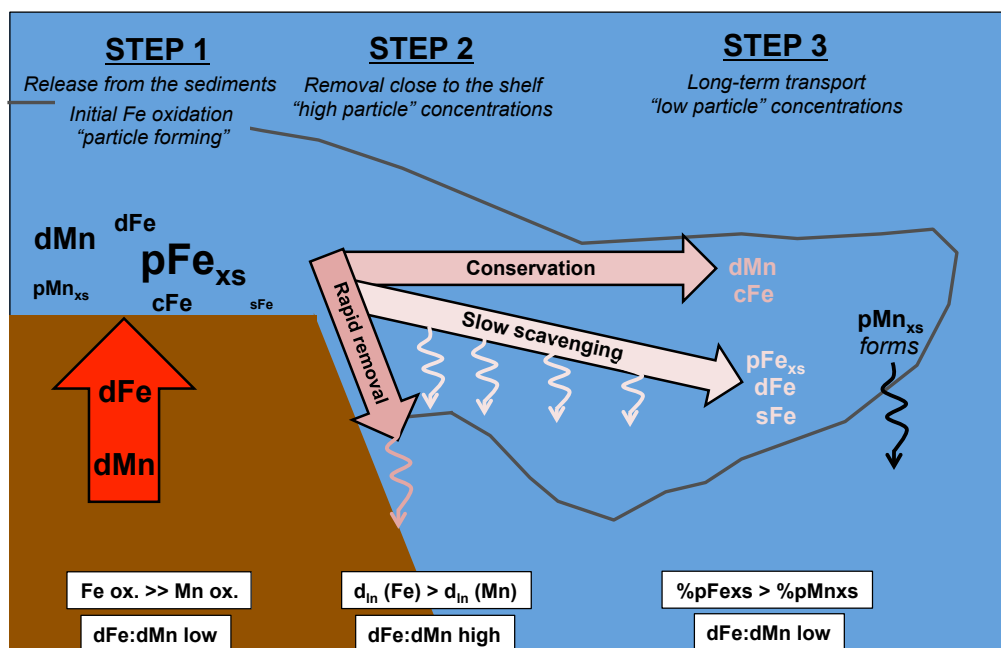


**Figure 4.18 Summary schematic of the major trends described in the text.** A three-step differentiation pattern between Fe and Mn is clearly demonstrated by 1) unequal oxidation kinetics leading to particle formation on the shelf following by 2) rapid removal of both species close to the shelf and 3) continued removal of Fe while Mn remains conserved. The size of the text on the shelf indicates relative concentrations of various Fe and Mn species. Squiggly arrows indicate removal from the water column, likely leading to eventual burial in the sediments.

The basic nature of the three-step decoupling found in this study is mirrored in buoyant hydrothermal fluids (Step 1) and neutrally-buoyant plumes (Steps 2 nearer the vent and Step 3 farther from the vent). For example, in the Southern East Pacific Rise (SEPR) hydrothermal plume study of Fitzsimmons et al. (2017), the scavenging regimes and subsequent distributions of Fe and Mn were different, with dMn conserved down the plume and dFe both removed and found to deepen with sinking particles. The authors of that study concluded that a reversible scavenging between the dissolved and particulate Fe phases was necessary to explain the distributions, and they proposed an essential role of dissolved organic ligands in driving the Fe exchange. The SEPR study used Fe

isotopes to show that Fe oxyhydroxide nanoparticles were scavenged more rapidly than the ligand-bound dFe compounds, and that was used as a framework for the difference between Step 2 and Step 3 dFe loss observed here (Figure 4.16).

In fact, the three-step differentiation proposed here both contradicts and supports our current understanding of residence time in the upper water column, namely that dFe is thought to be shorter-lived than dMn (Landing and Bruland, 1987; Bruland et al., 1994). Away from the shelf, dFe appears “longer-lived” than dMn, based on the longer  $d_{in}$ , which is controlled primarily by the soluble phase (Figure 4.16a, e, f). However, beyond this region of initial rapid removal, dFe, sFe, and pFe<sub>xs</sub> are slowly removed and dMn remains conserved, as in the SEPR plume (Fitzsimmons et al. 2017). Offshore, it may be the pMn<sub>xs</sub> that is responsible for scavenging of dFe and sFe far away from the shelf source (Cheize et al., 2019). The similar scavenging kinetics of pFe<sub>xs</sub> and cFe in the Arctic can be explained if cFe in the Arctic were largely inorganic in character, leading to similar cFe aggregation and sinking from the water column as pFe<sub>xs</sub>, as posited in Aguilar-Islas et al. (2013). However, farther offshore the cFe remains low and conserved, like dMn, indicating a different, perhaps organic, chemical composition of this offshore UHL cFe phase.

As the “Scavengers of the Sea” (Goldberg, 1954), the opposite distributions of particulate Fe oxides (over the shelf) and particulate Mn oxides (offshore in the halocline) will also affect the distributions of other scavenging-prone trace metals, both in the water column and in the sediments below. Previous studies have demonstrated that different elements have a tendency to sorb either to Fe oxyhydroxides (which are surface

neutral or slightly positively charged) compared to Mn oxides (which are surface negatively charged), based on the dominant inorganic speciation of the dissolved trace elements (Koschinsky and Hein, 2003). For example, trace metals found in seawater as weakly complexed cations (Byrne, 2002), such as most rare earth elements, are expected to sorb more readily to Mn oxides, while negatively charged carbonate and chloro species such as Sc, Cu, Ti, Zn (Byrne, 2002) are more readily absorbed to Fe oxides (Koschinsky and Hein, 2003). Thus, we might expect this first group to have higher abundances in slope/offshore sediments, while the second group may have higher abundances in shelf and near-shelf sediments. A recent study found high Fe:Mn ratios in Fe-Mn nodules just off of the Chukchi Shelf, indicative of Fe being “shuttled” efficiently off of the shelf and precipitating as Fe oxyhydroxides (Hein et al., 2017). These so-called “Fe shuttles” have been described in margin sediments and in oxygen minimum zones (OMZ) elsewhere (Raiswell, 2011; Scholz et al., 2011) and may be responsible for moving other elements offshore (Whitmore et al., 2019).

We also mention here the implications of a changing climate for the distribution and influence of Fe and Mn in the Western Arctic Ocean. It is established that the diagenetic cycling of Fe and Mn has great importance to the overall carbon budget along the Arctic shelves where organic matter export is “pulsed” seasonally (Vandieken et al., 2006; Magen et al., 2011). In light of a changing climate, increased ice melt will likely lead to an increase in pulses of organic matter to the seafloor (Magen et al., 2011). This will in turn increase the mobilization of redox-sensitive metals such as Fe and Mn,

which will subsequently oxidize and may then increase the scavenging of other metals throughout the water column.

#### 4.6. Conclusions

Dissolved Fe and Mn share many common sources and sinks in the global ocean, such as release from sediments, dust fluxes, hydrothermal venting, biological uptake, and scavenging to the particulate phase. Despite multiple field investigations demonstrating their decoupling, many studies continue to compare the two and use them to trace each other. The Western Arctic Ocean provided an ideal, simple case study for resolving how some of the chemical properties that differentiate Fe and Mn, such as the timescale of oxidation and stabilization by organic ligands, affect their distributions.

We described a three-step decoupling of Fe and Mn in both the dissolved and particulate phases from the shelf to the offshore halocline. The first step was the release of both dFe and dMn as a result of reductive dissimilation during the decay of organic matter in Chukchi Shelf porewaters, producing dFe and dMn fluxes that were immediately decoupled due to faster oxidation of Fe(II) in the presence of oxygen. The subsequent difference in oxidation timescale is illustrated by  $dFe \ll dMn$  and  $pMn_{xs} \ll pFe_{xs}$  over the Chukchi Shelf. These shelf fluxes were then entrained into the subsurface halocline water mass (UHL) and moved offshore, largely unaffected by significant mixing and *in situ* remineralization fluxes. The second step of Fe and Mn differentiation thus occurred within the UHL, where dFe,  $pFe_{xs}$ , sFe, cFe and dMn all decreased exponentially within 150 km of the shelf. This was interpreted to occur because of the scavenging and aggregation of the high particle environment near the shelf break, with

only the smallest soluble Fe, likely dominated by strong organic ligand complexes, somewhat protected from this removal. The third step of Fe and Mn differentiation was the continued slow removal of dFe, sFe, and pFe<sub>xs</sub> within the UHL between 150 and 1200 km offshore, while dMn and cFe were relatively conserved, possibly due to an equality of sources and sinks during offshore transport; pMn<sub>xs</sub> varied but was generally supplied over the offshore 1200 km interval.

Chemical oceanographers should note that Fe and Mn are thus not ideal tracers of each other in the global ocean, despite their similar sources. A correlation between the two could indicate the presence of a shared source, such as hydrothermal venting, diagenetic fluxes (as seen in this study), or dust input to the surface ocean. However, a lack of correlation in a system does not prevent one of these shared supply mechanisms as one may have been removed more than the other on various spatial scales. In fact, the different behaviors of Fe and Mn are widespread. The chemical properties of Fe and Mn that drive their unique reactivity and speciation, as examined here, also serve to decouple these two elements across temporal and spatial scales. Future studies should recognize the influence of Fe and Mn in both the dissolved and particulate phases on the distribution of other trace elements, especially in shelf-influenced oceanic margin regions.

#### **4.7. References**

Aagaard, Knut, LK Coachman, and Eddy Carmack. 1981. "On the halocline of the Arctic Ocean." *Deep Sea Research Part A. Oceanographic Research Papers* 28 (6):529-545.

- Aagaard, K., and AT Roach. 1990. "Arctic ocean-shelf exchange: Measurements in Barrow Canyon." *Journal of Geophysical Research: Oceans* 95 (C10):18163-18175.
- Aagaard, K., J. H. Swift, and E. C. Carmack. 1985. "Thermohaline circulation in the Arctic Mediterranean Seas." *Journal of Geophysical Research: Oceans* 90 (C3):4833-4846. doi: 10.1029/JC090iC03p04833.
- Aguilar-Islas, Ana M., Robert Rember, Shigeto Nishino, Takashi Kikuchi, and Motoyo Itoh. 2013. "Partitioning and lateral transport of iron to the Canada Basin." *Polar Science* 7 (2):82-99. doi: <http://dx.doi.org/10.1016/j.polar.2012.11.001>.
- Aguilar-Islas, A. M., R. D. Rember, C. W. Mordy, and J. Wu. 2008. "Sea ice-derived dissolved iron and its potential influence on the spring algal bloom in the Bering Sea." *Geophysical Research Letters* 35 (24):n/a-n/a. doi: 10.1029/2008GL035736.
- Anderson, L. G., Per S Andersson, Göran Björk, E Peter Jones, Sara Jutterström, and Iréne Wåhlström. 2013. "Source and formation of the upper halocline of the Arctic Ocean." *Journal of Geophysical Research: Oceans* 118 (1):410-421.
- Arimoto, RRABJCK, RA Duce, BJ Ray, and CK Unni. 1985. "Atmospheric trace elements at Enewetak Atoll: 2. Transport to the ocean by wet and dry deposition." *Journal of Geophysical Research: Atmospheres* 90 (D1):2391-2408.

- Balistrieri, L., PG Brewer, and JW Murray. 1981. "Scavenging residence times of trace metals and surface chemistry of sinking particles in the deep ocean." *Deep Sea Research Part A. Oceanographic Research Papers* 28 (2):101-121.
- Barbeau, K., E. L. Rue, K. W. Bruland, and A. Butler. 2001. "Photochemical cycling of iron in the surface ocean mediated by microbial iron(III)-binding ligands." *Nature* 413 (6854):409-413. doi: 10.1038/35096545.
- Bergquist, B. A., J. Wu, and E. A. Boyle. 2007. "Variability in oceanic dissolved iron is dominated by the colloidal fraction." *Geochimica et Cosmochimica Acta* 71 (12):2960-2974. doi: <http://dx.doi.org/10.1016/j.gca.2007.03.013>.
- Boyle, Edward A., Bridget A. Bergquist, Richard A. Kayser, and Natalie Mahowald. 2005. "Iron, manganese, and lead at Hawaii Ocean Time-series station ALOHA: Temporal variability and an intermediate water hydrothermal plume." *Geochimica et Cosmochimica Acta* 69 (4):933-952. doi: <https://doi.org/10.1016/j.gca.2004.07.034>.
- Bruland, K. W., and M. C. Lohan. 2003. "6.02 - Controls of Trace Metals in Seawater." In *Treatise on Geochemistry*, edited by Heinrich D. Holland and Karl K. Turekian, 23-47. Oxford: Pergamon.
- Bruland, K. W., Kristin J Orians, and James P Cowen. 1994. "Reactive trace metals in the stratified central North Pacific." *Geochimica et Cosmochimica Acta* 58 (15):3171-3182.

- Bucciarelli, Eva, Stéphane Blain, and Paul Tréguer. 2001. "Iron and manganese in the wake of the Kerguelen Islands (Southern Ocean)." *Marine Chemistry* 73 (1):21-36. doi: [https://doi.org/10.1016/S0304-4203\(00\)00070-0](https://doi.org/10.1016/S0304-4203(00)00070-0).
- Burdige, David J. 2006. *Geochemistry of marine sediments*: Princeton University Press.
- Byrne, Robert H. 2002. "Inorganic speciation of dissolved elements in seawater: the influence of pH on concentration ratios." *Geochemical Transactions* 3 (1):11. doi: 10.1186/1467-4866-3-11.
- Carpenter, James H. 1965. "The Chesapeake Bay Institute technique for the Winkler dissolved oxygen method." *Limnology and Oceanography* 10 (1):141-143.
- Charette, Matthew A., Lauren E. Kipp, Laramie T. Jensen, Jessica S. Dabrowski, Laura M. Whitmore, Jessica N. Fitzsimmons, Tatiana Williford, Adam Ulfsbo, Elizabeth Jones, Randelle M. Bundy, Sebastian M. Vivancos, Katharina Pahnke, Seth G. John, Yang Xiang, Mariko Hatta, Mariia V. Petrova, Lars-Eric Heimbürger-Boavida, Dorothea Bauch, Robert Newton, Angelica Pasqualini, Alison M. Agather, Rainer M.W. Amon, Robert F. Anderson, Per S. Andersson, Ronald Benner, Katlin L. Bowman, R. Lawrence Edwards, Sandra Gdaniec, Loes J.A. Gerringa, Aridane G. González, Mats Granskog, Brian Haley, Chad R. Hammerschmidt, Dennis A. Hansell, Paul B. Henderson, David C. Kadko, Karl Kaiser, Patrick Laan, Phoebe J. Lam, Carl H. Lamborg, Martin Levier, Xianglei Li, Andrew R. Margolin, Chris Measures, Rob Middag, Frank J. Millero, Willard S. Moore, Ronja Paffrath, H el ene Planquette, Benjamin Rabe, Heather Reader, Robert Rember, Micha J.A. Rijkenberg, Matthieu Roy-

- Barman, Michiel Rutgers van der Loeff, Mak Saito, Ursula Schauer, Peter Schlosser, Robert M. Sherrell, Alan M. Shiller, Hans Slagter, Jeroen E. Sonke, Colin Stedmon, Ryan J. Woosley, Ole Valk, Jan van Ooijen, and Ruifeng Zhang. 2020. "The Transpolar Drift as a Source of Riverine and Shelf-Derived Trace Elements to the Central Arctic Ocean." *Journal of Geophysical Research: Oceans* n/a (n/a):e2019JC015920. doi: 10.1029/2019jc015920.
- Chase, Zanna, Kenneth S. Johnson, Virginia A. Elrod, Joshua N. Plant, Steve E. Fitzwater, Lisa Pickell, and Carol M. Sakamoto. 2005. "Manganese and iron distributions off central California influenced by upwelling and shelf width." *Marine Chemistry* 95 (3):235-254. doi: <https://doi.org/10.1016/j.marchem.2004.09.006>.
- Chase, Zanna, Kenneth S. Johnson, Virginia A. Elrod, Joshua N. Plant, Steve E. Fitzwater, Lisa Pickell, and Carol M. Sakamoto. 2005. "Manganese and iron distributions off central California influenced by upwelling and shelf width." *Marine Chemistry* 95 (3):235-254. doi: <https://doi.org/10.1016/j.marchem.2004.09.006>.
- Cheize, M., H. F. Planquette, J. N. Fitzsimmons, E. Pelleret, R. M. Sherrell, C. Lambert, E. Bucciarelli, G. Sarthou, M. Le Goff, C. Liorzou, S. Chéron, E. Viollier, and N. Gayet. 2019. "Contribution of resuspended sedimentary particles to dissolved iron and manganese in the ocean: An experimental study." *Chemical Geology* 511:389-415. doi: <https://doi.org/10.1016/j.chemgeo.2018.10.003>.

- Cid, Abigail Parcasio, Seiji Nakatsuka, and Yoshiki Sohrin. 2012. "Stoichiometry among bioactive trace metals in the Chukchi and Beaufort Seas." *Journal of oceanography* 68 (6):985-1001.
- Corlett, W Bryce, and Robert S Pickart. 2017. "The Chukchi slope current." *Progress in Oceanography* 153:50-65.
- Cowen, James P., and Kenneth W. Bruland. 1985. "Metal deposits associated with bacteria: implications for Fe and Mn marine biogeochemistry." *Deep Sea Research Part A. Oceanographic Research Papers* 32 (3):253-272. doi: [https://doi.org/10.1016/0198-0149\(85\)90078-0](https://doi.org/10.1016/0198-0149(85)90078-0).
- Culberson, Charles H, George P Knapp, Marvel C Stalcup, Robert T Williams, and Frank Zemlyak. 1991. "A comparison of methods for the determination of dissolved oxygen in seawater."
- Cutter, G, P Andersson, Lou Codispoti, P Croot, R Francois, MC Lohan, H Obata, and Michiel Rutgers vd Loeff. 2010. Sampling and sample-handling protocols for GEOTRACES cruises. GEOTRACES.
- Fitzsimmons, Jessica N., and Edward A. Boyle. 2012. "An intercalibration between the GEOTRACES GO-FLO and the MITESS/Vanes sampling systems for dissolved iron concentration analyses (and a closer look at adsorption effects)." *Limnology and Oceanography: Methods* 10 (6):437-450. doi: 10.4319/lom.2012.10.437.
- Fitzsimmons, Jessica N, and Edward A Boyle. 2014. "Assessment and comparison of Anopore and cross flow filtration methods for the determination of dissolved

- iron size fractionation into soluble and colloidal phases in seawater." *Limnol. Oceanogr. Methods* 12:246-263.
- Fitzsimmons, Jessica N., and Edward A. Boyle. 2014. "Both soluble and colloidal iron phases control dissolved iron variability in the tropical North Atlantic Ocean." *Geochimica et Cosmochimica Acta* 125:539-550. doi: <http://dx.doi.org/10.1016/j.gca.2013.10.032>.
- Fitzsimmons, Jessica N., G. G. Carrasco, J. Wu, S. Roshan, M. Hatta, C. I. Measures, T. M. Conway, S. G. John, and E. A. Boyle. 2015. "Partitioning of dissolved iron and iron isotopes into soluble and colloidal phases along the GA03 GEOTRACES North Atlantic Transect." *Deep-Sea Research Part II: Topical Studies in Oceanography* 116:130-151. doi: 10.1016/j.dsr2.2014.11.014.
- Fitzsimmons, Jessica N., Seth G John, Christopher M Marsay, Colleen L Hoffman, Sarah L Nicholas, Brandy M Toner, Christopher R German, and Robert M Sherrell. 2017. "Iron persistence in a distal hydrothermal plume supported by dissolved–particulate exchange." *Nature Geoscience* 10 (3):195.
- Froelich, P. N., GP Klinkhammer, M Luedtke Bender, NA Luedtke, G Ross Heath, Doug Cullen, Paul Dauphin, Doug Hammond, Blayne Hartman, and Val Maynard. 1979. "Early oxidation of organic matter in pelagic sediments of the eastern equatorial Atlantic: suboxic diagenesis." *Geochimica et cosmochimica acta* 43 (7):1075-1090.
- German, C. R., K. A. Casciotti, J.-C. Dutay, L. E. Heimbürger, W. J. Jenkins, C. I. Measures, R. A. Mills, H. Obata, R. Schlitzer, A. Tagliabue, D. R. Turner, and

- H. Whitby. 2016. "Hydrothermal impacts on trace element and isotope ocean biogeochemistry." *Philosophical Transactions of the Royal Society A: Mathematical, Physical and Engineering Sciences* 374 (2081):20160035. doi: doi:10.1098/rsta.2016.0035.
- Gledhill, Martha, and Kristen N. Buck. 2012. "The Organic Complexation of Iron in the Marine Environment: A Review." *Frontiers in Microbiology* 3:69. doi: 10.3389/fmicb.2012.00069.
- Goldberg, Edward D. 1954. "Marine Geochemistry 1. Chemical Scavengers of the Sea." *The Journal of Geology* 62 (3):249-265. doi: 10.1086/626161.
- Granger, Julie, Daniel M. Sigman, Jonathan Gagnon, Jean-Eric Tremblay, and Alfonso Mucci. 2018. "On the Properties of the Arctic Halocline and Deep Water Masses of the Canada Basin from Nitrate Isotope Ratios." *Journal of Geophysical Research: Oceans* 123 (8):5443-5458. doi: 10.1029/2018jc014110.
- Hatta, M, CI Measures, KE Selph, M Zhou, and WT Hiscock. 2013. "Iron fluxes from the shelf regions near the South Shetland Islands in the Drake Passage during the austral-winter 2006." *Deep Sea Research Part II: Topical Studies in Oceanography* 90:89-101.
- Hatta, Mariko, Chris I Measures, Jingfeng Wu, Saeed Roshan, Jessica N Fitzsimmons, Peter Sedwick, and Pete Morton. 2015. "An overview of dissolved Fe and Mn distributions during the 2010–2011 US GEOTRACES north Atlantic cruises: GEOTRACES GA03." *Deep Sea Research Part II: Topical Studies in Oceanography* 116:117-129.

- Hein, James R., Natalia Konstantinova, Mariah Mikesell, Kira Mizell, Jessica N. Fitzsimmons, Phoebe J. Lam, Laramie T. Jensen, Yang Xiang, Amy Gartman, Georgy Cherkashov, Deborah R. Hutchinson, and Claire P. Till. 2017. "Arctic Deep Water Ferromanganese-Oxide Deposits Reflect the Unique Characteristics of the Arctic Ocean." *Geochemistry, Geophysics, Geosystems* 18 (11):3771-3800. doi: doi:10.1002/2017GC007186.
- Hioki, Nanako, Kenshi Kuma, Yuichirou Morita, Ryouhei Sasayama, Atsushi Ooki, Yoshiko Kondo, Hajime Obata, Jun Nishioka, Youhei Yamashita, Shigeto Nishino, Takashi Kikuchi, and Michio Aoyama. 2014. "Laterally spreading iron, humic-like dissolved organic matter and nutrients in cold, dense subsurface water of the Arctic Ocean." *Scientific Reports* 4 (1):6775. doi: 10.1038/srep06775.
- Hydes, D, M Aoyama, Alain Aminot, K Bakker, S Becker, S Coverly, Anne Daniel, A Dickson, O Grosso, and Roger Kerouel. 2010. "Determination of dissolved nutrients (N, P, Si) in seawater with high precision and inter-comparability using gas-segmented continuous flow analysers."
- Jakobsson, M, A Grantz, Y Kristoffersen, R Macnab, RW MacDonald, E Sakshaug, R Stein, and W Jokat. 2004. "The Arctic Ocean: Boundary conditions and background information." In *The organic carbon cycle in the Arctic Ocean*, 1-32. Springer.
- Jensen, L. T., N. J. Wyatt, W. M. Landing, and J. N. Fitzsimmons. 2020. "Assessment of the stability, sorption, and exchangeability of marine dissolved and colloidal

metals." *Marine Chemistry* 220:103754. doi:

<https://doi.org/10.1016/j.marchem.2020.103754>.

- Jensen, L. T., N. J. Wyatt, B. S. Twining, S. Rauschenberg, W. M. Landing, R. M. Sherrell, and J. N. Fitzsimmons. 2019. "Biogeochemical Cycling of Dissolved Zinc in the Western Arctic (Arctic GEOTRACES GN01)." *Global Biogeochemical Cycles* 33 (3):343-369. doi: 10.1029/2018gb005975.
- Johnson, Kenneth S, R Michael Gordon, and Kenneth H Coale. 1997. "What controls dissolved iron concentrations in the world ocean?" *Marine chemistry* 57 (3-4):137-161.
- Jones, E.P., and L. G. Anderson. 1986. "On the origin of the chemical properties of the Arctic Ocean halocline." *Journal of Geophysical Research: Oceans* 91 (C9):10759-10767. doi: 10.1029/JC091iC09p10759.
- Kadko, David, Frank J. Millero, Ryan Woosley, Dennis A. Hansell, James H. Swift, William M. Landing, William M. Jr. Smethie, and Peter Schlosser. 2016. Dissolved inorganic carbon, pH, alkalinity, temperature, salinity and other variables collected from discrete sample and profile observations using CTD, bottle and other instruments from HEALY in the Arctic Ocean, Beaufort Sea and Bering Sea from 2015-08-09 to 2015-10-13. edited by NOAA National Centers for Environmental Information.
- Kanna, Naoya, Takenobu Toyota, and Jun Nishioka. 2014. "Iron and macro-nutrient concentrations in sea ice and their impact on the nutritional status of surface

waters in the southern Okhotsk Sea." *Progress in Oceanography* 126:44-57.  
doi: <https://doi.org/10.1016/j.pocean.2014.04.012>.

Klunder, M. B., D. Bauch, P. Laan, H. J. W. de Baar, S. van Heuven, and S. Ober.  
2012. "Dissolved iron in the Arctic shelf seas and surface waters of the central  
Arctic Ocean: Impact of Arctic river water and ice-melt." *Journal of  
Geophysical Research: Oceans* 117 (C1):n/a-n/a. doi: 10.1029/2011JC007133.

Klunder, M. B., P. Laan, R. Middag, H. J. W. de Baar, and K. Bakker. 2012.  
"Dissolved iron in the Arctic Ocean: Important role of hydrothermal sources,  
shelf input and scavenging removal." *Journal of Geophysical Research:  
Oceans* 117 (C4):n/a-n/a. doi: 10.1029/2011JC007135.

Kondo, Yoshiko, Hajime Obata, Nanako Hioki, Atsushi Ooki, Shigeto Nishino,  
Takashi Kikuchi, and Kenshi Kuma. 2016. "Transport of trace metals (Mn, Fe,  
Ni, Zn and Cd) in the western Arctic Ocean (Chukchi Sea and Canada Basin) in  
late summer 2012." *Deep Sea Research Part I: Oceanographic Research  
Papers* 116:236-252. doi: <http://dx.doi.org/10.1016/j.dsr.2016.08.010>.

Koschinsky, Andrea, and James R. Hein. 2003. "Uptake of elements from seawater by  
ferromanganese crusts: solid-phase associations and seawater speciation."  
*Marine Geology* 198 (3):331-351. doi: [https://doi.org/10.1016/S0025-  
3227\(03\)00122-1](https://doi.org/10.1016/S0025-3227(03)00122-1).

Kuma, Kenshi, Jun Nishioka, and Katsuhiko Matsunaga. 1996. "Controls on iron (III)  
hydroxide solubility in seawater: the influence of pH and natural organic  
chelators." *Limnology and Oceanography* 41 (3):396-407.

- Lagerström, Maria, M. Field, Marie Seguret, Fisher E, Clark, and Robert Sherrell. 2013. "Automated on-line flow-injection ICP-MS determination of trace metals (Mn, Fe, Co, Ni, Cu and Zn) in open ocean seawater: Application to the GEOTRACES program." *Marine Chemistry* 155:71-80. doi: 10.1016/j.marchem.2013.06.001.
- Lam, Phoebe J., and James K. B. Bishop. 2008. "The continental margin is a key source of iron to the HNLC North Pacific Ocean." *Geophysical Research Letters* 35 (7). doi: 10.1029/2008gl033294.
- Landing, William M, and Kenneth W Bruland. 1987. "The contrasting biogeochemistry of iron and manganese in the Pacific Ocean." *Geochimica et Cosmochimica Acta* 51 (1):29-43.
- Lannuzel, Delphine, Andrew R Bowie, Pier C van der Merwe, Ashley T Townsend, and Véronique Schoemann. 2011. "Distribution of dissolved and particulate metals in Antarctic sea ice." *Marine Chemistry* 124 (1-4):134-146.
- Lewis, B. L., and W. M. Landing. 1991. "The biogeochemistry of manganese and iron in the Black Sea." *Deep Sea Research Part A. Oceanographic Research Papers* 38:S773-S803. doi: [https://doi.org/10.1016/S0198-0149\(10\)80009-3](https://doi.org/10.1016/S0198-0149(10)80009-3).
- Liu, Xuewu, and Frank J. Millero. 2002. "The solubility of iron in seawater." *Marine Chemistry* 77 (1):43-54. doi: [https://doi.org/10.1016/S0304-4203\(01\)00074-3](https://doi.org/10.1016/S0304-4203(01)00074-3).
- Luther, George W., Andrew S. Madison, Alfonso Mucci, Bjørn Sundby, and Véronique E. Oldham. 2015. "A kinetic approach to assess the strengths of ligands bound

to soluble Mn(III)." *Marine Chemistry* 173:93-99. doi:

<https://doi.org/10.1016/j.marchem.2014.09.006>.

Macdonald, R.W., E. C. Carmack, F. A. McLaughlin, K. Iseki, D. M. Macdonald, and M. C. O'Brien. 1989. "Composition and modification of water masses in the Mackenzie shelf estuary." *Journal of Geophysical Research: Oceans* 94 (C12):18057-18070. doi: 10.1029/JC094iC12p18057.

Macdonald, Robie W., and Charles Gobeil. 2012. "Manganese Sources and Sinks in the Arctic Ocean with Reference to Periodic Enrichments in Basin Sediments." *Aquatic Geochemistry* 18 (6):565-591. doi: 10.1007/s10498-011-9149-9.

Magen, Cédric, Alfonso Mucci, and Bjorn Sundby. 2011. "Reduction Rates of Sedimentary Mn and Fe Oxides: An Incubation Experiment with Arctic Ocean Sediments." *Aquatic Geochemistry* 17 (4):629-643. doi: 10.1007/s10498-010-9117-9.

Marsay, Chris M., Ana Aguilar-Islas, Jessica N. Fitzsimmons, Mariko Hatta, Laramie T. Jensen, Seth G. John, David Kadko, William M. Landing, Nathan T. Lanning, Peter L. Morton, Angelica Pasqualini, Sara Rauschenberg, Robert M. Sherrell, Alan M. Shiller, Benjamin S. Twining, Laura M. Whitmore, Ruifeng Zhang, and Clifton S. Buck. 2018. "Dissolved and particulate trace elements in late summer Arctic melt ponds." *Marine Chemistry* 204:70-85. doi: <https://doi.org/10.1016/j.marchem.2018.06.002>.

Martin, J. H., and G. A. Knauer. 1985. "Lateral transport of Mn in the north-east Pacific Gyre oxygen minimum." *Nature* 314 (6011):524-526. doi: 10.1038/314524a0.

- Measures, CI. 1999. "The role of entrained sediments in sea ice in the distribution of aluminium and iron in the surface waters of the Arctic Ocean." *Marine chemistry* 68 (1-2):59-70.
- Middag, R., H. J. W. de Baar, P. Laan, and M. B. Klunder. 2011. "Fluvial and hydrothermal input of manganese into the Arctic Ocean." *Geochimica et Cosmochimica Acta* 75 (9):2393-2408. doi: <http://dx.doi.org/10.1016/j.gca.2011.02.011>.
- Millero, Frank J., Sara Sotolongo, and Miguel Izaguirre. 1987. "The oxidation kinetics of Fe(II) in seawater." *Geochimica et Cosmochimica Acta* 51 (4):793-801. doi: [https://doi.org/10.1016/0016-7037\(87\)90093-7](https://doi.org/10.1016/0016-7037(87)90093-7).
- Münchow, Andreas, and Eddy C Carmack. 1997. "Synoptic flow and density observations near an Arctic shelf break." *Journal of physical Oceanography* 27 (7):1402-1419.
- Nakawo, M, and Nirmal Kumar Sinha. 1981. "Growth rate and salinity profile of first-year sea ice in the high Arctic." *Journal of Glaciology* 27 (96):315-330.
- Nakayama, Yuta, Satoshi Fujita, Kenshi Kuma, and Koji Shimada. 2011. "Iron and humic-type fluorescent dissolved organic matter in the Chukchi Sea and Canada Basin of the western Arctic Ocean." *Journal of Geophysical Research: Oceans* 116 (C7):n/a-n/a. doi: 10.1029/2010JC006779.
- Nealson, Kenneth H., Bradley M. Tebo, and Reinhardt A. Rosson. 1988. "Occurrence and Mechanisms of Microbial Oxidation of Manganese." In *Advances in Applied Microbiology*, edited by Allen I. Laskin, 279-318. Academic Press.

- Newton, Robert, Peter Schlosser, Richard Mortlock, James Swift, and Robie MacDonald. 2013. "Canadian Basin freshwater sources and changes: Results from the 2005 Arctic Ocean Section." *Journal of Geophysical Research: Oceans* 118 (4):2133-2154. doi: doi:10.1002/jgrc.20101.
- Nishimura, Shotaroh, Kenshi Kuma, Satoko Ishikawa, Aya Omata, and Sei-ichi Saitoh. 2012. "Iron, nutrients, and humic-type fluorescent dissolved organic matter in the northern Bering Sea shelf, Bering Strait, and Chukchi Sea." *Journal of Geophysical Research: Oceans* 117 (C2):n/a-n/a. doi: 10.1029/2011JC007355.
- Nishino, Shigeto, Koji Shimada, and Motoyo Itoh. 2005. "Use of ammonium and other nitrogen tracers to investigate the spreading of shelf waters in the western Arctic halocline." *Journal of Geophysical Research: Oceans* 110 (C10):n/a-n/a. doi: 10.1029/2003JC002118.
- Noble, Abigail E., Carl H. Lamborg, Dan C. Ohnemus, Phoebe J. Lam, Tyler J. Goepfert, Chris I. Measures, Caitlin H. Frame, Karen L. Casciotti, Giacomo R. DiTullio, Joe Jennings, and Mak A. Saito. 2012. "Basin-scale inputs of cobalt, iron, and manganese from the Benguela-Angola front to the South Atlantic Ocean." *Limnology and Oceanography* 57 (4):989-1010. doi: doi:10.4319/lo.2012.57.4.0989.
- Noble, Abigail E., Mak A. Saito, Kanchan Maiti, and Claudia R. Benitez-Nelson. 2008. "Cobalt, manganese, and iron near the Hawaiian Islands: A potential concentrating mechanism for cobalt within a cyclonic eddy and implications for the hybrid-type trace metals." *Deep Sea Research Part II: Topical Studies in*

- Oceanography* 55 (10):1473-1490. doi:  
<https://doi.org/10.1016/j.dsr2.2008.02.010>.
- Ohnemus, Daniel C., and Phoebe J. Lam. 2015. "Cycling of lithogenic marine particles in the US GEOTRACES North Atlantic transect." *Deep Sea Research Part II: Topical Studies in Oceanography* 116:283-302. doi:  
<https://doi.org/10.1016/j.dsr2.2014.11.019>.
- Oldham, Véronique E., Alfonso Mucci, Bradley M. Tebo, and George W. Luther III. 2017. "Soluble Mn(III)–L complexes are abundant in oxygenated waters and stabilized by humic ligands." *Geochimica et Cosmochimica Acta* 199:238-246. doi: <http://dx.doi.org/10.1016/j.gca.2016.11.043>.
- Oldham, Véronique E, Shannon M Owings, Matthew R Jones, Bradley M Tebo, and George W Luther III. 2015. "Evidence for the presence of strong Mn (III)-binding ligands in the water column of the Chesapeake Bay." *Marine Chemistry* 171:58-66.
- Raiswell, Robert. 2011. "Iron transport from the continents to the open ocean: The aging–rejuvenation cycle." *Elements* 7 (2):101-106.
- Rijkenberg, Micha J. A., Hans A. Slagter, Michiel Rutgers van der Loeff, Jan van Ooijen, and Loes J. A. Gerringa. 2018. "Dissolved Fe in the Deep and Upper Arctic Ocean With a Focus on Fe Limitation in the Nansen Basin." *Frontiers in Marine Science* 5 (88). doi: 10.3389/fmars.2018.00088.
- Rudels, B. 2015. "Arctic Ocean circulation, processes and water masses: A description of observations and ideas with focus on the period prior to the International

- Polar Year 2007–2009." *Progress in Oceanography* 132:22-67. doi:  
<http://dx.doi.org/10.1016/j.pocean.2013.11.006>.
- Rudnick, RL, and S Gao. 2003. "Composition of the continental crust." *The crust* 3:1-64.
- Rue, Eden L, and Kenneth W Bruland. 1995. "Complexation of iron (III) by natural organic ligands in the Central North Pacific as determined by a new competitive ligand equilibration/adsorptive cathodic stripping voltammetric method." *Marine chemistry* 50 (1-4):117-138.
- Saager, Paul M., Hein J. W. De Baar, and Peter H. Burkill. 1989. "Manganese and iron in Indian Ocean waters." *Geochimica et Cosmochimica Acta* 53 (9):2259-2267. doi: [https://doi.org/10.1016/0016-7037\(89\)90348-7](https://doi.org/10.1016/0016-7037(89)90348-7).
- Sakshaug, E. 2004. "Primary and secondary production in the Arctic Seas." In *The organic carbon cycle in the Arctic Ocean*, 57-81. Springer.
- Sanial, V, LE Kipp, PB Henderson, P van Beek, J-L Reyss, DE Hammond, NJ Hawco, MA Saito, JA Resing, and P Sedwick. 2017. "Radium-228 as a tracer of dissolved trace element inputs from the Peruvian continental margin." *Marine Chemistry*.
- Schlitzer, Reiner. 2016. "Ocean data view." <http://odv.awi.de>.
- Scholz, Florian, Christian Hensen, Anna Noffke, Anne Rohde, Volker Liebetrau, and Klaus Wallmann. 2011. "Early diagenesis of redox-sensitive trace metals in the Peru upwelling area – response to ENSO-related oxygen fluctuations in the

- water column." *Geochimica et Cosmochimica Acta* 75 (22):7257-7276. doi:  
<https://doi.org/10.1016/j.gca.2011.08.007>.
- Sedwick, P. N., P. R. Edwards, D. J. Mackey, F. B. Griffiths, and J. S. Parslow. 1997.  
"Iron and manganese in surface waters of the Australian subantarctic region."  
*Deep Sea Research Part I: Oceanographic Research Papers* 44 (7):1239-1253.  
doi: [https://doi.org/10.1016/S0967-0637\(97\)00021-6](https://doi.org/10.1016/S0967-0637(97)00021-6).
- Sherrell, Robert M., Amber L. Annett, Jessica N. Fitzsimmons, Vincent J. Rocanova,  
and Michael P. Meredith. 2018. "A "shallow bathtub ring" of local sedimentary  
iron input maintains the Palmer Deep biological hotspot on the West Antarctic  
Peninsula shelf." *Philosophical Transactions of the Royal Society A:  
Mathematical, Physical and Engineering Sciences* 376 (2122):20170171. doi:  
[doi:10.1098/rsta.2017.0171](https://doi.org/10.1098/rsta.2017.0171).
- Shimada, Koji, Motoyo Itoh, Shigeto Nishino, Fiona McLaughlin, Eddy Carmack, and  
Andrey Proshutinsky. 2005. "Halocline structure in the Canada Basin of the  
Arctic Ocean." *Geophysical Research Letters* 32 (3):n/a-n/a. doi:  
[10.1029/2004GL021358](https://doi.org/10.1029/2004GL021358).
- Sholkovitz, ER, EA Boyle, and NB Price. 1978. "The removal of dissolved humic acids  
and iron during estuarine mixing." *Earth and Planetary Science Letters* 40  
(1):130-136.
- Sholkovitz, Edward R. 1978. "The flocculation of dissolved Fe, Mn, Al, Cu, NI, Co and  
Cd during estuarine mixing." *Earth and Planetary Science Letters* 41 (1):77-86.

- Slagter, Hans A., Luis M. Laglera, Camila Sukekava, and Loes J. A. Gerringa. 2019. "Fe-Binding Organic Ligands in the Humic-Rich TransPolar Drift in the Surface Arctic Ocean Using Multiple Voltammetric Methods." *Journal of Geophysical Research: Oceans* 124 (3):1491-1508. doi: 10.1029/2018jc014576.
- Slagter, H. A., H. E. Reader, M. J. A. Rijkenberg, M. Rutgers van der Loeff, H. J. W. de Baar, and L. J. A. Gerringa. 2017. "Organic Fe speciation in the Eurasian Basins of the Arctic Ocean and its relation to terrestrial DOM." *Marine Chemistry* 197:11-25. doi: <https://doi.org/10.1016/j.marchem.2017.10.005>.
- Stumm, W, and JJ Morgan. 1981. "Aquatic Chemistry, 780 pp." *J. Wiley & Sons*.
- Sunda, WG, SA Huntsman, and GR Harvey. 1983. "Photoreduction of manganese oxides in seawater and its geochemical and biological implications." *Nature* 301 (5897):234-236.
- Sunda, William G. 2012. "Feedback interactions between trace metal nutrients and phytoplankton in the ocean." *Frontiers in Microbiology* 3. doi: 10.3389/fmicb.2012.00204.
- Sunda, William G., SA Huntsman, and GR Harvey. 1983. "Photoreduction of manganese oxides in seawater and its geochemical and biological implications." *Nature* 301 (5897):234.
- Sunda, William G, and Susan A Huntsman. 1994. "Photoreduction of manganese oxides in seawater." *Marine chemistry* 46 (1-2):133-152.
- Sunda, William G, and Susan A Huntsman. 1995. "Iron uptake and growth limitation in oceanic and coastal phytoplankton." *Marine Chemistry* 50 (1-4):189-206.

- Sunda, William G, and Susan A Huntsman. 1998. "Interactions among Cu<sup>2+</sup>, Zn<sup>2+</sup>, and Mn<sup>2+</sup> in controlling cellular Mn, Zn, and growth rate in the coastal alga *Chlamydomonas*." *Limnology and Oceanography* 43 (6):1055-1064.
- Tagliabue, Alessandro, Andrew R Bowie, Philip W Boyd, Kristen N Buck, Kenneth S Johnson, and Mak A Saito. 2017. "The integral role of iron in ocean biogeochemistry." *Nature* 543 (7643):51-59.
- Talley, Lynne D., George L. Pickard, William J. Emery, and James H. Swift. 2011. "Chapter 12 - Arctic Ocean and Nordic Seas." In *Descriptive Physical Oceanography (Sixth Edition)*, 401-436. Boston: Academic Press.
- Tebo, Bradley M. 1991. "Manganese(II) oxidation in the suboxic zone of the Black Sea." *Deep Sea Research Part A. Oceanographic Research Papers* 38:S883-S905. doi: [https://doi.org/10.1016/S0198-0149\(10\)80015-9](https://doi.org/10.1016/S0198-0149(10)80015-9).
- Tebo, Bradley M., John R. Bargar, Brian G. Clement, Gregory J. Dick, Karen J. Murray, Dorothy Parker, Rebecca Verity, and Samuel M. Webb. 2004. "BIOGENIC MANGANESE OXIDES: Properties and Mechanisms of Formation." *Annual Review of Earth and Planetary Sciences* 32 (1):287-328. doi: 10.1146/annurev.earth.32.101802.120213.
- Tovar-Sánchez, Antonio, Carlos M. Duarte, Juan C. Alonso, Silvia Lacorte, Romà Tauler, and Cristobal Galbán-Malagón. 2010. "Impacts of metals and nutrients released from melting multiyear Arctic sea ice." *Journal of Geophysical Research: Oceans* 115 (C7):n/a-n/a. doi: 10.1029/2009JC005685.

- Trefry, John H, Robert P Trocine, Lee W Cooper, and Kenneth H Dunton. 2014. "Trace metals and organic carbon in sediments of the northeastern Chukchi Sea." *Deep Sea Research Part II: Topical Studies in Oceanography* 102:18-31.
- Twining, B. S., S. Rauschenberg, and Pete Morton. 2017. "Trace metal contents of biogenic particles and phytoplankton in the upper Arctic Ocean and Arctic sea ice." ASLO Aquatic Sciences, Honolulu, HI.
- Twining, B. S., Sara Rauschenberg, Peter L. Morton, and Stefan Vogt. 2015. "Metal contents of phytoplankton and labile particulate material in the North Atlantic Ocean." *Progress in Oceanography* 137 (Part A):261-283. doi: <https://doi.org/10.1016/j.pocean.2015.07.001>.
- Vancoppenolle, Martin, Thierry Fichefet, and Cecilia M Bitz. 2006. "Modeling the salinity profile of undeformed Arctic sea ice." *Geophysical research letters* 33 (21).
- Vandieken, Verona, Maren Nickel, and Bo Barker Jørgensen. 2006. "Carbon mineralization in Arctic sediments northeast of Svalbard: Mn (IV) and Fe (III) reduction as principal anaerobic respiratory pathways." *Marine Ecology Progress Series* 322:15-27.
- Vieira, Lúcia H., Eric P. Achterberg, Jan Scholten, Aaron J. Beck, Volker Liebetrau, Matthew M. Mills, and Kevin R. Arrigo. 2019. "Benthic fluxes of trace metals in the Chukchi Sea and their transport into the Arctic Ocean." *Marine Chemistry* 208:43-55. doi: <https://doi.org/10.1016/j.marchem.2018.11.001>.

- von Langen, Peter J, Kenneth S Johnson, Kenneth H Coale, and Virginia A Elrod. 1997. "Oxidation kinetics of manganese (II) in seawater at nanomolar concentrations." *Geochimica et Cosmochimica Acta* 61 (23):4945-4954.
- Wells, Mark L. 2002. "Marine colloids and trace metals." *Biogeochemistry of marine dissolved organic matter*:367-404.
- Whitmore, Laura M., Peter L. Morton, Benjamin S. Twining, and Alan M. Shiller. 2019. "Vanadium cycling in the Western Arctic Ocean is influenced by shelf-basin connectivity." *Marine Chemistry* 216:103701. doi: <https://doi.org/10.1016/j.marchem.2019.103701>.
- Woodgate, Rebecca A., Knut Aagaard, James H. Swift, Kelly K. Falkner, and William M. Smethie. 2005. "Pacific ventilation of the Arctic Ocean's lower halocline by upwelling and diapycnal mixing over the continental margin." *Geophysical Research Letters* 32 (18):n/a-n/a. doi: 10.1029/2005GL023999.
- Yamashita, Youhei, Jun Nishioka, Hajime Obata, and Hiroshi Ogawa. 2020. "Shelf humic substances as carriers for basin-scale iron transport in the North Pacific." *Scientific Reports* 10 (1):4505. doi: 10.1038/s41598-020-61375-7.
- Yeats, PA, and PM Strain. 1990. "The oxidation of manganese in seawater: rate constants based on field data." *Estuarine, Coastal and Shelf Science* 31 (1):11-24.
- Zhang, Ruifeng, Laramie T. Jensen, Jessica N. Fitzsimmons, Robert M. Sherrell, and Seth John. 2019. "Dissolved cadmium and cadmium stable isotopes in the

western Arctic Ocean." *Geochimica et Cosmochimica Acta* 258:258-273. doi:  
<https://doi.org/10.1016/j.gca.2019.05.028>.

## 5. A NOVEL RELATIONSHIP BETWEEN DISSOLVED COPPER AND NICKEL IN THE WESTERN ARCTIC OCEAN (GEOTRACES GN01)

### 5.1. Introduction

Trace metals across the global ocean act as essential micronutrients as well as tracers of important biogeochemical processes based on their distribution and behavior. Nickel (Ni) is typically classified as a “nutrient-type” element based on its “macronutrient-like” profile shape, while copper (Cu) is classified as a “hybrid-type” element because it has a linearly-increasing concentration with depth, indicating that other abiotic processes are significant (Bruland et al., 2014). Copper is biologically active and serves as an essential metalloenzyme center for proteins such as cytochrome oxidase (Wood, 1978), iron acquisition proteins (Maldonado et al., 2006), and denitrification proteins (Granger and Ward, 2003), resulting in an essential cellular requirement for Cu (Ho et al., 2003) and potential co-limitation with other micronutrients (Annett et al., 2008). However, high concentrations of available Cu are known to be toxic to phytoplankton (Moffett et al., 1997), leading to surface complexation by organic ligands (>95%, (Coale and Bruland, 1988; Moffett and Brand, 1996)) that serves to buffer Cu to an acceptable level for optimal growth (Bruland et al., 2014).

Copper concentrations are depleted in surface waters due to this biological uptake, indicating its biological demand. However, Cu also increases linearly with depth (Jacquot and Moffett, 2015; Roshan and Wu, 2015), unlike most “nutrient-type” metals such as zinc, cadmium, and Ni, which follow a sharp concentration increase in the

nutricline and then have generally constant concentrations at depth, similar to major macronutrients. Scavenging is known to play a role in Cu removal in the deep water (Boyle et al., 1977; Moore, 1978; Noriki et al., 1998), explaining why its concentration does not increase as much over thermohaline circulation. However, copper's unique linear profile suggests a sediment/deep water source (Hines et al., 1984; Biller and Bruland, 2013) or possible reversible scavenging at depth, similar to thorium or Zn (Little et al., 2014b). Like iron, Cu is highly organically complexed throughout the water column (>99%, Cole and Bruland, 1988; Moffett, 1995; Buck and Bruland, 2005, Vraspir and Butler, 2009; Jacquot and Moffett, 2015). Margin and benthic sources are thought to be significant inputs of Cu to both surface and bottom waters (Boyle et al., 1981; Heggie et al., 1987), pointing to the important role of sediments alongside rivers and aerosol fluxes, which are the major external sources of Cu to the global ocean (Richon and Tagliabue, 2019).

Nickel also serves as an essential micronutrient and follows the “macronutrient-like” profile shape of surface depletion and regeneration with depth. As a protein metal center, it catalyzes the assimilation of urea in the enzyme urease and also serves as the center of a nickel superoxide dismutase enzyme (Dupont et al., 2008; Sunda, 2012; Twining and Baines, 2013). Nickel has been found to be co-limiting with nitrogen (Price and Morel, 1991), which is of particular interest in areas like the Arctic Ocean that are nitrogen limited (Taylor et al., 2013; Rijkenberg et al., 2018). While Ni speciation has been studied much less than metals such as iron and Cu, 10-60% of Ni is potentially bound by organic ligands (Donat et al., 1994; Saito et al., 2004; Vraspir and Butler,

2009). Unlike some other nutrient-type metals, Ni appears to have both shallow and deep water regeneration similar to phosphate and silicate, respectively (Sclater et al., 1976; Böning et al., 2015), which perhaps points to the important role of diatom activity in controlling Ni's global distribution and relationship to macronutrients (Twining and Baines, 2013; Böning et al., 2015; Middag et al., 2020). Beyond biological uptake and regeneration, the inputs of Ni to the ocean are not well constrained, although continental margin and river sources have been suggested to play a significant role (Westerlund et al., 1986; Bowie et al., 2002; Cameron and Vance, 2014).

Because of their different profile shapes and biogeochemical controls, Cu and Ni are not often directly compared in the ocean. Some early studies of trace metals predicated on establishing baseline global trace metal distributions did compare Cu and Ni alongside other nutrient-type elements such as Cd and Zn (Bruland, 1980; Boyle et al., 1981; Dickson and Hunter, 1981; Spivack et al., 1983; Danielsson et al., 1985; Nolting and de Baar, 1994; Yeats et al., 1995; Noriki et al., 1998), but these studies very rarely juxtaposed Cu and Ni directly. Notably, Cu and Ni have both been observed to be complexed by marine humics (Whitby and Van den Berg, 2014; Abbualhaija et al., 2015) and may compete for similar ligand groups as divalent metals in the open ocean (Boiteau et al., 2016). Copper has anthropogenic sources, is prone to scavenging and is highly complexed by organic ligands, while Ni follows typical macronutrient distributions and has less well-constrained chemical speciation. However, a comparison of the two is not without merit, as both share riverine and continental sources (Böning et al., 2015; Richon and Tagliabue, 2019) and some nutrient-like dynamics.

The Arctic Ocean is an enclosed basin dominated by continental shelf area (>50%, (Jakobsson et al., 2004)) and riverine input (Ekwurzel et al., 2001), representing a potentially large source of Cu and Ni. Additionally, the Arctic Ocean is a point of mixing between the North Atlantic and North Pacific Oceans, which have starkly different trace metal signatures (Sunda, 2012). Prior studies of trace metals in the Arctic have noted high Cu, Ni, and other trace metal concentrations in surface and subsurface waters (Moore, 1981; Danielsson and Westerlund, 1983; Yeats, 1988; Yeats and Westerlund, 1991; Middag et al., 2011; Cid et al., 2012; Klunder et al., 2012b; Klunder et al., 2012a; Kondo et al., 2016; Jensen et al., 2019). The origin of these subsurface enrichments in the Western Arctic is the Chukchi Shelf and the upper halocline water mass that advect shelf material offshore into the central Arctic (Cid et al., 2012; Kondo et al., 2016; Jensen et al., 2019). Notably, Cu and Ni appear to share the same profile shape in the Arctic Ocean (Cid et al., 2012; Kondo et al., 2016) with high surface concentrations that decrease with depth, a direct contradiction to their typical global distribution. In fact, Cu and Ni appear to be linearly correlated in this region (Figure 5.1).

Here, we use the U.S. Arctic GEOTRACES GN01 section in the Western Arctic (Figure 5.2) to rigorously juxtapose marine Cu and Ni cycling, with a primary motivation to understand why they share a surprisingly similar distribution in the Arctic Ocean that is absent in other global ocean basins. Our null hypothesis is based on their different “elemental personalities” suggested by studies of the other major ocean basins: Ni should follow macronutrient silicate and phosphate distributions, while Cu and

should exhibit signs of scavenging and linear regeneration with depth. This does not appear to be the whole story for these metals in the Arctic, which has a wealth of important trace metal sources to shallow waters such as riverine inputs, sea ice melt, and the shelf-derived halocline. Using the framework of the Cu-Ni linear correlation observed in the Arctic, we will answer the following questions: 1) What processes cause Cu and Ni to be linearly correlated in the Western Arctic Ocean, particularly in the surface? and 2) How does this compare to the Cu-Ni relationship in the rest of the global ocean?

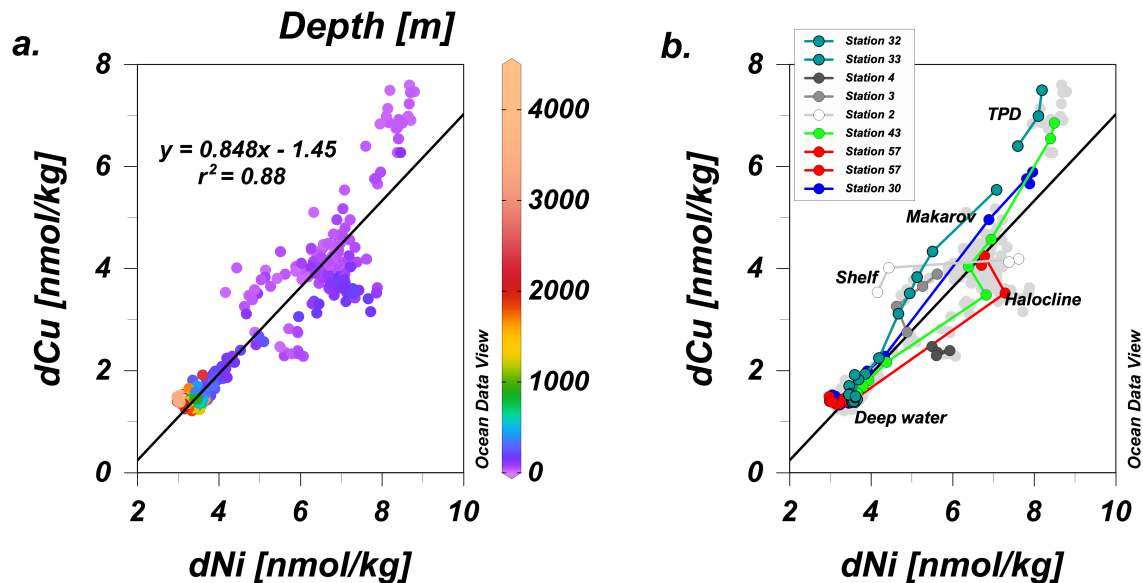


**Figure 5.1** Linear correlation of Cu and Ni in the Western Arctic Ocean on GEOTRACES GN01 (excluding Station 1 in the Pacific). a) Ni vs. Cu across the whole water column with depth by color, which highlights that the Cu-Ni linear relationship is primarily driven by surface samples. b) The same Ni vs. Cu relationship (gray dots in background) and slope (black line) but with individual stations highlighted in color to emphasize certain oceanographic features, including the Bering Strait and Shelf (dark gray, Stations 2,3,4), the Canada Basin and Upper Halocline Layer (green and red, Stations 43 and 57, respectively), the Eurasian-influenced Makarov Basin (teal, Station 32), and the riverine-influenced Transpolar Drift (teal, Stations 32, 33).

## 5.2. Methods

### 5.2.1. Sample collection

Seawater samples for this study were collected along the 2015 U.S. Arctic GEOTRACES GN01 cruise departing from Dutch Harbor, AK aboard the USCGC *Healy* on 9 August 2015 and returning 12 October 2015. The cruise originated in the North Pacific (Station 1, Figure 5.2) and continued through the Bering Strait northward along 170-180°W across the western Chukchi Shelf to the North Pole (“northbound”) and then back along 150°W to terminate again on the eastern Chukchi Shelf (“southbound”). Full depth samples were taken along the Bering Strait, Chukchi Shelf, and Canada, Makarov, and Amundsen basins (Figure 5.2). Additionally, shallow casts collected clean near-surface samples (1-20 m) through ice holes at select stations (Stations 31, 33, 39, 42, 43, 46) north of 84°N (blue, Figure 5.2) and within the marginal ice zone (orange, Figure 5.2).

Dissolved trace metals Cu and Ni were collected following established trace metal clean GEOTRACES protocols (Cutter et al., 2010; Cutter and Bruland, 2012). Briefly, seawater was collected using a trace metal clean CTD rosette (Seabird) on a Vectran cable, mounted with 24 x 12 L GO-Flo bottles. The GO-Flo bottles were tripped at the desired sampling depth on ascent at ~3 m/min, and upon recovery each bottle was immediately moved into a clean, positive pressure sampling area and pressurized (~0.5 atm) with HEPA-filtered air. Each GO-Flo bottle was fitted with a 0.2 um AcroPak-200 polyethersulfone filter capsule (Pall), and seawater was filtered into an acid cleaned 250

mL low density polyethylene (LDPE) Nalgene bottle following three 10% volume rinses of the bottle, cap, and threads.

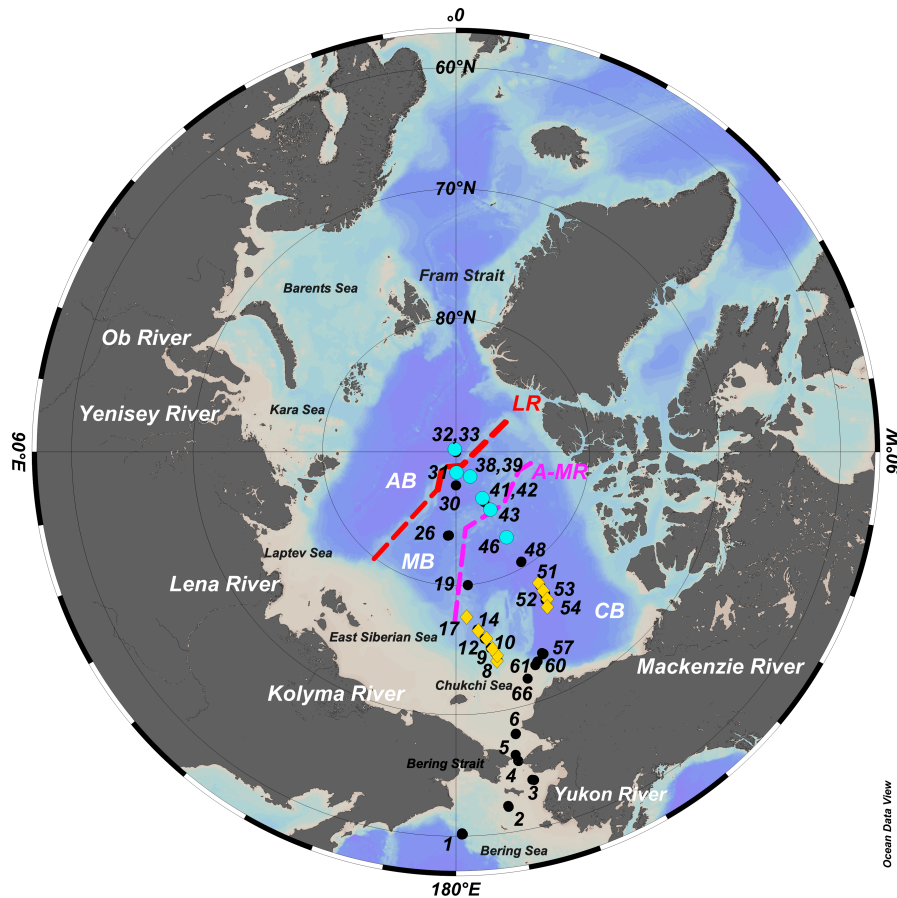


**Figure 5.2** U.S. GEOTRACES Arctic GN01 transect labeled with relevant stations, rivers, seas, and bathymetric features identified. Blue dots = ice Stations 31, 33, 39, 42, 43, gold diamonds = MIZ Stations 8, 9, 10, 12, 52, 53, 54, black dots = full depth stations. AB = Amundsen Basin, MB = Makarov Basin, CB = Canada Basin, LR = Lomonosov Ridge, A-MR = Alpha-Mendeleev Ridge. Stations 2-5 are considered “Bering Strait” while stations 6-8, 66-61 are “Chukchi Shelf.” Stations 8-31 are “northbound” transect, Station 32 is the North Pole, and Stations 38-66 are “southbound” transect. Blue dots are ice stations (Stations 31, 33, 39, 42, 43, 46) and orange diamonds are within the MIZ (Stations 8-17, 51-54). Station 1 is the North Pacific endmember.

Surface and ice hole dissolved samples (Stations 31, 33, 39, 42, 43, 46) were collected by small boat (~1 m), or through holes drilled through the sea ice at 1, 5, and

20 m depth using a polypropylene high-head battery-powered motor diaphragm pump with ½-inch FEP-lined Tygon tubing (Cole Parmer) fitted with a 0.2 µm AcroPak filter. Samples were subsequently filtered on the ice into a 25 L acid-cleaned LDPE carboy and immediately subsampled into clean LDPE bottles on the ship. All samples were promptly acidified in a clean area to pH<2 (0.012M HCl, Optima, Fisher Scientific) according to Fitzsimmons & Boyle (2012).

### **5.2.2. Analysis**

Following at least 9 months of acidification to allow adequate desorption from bottle walls (Jensen et al., 2020) samples were pre-concentrated for dissolved Cu and Ni using a SeaFAST-pico system (ESI) at Texas A&M University coupled with an isotope dilution and standard curve method following (Lagerström et al., 2013) and fully described in (Jensen et al., 2020). A 10 mL aliquot of sample was taken up by the SeaFAST system following equilibration with <sup>65</sup>Cu and <sup>62</sup>Ni spike and subsequently buffered to pH 6.2±0.3 and loaded onto a column containing Nobias-chelate PA1 resin. The sample was then back-eluted with 10% (v/v) HNO<sub>3</sub> (Optima, Fisher Scientific) into a 400 uL eluent (25x pre-concentration). This eluent was then promptly analyzed in medium resolution on a Thermo Element XR high-resolution inductively-coupled plasma mass spectrometer (HR-ICP-MS) at the R. Ken Williams Radiogenic laboratory at Texas A&M University. Accuracy, precision, procedural blanks, and limits of detection of these measurements are summarized in Table 1.

**Table 5.1.1** Reported values of consensus SAFe D1, D2, and S solutions, as well as blanks and detection limits for dissolved Cu and Ni over the analytical sessions used for GN01 samples.

CRM	n	Element (nmol/kg)	
		Ni	Cu
<b>SAFe D1</b>	35	8.609	2.035
<b>stdev</b>		0.176	0.081
Consensus (May 2013)		8.580	2.270
stdev		0.260	0.110
<b>SAFe D2</b>	32	8.714	2.192
<b>stdev</b>		0.166	0.099
Consensus (May 2013)		8.630	2.280
stdev		0.250	0.150
<b>SAFe S</b>	4	2.401	0.544
<b>stdev</b>		0.020	0.013
Consensus (May 2013)		2.280	0.520
stdev		0.090	0.050
<b>Element (pmol/kg)</b>			
	n	Ni	Cu
<b>Average blank</b>	31	15.2	12.4
<b>Detection limit (3*stdev of blank)</b>	29	8.45	5.08

### 5.3. Results

#### 5.3.1. Hydrography

The Arctic Ocean is an isolated basin, dominated by shallow continental shelves and limited in exchange with the Pacific and Atlantic Oceans to relatively shallow sills (50 and 2600 m, respectively). In addition, it has year-round ice coverage, and it receives 11% of the global riverine flux despite comprising only 1% of the ocean by volume (Opsahl and Benner, 1999). This leads to a large freshwater reservoir in the surface Arctic and water masses dictated largely by changes in salinity due to brine rejection during sea ice formation and the relatively isothermal nature of polar oceans.

The surface Arctic is commonly referred to as the polar mixed layer (PML) and extends from approximately 0 to 50 m (Talley et al., 2011; Rudels, 2015). In the Western Arctic, this is comprised mainly of Pacific waters advected through the Bering Strait (50 m sill), riverine discharge, and ice melt, and it has a low salinity of 22 to 31 and a potential temperature ranging -1.8 to 1.8°C along the GN01 transect. This layer is well ventilated and well-mixed itself, but its low salinity generally prevents ventilation of the underlying denser water masses. A prominent feature of the PML is the surface transpolar drift (TPD) current that brings Eurasian shelf-modified river water across the middle of the Arctic Ocean and out through the Fram Strait and Canadian Archipelago (Rudels, 2015). The TPD is characterized by high organic matter and other markers of terrigenous inputs, as well as elevated trace metals (Charette et al., 2020). For the purposes of this study, we consider the PML to extend from the surface to where the salinity sharply increases, indicating the first subsurface water mass: the halocline.

The halocline of the Arctic Ocean, directly below the PML, is a unique feature formed on Arctic continental shelves as a result of brine rejection during sea ice formation (Aagaard et al., 1981). The Canada Basin of the Western Arctic presents with a so-called “double” halocline feature, due to the presence of advected Pacific waters over the Chukchi Shelf. As brine is rejected during sea ice formation on the shallow Chukchi Shelf, a cold, salty water mass forms and subducts under the PML and extends well into the Canada basin, forming the Upper Halocline Layer (UHL, S 31-33.1, ~50-150 m; (Aagaard et al., 1981; Shimada et al., 2005; Woodgate et al., 2005)). Often, we delineate the UHL with its elevated silica ( $\text{Si}$ ) > 25  $\mu\text{mol/kg}$  (Jones and Anderson, 1986;

Anderson et al., 2013) (Figure 5.3). Below this, there is a Lower Halocline Layer (LHL, S 33.1-34.7, ~150-300 m), which originates from Atlantic-derived shelf waters mixed with UHL waters (Jones and Anderson, 1986). The Makarov basin has a “single” halocline, or change in salinity (S 31-34.3, ~50-100m), which is primarily derived from the Eurasian (Eastern Arctic) shelves mixed with some Pacific-derived water (Rudels, 2015). Likewise, Station 32 in the Amundsen Basin has a single, Eurasian-influenced halocline (S 32.7-34.7) (Rudels et al., 2004).

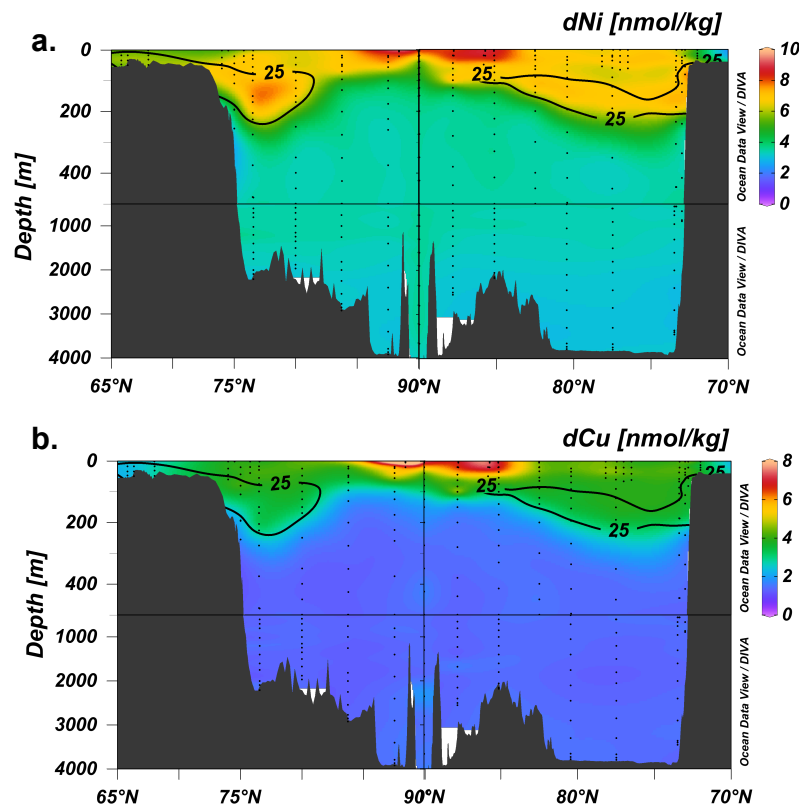


**Figure 5.3** Full depth sections of dissolved a) Ni and b) Cu across the GN01 transect, with the northbound (170-180°W) section on the left and the southbound section (150°W) on the right; the North Pole is the black line in the middle. The top section of each panel is zoomed to the upper 500 m and the bottom section from 500-4000m. Black contours are Si = 25 umol/kg to indicate the bounds of the UHL as described in the text.

Below the halocline layers across all basins are the intermediate Atlantic waters and deep waters. The upper Atlantic layer, called the Fram Strait Branch (FSB, (Rudels et al., 2004)), has a noticeable maximum in potential temperature of  $\theta > 0^\circ\text{C}$  and sits between ~350 and 800 m. Below this, there is another Atlantic-derived layer known as the Barents Sea Branch, which has a different water mass history, including mixing from the shallower Barents Sea (Woodgate et al., 2001; Schauer et al., 2002). Below the Atlantic layers are the homogenous, poorly ventilated Arctic deep waters (Aagaard et al., 1985; Talley et al., 2011). More detail on hydrography and water mass specifications made here for the GN01 transect can be found in (Jensen et al., 2019). For the purposes of this study, the stations and geographic areas of interest are defined and labeled in Figure 2.

### **5.3.2. Copper and Nickel in the Arctic Ocean**

The major result of this study is that dissolved Cu and Ni share a similar distribution (Figure 5.3) in the Western Arctic Ocean that is unexpected based on prior studies of these elements in other major ocean basins (Figure 5.4). Importantly, copper and Ni distributions are different in the Arctic than in these other ocean basins in three major ways. First, Arctic Cu concentration ranges extend to greater concentrations than found in other major ocean basins (Figure 5.4). Second, Arctic profile shapes of Cu and Ni are unique and do not follow the strict “hybrid-type” and “nutrient-type” profile shapes, respectively, observed in rest of the global ocean (Figure 5.4); we note that this was also true for Zn (Jensen et al. 2019), Cd (Zhang et al. 2019), and Co (Bundy et al. 2020) along the GN01 Western Arctic transect. Finally, copper and Ni in the Arctic

appear very similar to each other in profile shape (Figure 5.4) and share a remarkable linear correlation in the Arctic (Figure 5.1). A potentially important clue in resolving these unique observations is that the high Cu and Ni concentrations driving the linear Cu-Ni relationship mostly come from surface and intermediate waters (upper 500 m, cold colors in Figure 5.1a), while deeper Arctic waters have low, homogenous concentrations (hot colors in Figure 5.1a). In order to identify the chemical processes responsible for these unique Cu and Ni distributions, the following sections will summarize the distribution of Cu and Ni with depth within each major water mass and geographic area of the Arctic Ocean, especially comparing Cu and Ni with other chemical tracers diagnostic of individual fluxes or ocean processes.

#### **5.3.2.1. Surface distribution of Cu and Ni**

Why do Cu and Ni share a maximum in Arctic surface waters that is immediately evident in profile shape and drives their linear relationship?

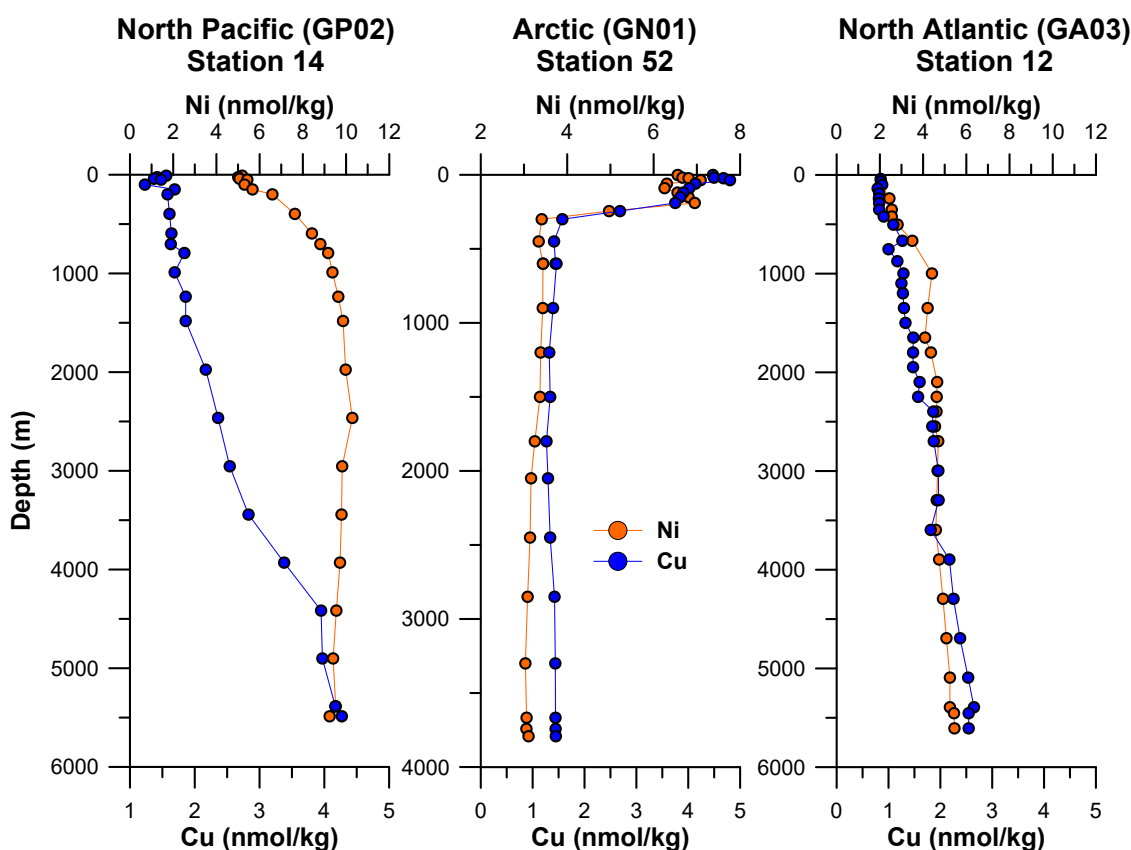


**Figure 5.4** Global comparison of the profile shapes of Cu (blue) and Ni (orange) in the Arctic (GEOTRACES GN01, Station 52) to other major ocean basins. Data taken from the subarctic North Pacific (GEOTRACES GP02, Station 14, 47°N, 170°W) and the subtropical Western North Atlantic (GEOTRACES GA03, Station 12, 29.7°N, 56.8°W). Data from Schlitzer et al. (2018). The concentration range of the nickel axis in the middle Arctic Ocean panel is smaller than in the other two panels to emphasize overlap in profile shape between Cu and Ni in the Arctic Ocean.

Arctic surface concentrations of Ni and Cu were noticeably higher than surface concentrations in the Atlantic and Pacific (Figure 5.4). In the surface Western Arctic, dissolved Cu averaged  $4.57 \pm 1.50$  nmol/kg across the entire transect (excluding Station 1 in the Pacific), while Ni averaged  $6.59 \pm 1.25$  nmol/kg. This is significantly higher than global averages of  $0.80 \pm 0.64$  and  $3.18 \pm 1.53$  nmol/kg reported for surface Cu and Ni, respectively (Schlitzer et al., 2018). Additionally, the Cu-Ni relationship was high

and strong in the surface waters 0-20 m depth (Cu-Ni slope = 1.05,  $r^2 = 0.76$ ). What processes are responsible for these uniquely high concentrations? We put forward three hypothesized fluxes that are each tested below: sea ice melt, riverine fluxes, and continental shelf inputs.

#### **5.3.2.2. Sea ice melt in the Marginal Ice Zone (MIZ)**

Sea ice melt can be a potentially large source of trace metals to surface seawater (Hölemann et al., 1999; Measures, 1999; Aguilar-Islas et al., 2008; Tovar-Sánchez et al., 2010; Lannuzel et al., 2016), as metals and nutrients are incorporated in brine channels within sea ice. Additionally, sea ice may carry ice rafted sediments (Measures, 1999) that can deliver trace metals from the shelves to anywhere in the Arctic where ice is melting (Kadko et al., 2016; Krumpen et al., 2019). Concentrations of Cu and Ni in Arctic sea ice have a wide range, from 11 to 440 nM and 1 to 850 nM, respectively (Hölemann et al., 1999; Tovar-Sánchez et al., 2010; Marsay et al., 2018), which could thus act as a source or a diluent of surface Arctic seawater dissolved Cu and Ni concentrations upon melting. Notably, the sea ice Cu and Ni concentrations measured on the GN01 cruise were on the low end of this range (Marsay et al., 2018):  $0.67 \pm 0.44$  nmol/kg for Cu and  $0.75 \pm 0.47$  nmol/kg for Ni. Both of these are significantly lower than surface Arctic seawater concentrations, hinting that sea ice might not be the source of the high seawater Cu and Ni concentrations that we seek.

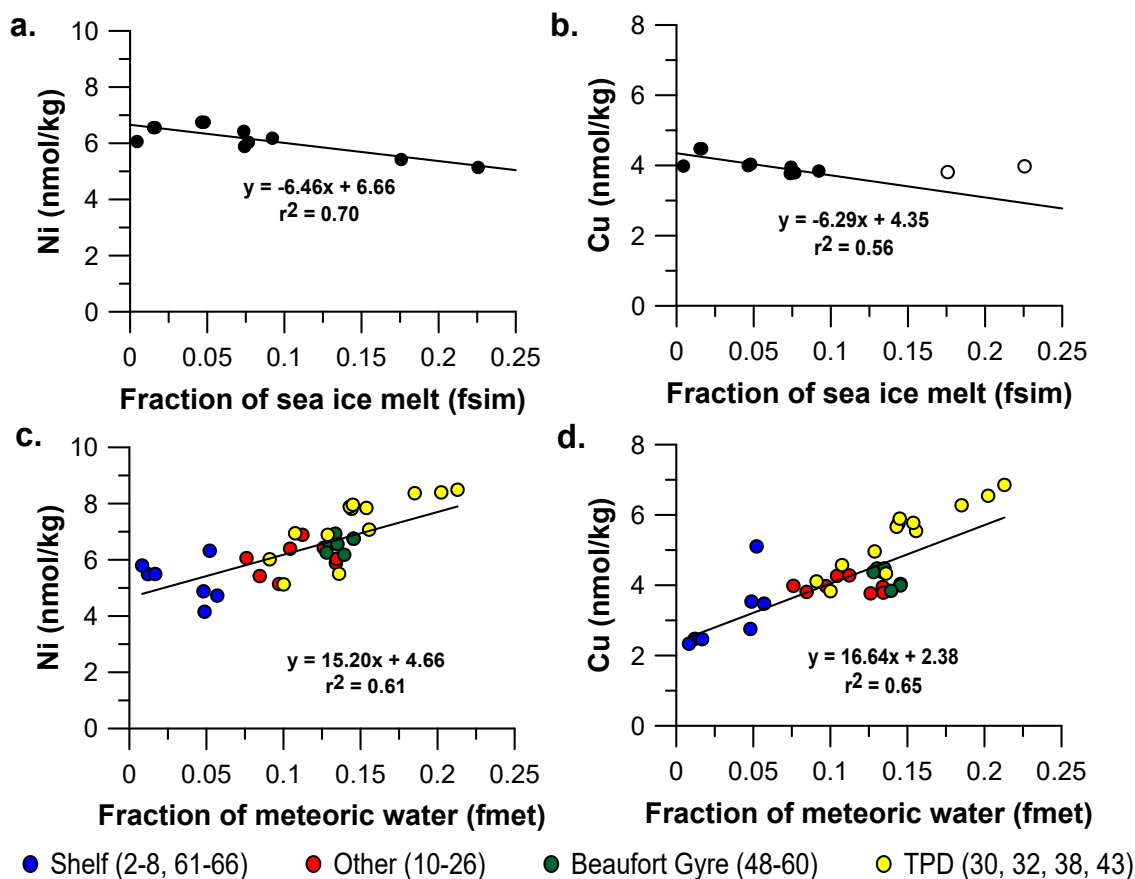


**Figure 5.5** Plots of surface seawater Ni and Cu vs fsim and fmet (a,b) vs fsim to identify sea ice melt influences and fmet (c,d) to identify riverine/snow influences on their distributions. Color legend refers to the fmet plots to demonstrate what stations are dominating the trend. All data is surface except for TPD (yellow) where data from the surface to 80 m is included to show the influence of the TPD at these stations (Charette et al. 2020). In plot b) Stations 8 and 9 are omitted (open circles) due to shelf influence.

Nonetheless, we employed the tracers  $\delta^{18}\text{O}$  and salinity to obtain the fraction of water contributed by sea ice melt (“fsim”, Figure 5.5) (Newton et al., 2013) at stations designated within the “marginal ice zone” (MIZ, Stations 8-17, 51-57), defined as stations where ice was present but coverage was <100%. Both Cu and Ni had negative relationships with fsim (Figure 5.5), indicating that sea ice melt acted as a diluent rather

than a source to surface waters, in accordance with the low measured sea ice concentrations (Marsay et al., 2018). In the case of Ni, this relationship encompassed all MIZ stations ( $r^2 = 0.61$ ), but for Cu the relationship excluded Stations 8 and 9 over the Chukchi Shelf, which are known from prior studies of other elements to receive shelf fluxes that could affect the relationship of metals to sea ice melt along this transect (Jensen et al., 2019). These stations deviated positively from the otherwise negatively decreasing linear relationship between Cu and  $f_{sim}$ , indicating a shelf source of Cu (also see 4.3.3.3 below) and thus were thus neglected in the  $f_{sim}$  correlation statistics for Cu. Sea ice melt therefore is not the source of the surface seawater concentration maxima for Cu and Ni in the Western Arctic and in fact only serves to dilute these concentrations upon melting.

#### **5.3.2.3. Riverine inputs of Copper and Nickel**

The surface PML, where dissolved Cu and Ni were highest, also has very low salinity, which can be ascribed to sea ice melt but is usually attributed to the large volume of riverine freshwaters carried into the Arctic Ocean. Arctic rivers such as the Yukon, Ob, Yenisey, and Lena rivers have elevated concentrations of Cu and Ni, ranging from 10-74 and 4-48 nmol/kg, respectively (Heggie, 1982; Martin et al., 1993; Dai and Martin, 1995; Hölemann et al., 1995; Guieu et al., 1996; Bradley et al., 1997; Hölemann et al., 1999; Hölemann et al., 2005), indicating that they may be the source of the elevated surface seawater Cu and Ni.

To assess the potential riverine source, we once again used the tracers  $\delta^{18}\text{O}$  and salinity to elucidate the fraction of meteoric water contribution (“ $f_{met}$ ”, Figure 5.5) in

the surface ocean; meteoric water contains contributions from both river water and precipitation (rain or snow). Copper and Ni both had a significant, positive correlation to  $f_{met}$  in the surface waters across the entire transect (Figure 5.5) with  $r^2 = 0.65$  and  $0.61$ , respectively. Notably, the TPD carried the highest fractions of meteoric water and thus appeared to drive the correlation significantly for both Cu and Ni (Figure 5.5, yellow circles, Charette et al. 2020). The shelf stations had overall low  $f_{met}$  and lower concentrations of Cu and Ni, despite the known presence of the Yukon River outflow near Stations 2 and 3 (Figure 5.2). The Beaufort Gyre (Stations 48-60), which also holds a significant freshwater reservoir (Proshutinsky et al., 2009), had values tightly clustered in the middle of the Cu-Ni- $f_{met}$  correlations; this suggests that rivers supplied an intermediate freshwater flux to the Beaufort gyre compared to the TPD (high) and shelf stations (low), and accordingly intermediate Cu and Ni.

Importantly, the fact that all surface sites in the Western Arctic fell on a single relationship with  $f_{met}$  suggests that all rivers sourcing this region must each supply similar concentrations of Cu and of Ni. In fact, when the overall relationship between  $f_{met}$  and Cu and Ni was extrapolated to a 100% meteoric water, a riverine end-member concentration of approximately 19 nmol/kg for Cu and 19.9 nmol/kg for Ni can be calculated, which was within error of the currently known Arctic river concentrations listed above. These strong correlations between Cu and Ni and  $f_{met}$ , in addition to the fact that the highest concentrations observed in the GN01 dataset are surface samples within the riverine-influenced TPD, make it fairly easy to conclude that rivers play a

significant role in driving the observed Cu and Ni concentration enrichments and linear correlations in Western Arctic seawater.

#### **5.3.2.4. Modifications across the Bering Strait and Chukchi Shelf**

The third potential Cu and Ni surface source that we investigated was benthic fluxes from the Bering and Chukchi continental shelves. We suspected shelf inputs because Cu is traditionally thought to have a benthic source (Boyle et al., 1981; Richon and Tagliabue, 2019), and other metals such as Zn (Jensen et al. 2019), Fe, and Mn (Section 4) all had benthic fluxes from the Chukchi shelf driven by porewater respiration during this GN01 study.

An examination of the Cu and Ni distributions during GN01 showed that both Cu and Ni had noticeable increases in surface concentrations, from the North Pacific “end member” at Station 1 across the Bering Strait and Chukchi Shelf (Figure 5.6). This increase was most noticeable for Cu, which increased gradually by ~2 nmol/kg from Station 1 ( $1.84 \pm 0.09$  nmol/kg) to the Chukchi Shelf break at stations 8 and 61 ( $3.89 \pm 0.53$  nmol/kg). Surprisingly, however, the concentrations at each of these shelf stations were constant with depth (Figure 5.6a, inset), indicative of strong mixing, and making it challenging to identify a clear benthic source (which was identified for Zn, Fe, and Mn for these same samples by a bottom water concentration maximum; Jensen et al. 2019, in review). In the surface of these shelf stations, Cu shared a correlation to *fmet* (Figure 5d), except at Stations 2 and 3 where *fmet* values were the highest along the Strait and Shelf ( $>0.03$ ). The elevated Cu throughout the water column suggested that while Cu is

partially influenced by river water, especially in the surface, there could be another benthic source or lack of surface biological that we saw with other elements.

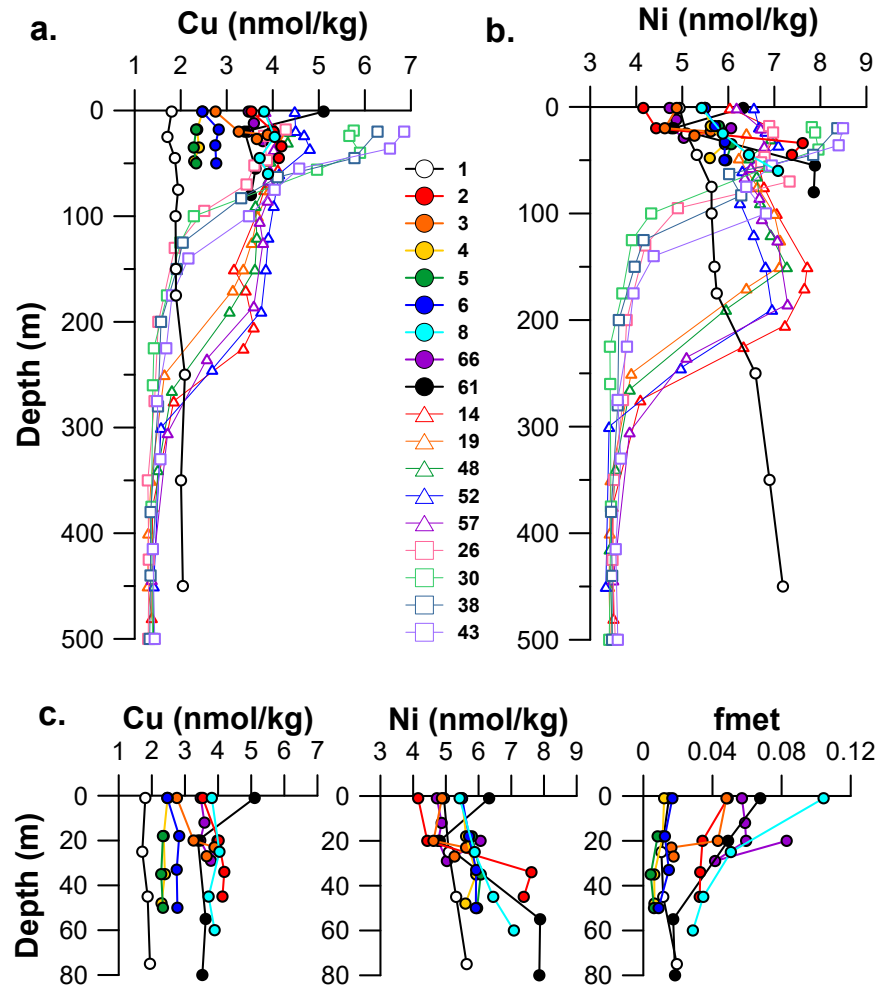


**Figure 5.6** Profile overlay of the concentrations of a) Cu and b) Ni across the entire transect in the upper 500 m of the water column (Station 32 in Amundsen Basin excluded). A grouping of Bering and Chukchi Shelf stations (Stations 2-8, 61-66, closed circle symbols) demonstrate the increase in Cu and Ni in the upper water column moving from Station 1 across the continental shelf. Offshore there are higher Cu and Ni concentrations in the UHL of the Canada Basin (Stations 14, 19, 48-57 open triangle symbols) then in the halocline of the Makarov Basin (Stations 26-43, open square symbols). c) the distribution of Cu, Ni and fractional meteoric water (fmet) from left to right across the shelf in more detail.

Dissolved Ni also increased along the shelf from ~5.0 nmol/kg at Pacific Station 1 to 5.5-6.0 nmol/kg at the shelf break, averaging  $5.67 \pm 1.02$  nmol/kg over the shelf as a whole (Figure 5.6b). However, there were two differences in the Ni increase over the shelf compared to Cu. First, the increase was smaller in magnitude and more spatially sporadic than for Cu, not following Cu's general northward increase. Additionally, Ni profiles were not constant with depth (Figure 5.6b), as for Cu, and instead increased significantly with depth, sometimes with gradients of 2-3 nmol/kg Ni between surface and bottom over the shelf (Figure 5.6b), pointing to a benthic source and/or a strong surface sink due to biological uptake, in line with macronutrient trends (Jensen et al., 2019). Unlike Cu, there was no relationship between Ni and fmet along the Strait and Shelf stations (Figure 5.4c, blue), indicating that riverine sources were not as significant in driving Ni concentrations at these stations. Instead, benthic fluxes appear to drive the increasing Ni over the Bering and Chukchi Shelves.

Interestingly, Cu and Ni shared no relationship along the Strait and Shelf stations despite both elements increasing in concentration (Figure 5.7a), suggesting that different dominant processes were controlling each. Nickel can be sourced from sediments, particularly accompanying other biological fluxes such as organic matter (Böning et al., 2015). Previous studies have established that benthic fluxes from the Chukchi Shelf can control trace metal distributions in the rest of the Western Arctic in two different ways: dissolved Fe and Mn are supplied by reductive dissolution of Chukchi Shelf sediments (Aguilar-Islas et al., 2013; Kondo et al., 2016; Jensen et al., in review), while dissolved Zn is supplied by porewater fluxes of remineralized Zn-rich organic matter (Jensen et al.,

2019). We compare to each of these metals in order to elucidate which of these mechanisms might be causing any benthic fluxes of Cu and Ni.

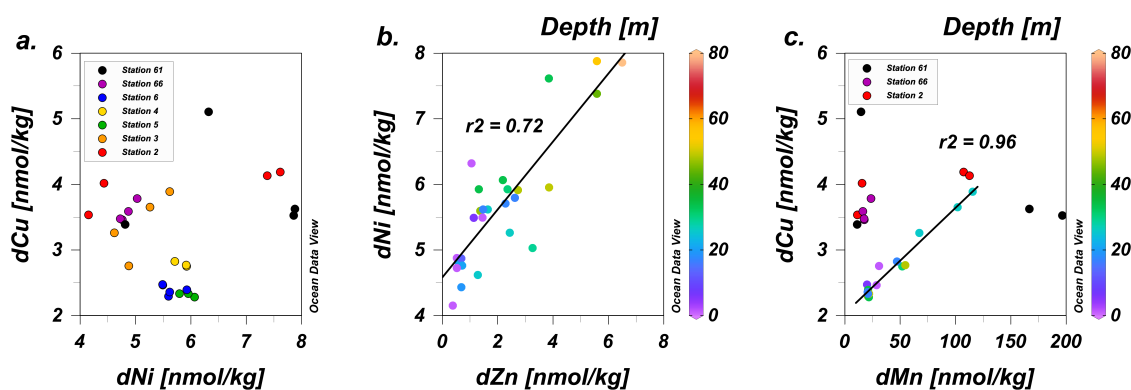


**Figure 5.7** Ni and Cu across the Shelf and Strait. a) Ni vs. Cu across the Strait and Shelf (Stations 2-6, 61-66) with each separate station highlighted showing that there is no relationship, b) Zn vs Ni with color by depth and c) Mn vs Cu with color by depth. Stations 2, 61, 66 are excluded from the regression in plot c, as explained in the text, but are included in the plot for reference.

Dissolved Ni shared a decently strong correlation with Zn along the Strait and Shelf stations ( $r^2 = 0.72$ , Figure 5.7b). Like Zn, Ni shared a correlation at these sites with the macronutrient silicate (Si), which is known to be released in sediments along the Chukchi Shelf alongside Zn (Jensen et al., 2019), suggesting that the Ni flux from sediments was also driven by regeneration of diatomaceous Ni into porewaters. This is consistent with a greater Ni demand for both the frustules and cellular enzymes of diatoms compared to other phytoplankton groups (Twining et al. 2012), which might produce a similar Si, Zn, and Ni flux from Chukchi Shelf sediments.

In contrast, copper appeared to have a strong correlation only to Mn ( $r^2 = 0.96$ , Figure 5.7c), and only along a subset of Strait and Shelf stations, suggesting that the

same reductive dissolution processes associated with diagenesis that control the Chukchi Shelf Mn distribution might also be partially responsible for Cu fluxes. However, Stations 61 and 66 fell off this trend due to extremely high Mn fluxes, and Station 2 also fell off this trend, perhaps due to riverine fluxes of Cu ( $f_{met} = 0.048$ ). These trends confirm a dominant benthic source for Ni over the Bering and Chukchi Shelves, derived from remineralization of diatoms in sediment porewaters, similar to Zn and Si (Jensen et al. 2019), and a less dominant shelf-derived source for Cu, possibly related to reductive dissolution of Mn in shelf porewaters, though riverine fluxes may play an equal or greater role in determining the Cu distribution.

#### **5.3.2.5. Halocline (UHL)**

Concentrations of Cu and Ni were elevated not only in the surface but also throughout the UHL in the Canada Basin (Figures 5.3, 5.6), similar to previous findings ((Cid et al., 2012; Kondo et al., 2016; Jensen et al., 2019); Section 4). Within these UHL bounds, Cu averaged  $3.74 \pm 0.26$  nmol/kg, which was lower than its surface concentrations directly above ( $4.25 \pm 0.29$  nmol/kg; Figure 5.6). In contrast, Ni averaged  $7.08 \pm 0.32$  nmol/kg in the UHL of the Canada Basin, which was on average slightly higher than its surface concentrations directly above ( $6.73 \pm 0.33$  nmol/kg; Figure 5.6), requiring an additional UHL source. The UHL is known to be formed from salty waters released during brine rejection on the Chukchi Shelf (Shimada et al., 2005; Woodgate et al., 2005), which are transported along shelf bottom waters before being advected offshore as the UHL; during this transport, they acquire high macronutrients and Zn that remain relatively undiluted offshore (Jensen et al., 2019). Concentrations of Cu in the

UHL were within error of Shelf concentrations, but for Ni the UHL concentrations matched the more elevated bottom water concentrations from the shelf, causing an apparent UHL enrichment in Ni compared to Cu. In contrast, the Makarov halocline did not carry any Cu or Ni enrichments, confirming that the benthic shelf source is specific to the shallow Chukchi Shelf, as observed for Zn (Jensen et al., 2019).

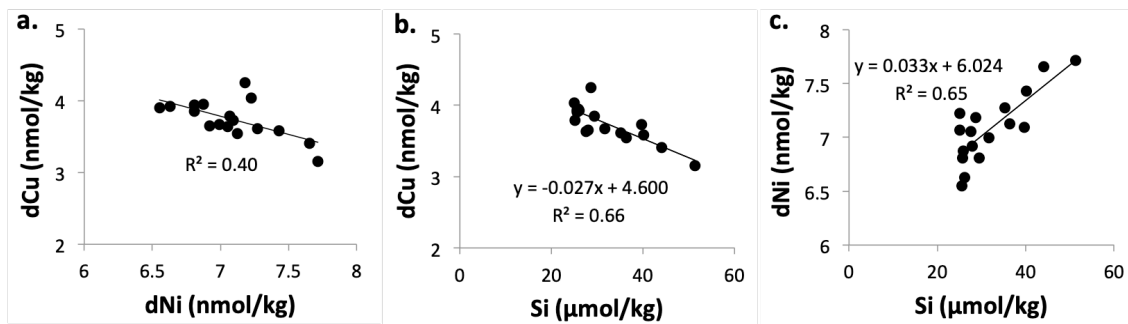


**Figure 5.8** Correlations between Cu, Ni, and Si within the halocline (Stations 8-19, 46-60). a) Ni vs Cu, b) Si vs Cu, c) Si vs Ni. Linear correlations are shown where relationships are significant.

This apparent increase in Ni compared to Cu in the UHL caused a deviation in the linear correlation between Cu and Ni at UHL depths (Figure 5.1). While Cu and Ni were not significantly correlated in the UHL, Ni was positively correlated to the UHL tracer Si ( $r^2 = 0.65$ ), indicative of mixing within water masses above/below the UHL. In contrast, Cu was negatively correlated to Si in the UHL ( $r^2 = 0.65$ ), indicative of removal relative to Si perhaps by scavenging (Figure 5.8). However, upon more rigorous examination, Cu does not appear to be appreciably scavenged within the UHL. The log-scale distance of transport ( $d_{1/e}$ ), which is a metric of how far a species is preserved within a water mass before being reduced to  $1/e$  of its original concentration (Johnson et

al., 1997), has been used in the Arctic in previous studies with Fe, Mn, and particulate phases ((Aguilar-Islas et al., 2013); Section 4) to demonstrate the distances over which these species are net removed by scavenging/aggregation within the UHL. Following the same methods of Jensen et al. (in review), we took an average of Cu within the bounds of the halocline ( $Si > 25 \mu\text{mol/kg}$ , salinity 31-33.1) at Stations 8-19, 46-60 and plotted the natural log (ln) of these averages versus distance from the 100 m isobath (Figure 5.9a). This yielded a  $d_{in}$  value of  $1,400 \pm 860$  km within 200 km of the shelf, a much greater scavenging distance than either dissolved Fe or Mn (74 and 43 km, respectively), both of which were rapidly scavenged. Beyond 200 km, there was no relationship for Cu, and Ni remained conserved throughout (Figure 5.9b). Thus, at least within the particle loads of the UHL, scavenging of Cu is slow but perhaps significant enough to cause the slight decoupling of Cu and Ni with the UHL water mass.

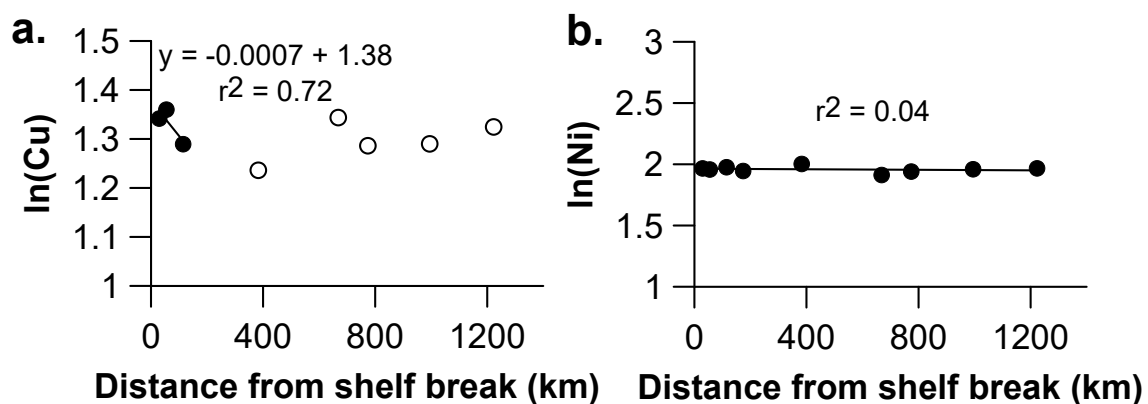


**Figure 5.9** Plot of the distance from the shelf break vs natural log of a) Cu and b) Ni. This plot is truncated for Cu to the initial 200 km to demonstrate where the potential relationship is present (following Section 4).

### 5.3.2.6. Atlantic layer (AL)

The Atlantic layer (AL, ~250-600 m depth) originates in the Atlantic Ocean, flowing first through the Eastern Arctic and cycling slowly into the Western Arctic, traceable by a maximum in potential temperature (Rudels, 2015). Tracking the inventory of Cu and Ni within this water mass as it ages allows a distinction between conservative mixing of water masses (linear relationship with  $\theta_{\max}$  at each station), regeneration inputs of Cu and Ni (curved upward relationship with  $\theta_{\max}$ ), or scavenging losses of Cu or Ni (curved downward relationship with  $\theta_{\max}$ ). Previous studies found that nutrient-type metals such as Zn and Cd had a linear negative correlation with  $\theta_{\max}$ , indicating loss during aging due to conservative mixing with the halocline above (Jensen et al., 2019; Zhang et al., 2019). Nickel concentrations did not change at all across the range of  $\theta_{\max}$  (Figure 5.10), indicating that AL Ni is not significantly mixed, regenerated, or scavenged but instead is highly constant. We might expect hybrid-type Cu to exhibit scavenging behavior within the aging AL. Indeed, there was slightly higher Cu at the station of lowest  $\theta_{\max}$ , which likely had the most significant mixing with the UHL layer above and thus the highest Cu, but the trendline was not significantly linear nor curvilinear to distinguish conservative mixing from scavenging, respectively. There was no correlation between Cu and Ni within this layer due to limited concentration ranges, and again any Cu scavenging could not be quantified.

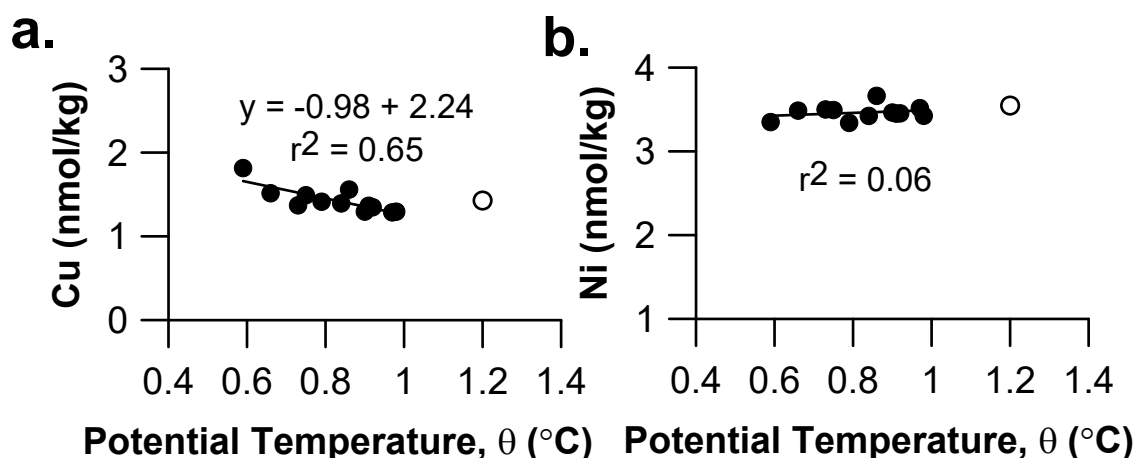


**Figure 5.10** Plots of Cu and Ni within the Atlantic layer. a) Ni and b) Cu vs potential temperature at the maximum within the Atlantic layer. Station 32 (open circle) is not included in plots (a) and (b) because it is in the Amundsen Basin.

### 5.3.2.7. Deep water

Both Cu and Ni shared low and constant deep water concentrations along the entire transect, with a range too small to allow a significant linear relationship between them within these depths. However, these low values appeared to “anchor” the overall GN01 linear correlation (Figure 5.1). As was observed for nutrient-type metals Zn and Cd along this transect (Jensen et al., 2019; Zhang et al., 2019), concentrations of Cu and Ni were remarkably low and constant below 1800 m, the Lomonosov Ridge sill depth (Figures 3, 4), with  $\text{Cu} = 1.39 \pm 0.08 \text{ nmol/kg}$  and  $\text{Ni} = 3.11 \pm 0.08 \text{ nmol/kg}$ . These were the lowest concentrations along the entire transect and a clear contrast to global averages for Cu and Ni below 1000 m which are  $2.60 \pm 1.02 \text{ nmol/kg}$  and  $7.76 \pm 1.56 \text{ nmol/kg}$ , respectively (Schlitzer et al., 2018). Although Cu and Ni did not share a significant relationship below 1800 m, Ni shared a positive correlation to phosphate below 1800 m.

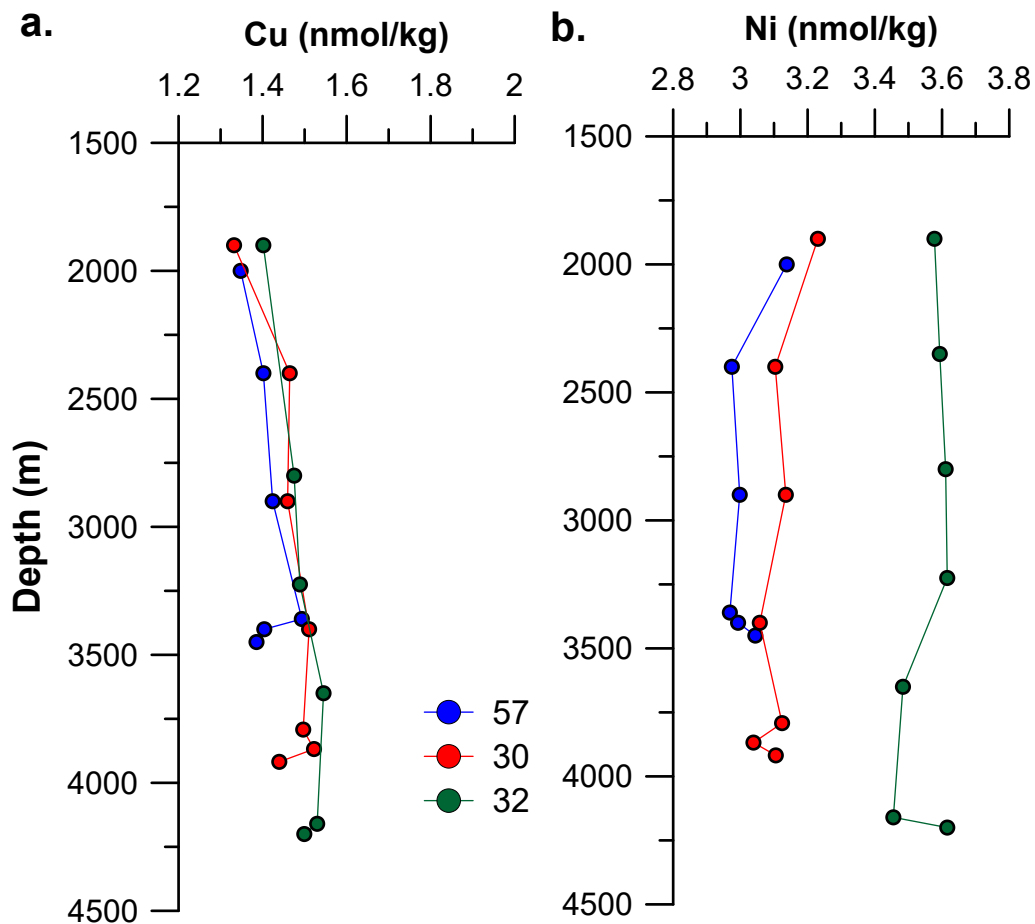


**Figure 5.11** Copper and nickel in Arctic deep water. a) Cu and b) Ni below 1800m in the Canada Basin (Station 48, blue), Makarov Basin (Station 30, red), Amundsen Basin (Station 32, green). There is a clear disparity between the Amundsen Basin and the other two basins.

Additionally, Cu and Ni appeared to vary in the deep water (>2000 m) of each basin of the Arctic Ocean across this transect: the Amundsen Basin (Station 32), the Makarov Basin (Stations 26-43, excluding 32), and the Canada Basin (Stations 14, 19, 48-57). The Lomonosov Ridge prohibits significant exchange between the Amundsen and Makarov basins below 1800 m, and the Alpha-Mendelev Ridge restricts exchange between the Makarov and Canada basins below 2,200 m. Below 2,000 m, both Cu and

Ni seemed to decrease between the Amundsen and Amerasian (Canada and Makarov) basins (Figure 5.11) where Cu =  $1.51 \pm 0.03$  nmol/kg,  $1.38 \pm 0.09$  nmol/kg, and  $1.39 \pm 0.07$  nmol/kg within the Amundsen, Makarov, and Canada basins, respectively. The Amundsen Basin average concentration below 2000 m was significantly greater (2-tailed *t*-test,  $p < 0.05$ ) than the average concentrations below 2000 m within the Canada and Makrov basins.

For Ni, these averages among the three basins were  $3.56 \pm 0.07$  nmol/kg,  $3.15 \pm 0.06$  nmol/kg, and  $3.09 \pm 0.09$  nmol/kg, respectively. The average differences between all three basins were statistically significant (2-tailed *t*-test,  $p < 0.05$ ), suggesting that Ni appreciably decreases in the deep water layers between the Amundsen, Makarov and Canada basins. This indicated that Ni was either removed or mixed out as water circulates slowly between the basins on the timescale of centuries (Timmermans et al., 2003; Rudels et al., 2004; Tanhua et al., 2009). Given this long circulation time and the typical age of Canada Basin deep water (300-500 years, (Tanhua et al., 2009; Schlosser et al. 1994)), it is possible that the Ni in the Canada and Makarov basin deep water was supplied at a time when the micronutrient dynamics were very different in the North Atlantic, as has been proposed for Cd (Zhang et al., 2019). For Cu, there was only a significant decrease moving across the Lomonosov Ridge, and both trends were primarily driven by noticeably higher concentrations of both Cu and Ni at Station 32 below 2000 m (Figure 5.11), reflecting the influence of long timescale circulation on trace metal concentrations in the absence of large regenerative inputs.

Additionally, both Cu and Ni appeared to be affected by benthic nepheloid layers (BNLs) that were intermittently present along the transect. Although most full-depth stations (14, 19, 26, 30, 32, 38, 48, 52, 57) showed evidence of BNLs via reduction in the transmissometry sensor data (Gardner et al., 2018), particulate aluminum in the large size fraction, a metric of BNL resuspension, was particularly elevated at Stations 14, 19, 26, 30, 32, 48, and 57 (Yang and Lam, in review). At these stations, Cu and Ni both showed variation in the bottom-most samples. At stations 14, 19, and 26, dissolved Cu became elevated near the bottom, indicating release from resuspended sediments (Boyle et al., 1977), while Ni appeared to slowly decrease. Although there is little global precedence for Ni scavenging in nepheloid layers, research in the central Arctic basin shows evidence of elevated Ni in Mn-rich sediments likely as a result of water column scavenging (Marz et al., 2011). This theory aligns well with the prolonged decrease in Ni observed at these stations over the course of at least 1000m. In contrast, at Stations 30, 32, 48, and 57, dissolved Cu decreased, and Ni increased sharply in the BNL (Figure 5.11). This highlights the more common dynamic between scavenging that is often observed for dissolved Cu within BNLs (Jacquot and Moffett, 2015; Sherrell and Boyle, 1992) and resuspension more often observed for elements like Ni (Sherrell and Boyle, 1992; Loscher, 1999).

#### **5.4. Discussion**

The GN01 dissolved Cu and Ni results showed that the concentration range, profile shapes, and relationship of dissolved Cu and Ni are unique in the Arctic Ocean, driven mostly by uniquely high surface and halocline concentrations. To put these

observations in the context of the global ocean, we set out to answer two major questions: 1) What processes cause Cu and Ni to be linearly correlated in the Western Arctic Ocean, particularly in surface waters? and 2) How does this compare to the Cu-Ni relationship in the rest of the global ocean?

#### **5.4.1. What causes the Cu-Ni linear correlation in the Arctic?**

A linear relationship implies that similar processes must be driving the distribution of Cu and Ni in the Western Arctic, particularly in surface waters, where the correlation is strongest and both Cu and Ni have especially elevated concentrations (Figure 1). Candidate external fluxes that could be responsible for aligned surface Cu and Ni fluxes include river discharge, Chukchi shelf inputs, and sea ice melt. Sea ice melt was quickly eliminated, as both Cu and Ni were diluted, not supplied, by sea ice melt (Figure 5.5). In contrast, both Cu and Ni shared a significant, positive correlation to *f<sub>met</sub>* (a tracer of meteoric water, including rivers) in surface waters, highlighting the importance of river water to the supply of both metals to the Western Arctic. Possible riverine sources to the Western Arctic are the Yukon and Mackenzie Rivers in Alaska and the Lena and Kolyma Rivers from Asia that feed into the TPD, which carry elevated Cu and Ni to the central Arctic ((Charette et al., 2020); Figure 5c,d).

The concentrations of Ni and Cu must each be fairly similar across any river significantly contributing to the Western Arctic surface waters, in order to maintain single respective relationships with *f<sub>met</sub>* across the entire surface Western Arctic. However, one contrast between Cu and Ni river fluxes was that, for nickel, the overall *f<sub>met</sub>* relationship was driven primarily by the TPD samples (Figure 5.5c), while Ni was

not correlated to fmet individually for stations along the shelf, within the Beaufort Gyre, or along the northbound GN01 route (“Other”, Figure 5.5c). In contrast, Cu did share individual correlations to fmet at stations along the shelf, as well as the TPD, indicating that riverine fluxes are critical for setting surface Arctic Cu distributions, as suggested by prior studies (Little et al., 2014a; Richon and Tagliabue, 2019). This is in line with what we know about the role of organic ligands in stabilizing Cu, particularly in estuarine environments (Laglera and van den Berg, 2003, Whitby and van den Verg, 2014; Abualhaija et al., 2015). Previous studies in the Arctic highlight the role of terrestrially-derived humic substances entering the Arctic via the TPD and other river sources in controlling Fe distribution and speciation (Slagter et al., 2017; Slagter et al. 2019). Given that Cu may be bound up to 69% by these same humic substances (Abualhaija et al, 2015), we suggest that river-derived organic matter may be preferentially stabilizing Cu over Ni. Similar ligands can also bind Ni(II) in marine and estuarine environments, but Cu(II)-humic complexes are more preferred following the Irving Williams Series (Irving and Williams, 1953), and Cu often outcompetes Ni for stronger ligands (Boiteau et al., 2016). Based on these results, Cu appears to be more significantly controlled by riverine fluxes than Ni, and rivers are likely the dominant driver of the increase in Cu moving from the North Pacific (Station 1) through the Bering Strait and Chukchi Shelf.

Nickel’s poorer correlation with fmet outside of the TPD, and yet increasing concentrations across the Bering Strait, requires an additional process, which comes in the form of benthic fluxes along the Bering and Chukchi Shelves. Nickel, like Zn, is

intimately tied to the biological cycling of diatoms, as it is present in both the frustule (“hard”) portion as well as the organic (“soft”) matter (Twining et al., 2012; Boning et al., 2015). This leads to a global correlation of Ni to both Si and P, and this correlation holds over the Chukchi Shelf and within the halocline in the Arctic. As shown previously for GN01, Zn has a bottom water source along the Chukchi Shelf that results from porewater remineralization of cells containing high Zn:Carbon ratios (Jensen et al., 2019); this signal is then entrained into the halocline, along with macronutrients like Si, and extends offshore into the Central Arctic. Nickel is directly correlated to Zn and Si at these sites, with clear concentration maxima in Shelf bottom waters, and must thus be sourced by similar porewater cellular remineralization mechanisms. Copper, in contrast, has a less clear sediment source, as it shows no bottom water enrichment. However, it had a strong correlation with dissolved Mn at some of the shelf stations (Figure 5.7c), perhaps pointing to a reductive porewater source (Section 4; (Vieira et al., 2019)), as has been posited by other studies in the same region with a similar correlation with Mn as here (Cid et al., 2012). Thus, while reductive sediments may provide some source of Cu to the Chukchi Shelf, these sediment fluxes are likely not greater than the riverine input observed over the shelf or the surface across the rest of the Western Arctic.

What makes a linear relationship between Cu and Ni most surprising is that Ni is a “nutrient-type” metal, while Cu is a “hybrid-type” metal, which means that it should also undergo some amount of scavenging that Ni does not experience. Why wouldn’t Cu scavenging in the Western Arctic decouple the Cu and Ni distributions? One observation is that surface concentrations drive the linear Cu-Ni correlation, and these waters may be

too young to have experienced sufficient Cu scavenging. Additionally, if there is any deviation from the linear Cu-Ni relationship, there is a reduction of Cu in the UHL of offshore waters, while Ni remained as high as in bottom waters of the Shelf stations (Figures 1, 2, 6), which would be consistent with some Cu scavenging. While Ni remained elevated and directly correlated with the macronutrients in the UHL, there was a slight decrease in Cu concentrations within 200 km of the shelf break (Figure 5.9a), within the first “scavenging regime” identified for Fe and Mn (Section 4). This indicates that slow removal of Cu is occurring at least within the Fe particle-rich halocline close to shore, contributing to the negative Cu-Ni relationship at these stations. This Cu-Ni decoupling, however, is very small, even within the UHL.

Arctic deep waters, which should be excellent indicators of scavenging given their large age gradient (200-500 years, (Tanhua et al., 2009)) and negligible remineralization inputs under the ice that might otherwise complicate deepwater scavenging trends, surprisingly recorded decreases in both Cu and Ni with increasing age below 2000 m. As Ni scavenging has never been postulated in any other region, we must consider other complicating factors such as mixing, variable benthic fluxes across basins, and cascading brines down the continental slopes into deep waters (Aagaard, 1981) as present in Arctic deep waters. Considering that other trace elements (e.g. Cd, P; (Zhang et al., 2019)) showed perplexing deepwater distributions across basins, we will not attempt to use deep waters to attribute the presence of any Cu scavenging. Instead, we will simply note that the average concentrations below 1000 m for Cu and Ni ( $1.39 \pm 0.10$  nmol/kg and  $3.24 \pm 0.18$  nmol/kg, respectively) compare well to the upper water

column of the North Atlantic north of 30°N (<2600 m, (Jacquot and Moffett, 2015; Schlitzer et al., 2018; Middag et al., 2020)) where  $\text{Cu} = 1.09 \pm 0.30 \text{ nmol/kg}$  and  $\text{Ni} = 3.78 \pm 1.04 \text{ nmol/kg}$ , assuming that water above the sill depth of the Fram Strait (2600 m) may eventually exchange with the Arctic Ocean.

Thus, in summary, we find that the unique linear relationship between Cu and Ni in the Western Arctic can be explained by similar large riverine (especially Cu) and sediment (especially Ni) fluxes of both Cu and Ni, with minor differences over the Bering and Chukchi Shelves that may contribute to some decoupling of the two metals in that region. It is also supported by only slow scavenging of Cu, at least over the timescales relevant to surface and UHL waters that dominate the upper ocean Cu-Ni trend.

#### **5.4.2. Copper and Nickel global relationship**

Globally, Cu and Ni do not share a linear relationship and are not typically compared. When plotted against each other outside of the Arctic Ocean, the relationship is overall nonlinear, with clear geographic variation (Figure 5.12). Of all the ocean basins, Cu and Ni appear more closely related in the North Atlantic (GA03) where concentrations are lower, as expected for nutrient-type metals (Figure 5.12). By the time water reaches the North Pacific (Cruise GP02), there is a much wider range in concentrations of both metals, and a “kink” in the relationship is readily observed. This “kink” occurs in every global ocean basin currently in the GEOTRACES Intermediate Data Product, where both Cu and Ni steadily increase linearly until a breakpoint around 1000 m depth, where Cu appears to increase, and Ni remains relatively constant.

This observation calls forth other known “kinks” in metal-nutrient relationships as described for Ni, Cd, Zn, and P (Cullen, 2006; Middag et al., 2018; Middag et al., 2019; Middag et al., 2020), which were determined to be a product of water mass mixing with variable preformed concentrations of micro and macronutrients within major ocean basins. For example, Middag et al. (2020) tied the Ni-PO<sub>4</sub> “kink” to multiple regressions resulting from the merging of water masses of Nordic and Antarctic origin, resulting in an apparent “kink” or “zig-zag” as the steepness in the slope abruptly changed with depth during the intrusion of Atlantic-origin water masses, which carry different preformed nutrient concentrations. However, for Cu and Ni, the relationship appears linear above 1000 m globally and then increases non-linearly with increasing depth, becoming nonlinear. In the upper 1000 m, the slope is primarily governed by the concurrent uptake and regeneration of Cu and Ni. Below 1000 m, the base of the major oceanic thermocline, Ni is largely constant with depth and carries a preformed Ni concentration, while Cu is reversibly scavenged and continues to increase in concentration toward the bottom. As both Cu and Ni are accumulated during thermohaline circulation moving from the North Atlantic to the North Pacific (Sunda 2012; Bruland et al., 2014), the “breakpoint” (linear to nonlinear) of the Cu-Ni kink is shifted to substantially higher (~4 to 10 nmol/kg) Ni concentrations but only slightly higher (~1.5 to 2.0 nmol/kg) Cu concentrations. The influence of preformed concentrations of Cu and Ni are most apparent here, especially within Antarctic-origin deep water.

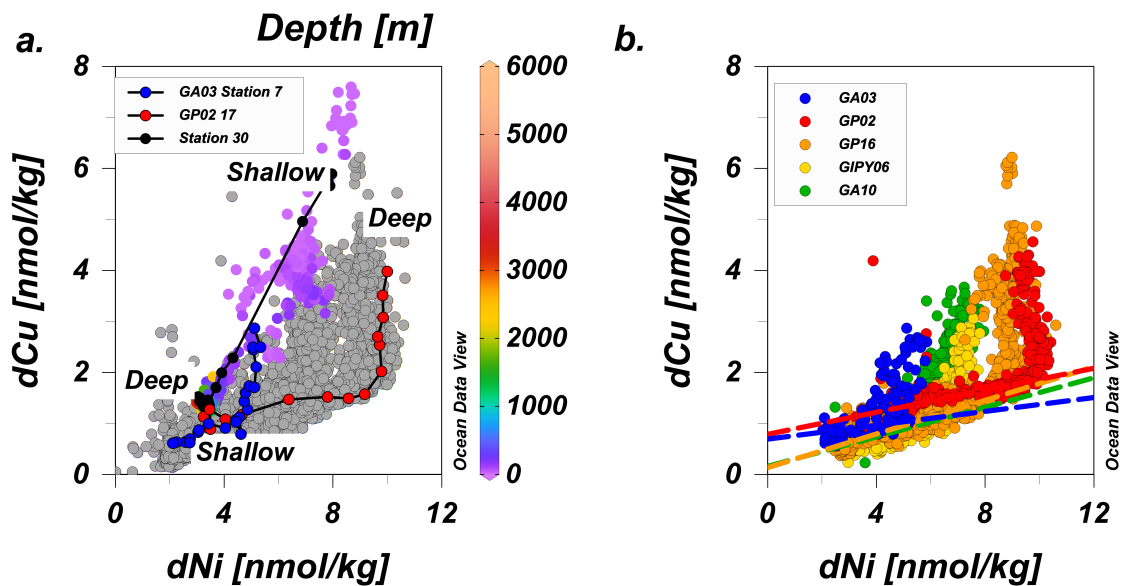


**Figure 5.12** Global comparison of Cu/Ni relationship to this study. a) Cu vs. Ni globally (grey) with this study highlighted (color by depth), Station 30 (black, this study), North Pacific (red, GP02), and North Atlantic (blue, GA03). b) global relationship is highlighted by geographic region demonstrating that the observed “kink” moves to higher Cu and Ni concentrations and the regressions within the water column (<1000m) that are highlighted become steeper moving from the North Atlantic (blue) to the North Pacific (red). Data from Schlitzer et al. (2018).

If the global ocean Cu-Ni relationship has a kink due to concurrent uptake and shallow regeneration of Cu and Ni above 1000 m and deep water preformed concentrations and Cu scavenging below 1000 m, what would we expect to see in the Arctic Ocean? The upper water column of the Arctic Ocean is elevated for both Cu and Ni (Figure 5.6) as a result of riverine and sedimentary inputs of both Cu and Ni that are not significantly removed via biological uptake, much like high surface concentrations observed for dissolved Mn (Section 4) and Co (Bundy et al., 2020). The absence of a vertical biological pump maintains the high Cu and Ni concentrations throughout the upper 500 m as well as the linear relationship, with some deviation occurring in the Canada Basin halocline due to external inputs. In global deep waters that should carry

performed Cu and Ni, the Arctic deep water is primarily derived from the North Atlantic (Rudels, 2015) where Cu and Ni are generally low. Thus, the deep water concentrations in this study are low and homogenous, which when mixed with the high surface values help regulate the strong, linear relationship throughout the Arctic water column. Unlike in the rest of the global ocean, where there is sufficient Ni and Cu concentration in deep waters to observe a decoupling due to Cu scavenging, Arctic deep water concentrations of Cu and Ni are too low, and thus they simply cluster homogeneously at the base of the Arctic's 1:1 Cu-Ni relationship.

To reinforce these process attributions in the Arctic Cu-Ni trend, we test the null hypothesis that the Cu-Ni relationship in the upper 1000 m waters of the Western Arctic should reflect a mixture of the the North Atlantic and North Pacific Cu-Ni slopes, as these oceans known to mix in the Arctic. Instead, the steep Cu-Ni slope across the entire water column ( $\text{Cu/Ni} = 0.848 \pm 0.02$ ,  $r^2 = 0.88$ ) is higher than anywhere else in the global ocean, by far. Globally, the average relationship between Cu and Ni above 1000 m appears linear but has a shallow slope ( $\text{Cu/Ni slope} = 0.193 \pm 0.003$ ,  $r^2 = 0.70$ ). While this is a significantly shallower slope than in the Arctic, there is also a global trend, where the Cu/Ni slope is steepest in the Southern hemisphere and shallower in the North Atlantic and the North Pacific. For instance, in the North Atlantic, the relationship is shallow and weak ( $\text{Cu/Ni} = 0.067 \pm 0.023$ ,  $r^2 = 0.17$ , GA03), while in the North Pacific the correlation is stronger but only a mildly steeper slope ( $\text{Cu/Ni} = 0.108 \pm 0.008$ ,  $r^2 = 0.65$ , GP02). Thus, it is even more difficult to explain the Arctic Cu/Ni relationship (which had the steepest slope) as a mixture of the North Atlantic and Pacific slopes

(which were the shallowest globally). The Southern hemisphere zonal transects had significantly higher Cu/Ni slopes (Table 5.2). Much of this is driven by the y-intercept (Cu concentration when the Ni is extrapolated to 0 concentration), which was extremely low across the 3 Southern hemisphere sections ( $<0.2 \mu\text{mol/kg}$ ), allowing for the sharpest increase in concentrations with depth and thus steepest slopes, but was a higher  $\sim 0.7 \text{ nmol/kg}$  in the two Northern hemisphere sections, creating more shallow slopes. This elevated y-intercept is attributed to particularly high dissolved Cu concentrations in the North Pacific (GP02, (Schlitzer et al., 2018)) and particularly low dissolved Ni concentrations in the North Atlantic (GA03). In the Southern hemisphere, low surface Cu and Ni concentrations in the gyres combined with shallow influence of Antarctic intermediate waters carrying elevated Ni concentrations contributes to the steeper slopes. In fact in the South Atlantic, the confluence of Nordic and Antarctic waters causes an abrupt shift in the slope of Cu-Ni below 1000m, observed along GA10, not unlike the observed kink described for Ni- $\text{PO}_4$  in the same region (Middag et al., 2020). The Arctic appears to eschew the typical global relationships where Cu and Ni are low in the surface and increase with depth, leading to a dynamic upper 500 m Cu-Ni relationship driven by river and shelf fluxes and mixing and slow scavenging (for Cu) at depth.

**Table 5.2** Table of global Cu-Ni slopes along zonal GEOTRACES transects. The values of the slopes and y-intercepts (y-int) are bolded and their corresponding errors are shown below in the split cell. The approximate latitude of the transect is shown in the far right column to demonstrate the movement from the Atlantic basin (GA03, GA10) to the Pacific basin (GP13, GP16, GP02). Data from Schlitzer et al. (2018).

<b>Cruise</b>	<b>Cu-Ni slope</b>	<b>y-int (nmol/kg)</b>	<b>r2</b>	<b>Approx. latitude</b>
GA03	<b>0.068</b> 0.024	<b>0.692</b> 0.078	0.17	18°N
GA10	<b>0.145</b> 0.009	<b>0.158</b> 0.038	0.68	40°S
GP13	<b>0.197</b> 0.006	<b>-0.049</b> 0.019	0.67	30°S
GP16	<b>0.165</b> 0.006	<b>0.134</b> 0.031	0.67	15°S
GP02	<b>0.108</b> 0.008	<b>0.787</b> 0.062	0.65	50°N

## 5.5. Conclusions

Copper and Ni share a globally unprecedented relationship in the Western Arctic Ocean that reflects the unique fluxes into this basin and the subsequent novel distributions of trace metals. The profile shapes for Ni and Cu are noticeably different than in other global ocean basins, with high surface concentrations far surpassing global averages and a decrease with depth to low and homogenous concentrations below 1000 m. This echoes studies of other metals in the Western Arctic, in particular Mn and Co, which both appear to share a similar profile shape (Section 4; (Bundy et al., 2020)) that is distinct from the profile shapes of these same metals in other global ocean basins. However, Arctic Cu and Ni distributions are similar enough, especially in the upper 500 m, that they are linearly correlated throughout the water column ( $\text{Cu/Ni} = 0.848 \pm 0.02$ ,  $r^2 = 0.88$ ). This is driven by the high surface concentrations, supplied by river fluxes (more for Cu) and benthic porewater fluxes (more for Ni) over the Bering and Chukchi

Shelves, which mix mostly linearly with low and homogenous deep water concentrations, demonstrating only mild Cu-Ni decoupling in the upper halocline layer. These particular sources are abundant in the Western Arctic Ocean due to the prevalence of river discharge and freshwater volume (Carmack et al., 2008; Yamamoto-Kawai et al., 2008) as the broad, shallow continental shelves that account for more than 50% of the ocean by area (Jakobsson et al., 2004). In particular, our conclusion that the riverine flux of Cu is especially high in this region aligns well with current literature suggesting that the river flux of Cu is far greater and more dominant than previously established, lowering the residence time in the ocean considerably (Richon and Tagliabue, 2019).

The novel relationship between Cu and Ni is largely absent in the Atlantic, Indian, Southern, and Pacific Oceans. Much like metal-macronutrient relationships, there is a pronounced kink in the global Cu vs. Ni plot at ~1000 m depth and appears to move more positively along the Ni axis. This must to some extent be linked to the fact that Cu has a linearly increasing concentration with depth, usually attributed to its reversibly scavenged characteristics (Bruland et al., 2014; Richon and Tagliabue, 2019), while Ni distributions are set only by water mass mixing and the biological pump. Scavenging is uniquely low in the Western Arctic for Cu, as well as for Co and to some extent Mn (Section 4; (Bundy et al., 2020)), contributing to the unique relationship between Cu and Ni in the Western Arctic. While there are many studies of the chemical complexation of the organic species that bind Cu in seawater, there are no studies of copper organic complexation in the Arctic basin, which might help explain why it is particularly stable against scavenging in this ocean basin. More work is needed on Arctic Cu and Ni distributions, as well as the

chemical complexation of Cu and Ni, in order to demonstrate whether this unique Cu-Ni behavior is pan-Arctic or merely a reflection of processes endemic to the Western Arctic.

## 5.6. References

- Aagaard, K. 1981. "On the deep circulation in the Arctic Ocean." *Deep Sea Research Part A. Oceanographic Research Papers* 28 (3):251-268. doi: [http://dx.doi.org/10.1016/0198-0149\(81\)90066-2](http://dx.doi.org/10.1016/0198-0149(81)90066-2).
- Aagaard, Knut, LK Coachman, and Eddy Carmack. 1981. "On the halocline of the Arctic Ocean." *Deep Sea Research Part A. Oceanographic Research Papers* 28 (6):529-545.
- Aagaard, K., J. H. Swift, and E. C. Carmack. 1985. "Thermohaline circulation in the Arctic Mediterranean Seas." *Journal of Geophysical Research: Oceans* 90 (C3):4833-4846. doi: 10.1029/JC090iC03p04833.
- Abualhaija, Mahmoud M., Hannah Whitby, and Constant M. G. van den Berg. 2015. "Competition between copper and iron for humic ligands in estuarine waters." *Marine Chemistry* 172:46-56. doi: <https://doi.org/10.1016/j.marchem.2015.03.010>.
- Aguilar-Islas, Ana M., Robert Rember, Shigeto Nishino, Takashi Kikuchi, and Motoyo Itoh. 2013. "Partitioning and lateral transport of iron to the Canada Basin." *Polar Science* 7 (2):82-99. doi: <http://dx.doi.org/10.1016/j.polar.2012.11.001>.
- Aguilar-Islas, A. M., R. D. Rember, C. W. Mordy, and J. Wu. 2008. "Sea ice-derived dissolved iron and its potential influence on the spring algal bloom in the Bering

Sea." *Geophysical Research Letters* 35 (24):n/a-n/a. doi:  
10.1029/2008GL035736.

Anderson, L. G., Per S Andersson, Göran Björk, E Peter Jones, Sara Jutterström, and Iréne Wåhlström. 2013. "Source and formation of the upper halocline of the Arctic Ocean." *Journal of Geophysical Research: Oceans* 118 (1):410-421.

Annett, Amber L, Suzanne Lapi, Thomas J Ruth, and Maria T Maldonado. 2008. "The effects of Cu and Fe availability on the growth and Cu: C ratios of marine diatoms." *Limnology and oceanography* 53 (6):2451-2461.

Biller, Dondra V., and Kenneth W. Bruland. 2013. "Sources and distributions of Mn, Fe, Co, Ni, Cu, Zn, and Cd relative to macronutrients along the central California coast during the spring and summer upwelling season." *Marine Chemistry* 155:50-70. doi: <https://doi.org/10.1016/j.marchem.2013.06.003>.

Boiteau, Rene M., Claire P. Till, Angel Ruacho, Randelle M. Bundy, Nicholas J. Hawco, Amy M. McKenna, Katherine A. Barbeau, Kenneth W. Bruland, Mak A. Saito, and Daniel J. Repeta. 2016. "Structural Characterization of Natural Nickel and Copper Binding Ligands along the US GEOTRACES Eastern Pacific Zonal Transect." *Frontiers in Marine Science* 3 (243). doi: 10.3389/fmars.2016.00243.

Böning, Philipp, Tim Shaw, Katharina Pahnke, and Hans-Jürgen Brumsack. 2015. "Nickel as indicator of fresh organic matter in upwelling sediments." *Geochimica et Cosmochimica Acta* 162:99-108. doi:  
<http://dx.doi.org/10.1016/j.gca.2015.04.027>.

- Bowie, Andrew R., David J. Whitworth, Eric P. Achterberg, R. Fauzi C. Mantoura, and Paul J. Worsfold. 2002. "Biogeochemistry of Fe and other trace elements (Al, Co, Ni) in the upper Atlantic Ocean." *Deep Sea Research Part I: Oceanographic Research Papers* 49 (4):605-636. doi: [https://doi.org/10.1016/S0967-0637\(01\)00061-9](https://doi.org/10.1016/S0967-0637(01)00061-9).
- Boyle, Edward A., Sarah S. Husted, and Susan P. Jones. 1981. "On the distribution of copper, nickel, and cadmium in the surface waters of the North Atlantic and North Pacific Ocean." *Journal of Geophysical Research: Oceans* 86 (C9):8048-8066. doi: 10.1029/JC086iC09p08048.
- Boyle, E. A., FR Sclater, and JM Edmond. 1977. "The distribution of dissolved copper in the Pacific." *Earth and planetary science letters* 37 (1):38-54.
- Bradley, S. Moran, and Wendy L. Woods. 1997. "Cd, Cr, Cu, Ni and Pb in the water column and sediments of the Ob-Irtysh Rivers, Russia." *Marine Pollution Bulletin* 35 (7):270-279. doi: [https://doi.org/10.1016/S0025-326X\(97\)00087-8](https://doi.org/10.1016/S0025-326X(97)00087-8).
- Bruland, K. W. 1980. "Oceanographic distributions of cadmium, zinc, nickel, and copper in the North Pacific." *Earth and Planetary Science Letters* 47 (2):176-198.
- Bruland, K. W., R. Middag, and M. C. Lohan. 2014. "8.2 - Controls of Trace Metals in Seawater." In *Treatise on Geochemistry (Second Edition)*, edited by Heinrich D. Holland and Karl K. Turekian, 19-51. Oxford: Elsevier.
- Bundy, R. M., A. Tagliabue, N. J. Hawco, P. L. Morton, B. S. Twining, M. Hatta, A. Noble, M. R. Cape, S. G. John, J. T. Cullen, and M. A. Saito. 2020. "Elevated

sources of cobalt in the Arctic Ocean." *Biogeosciences Discuss.* 2020:1-46. doi: 10.5194/bg-2020-84.

Cameron, Vyllinniskii, and Derek Vance. 2014. "Heavy nickel isotope compositions in rivers and the oceans." *Geochimica et Cosmochimica Acta* 128:195-211.

Carmack, Eddy, Fiona McLaughlin, Michiyo Yamamoto-Kawai, Motoyo Itoh, Koji Shimada, Richard Krishfield, and Andrey Proshutinsky. 2008. "Freshwater storage in the Northern Ocean and the special role of the Beaufort Gyre." In *Arctic–subArctic ocean fluxes*, 145-169. Springer.

Charette, Matthew A., Lauren E. Kipp, Laramie T. Jensen, Jessica S. Dabrowski, Laura M. Whitmore, Jessica N. Fitzsimmons, Tatiana Williford, Adam Ulfsbo, Elizabeth Jones, Randelle M. Bundy, Sebastian M. Vivancos, Katharina Pahnke, Seth G. John, Yang Xiang, Mariko Hatta, Mariia V. Petrova, Lars-Eric Heimbürger-Boavida, Dorothea Bauch, Robert Newton, Angelica Pasqualini, Alison M. Agather, Rainer M.W. Amon, Robert F. Anderson, Per S. Andersson, Ronald Benner, Katlin L. Bowman, R. Lawrence Edwards, Sandra Gdaniec, Loes J.A. Gerringa, Aridane G. González, Mats Granskog, Brian Haley, Chad R. Hammerschmidt, Dennis A. Hansell, Paul B. Henderson, David C. Kadko, Karl Kaiser, Patrick Laan, Phoebe J. Lam, Carl H. Lamborg, Martin Levier, Xianglei Li, Andrew R. Margolin, Chris Measures, Rob Middag, Frank J. Millero, Willard S. Moore, Ronja Paffrath, H el ene Planquette, Benjamin Rabe, Heather Reader, Robert Rember, Micha J.A. Rijkenberg, Matthieu Roy-Barman, Michiel Rutgers van der Loeff, Mak Saito, Ursula Schauer, Peter Schlosser, Robert M. Sherrell,

- Alan M. Shiller, Hans Slagter, Jeroen E. Sonke, Colin Stedmon, Ryan J. Woosley, Ole Valk, Jan van Ooijen, and Ruifeng Zhang. 2020. "The Transpolar Drift as a Source of Riverine and Shelf-Derived Trace Elements to the Central Arctic Ocean." *Journal of Geophysical Research: Oceans* n/a (n/a):e2019JC015920. doi: 10.1029/2019jc015920.
- Cid, Abigail Parcasio, Seiji Nakatsuka, and Yoshiki Sohrin. 2012. "Stoichiometry among bioactive trace metals in the Chukchi and Beaufort Seas." *Journal of oceanography* 68 (6):985-1001.
- Coale, Kenneth H, and Kenneth W Bruland. 1988. "Copper complexation in the Northeast Pacific." *Limnology and Oceanography* 33 (5):1084-1101.
- Cullen, Jay T. 2006. "On the nonlinear relationship between dissolved cadmium and phosphate in the modern global ocean: Could chronic iron limitation of phytoplankton growth cause the kink?" *Limnology and Oceanography* 51 (3):1369-1380. doi: 10.4319/lo.2006.51.3.1369.
- Cutter, G, P Andersson, Lou Codispoti, P Croot, R Francois, MC Lohan, H Obata, and Michiel Rutgers vd Loeff. 2010. Sampling and sample-handling protocols for GEOTRACES cruises. GEOTRACES.
- Cutter, Gregory A., and Kenneth W. Bruland. 2012. "Rapid and noncontaminating sampling system for trace elements in global ocean surveys." *Limnology and Oceanography: Methods* 10 (6):425-436. doi: doi:10.4319/lom.2012.10.425.
- Dai, Min-Han, and Jean-Marie Martin. 1995. "First data on trace metal level and behaviour in two major Arctic river-estuarine systems (Ob and Yenisey) and in

- the adjacent Kara Sea, Russia." *Earth and Planetary Science Letters* 131 (3):127-141. doi: [http://dx.doi.org/10.1016/0012-821X\(95\)00021-4](http://dx.doi.org/10.1016/0012-821X(95)00021-4).
- Danielsson, Lars-Göran, Bertil Magnusson, and Stig Westerlund. 1985. "Cadmium, copper, iron, nickel and zinc in the north-east Atlantic Ocean." *Marine Chemistry* 17 (1):23-41. doi: [https://doi.org/10.1016/0304-4203\(85\)90034-9](https://doi.org/10.1016/0304-4203(85)90034-9).
- Danielsson, Lars-Göran, and Stig Westerlund. 1983. "Trace Metals in the Arctic Ocean." In *Trace Metals in Sea Water*, edited by C. S. Wong, Edward Boyle, Kenneth W. Bruland, J. D. Burton and Edward D. Goldberg, 85-95. Boston, MA: Springer US.
- Dickson, R. J., and K. A. Hunter. 1981. "Copper and nickel in surface waters of Otago Harbour." *New Zealand Journal of Marine and Freshwater Research* 15 (4):475-480. doi: 10.1080/00288330.1981.9515939.
- Donat, John R, Kathy A Lao, and Kenneth W Bruland. 1994. "Speciation of dissolved copper and nickel in South San Francisco Bay: a multi-method approach." *Analytica Chimica Acta* 284 (3):547-571.
- Dupont, Christopher L., Katherine Barbeau, and Brian Palenik. 2008. "Ni Uptake and Limitation in Marine Synechococcus Strains." *Applied and Environmental Microbiology* 74 (1):23-31. doi: 10.1128/aem.01007-07.
- Ekwuzel, Brenda, Peter Schlosser, Richard A. Mortlock, Richard G. Fairbanks, and James H. Swift. 2001. "River runoff, sea ice meltwater, and Pacific water distribution and mean residence times in the Arctic Ocean." *Journal of Geophysical Research: Oceans* 106 (C5):9075-9092. doi: 10.1029/1999JC000024.

- Gardner, Wilford D., Mary Jo Richardson, and Alexey V. Mishonov. 2018. "Global assessment of benthic nepheloid layers and linkage with upper ocean dynamics." *Earth and Planetary Science Letters* 482 (Supplement C):126-134. doi: <https://doi.org/10.1016/j.epsl.2017.11.008>.
- Granger, Julie, and Bess B. Ward. 2003. "Accumulation of nitrogen oxides in copper-limited cultures of denitrifying bacteria." *Limnology and Oceanography* 48 (1):313-318. doi: 10.4319/lo.2003.48.1.0313.
- Guieu, Cécile, Wei Wen Huang, Jean-Marie Martin, and Yoon Yi Yong. 1996. "Outflow of trace metals into the Laptev Sea by the Lena River." *Marine Chemistry* 53 (3-4):255-267.
- Heggie, David, Gary Klinkhammer, and Douglas Cullen. 1987. "Manganese and copper fluxes from continental margin sediments." *Geochimica et Cosmochimica Acta* 51 (5):1059-1070.
- Heggie, David T. 1982. "Copper in surface waters of the Bering Sea." *Geochimica et Cosmochimica Acta* 46 (7):1301-1306. doi: [https://doi.org/10.1016/0016-7037\(82\)90014-X](https://doi.org/10.1016/0016-7037(82)90014-X).
- Hines, Mark E., Wm Berry Lyons, Peter B. Armstrong, William H. Orem, Mary Jo Spencer, Henri E. Gaudette, and Galen E. Jones. 1984. "Seasonal metal remobilization in the sediments of Great Bay, New Hampshire." *Marine Chemistry* 15 (2):173-187. doi: [https://doi.org/10.1016/0304-4203\(84\)90014-8](https://doi.org/10.1016/0304-4203(84)90014-8).

- Ho, Tung-Yuan, Antonietta Quigg, Zoe V Finkel, Allen J Milligan, Kevin Wyman, Paul G Falkowski, and François MM Morel. 2003. "The elemental composition of some marine phytoplankton." *Journal of phycology* 39 (6):1145-1159.
- Hölemann, Jens, M Schirmacher, and A Prange. 1995. "Transport and distribution of trace elements in the Laptev Sea. First results of the TRANSDRIFT expeditions." *Berichte zur Polarforschung*, 176. 297 (302).
- Hölemann, JA, M Schirmacher, and A Prange. 1999. "Dissolved and particulate major and trace elements in newly formed ice from the Laptev Sea (Transdrift III, October 1995)." In *Land-Ocean Systems in the Siberian Arctic*, 101-111. Springer.
- Hölemann, J. A., M. Schirmacher, and A. Prange. 2005. "Seasonal variability of trace metals in the Lena River and the southeastern Laptev Sea: Impact of the spring freshet." *Global and Planetary Change* 48 (1–3):112-125. doi: <http://dx.doi.org/10.1016/j.gloplacha.2004.12.008>.
- Irving, H., and R.J.P. Williams. 1953. "637. The stability of transition-metal complexes." *Journal of the Chemical Society (Resumed)*:3192-3210.
- Jacquot, Jeremy E., and James W. Moffett. 2015. "Copper distribution and speciation across the International GEOTRACES Section GA03." *Deep Sea Research Part II: Topical Studies in Oceanography* 116:187-207. doi: <https://doi.org/10.1016/j.dsr2.2014.11.013>.
- Jakobsson, M, A Grantz, Y Kristoffersen, R Macnab, RW MacDonald, E Sakshaug, R Stein, and W Jokat. 2004. "The Arctic Ocean: Boundary conditions and

background information." In *The organic carbon cycle in the Arctic Ocean*, 1-32. Springer.

Jensen, L. T., N. J. Wyatt, W. M. Landing, and J. N. Fitzsimmons. 2020. "Assessment of the stability, sorption, and exchangeability of marine dissolved and colloidal metals." *Marine Chemistry* 220:103754. doi:

<https://doi.org/10.1016/j.marchem.2020.103754>.

Jensen, L. T., N. J. Wyatt, B. S. Twining, S. Rauschenberg, W. M. Landing, R. M. Sherrell, and J. N. Fitzsimmons. 2019. "Biogeochemical Cycling of Dissolved Zinc in the Western Arctic (Arctic GEOTRACES GN01)." *Global Biogeochemical Cycles* 33 (3):343-369. doi: 10.1029/2018gb005975.

Johnson, Kenneth S, R Michael Gordon, and Kenneth H Coale. 1997. "What controls dissolved iron concentrations in the world ocean?" *Marine chemistry* 57 (3-4):137-161.

Jones, E.P., and L. G. Anderson. 1986. "On the origin of the chemical properties of the Arctic Ocean halocline." *Journal of Geophysical Research: Oceans* 91 (C9):10759-10767. doi: 10.1029/JC091iC09p10759.

Kadko, David, Ben Galfond, William M. Landing, and Rachel U. Shelley. 2016. "Determining the pathways, fate, and flux of atmospherically derived trace elements in the Arctic ocean/ice system." *Marine Chemistry* 182 (Supplement C):38-50. doi: <https://doi.org/10.1016/j.marchem.2016.04.006>.

Klunder, M. B., D. Bauch, P. Laan, H. J. W. de Baar, S. van Heuven, and S. Ober. 2012. "Dissolved iron in the Arctic shelf seas and surface waters of the central Arctic

- Ocean: Impact of Arctic river water and ice-melt." *Journal of Geophysical Research: Oceans* 117 (C1):n/a-n/a. doi: 10.1029/2011JC007133.
- Klunder, M. B., P. Laan, R. Middag, H. J. W. de Baar, and K. Bakker. 2012. "Dissolved iron in the Arctic Ocean: Important role of hydrothermal sources, shelf input and scavenging removal." *Journal of Geophysical Research: Oceans* 117 (C4):n/a-n/a. doi: 10.1029/2011JC007135.
- Kondo, Yoshiko, Hajime Obata, Nanako Hioki, Atsushi Ooki, Shigeto Nishino, Takashi Kikuchi, and Kenshi Kuma. 2016. "Transport of trace metals (Mn, Fe, Ni, Zn and Cd) in the western Arctic Ocean (Chukchi Sea and Canada Basin) in late summer 2012." *Deep Sea Research Part I: Oceanographic Research Papers* 116:236-252. doi: <http://dx.doi.org/10.1016/j.dsr.2016.08.010>.
- Kruppen, Thomas, H Jakob Belter, Antje Boetius, Ellen Damm, Christian Haas, Stefan Hendricks, Marcel Nicolaus, Eva-Maria Nöthig, Stephan Paul, and Ilka Peeken. 2019. "Arctic warming interrupts the Transpolar Drift and affects long-range transport of sea ice and ice-rafted matter." *Scientific reports* 9 (1):1-9.
- Lagerström, Maria, M. Field, Marie Seguret, Fisher E, Clark, and Robert Sherrell. 2013. "Automated on-line flow-injection ICP-MS determination of trace metals (Mn, Fe, Co, Ni, Cu and Zn) in open ocean seawater: Application to the GEOTRACES program." *Marine Chemistry* 155:71-80. doi: 10.1016/j.marchem.2013.06.001.
- Lannuzel, Delphine, Martin Vancoppenolle, Pier Van der Merwe, Jeroen De Jong, Klaus Martin Meiners, Marco Grotti, Jun Nishioka, and Véronique Schoemann. 2016. "Iron in sea ice: Review and new insights." *Elem Sci Anth* 4.

- Little, S.H., D Vance, C Walker-Brown, and WM Landing. 2014. "The oceanic mass balance of copper and zinc isotopes, investigated by analysis of their inputs, and outputs to ferromanganese oxide sediments." *Geochimica et Cosmochimica Acta* 125:673-693.
- Little, S. H., D. Vance, C. Walker-Brown, and W. M. Landing. 2014. "The oceanic mass balance of copper and zinc isotopes, investigated by analysis of their inputs, and outputs to ferromanganese oxide sediments." *Geochimica et Cosmochimica Acta* 125:673-693. doi: <https://doi.org/10.1016/j.gca.2013.07.046>.
- Löscher, Bettina M. 1999. "Relationships among Ni, Cu, Zn, and major nutrients in the Southern Ocean." *Marine Chemistry* 67 (1):67-102. doi: [https://doi.org/10.1016/S0304-4203\(99\)00050-X](https://doi.org/10.1016/S0304-4203(99)00050-X).
- Maldonado, Maria T., Andrew E. Allen, Joanne S. Chong, Kevin Lin, Dan Leus, Nataliya Karpenko, and Shannon L. Harris. 2006. "Copper-dependent iron transport in coastal and oceanic diatoms." *Limnology and Oceanography* 51 (4):1729-1743. doi: 10.4319/lo.2006.51.4.1729.
- Marsay, Chris M., Ana Aguilar-Islas, Jessica N. Fitzsimmons, Mariko Hatta, Laramie T. Jensen, Seth G. John, David Kadko, William M. Landing, Nathan T. Lanning, Peter L. Morton, Angelica Pasqualini, Sara Rauschenberg, Robert M. Sherrell, Alan M. Shiller, Benjamin S. Twining, Laura M. Whitmore, Ruifeng Zhang, and Clifton S. Buck. 2018. "Dissolved and particulate trace elements in late summer Arctic melt ponds." *Marine Chemistry* 204:70-85. doi: <https://doi.org/10.1016/j.marchem.2018.06.002>.

- Martin, JM, DM Guan, F Elbaz-Poulichet, AJ Thomas, and VV Gordeev. 1993. "Preliminary assessment of the distributions of some trace elements (As, Cd, Cu, Fe, Ni, Pb and Zn) in a pristine aquatic environment: the Lena River estuary (Russia)." *Marine Chemistry* 43 (1-4):185-199.
- März, C., A. Stratmann, J. Matthiessen, A. K. Meinhardt, S. Eckert, B. Schnetger, C. Vogt, R. Stein, and H. J. Brumsack. 2011. "Manganese-rich brown layers in Arctic Ocean sediments: Composition, formation mechanisms, and diagenetic overprint." *Geochimica et Cosmochimica Acta* 75 (23):7668-7687. doi: <https://doi.org/10.1016/j.gca.2011.09.046>.
- Measures, C. I. 1999. "The role of entrained sediments in sea ice in the distribution of aluminium and iron in the surface waters of the Arctic Ocean." *Marine Chemistry* 68 (1-2):59-70. doi: [http://dx.doi.org/10.1016/S0304-4203\(99\)00065-1](http://dx.doi.org/10.1016/S0304-4203(99)00065-1).
- Middag, R, HJW de Baar, and KW Bruland. 2019. "The relationships between dissolved zinc and major nutrients phosphate and silicate along the GEOTRACES GA02 transect in the West Atlantic Ocean." *Global Biogeochemical Cycles* 33 (1):63-84.
- Middag, Rob, Hein JW de Baar, Kenneth W Bruland, and Steven MAC van Heuven. 2020. "The distribution of nickel in the west-Atlantic Ocean, its relationship with phosphate and a comparison to cadmium and zinc." *Frontiers in Marine Science* 7:105.
- Middag, R., H. J. W. de Baar, P. Laan, and M. B. Klunder. 2011. "Fluvial and hydrothermal input of manganese into the Arctic Ocean." *Geochimica et*

- Cosmochimica Acta* 75 (9):2393-2408. doi:  
<http://dx.doi.org/10.1016/j.gca.2011.02.011>.
- Moffett, James W., and Larry E Brand. 1996. "Production of strong, extracellular Cu chelators by marine cyanobacteria in response to Cu stress." *Limnology and Oceanography* 41 (3):388-395.
- Moffett, James W., Larry E. Brand, Peter L. Croot, and Katherine A. Barbeau. 1997. "Cu speciation and cyanobacterial distribution in harbors subject to anthropogenic Cu inputs." *Limnology and Oceanography* 42 (5):789-799. doi:  
[10.4319/lo.1997.42.5.0789](https://doi.org/10.4319/lo.1997.42.5.0789).
- Moore, R. M. 1978. "The distribution of dissolved copper in the eastern Atlantic Ocean." *Earth and planetary science letters* 41 (4):461-468.
- Moore, R. M. 1981. "Oceanographic distributions of zinc, cadmium, copper and aluminium in waters of the central arctic." *Geochimica et Cosmochimica Acta* 45 (12):2475-2482. doi: [http://dx.doi.org/10.1016/0016-7037\(81\)90099-5](http://dx.doi.org/10.1016/0016-7037(81)90099-5).
- Newton, Robert, Peter Schlosser, Richard Mortlock, James Swift, and Robie MacDonald. 2013. "Canadian Basin freshwater sources and changes: Results from the 2005 Arctic Ocean Section." *Journal of Geophysical Research: Oceans* 118 (4):2133-2154. doi: [doi:10.1002/jgrc.20101](https://doi.org/10.1002/jgrc.20101).
- Nolting, R. F., and H. J. W. de Baar. 1994. "Behaviour of nickel, copper, zinc and cadmium in the upper 300 m of a transect in the Southern Ocean (57°–62°S, 49°W)." *Marine Chemistry* 45 (3):225-242. doi: [https://doi.org/10.1016/0304-4203\(94\)90006-X](https://doi.org/10.1016/0304-4203(94)90006-X).

- Noriki, Shinichiro, Yoshihiro Arashitani, Masayuki Minakawa, Koh Harada, and Shizuo Tsunogai. 1998. "Vertical cycling of Cu and Ni in the western North and Equatorial Pacific." *Marine chemistry* 59 (3-4):211-218.
- Opsahl, Stephen, Ronald Benner, and Rainer M. W. Amon. 1999. "Major flux of terrigenous dissolved organic matter through the Arctic Ocean." *Limnology and Oceanography* 44 (8):2017-2023. doi: 10.4319/lo.1999.44.8.2017.
- Price, NM, and Francois MM Morel. 1991. "Colimitation of phytoplankton growth by nickel and nitrogen." *Limnology and Oceanography* 36 (6):1071-1077.
- Proshutinsky, Andrey, Richard Krishfield, Mary-Louise Timmermans, John Toole, Eddy Carmack, Fiona McLaughlin, William J Williams, Sarah Zimmermann, Motoyo Itoh, and Koji Shimada. 2009. "Beaufort Gyre freshwater reservoir: State and variability from observations." *Journal of Geophysical Research: Oceans* 114 (C1).
- Richon, Camille, and Alessandro Tagliabue. 2019. "Insights Into the Major Processes Driving the Global Distribution of Copper in the Ocean From a Global Model." *Global Biogeochemical Cycles* 33 (12):1594-1610. doi: 10.1029/2019gb006280.
- Rijkenberg, Micha J. A., Hans A. Slagter, Michiel Rutgers van der Loeff, Jan van Ooijen, and Loes J. A. Gerringa. 2018. "Dissolved Fe in the Deep and Upper Arctic Ocean With a Focus on Fe Limitation in the Nansen Basin." *Frontiers in Marine Science* 5 (88). doi: 10.3389/fmars.2018.00088.

- Roshan, Saeed, and Jingfeng Wu. 2015. "The distribution of dissolved copper in the tropical-subtropical north Atlantic across the GEOTRACES GA03 transect." *Marine Chemistry* 176:189-198.
- Rudels, B. 2015. "Arctic Ocean circulation, processes and water masses: A description of observations and ideas with focus on the period prior to the International Polar Year 2007–2009." *Progress in Oceanography* 132:22-67. doi: <http://dx.doi.org/10.1016/j.pocean.2013.11.006>.
- Rudels, B., E. Peter Jones, Ursula Schauer, and Patrick Eriksson. 2004. "Atlantic sources of the Arctic Ocean surface and halocline waters." *Polar Research* 23 (2):181-208. doi: 10.1111/j.1751-8369.2004.tb00007.x.
- Saito, Mak A., James W. Moffett, and Giacomo R. DiTullio. 2004. "Cobalt and nickel in the Peru upwelling region: A major flux of labile cobalt utilized as a micronutrient." *Global Biogeochemical Cycles* 18 (4). doi: 10.1029/2003gb002216.
- Schauer, Ursula, B Rudels, EP Jones, LG Anderson, RD Muench, G Björk, JH Swift, V Ivanov, and A-M Larsson. 2002. "Confluence and redistribution of Atlantic water in the Nansen, Amundsen and Makarov basins." *Annales Geophysicae*.
- Schlitzer, Reiner, Robert F. Anderson, Elena Masferrer Dodas, Maeve Lohan, Walter Geibert, Alessandro Tagliabue, Andrew Bowie, Catherine Jeandel, Maria T. Maldonado, William M. Landing, Donna Cockwell, Cyril Abadie, Wafa Abouchami, Eric P. Achterberg, Alison Agather, Ana Aguliar-Islas, Hendrik M. van Aken, Morten Andersen, Corey Archer, Maureen Auro, Hein J. de Baar,

Oliver Baars, Alex R. Baker, Karel Bakker, Chandranath Basak, Mark Baskaran, Nicholas R. Bates, Dorothea Bauch, Pieter van Beek, Melanie K. Behrens, Erin Black, Katrin Bluhm, Laurent Bopp, Heather Bouman, Katlin Bowman, Johann Bown, Philip Boyd, Marie Boye, Edward A. Boyle, Pierre Branellec, Luke Bridgestock, Guillaume Brissebrat, Thomas Browning, Kenneth W. Bruland, Hans-Jürgen Brumsack, Mark Brzezinski, Clifton S. Buck, Kristen N. Buck, Ken Buesseler, Abby Bull, Edward Butler, Pinghe Cai, Patricia Cámara Mor, Damien Cardinal, Craig Carlson, Gonzalo Carrasco, Núria Casacuberta, Karen L. Casciotti, Maxi Castrillejo, Elena Chamizo, Rosie Chance, Matthew A. Charette, Joaquin E. Chaves, Hai Cheng, Fanny Chever, Marcus Christl, Thomas M. Church, Ivía Closset, Albert Colman, Tim M. Conway, Daniel Cossa, Peter Croot, Jay T. Cullen, Gregory A. Cutter, Chris Daniels, Frank Dehairs, Feifei Deng, Huong Thi Dieu, Brian Duggan, Gabriel Dulaquais, Cynthia Dumousseaud, Yolanda Echegoyen-Sanz, R. Lawrence Edwards, Michael Ellwood, Eberhard Fahrbach, Jessica N. Fitzsimmons, A. Russell Flegal, Martin Q. Fleisher, Tina van de Flierdt, Martin Frank, Jana Friedrich, Francois Fripiat, Henning Fröllje, Stephen J. G. Galer, Toshitaka Gamo, Raja S. Ganeshram, Jordi Garcia-Orellana, Ester Garcia-Solsona, Melanie Gault-Ringold, Ejin George, Loes J. A. Gerringa, Melissa Gilbert, Jose M. Godoy, Steven L. Goldstein, Santiago R. Gonzalez, Karen Grissom, Chad Hammerschmidt, Alison Hartman, Christel S. Hassler, Ed C. Hathorne, Mariko Hatta, Nicholas Hawco, Christopher T. Hayes, Lars-Eric Heimbürger, Josh Helgoe, Maija Heller, Gideon M. Henderson, Paul B.

Henderson, Steven van Heuven, Peng Ho, Tristan J. Horner, Yu-Te Hsieh, Kuo-Fang Huang, Matthew P. Humphreys, Kenji Isshiki, Jeremy E. Jacquot, David J. Janssen, William J. Jenkins, Seth John, Elizabeth M. Jones, Janice L. Jones, David C. Kadko, Rick Kayser, Timothy C. Kenna, Roulin Khondoker, Taejin Kim, Lauren Kipp, Jessica K. Klar, Maarten Klunder, Sven Kretschmer, Yuichiro Kumamoto, Patrick Laan, Marie Labatut, Francois Lacan, Phoebe J. Lam, Myriam Lambelet, Carl H. Lamborg, Frédéric A. C. Le Moigne, Emilie Le Roy, Oliver J. Lechtenfeld, Jong-Mi Lee, Pascale Lherminier, Susan Little, Mercedes López-Lora, Yanbin Lu, Pere Masque, Edward Mawji, Charles R. McClain, Christopher Measures, Sanjin Mehic, Jan-Lukas Menzel Barraqueta, Pier van der Merwe, Rob Middag, Sebastian Mieruch, Angela Milne, Tomoharu Minami, James W. Moffett, Gwenaelle Moncoiffe, Willard S. Moore, Paul J. Morris, Peter L. Morton, Yuzuru Nakaguchi, Noriko Nakayama, John Niedermiller, Jun Nishioka, Akira Nishiuchi, Abigail Noble, Hajime Obata, Sven Ober, Daniel C. Ohnemus, Jan van Ooijen, Jeanette O'Sullivan, Stephanie Owens, Katharina Pahnke, Maxence Paul, Frank Pavia, Leopoldo D. Pena, Brian Peters, Frederic Planchon, Helene Planquette, Catherine Pradoux, Viena Puigcorbé, Paul Quay, Fabien Queroue, Amandine Radic, S. Rauschenberg, Mark Rehkämper, Robert Rember, Tomas Remenyi, Joseph A. Resing, Joerg Rickli, Sylvain Rigaud, Micha J. A. Rijkenberg, Stephen Rintoul, Laura F. Robinson, Montserrat Roca-Martí, Valenti Rodellas, Tobias Roeske, John M. Rolison, Mark Rosenberg, Saeed Roshan, Michiel M. Rutgers van der Loeff, Evgenia Ryabenko, Mak A. Saito,

Lesley A. Salt, Virginie Sanial, Geraldine Sarthou, Christina Schallenberg, Ursula Schauer, Howie Scher, Christian Schlosser, Bernhard Schnetger, Peter Scott, Peter N. Sedwick, Igor Semiletov, Rachel Shelley, Robert M. Sherrell, Alan M. Shiller, Daniel M. Sigman, Sunil Kumar Singh, Hans A. Slagter, Emma Slater, William M. Smethie, Helen Snaith, Yoshiki Sohrin, Bettina Sohst, Jeroen E. Sonke, Sabrina Speich, Reiner Steinfeldt, Gillian Stewart, Torben Stichel, Claudine H. Stirling, Johnny Stutsman, Gretchen J. Swarr, James H. Swift, Alexander Thomas, Kay Thorne, Claire P. Till, Ralph Till, Ashley T. Townsend, Emily Townsend, Robyn Tuerena, Benjamin S. Twining, Derek Vance, Sue Velazquez, Celia Venchiarutti, Maria Villa-Alfageme, Sebastian M. Vivancos, Antje H. L. Voelker, Bronwyn Wake, Mark J. Warner, Ros Watson, Evaline van Weerlee, M. Alexandra Weigand, Yishai Weinstein, Dominik Weiss, Andreas Wisotzki, E. Malcolm S. Woodward, Jingfeng Wu, Yingzhe Wu, Kathrin Wuttig, Neil Wyatt, Yang Xiang, Ruifang C. Xie, Zichen Xue, Hisayuki Yoshikawa, Jing Zhang, Pu Zhang, Ye Zhao, Linjie Zheng, Xin-Yuan Zheng, Moritz Zieringer, Louise A. Zimmer, Patrizia Ziveri, Patricia Zunino, and Cheryl Zurbrugg. 2018. "The GEOTRACES Intermediate Data Product 2017." *Chemical Geology* 493:210-223. doi: <https://doi.org/10.1016/j.chemgeo.2018.05.040>.

Schlosser, Peter, Bernd Kromer, Gote Östlund, Brenda Ekwurzel, Gerhard Bönisch, HH Loosli, and Roland Purtschert. 1994. "On the  $^{14}\text{C}$  and  $^{39}\text{Ar}$  Distribution in the Central Arctic Ocean: Implications for Deep Water Formation 1." *Radiocarbon* 36 (3):327-343.

- Sclater, FR, Edward Boyle, and JM Edmond. 1976. "On the marine geochemistry of nickel." *Earth and Planetary Science Letters* 31 (1):119-128.
- Sherrell, Robert M., and Edward A. Boyle. 1992. "The trace metal composition of suspended particles in the oceanic water column near Bermuda." *Earth and Planetary Science Letters* 111 (1):155-174. doi: [https://doi.org/10.1016/0012-821X\(92\)90176-V](https://doi.org/10.1016/0012-821X(92)90176-V).
- Shimada, Koji, Motoyo Itoh, Shigeto Nishino, Fiona McLaughlin, Eddy Carmack, and Andrey Proshutinsky. 2005. "Halocline structure in the Canada Basin of the Arctic Ocean." *Geophysical Research Letters* 32 (3):n/a-n/a. doi: [10.1029/2004GL021358](https://doi.org/10.1029/2004GL021358).
- Slagter, Hans A., Luis M. Laglera, Camila Sukekava, and Loes J. A. Gerringa. 2019. "Fe-Binding Organic Ligands in the Humic-Rich TransPolar Drift in the Surface Arctic Ocean Using Multiple Voltammetric Methods." *Journal of Geophysical Research: Oceans* 124 (3):1491-1508. doi: [10.1029/2018jc014576](https://doi.org/10.1029/2018jc014576).
- Slagter, H. A., H. E. Reader, M. J. A. Rijkenberg, M. Rutgers van der Loeff, H. J. W. de Baar, and L. J. A. Gerringa. 2017. "Organic Fe speciation in the Eurasian Basins of the Arctic Ocean and its relation to terrestrial DOM." *Marine Chemistry* 197:11-25. doi: <https://doi.org/10.1016/j.marchem.2017.10.005>.
- Spivack, A. J., S. S. Husted, and E. A. Boyle. 1983. "Copper, Nickel and Cadmium in the Surface Waters of the Mediterranean." In *Trace Metals in Sea Water*, edited by C. S. Wong, Edward Boyle, Kenneth W. Bruland, J. D. Burton and Edward D. Goldberg, 505-512. Boston, MA: Springer US.

- Sunda, William G. 2012. "Feedback interactions between trace metal nutrients and phytoplankton in the ocean." *Frontiers in Microbiology* 3. doi: 10.3389/fmicb.2012.00204.
- Talley, Lynne D., George L. Pickard, William J. Emery, and James H. Swift. 2011. "Chapter 12 - Arctic Ocean and Nordic Seas." In *Descriptive Physical Oceanography (Sixth Edition)*, 401-436. Boston: Academic Press.
- Tanhua, Toste, E. Peter Jones, Emil Jeansson, Sara Jutterström, William M. Smethie, Douglas W. R. Wallace, and Leif G. Anderson. 2009. "Ventilation of the Arctic Ocean: Mean ages and inventories of anthropogenic CO<sub>2</sub> and CFC-11." *Journal of Geophysical Research: Oceans* 114 (C1):n/a-n/a. doi: 10.1029/2008JC004868.
- Taylor, Rebecca L, David M Semeniuk, Christopher D Payne, Jie Zhou, Jean-Éric Tremblay, Jay T Cullen, and Maria T Maldonado. 2013. "Colimitation by light, nitrate, and iron in the Beaufort Sea in late summer." *Journal of Geophysical Research: Oceans* 118 (7):3260-3277.
- Timmermans, M-L., Chris Garrett, and Eddy Carmack. 2003. "The thermohaline structure and evolution of the deep waters in the Canada Basin, Arctic Ocean." *Deep Sea Research Part I: Oceanographic Research Papers* 50 (10):1305-1321. doi: [https://doi.org/10.1016/S0967-0637\(03\)00125-0](https://doi.org/10.1016/S0967-0637(03)00125-0).
- Tovar-Sánchez, Antonio, Carlos M. Duarte, Juan C. Alonso, Silvia Lacorte, Romà Tauler, and Cristobal Galbán-Malagón. 2010. "Impacts of metals and nutrients released from melting multiyear Arctic sea ice." *Journal of Geophysical Research: Oceans* 115 (C7):n/a-n/a. doi: 10.1029/2009JC005685.

- Twining, B. S., and Stephen B Baines. 2013. "The trace metal composition of marine phytoplankton." *Annual review of marine science* 5:191-215.
- Vieira, Lúcia H., Eric P. Achterberg, Jan Scholten, Aaron J. Beck, Volker Liebetrau, Matthew M. Mills, and Kevin R. Arrigo. 2019. "Benthic fluxes of trace metals in the Chukchi Sea and their transport into the Arctic Ocean." *Marine Chemistry* 208:43-55. doi: <https://doi.org/10.1016/j.marchem.2018.11.001>.
- Vraspir, Julia M, and Alison Butler. 2009. "Chemistry of marine ligands and siderophores."
- Westerlund, Stig F. G., Leif G. Anderson, Per O. J. Hall, Åke Iverfeldt, Michiel M. Rutgers Van Der Loeff, and Bjørn Sundby. 1986. "Benthic fluxes of cadmium, copper, nickel, zinc and lead in the coastal environment." *Geochimica et Cosmochimica Acta* 50 (6):1289-1296. doi: [https://doi.org/10.1016/0016-7037\(86\)90412-6](https://doi.org/10.1016/0016-7037(86)90412-6).
- Whitby, Hannah, and Constant MG van den Berg. 2015. "Evidence for copper-binding humic substances in seawater." *Marine Chemistry* 173:282-290.
- Wood, Paul M. 1978. "Interchangeable Copper and Iron Proteins in Algal Photosynthesis: Studies on Plastocyanin and Cytochrome c-552 in *Chlamydomonas*." *European journal of biochemistry* 87 (1):9-19.
- Woodgate, Rebecca A., Knut Aagaard, Robin D. Muench, John Gunn, Göran Björk, Bert Rudels, A. T. Roach, and Ursula Schauer. 2001. "The Arctic Ocean Boundary Current along the Eurasian slope and the adjacent Lomonosov Ridge: Water mass properties, transports and transformations from moored instruments." *Deep Sea*

*Research Part I: Oceanographic Research Papers* 48 (8):1757-1792. doi:  
[https://doi.org/10.1016/S0967-0637\(00\)00091-1](https://doi.org/10.1016/S0967-0637(00)00091-1).

- Woodgate, Rebecca A., Knut Aagaard, James H. Swift, Kelly K. Falkner, and William M. Smethie. 2005. "Pacific ventilation of the Arctic Ocean's lower halocline by upwelling and diapycnal mixing over the continental margin." *Geophysical Research Letters* 32 (18):n/a-n/a. doi: 10.1029/2005GL023999.
- Xiang, Y., and P.J. Lam "Size-fractionated marine suspended particle dynamics in the Western Arctic Ocean from the U.S. GEOTRACES Arctic cruise (GN01)." (in review at *Journal of Geophysical Research*).
- Yamamoto-Kawai, M, FA McLaughlin, EC Carmack, S Nishino, and K Shimada. 2008. "Freshwater budget of the Canada Basin, Arctic Ocean, from salinity,  $\delta^{18}\text{O}$ , and nutrients." *Journal of Geophysical Research: Oceans* 113 (C1).
- Yeats, Philip A. 1988. "Manganese, nickel, zinc and cadmium distributions at the Fram-3 and Cesar Ice Camps in the Arctic Ocean." *Oceanologica acta* 11 (4):383-388.
- Yeats, Philip A., and Stig Westerlund. 1991. "Trace metal distributions at an Arctic Ocean ice island." *Marine Chemistry* 33 (3):261-277. doi:  
[http://dx.doi.org/10.1016/0304-4203\(91\)90071-4](http://dx.doi.org/10.1016/0304-4203(91)90071-4).
- Yeats, P. A., S. Westerlund, and A. R. Flegal. 1995. "Cadmium, copper and nickel distributions at four stations in the eastern central and south Atlantic." *Marine Chemistry* 49 (4):283-293. doi: [https://doi.org/10.1016/0304-4203\(95\)00018-M](https://doi.org/10.1016/0304-4203(95)00018-M).
- Zhang, Ruifeng, Laramie T. Jensen, Jessica N. Fitzsimmons, Robert M. Sherrell, and Seth John. 2019. "Dissolved cadmium and cadmium stable isotopes in the western

Arctic Ocean." *Geochimica et Cosmochimica Acta* 258:258-273. doi:

<https://doi.org/10.1016/j.gca.2019.05.028>.

## 6. BIOGEOCHEMICAL CYCLING OF COLLOIDAL TRACE METALS IN THE ARCTIC CRYOSPHERE

### 6.1. Introduction

Polar regions such as the Arctic Ocean and Southern Ocean are highly susceptible to a warming climate, particularly with respect to sea ice coverage and riverine fluxes. Evidence of climate-induced changes to the hydrologic cycle are most pronounced in the Arctic and are evident in trends of increasing water temperature, permafrost thaw, riverine discharge, and sea ice melt (Peterson et al., 2002; Frey and McClelland, 2009; Macdonald et al., 2015b; Spencer et al., 2015). The Arctic Ocean, which already receives 11% of total global river water flux to just 1% of the world's ocean volume (Opsahl et al., 1999), will feel this freshening more acutely due to the isolated nature of the basin. Furthermore, freshening of the Fram Strait, the Arctic's connection to the far North Atlantic, is expected to result in a direct global impact of increased freshwater discharge to the Arctic, as negative salinity anomalies found in the North Atlantic can be explained by Arctic freshening, potentially affecting the formation of deep water in the North Atlantic and thus global overturning circulation (Dickson et al., 2002; Karcher et al., 2012).

Importantly, these climate changes are not just physical but also biogeochemical, with impacts on biology and chemistry such as increased nutrient load in Arctic river fluxes (Macdonald et al., 2015a). This is felt acutely in the surface Arctic, where much of the freshwater inventory is stored in the cryosphere, defined here as glaciers, sea ice,

snow, melt ponds, and boreal freshwaters that may flow through recently thawed permafrost (Figure 6.1). Freshwater sources such as rivers and sea ice may be responsible for supplying essential nutrients into the central Arctic where ice coverage is more extensive than in the productive, open coastal regions. Among these essential nutrients are trace metals, which can act as micronutrients by serving as metal centers in important metabolic enzymes in photosynthesis, nitrogen fixation, and carbon uptake/usage (Sunda, 2012; Bruland et al., 2014). In particular, Arctic rivers have high trace metal and nutrient loadings (Dai and Martin, 1995; Hölemann et al., 2005; Holmes et al., 2019) that can be transported well into the central Arctic along surface currents (Charette et al., 2020). Likewise, sea ice, especially “dirty ice” laden with shelf sediments, can supply a large flux of nutrients and trace metals (Hölemann et al., 1999; Aguilar-Islas et al., 2008; Tovar-Sánchez et al., 2010) to the surface Arctic upon melting (Measures, 1999).

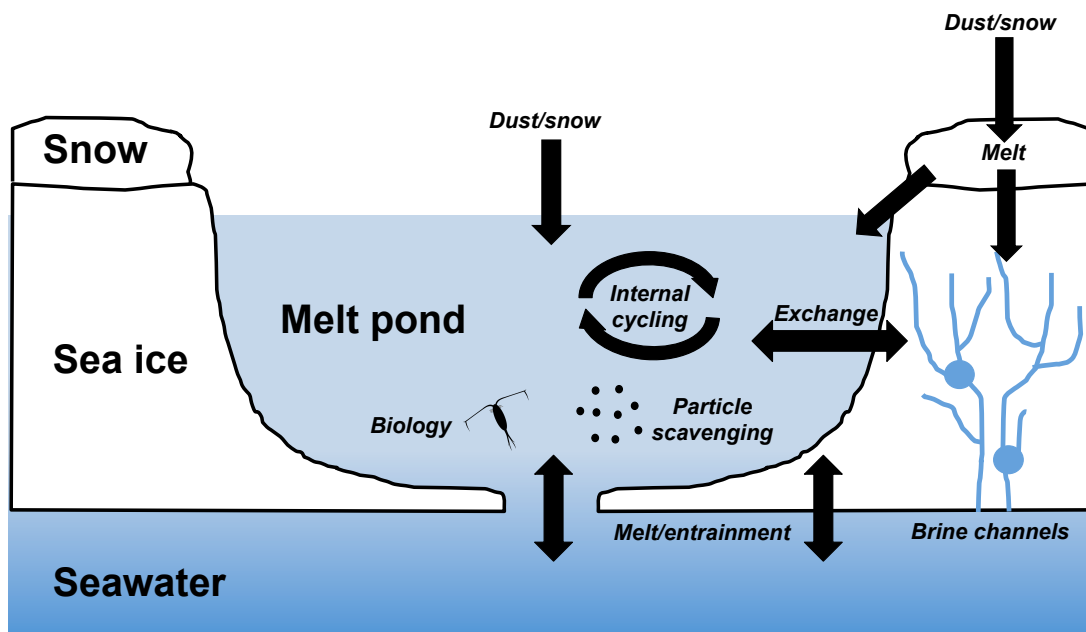


**Figure 6.1** Schematic of freshwater pools in the Arctic cryosphere. Side view of snow, sea ice, melt pond, and the underlying seawater with major points of exchange and likely processes affecting colloidal trace metals. Modified from Marsay et al. (2018b).

As climate change accelerates both riverine discharge and sea ice melting we can expect these cryospheric inventories of nutrients and metals such as sea ice, melt ponds, and river water to gain heightened importance. These inputs will be discharged directly into the surface Arctic, which is expected to become fresher, more stratified, and less limited by light (Aleksi et al., 2016), as sea ice coverage is reduced. This is likely to lead to a change in community composition of phytoplankton in surface waters, as well as the potential limitation to primary production by nutrients and metals alongside or even instead of known limiting factors like light (Arrigo et al., 2012; Taylor et al., 2013; Rijkenberg et al., 2018). Macronutrient and organic matter fluxes have been well reported in prior studies of the Arctic Ocean, but trace metals have been studied much less, despite their importance in influencing productivity and community composition.

Advances in trace metal sampling technology and a renewed international focus on the rapidly changing Arctic ecosystem have led to multiple surveys of trace metals, especially in the Eastern Arctic (Middag et al., 2009; Middag et al., 2011; Klunder et al., 2012b; Klunder et al., 2012a; Charette et al., 2020) and more recently in the Western Arctic (Nakayama et al., 2011; Cid et al., 2012; Nishimura et al., 2012; Aguilar-Islas et al., 2013; Kondo et al., 2016; Jensen et al., 2019).

The fate and transport of trace metals is also subject to changes in their physicochemical speciation, which is their molecular size and chemical composition. For example, a metal complex's size can affect its scavenging/aggregation fate with respect to settling (Wu et al., 2001; Cullen et al., 2006; Fitzsimmons et al., 2017; Section 4). Furthermore, a metal's chemical composition, such as its complexation with organic ligands or partitioning into an inorganic nanoparticle (Gledhill & Buck 2012), can directly affect its bioavailability to phytoplankton (Rue and Bruland, 1995; Chen and Wang, 2001; Chen et al., 2003). Thus, the physicochemical speciation of trace metals will play an important role in determining the ultimate fate of any increased fluxes due to climate change.

Typically, trace metals are supplied to the surface ocean by aerosol deposition, riverine/freshwater discharge, or continental margin influence such as shelf sediments. Certain trace metal fluxes carry unique chemical speciation that can differ from the seawater into which they are deposited, such as river (Dammshäuser and Croot, 2012; Gledhill and Buck, 2012; Oldham et al., 2017; Slagter et al., 2019) and aerosol inputs (Bergquist et al., 2007; Fitzsimmons and Boyle, 2014b; Fitzsimmons et al., 2015; Kunde

et al., 2019). Uniquely, wet aerosol deposition in the Arctic, as snow, settles upon sea ice, rather than directly into the surface ocean, and often will contribute to melt ponds on the surface of sea ice before mixing with sea ice or seawater directly (Figure 6.1). Thus, snow, sea ice, and melt pond reservoirs act as “incubators” of these trace metals, for various periods of time, with the ability to change their physicochemical speciation through biotic and abiotic particle interactions before being released into the surface seawater. Sea ice, in particular, is host to many physical, biotic, and abiotic processes that can affect aggregation and disaggregation of particles and colloids (Weeks and Ackley, 1982; Dieckmann et al., 2010).

Size speciation of dissolved trace metals is operationally defined here through ultrafiltration into a soluble or “truly dissolved” phase ( $<10$  kDa, which is  $\sim 0.003$   $\mu\text{m}$  for globular proteins, (Erickson, 2009)) and a colloidal phase ( $0.003$   $\mu\text{m}$  –  $0.2$   $\mu\text{m}$ ), which together add up to the total dissolved phase ( $<0.2$   $\mu\text{m}$ ). Marine colloids are thought to be composed of macromolecules and are thus largely organic in nature (Guo and Santschi, 1997). The organic nature of marine colloids has led scientists to connect a metal’s proclivity to bind to organic ligands to an increase in their colloidal abundance, which has proven true for Fe, Al, and Ti (Dammshäuser and Croot, 2012), despite that these compounds can also form inorganic nanoparticles even without organic complexation. Importantly, presence in the colloidal size fraction does not preclude an organic chemical composition, and presence in the soluble size fraction can include inorganic nanoparticulate species; thus, size partitioning does not define chemical complexation, and vice versa, as they are independent. Nonetheless, the colloidal phase is thought to be

an intermediary between the soluble (most bioavailable) and particulate (less available) phase, as well as potentially bioavailable to phytoplankton. While sources of colloids can vary from estuaries to sediment resuspension, their *in situ* cycling and aggregation-disaggregation dynamics dominate marine colloid production in the water column (Guo and Santschi, 1997). In the Arctic Ocean, these factors are all at play.

Colloidal species of Fe have been best studied in the global ocean, and a GEOTRACES section of colloidal Fe from the North Atlantic (GA03, (Fitzsimmons et al., 2015)) provided a working model against which to test metal speciation in other ocean basins. This model suggested that Fe supplied from external sources such as dust and sediments were rich in colloids (up to 90%), while older dissolved Fe supplied by remineralization was partitioned approximately 50% colloidal and 50% soluble. Thus, in the riverine- and sediment-rich Arctic, both strong sources of colloidal Fe (Wells et al., 200; Fitzsimmons et al., 2014), we expected to see a dominance of colloidal Fe species. However, results from the U.S. GEOTRACES GN01 study of the Western Arctic showed that colloidal Fe is a lower fraction of dissolved Fe ( $25 \pm 16\%$ ) in the Arctic water column (Section 4), compared to the North Atlantic. So, why are colloidal Fe loadings so low, and does this extend to other metals? Overall, there is little to no colloidal data in the Arctic Ocean except in river estuaries, where colloids appear to be rapidly attenuated due to flocculation (Pokrovsky et al., 2014). For dissolved Fe, colloids appear only to be enriched on the shelf ( $65 \pm 22\%$ , Section 4) and likewise rapidly removed away from that source (Section 4). This suggests that either external sources to

the Arctic have fewer Fe colloids or that perhaps longer incubation times, such as within the cryosphere, result in scavenging removal of colloids.

Here, we use a unique and opportunistic sample set from the U.S GEOTRACES GN01 Western Arctic cruise where the size partitioning of a suite of trace metals (Mn, Fe, Ni, Cu, Zn, and Cd) was studied in six locations across four different cryospheric pools: snow, sea ice, melt ponds, and the underlying seawater. We aim to answer the following questions: 1) Do cryospheric freshwater pools have high %colloids and if so, for which metals? 2) As suggested for dissolved Fe above, is aggregation and/or scavenging a pathway for a decrease in metals during the incubation of waters in freshwater pools before it is sourced to the underlying seawater? Previous work on this sample set has identified several potential processes occurring over time in the freshwater cryosphere [Marsay et al., 2018b), such as biological activity, particle scavenging, mixing of melt waters, and brine rejection (Figure 6.1), a complex physical process occurring in sea ice (Weeks and Ackley, 1982). Here, we attempt to use chemical tracers to tease out the strength of these processes in different samples, in order to resolve the variability in metal size partitioning observed in this dataset.

## **6.2. Methods**

### **6.2.1. Sample collection**

The U.S. Arctic GEOTRACES GN01 cruise left Dutch Harbor, AK on the 9<sup>th</sup> August 2015 aboard the USCGC *Healy* moving northward through the Bering Strait and Chukchi Shelf and across the Canada and Makarov basins along ~170°W to the North Pole and then southward along 150°W to terminate sample collection on the Chukchi

Shelf and return to Dutch Harbor on 12<sup>th</sup> October 2015. At six designated ice stations (Stations 31, 33, 39, 42, 43, 46) occupied north of 80°N (Figure 6.2) trace metal clean samples were taken from snow, sea ice, and underlying seawater (1, 5, and 20 m depth) through ice holes. At five of these six ice stations (Stations 33, 39, 42, 43, 46), samples were also collected from melt ponds that had formed on the sea ice. All ice stations were selected at locations where sampling was deemed to be safe for collection and close to a full water column station for comparison.

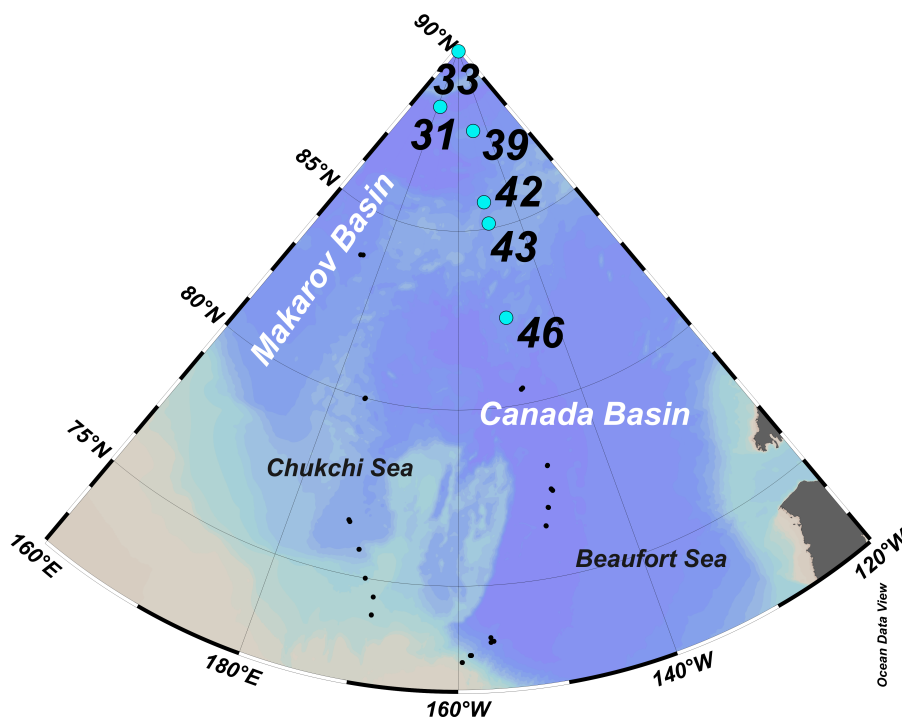


**Figure 6.2** Map of samples sites in this study as part of U.S. Arctic GEOTRACES GN01 cruise (2015). Relevant ice stations are shown as blue dots, and full-water column stations are shown as smaller black dots (Jensen et al. 2019 for Zn, Zhang et al. 2020 for Cd, Jensen et al. in review for Fe and Mn). Snow, sea ice, and under ice-seawater samples were collected at Stations 31, 33, 39, 42, 43, and 46, and melt pond samples were taken at these same stations except Station 31. Chukchi and Beaufort seas as well as the Canada and Makarov basins are labeled for spatial reference.

Bulk snow samples at each of the six stations were collected for contamination prone elements using an acid-cleaned high density polyethylene (HDPE) shovel and were placed into an acid-washed low density polyethylene (LDPE) bag. On board the ship, snow samples were melted, homogenized, and subsequently filtered through a 0.2  $\mu\text{m}$  filter (Supor) and subsampled into 250 mL (for dissolved concentrations) and 500 mL (for ultrafiltration) LDPE bottles (Nalgene) that had been previously acid cleaned (Fitzsimmons and Boyle, 2012). Likewise, bulk sea ice was collected at each station using a trace metal clean ice corer and homogenized from four separate cores at each locations. Once melted, the resulting water was filtered through a 0.2 $\mu\text{m}$  filter (Supor) into a 25 L acid-washed carboy and subsampled into acid cleaned 250 mL and 500 mL LDPE bottles, as for the snow samples. Water collected at 1, 5, and 20 meters below the ice used a battery powered pump and Teflon-lined PVC tubing and was directly filtered (0.2  $\mu\text{m}$ , Supor) into a 25 L carboy and subsampled directly into previously acid cleaned LDPE bottles. Methods for melt pond sampling and subsampling are described in (Marsay et al., 2018b), and all melt pond data reported here are published in that study.

### **6.2.2. Ultrafiltration**

The subsamples from snow, sea ice, melt ponds, and seawater were ultrafiltered on board the ship within 3 hours of subsampling, in a trace metal clean environment under positive pressure via HEPA-filtered air. The full methods for the ultrafiltrations are described in (Jensen et al., 2020) and (Fitzsimmons and Boyle, 2014a). Briefly, the cross flow filtration (CFF) used a membrane with a 10 kDa pore size ( $\sim 0.003 \mu\text{m}$  for

globular proteins, (Erickson, 2009)) and a Masterflex pump with FEP tubing. The pump, filter, and tubing were all cleaned and conditioned following the methods of (Fitzsimmons and Boyle, 2014a) and calibrated and conditioned with 100-500 mL of sample seawater as volume allowed. Importantly, this method set the permeate and retentate flows to be equal at 12.5mL/min with an overall pump flow rate of 25 mL/min and does not return the retentate solution to the feed water, effectively rendering this CFF method as “single-pass” ultrafiltration, utilizing high back-pressure on the retentate flow to force permeate solution through the membrane. The permeate and retentate fractions were each collected into 60 mL LDPE (Nalgene) bottles following three 10% rinses of the bottles, caps, and threads. All samples were promptly acidified to pH<2 (0.012 M HCl, Optima, Fisher Scientific).

The dissolved (dMe) and permeate solutions were analyzed for their concentrations, and permeate concentration was taken as the soluble metal (sMe) concentration. Colloidal (cMe) concentrations of each metal were determined by subtracting the soluble (sMe) concentration from the overall dissolved concentration:  $[cMe] = [dMe] - [sMe]$ , where Me = Mn, Fe, Ni, Cu, Zn, or Cd. In the text, we often refer to %cMe to denote the contribution of colloids to the overall dissolved phase, which is calculated as:  $\%cMe = 1 - ([sMe]/[dMe])$ . The retentate solutions were also analyzed for their concentrations to assess total metal recovery through the CFF system. As soluble compounds are present in the retentate solution, and colloids are concentrated into this solution, we used the following equation to calculate recovery (Fitzsimmons and Boyle, 2014):

$$\%Recovery = \frac{[permeate] + \frac{([retentate] - [permeate])}{CF}}{[dissolved]} \quad (6.1)$$

where the CF = concentration factor is ~2 for all samples. Recoveries for all samples were assessed, and only samples where %Recovery > %sMe were used in this analysis, as otherwise poor ultrafiltration recovery could be confused with high colloidal loadings. Only Cu colloids were eliminated in the snow samples throughout, due to poor recovery, and all metal data from the snow sample at Station 39 were also eliminated due to low recovery, except Fe.

### 6.2.3. Analyses

Acidified samples sat for at minimum nine months at room temperature following acidification, allowing for optimal desorption of metals from bottle walls (Jensen et al. 2020). After this time, samples were initially pre-concentrated for dissolved and colloidal trace metals using a SeaFAST-pico system (ESI, Omaha, NE) at Texas A&M University following the isotope dilution ICP-MS methods of Lagerström et al. (2013) and Jensen et al. (2020). Exact spike concentrations and details of the matrix-matched standard curve used for Mn can be found in (Jensen et al., 2020). Briefly, a 10 mL aliquot of seawater was loaded into the SeaFAST system, buffered to pH ~6.3 with an ammonium acetate buffer (Optima, Fisher Scientific), and loaded onto a column containing Nobias-chelate PA1 resin. After equilibration with the resin, samples were back-eluted using 10% (v/v) nitric acid (Optima) into a 400 µL eluent (25x pre-concentration factor) for analysis. Eluents were subsequently analyzed in medium (Mn, Fe, Ni, Cu, Zn) and low (Cd) resolution on a Thermo Element XR high-resolution inductively-coupled plasma mass spectrometer (HR-ICP-MS) at the R. Ken Williams

Radiogenic laboratory at Texas A&M University. The accuracy, precision, and limits of detection for these elements are summarized in Table 6.1.

**Table 6.1** Values for SAFe D1 consensus materials for elements reported in this study (nmol/kg). Average blank and detection limit (3\*standard deviation of the blank) are reported below (pmol/kg).

CRM	Element (nmol/kg)						
	n	Fe	Zn	Cd	Ni	Cu	Mn
SAFe D1	12	0.668	7.441	1.024	2.159	8.747	0.392
1SD		0.058	0.223	0.026	0.128	0.194	0.026
Consensus (May 2013)		0.670	7.400	0.991	2.270	8.580	0.350
1SD		0.040	0.350	0.031	0.110	0.260	0.050
	Element (pmol/kg)						
	n	Fe	Zn	Cd	Ni	Cu	Mn
Detection limit (3*1SD)	6	43.2	61.6	0.5	14.8	16.4	0.20

### 6.3. Results

In order to assess whether colloids were more abundant in cryospheric freshwater sources (snow, melt ponds, and sea ice) than in the underlying seawater into which they melt, we first examined the colloid contributions and spatial variability within the surface seawater itself. We present colloidal loadings as both a contribution of colloids to the overall dissolved phase (“%colloids” or “%cMe”) and as a concentration ([colloids] or [cMe]) for each metal. It was immediately evident that %colloids were remarkably consistent across all six ice hole stations within the upper 20 m (1, 5, and 20 m depth seawater values averaged, Table 6.2), despite variable total dissolved metal concentrations. Colloidal contributions were low in seawater for Mn and Cd (%cMn = 0 ± 1% and %cCd = 1 ± 1%), while colloids were significant fractions of the dissolved phase for Fe, Cu, Zn, and Ni (%cFe = 38 ± 3%, %cCu = 28 ± 2%, %cZn = 22 ± 8%,

%cNi =  $13 \pm 2\%$ ). This compared well to the average of %cFe found in the surface waters of the open Western Arctic ( $40 \pm 15\%$ , Chapter 4). As a comparison, %cFe in the larger 0.02-0.20  $\mu\text{m}$  colloidal size fractions was higher (50-90% of the dissolved phase) in the North Atlantic (Fitzsimmons et al., 2015), due to dust inputs. While few published values exist for the colloids of the other elements, these values were very consistent with previously analyzed ultrafiltered samples from the California Current, the Western Antarctic Peninsula, and the Gulf of Mexico (Fitzsimmons and Jensen, unpublished) for %cNi, %cCu, %cCd, and %cMn, while %cFe and %cZn appear to vary more globally with space and depth; this global comparison is the subject of another paper. Overall, within the surface Arctic, the surface seawater trends were very well resolved (Table 6.2).

Overall, colloids were statistically a greater proportion of the dissolved metal pool of cryospheric samples (snow, melt pond, and sea ice) than underlying seawater for Fe, Zn, Cd, Ni, Cu, and Mn, as determined by a two-tailed *t*-test (Table 6.2,  $p < 0.05$ ). They were also, generally, much more variable and less precise than the %colloids found in the surface seawater. Across all three freshwater pools, %cMn =  $25 \pm 38\%$ , %cFe =  $69 \pm 18\%$ , %cNi =  $41 \pm 21\%$ , %cCu =  $23 \pm 30\%$ , %cZn =  $64 \pm 29\%$ , %cCd =  $44 \pm 40\%$ . Note that the standard deviations are often 50% or more of the mean values, indicative of the heterogeneity of our sample set. In prior studies of polar freshwater pools, with which we might compare our size-fractionated metal concentration results, analogous data are very limited. However, studies in Antarctic sea ice found %cFe and %cMn ranges of  $75 \pm 30\%$  and  $76 \pm 19\%$ , respectively (Lannuzel et al., 2014), which agrees well with our

%cFe value of  $67 \pm 14\%$  for Arctic sea ice but is significantly different from our Arctic sea ice %cMn value of  $12 \pm 20\%$  (Table 6.2). Overall, these Antarctic data reinforce our observation that colloidal contribution to the dissolved phase is larger and more variable in cryospheric freshwaters than typically found in seawater.

Colloidal metals are known to aggregate or transform across salinity gradients (Gunnars et al., 2002), and thus it is useful to assess whether there is a pattern in %cMe across the cryospheric pools at each sampling site to elucidate which of these may be significant transformations. For the purposes of this analysis, we have assumed that any colloidal aggregation would proceed from snow (a “young” atmospheric source), to melt ponds and sea ice, and finally to the underlying seawater. In ordering the %colloids for each element in this way we noticed that Fe, Zn, Ni and sometimes Cd and Mn all had their %colloids decrease moving snow to melt pond to sea ice to seawater (see Figure 6.3, Station 33 as example). This was particularly evident at Stations 31, 33, and 46.

**Table 6.2** Summary of %colloids within each pool (snow, melt pond, sea ice, and underlying seawater from 0-20m) and the number of measurements incorporated from each pool (*n*). Percentage values are reported as mean ± 1SD. Average cryosphere values represent a combined average of snow, melt pond and sea ice and associated ± 1SD. \*%colloids is significantly greater than the underlying seawater, using a 2-tailed t-test (*p* < 0.05).

<b>Pool</b>	<b><i>n</i></b>	<b>Fe</b>	<b>Zn</b>	<b>Cd</b>	<b>Ni</b>	<b>Cu</b>	<b>Mn</b>
<b>Snow</b>	<b>6</b>	74 ± 20%	70 ± 37%	79 ± 47%	48 ± 30%	-	56 ± 52%
<b>Melt pond</b>	<b>5</b>	67 ± 24%	90 ± 25%	25 ± 18%	34 ± 17%	41 ± 13%	4 ± 3%
<b>Sea ice</b>	<b>6</b>	67 ± 14%	50 ± 26%	37 ± 39%	40 ± 16%	20 ± 15%	12 ± 20%
<b>Average cryospheric freshwaters</b>	<b>17</b>	<b>69 ± 18% *</b>	<b>64 ± 28% *</b>	<b>44 ± 40% *</b>	<b>41 ± 21% *</b>	<b>30 ± 17%</b>	<b>25 ± 38% *</b>
<b>Seawater</b>	<b>18</b>	38 ± 3%	26 ± 13%	1 ± 1%	13 ± 2%	28 ± 2%	0 ± 1%

Stations 31 (Figure 6.4) and 33 (Figure 6.3) nearest the North Pole had high concentrations dissolved and colloidal Fe and Zn concentrations in snow ( $>7$  nmol/kg for cFe and  $>20.71$  nmol/kg for cZn at both stations), leading to large colloidal contributions of 91 and 97% for %cFe and 97 and 96% for %cZn at Stations 31 and 33, respectively. However, at these same stations, the colloidal concentrations and %colloids were much lower in surface seawater, even in the top 1 m, for both Fe (43% and 37% colloidal, respectively) and Zn (0% and 36% colloidal). Together, these increased aerosol fluxes to the snow create a clear decreasing trend of %cFe and %cZn, as well as a decrease in [cFe] and [cZn], moving from the snow, to the sea ice and melt ponds, to surface seawater (Figure 6.3; Figure 6.4). Station 46 (Figure 6.5) also shared this pattern of decreasing %colloids for Fe and Zn from snow to seawater, but it had much lower [cFe] and [cZn] in snow (1.04 and 7.67 nmol/kg, respectively) and seawater (0.04 and 0.16 nmol/kg, respectively), although the %cFe and %cZn were still high (87% and 94%, respectively).

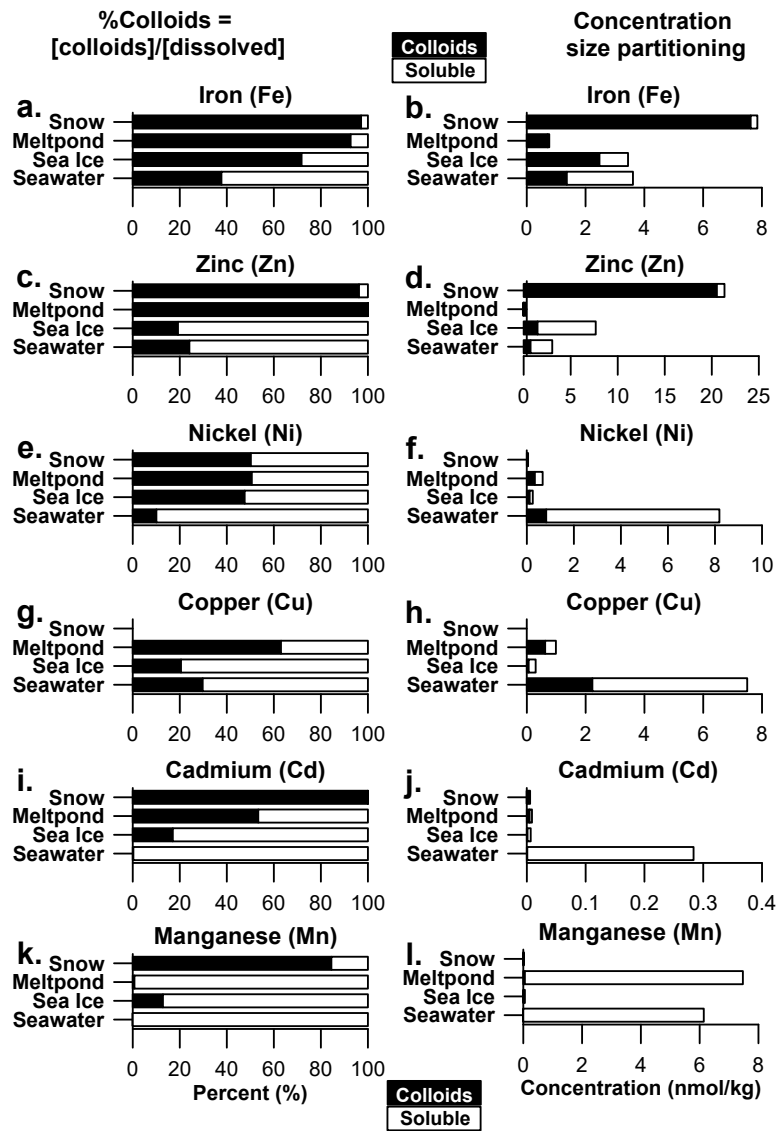


**Figure 6.3** Station 33 %Colloidal = [colloid]/[dissolved] for each metal (left) and the size partitioned concentrations (right) across each cryospheric pool. Colloids are represented by black bars and the soluble phase by white bars. This station was chosen as an example to illustrate an “aerosol-dominated” station where snow inputs of lithogenic metals were high, which was also true at Station 31. Note that Copper has no data for the snow pool.

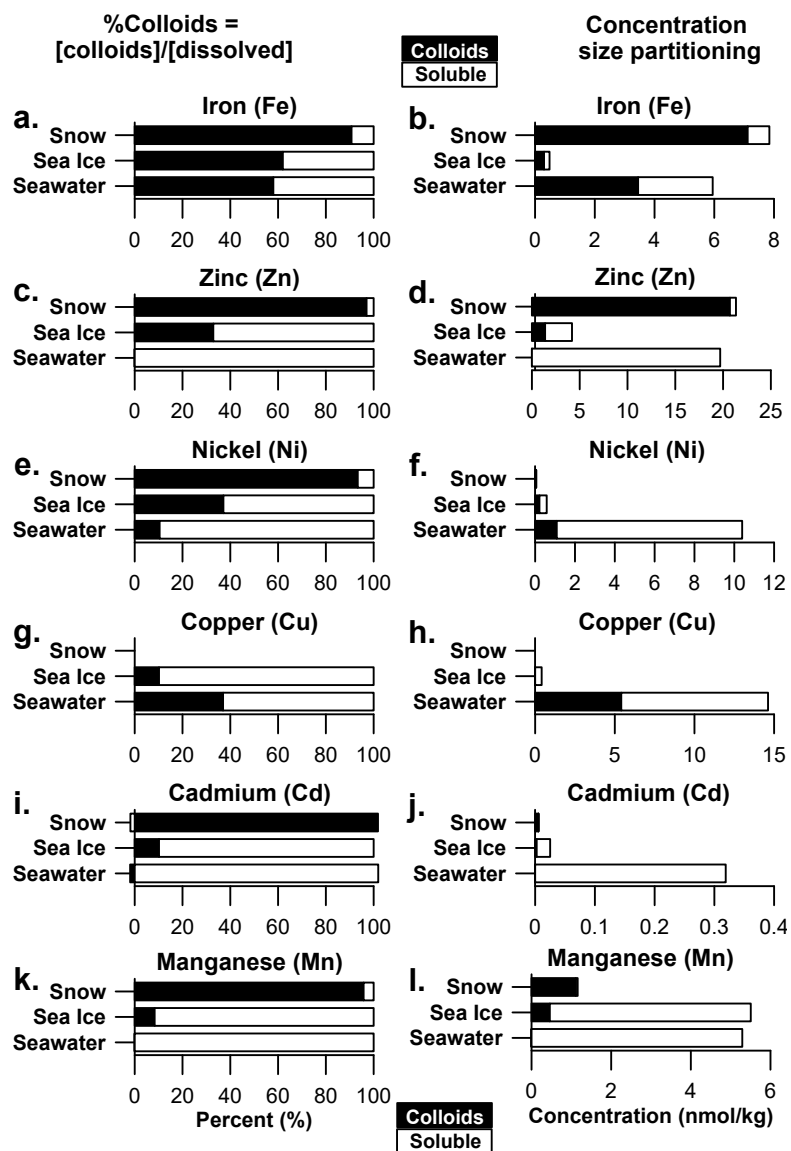


**Figure 6.4** Station 31 %Colloidal = [colloid]/[dissolved] for each metal (left) and the size partitioned concentrations (right) across each cryospheric pool. Colloids are represented by black bars and the soluble phase by white bars. This station was chosen as an example to illustrate an “aerosol-dominated” station where snow inputs of lithogenic metals were high, which was also true at Station 31. Note that Copper has no data for the snow pool. Also, no melt pond samples were collected at this station.

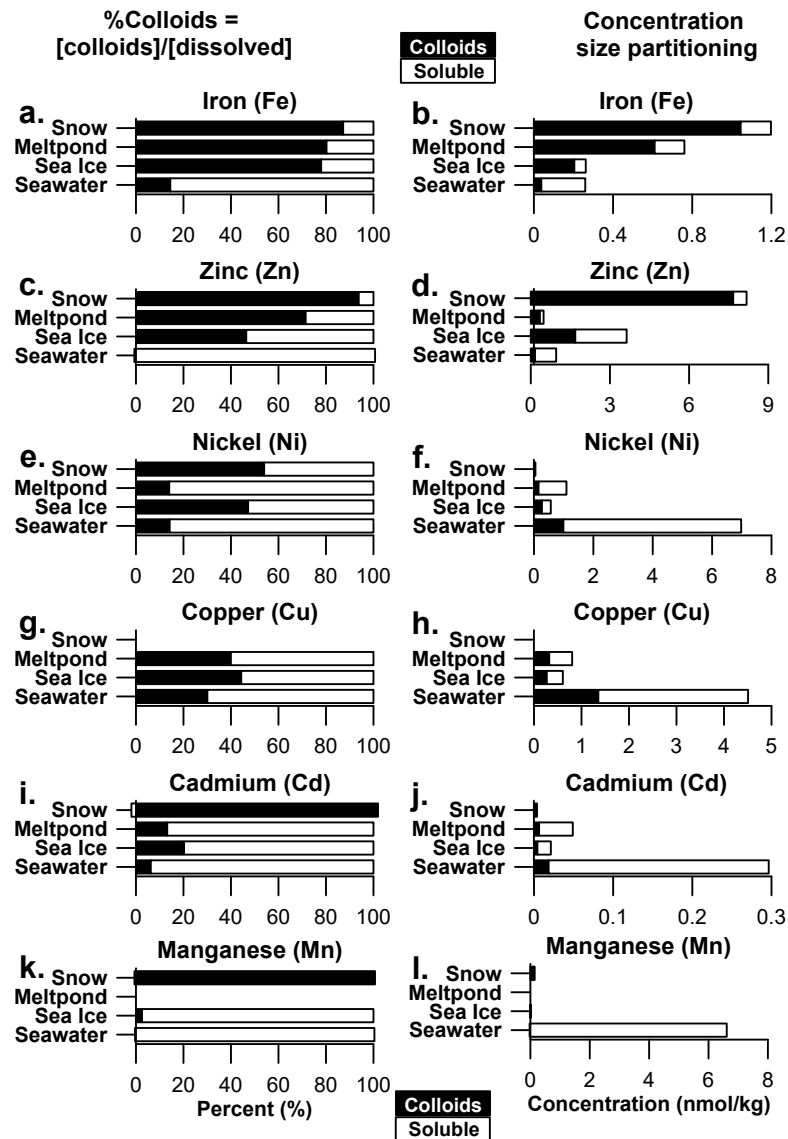


**Figure 6.5** Station 46 %Colloidal = [colloid]/[dissolved] for each metal (left) and the size partitioned concentrations (right) across each cryospheric pool. Colloids are represented by black bars and the soluble phase by white bars. This station was chosen as an example to illustrate an “aerosol-dominated” station where snow inputs of lithogenic metals were high, which was also true at Station 31. Note that Copper has no data for the snow pool.

At these same stations, the other metals studied – Ni, Cu, Mn, and Cd – shared some general decrease in %colloids, although [colloids] overall very low in the

cryospheric freshwaters compared to the underlying seawater (Figure 6.3, 6.4, 6.5). For instance, at Station 31 in the snow %cNi was 93%, %cMn was 96%, and %cCd was 100%. These values decreased to 10%, 0% and 0%, respectively, in the underlying seawater. While this greater %colloids in the freshwater sources could thus act as a source of colloidal metals upon melting, the trend in colloidal concentrations told a different story, as for example cNi at Station 31 increased from 0.05 nmol/kg in the snow to 1.08 nmol/kg in the underlying seawater (Figure 6.4). While [cMn] and [cCd] did have higher concentrations in snow than seawater, their overall dissolved concentrations actually increased towards the seawater below, driven by an increase in smaller soluble-sized species (Figure 6.3, 6.4, 6.5), actually far exceeding the cryospheric concentrations such that melting of these cryospheric freshwaters would not significantly increase the seawater inventories. Copper appeared to show very little variation in %colloidal space (mostly 20-40% colloids across all sample types), although this may be due in part to the lack of Cu size partitioning data for snow in this study.

The other three stations we sampled – Station 39, 42, and 43 – appeared to have more “seawater-like” cryospheric freshwater pools, as supported by a higher salinity in melt ponds, suggesting that more seawater had mixed into the melt pond (Marsay et al., 2018b). This was also reflected in the %colloids and [colloids] across all three freshwater pools (Figures 6.6, 6.7, 6.8), which matched the underlying seawater much more than at the “aerosol-dominated” stations, especially for Fe and Zn. Rather than a decrease in Fe or Zn %colloids moving between each pool, snow %colloids were lower overall, close to underlying seawater %colloids, and the maximum %colloids was more

likely to be found in the melt pond (Stations 39, 42) or sea ice (Station 43) pools. This may also be explained by a lack of recent aerosol supply at these stations, as particulate metal concentrations were also lower in the cryospheric freshwater samples at this station (Kadko et al., 2018). For Fe, [colloids] actually appeared to increase moving snow to melt pond to sea ice to seawater across these three stations (Figures 6.6, 6.7, 6.8), while Zn was more variable, with no clear pattern (Figures 6.6, 6.7, 6.8). Likewise for the other elements, broad patterns were more obscure across the three stations although the underlying seawater continued to be majority soluble and higher in overall dissolved concentration for Ni, Cu, Mn, and Cd (Figure 6.6, 6.7, 6.8).

#### **6.4. Discussion**

We put forward two guiding questions: 1) Do cryospheric freshwater pools have high %colloids and if so, for which metals? and 2) Is aggregation and/or scavenging a pathway for a decrease in metals during the incubation of waters in freshwater pools before it is sourced to the underlying seawater? To answer these questions, we can begin by grouping the stations by processes that govern them as well as group elements where speciation trends were similar. We suggested in the Results section above that Stations 31 and 33 (Figures 3, 4) are most influenced by high/recent aerosol fluxes, while surface seawater at Stations 39, 42, and 43 is in the trajectory of the transpolar drift (TPD), and Station 46 (Figure 6.3) can be considered a “pure” station, absent these other special influences. As noted in the Results section and Figures 3, 4, and 5, metal pairings of Fe and Zn, Ni and Cu, and Mn and Cd appear to share similar trends in both %colloidal and [colloid] characteristics.

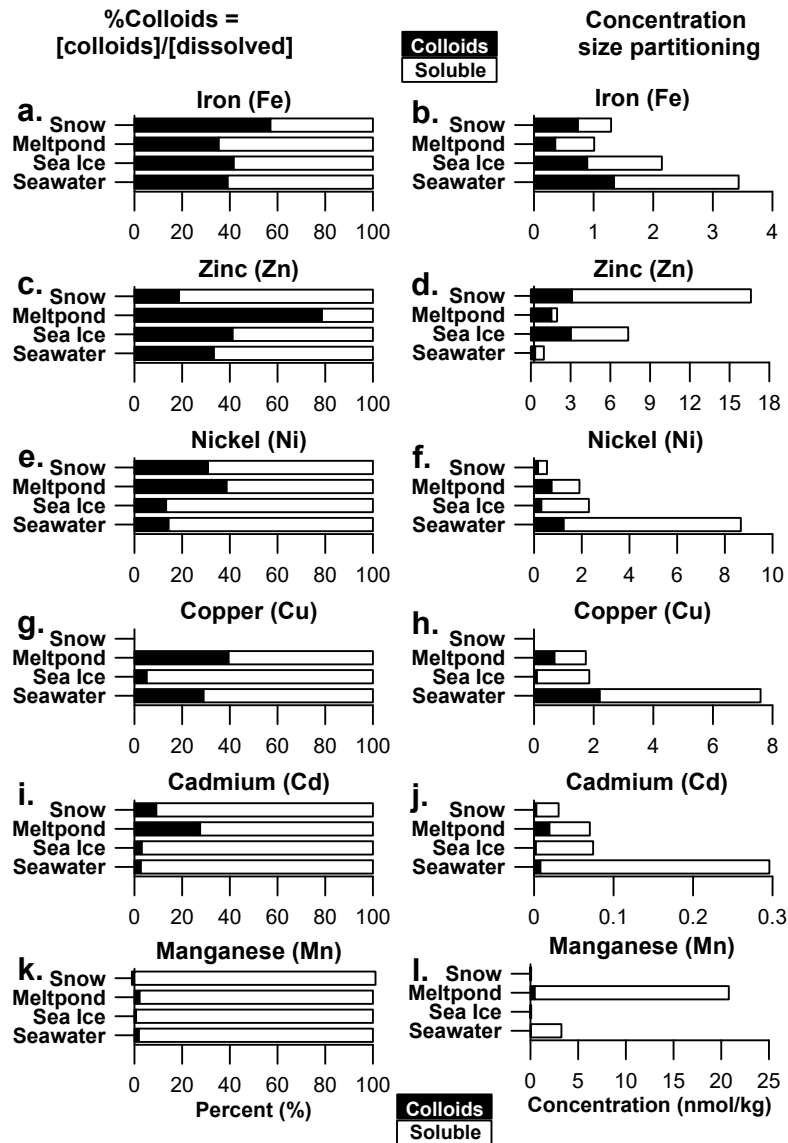


**Figure 6.6** Station 42 %Colloidal = [colloid]/[dissolved] for each metal (left) and the size partitioned concentrations (right) across each cryospheric pool. Colloids are represented by black bars and the soluble phase by white bars. This station was chosen as an example to illustrate an “TPD-dominated” station where snow inputs of lithogenic metals were high, which was also true at Stations 39 and 43. Note that Copper has no data for the snow pool.

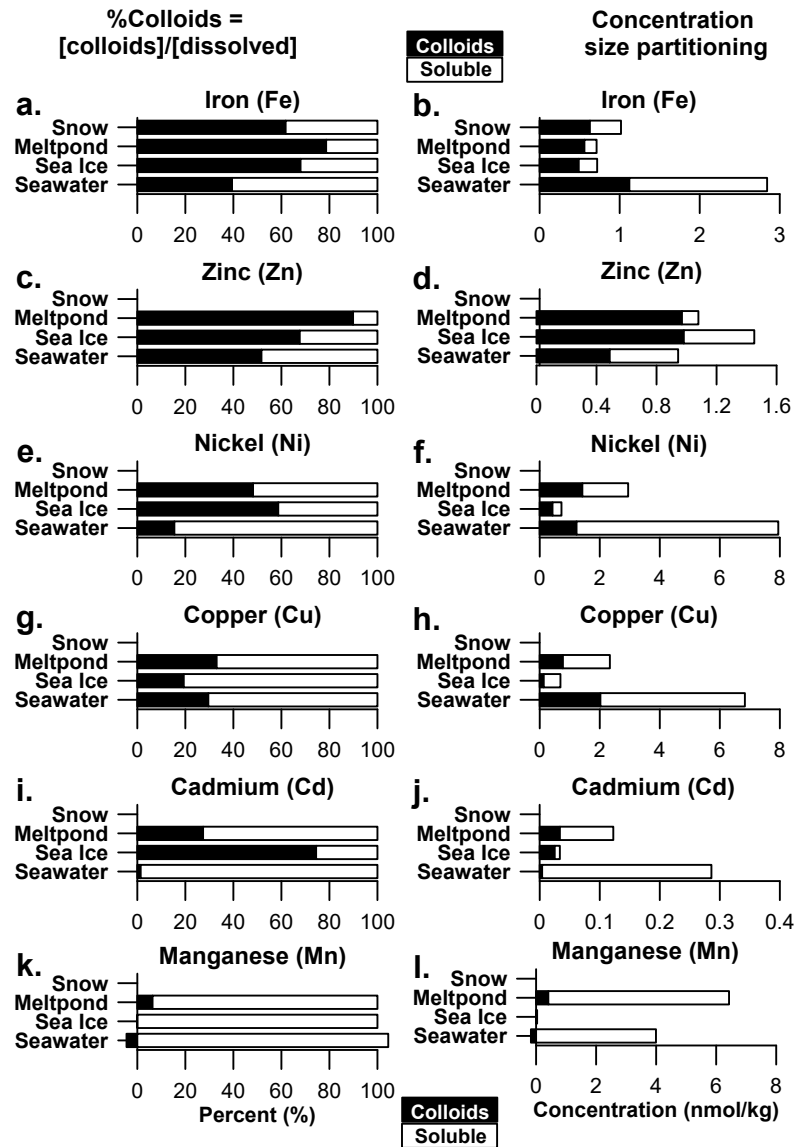


**Figure 6.7** Station 39 %Colloidal = [colloid]/[dissolved] for each metal (left) and the size partitioned concentrations (right) across each cryospheric pool. Colloids are represented by black bars and the soluble phase by white bars. This station was chosen as an example to illustrate an “TPD-dominated” station where snow inputs of lithogenic metals were high, which was also true at Stations 42 and 43. Note there is no snow data for all elements except Fe at this station.

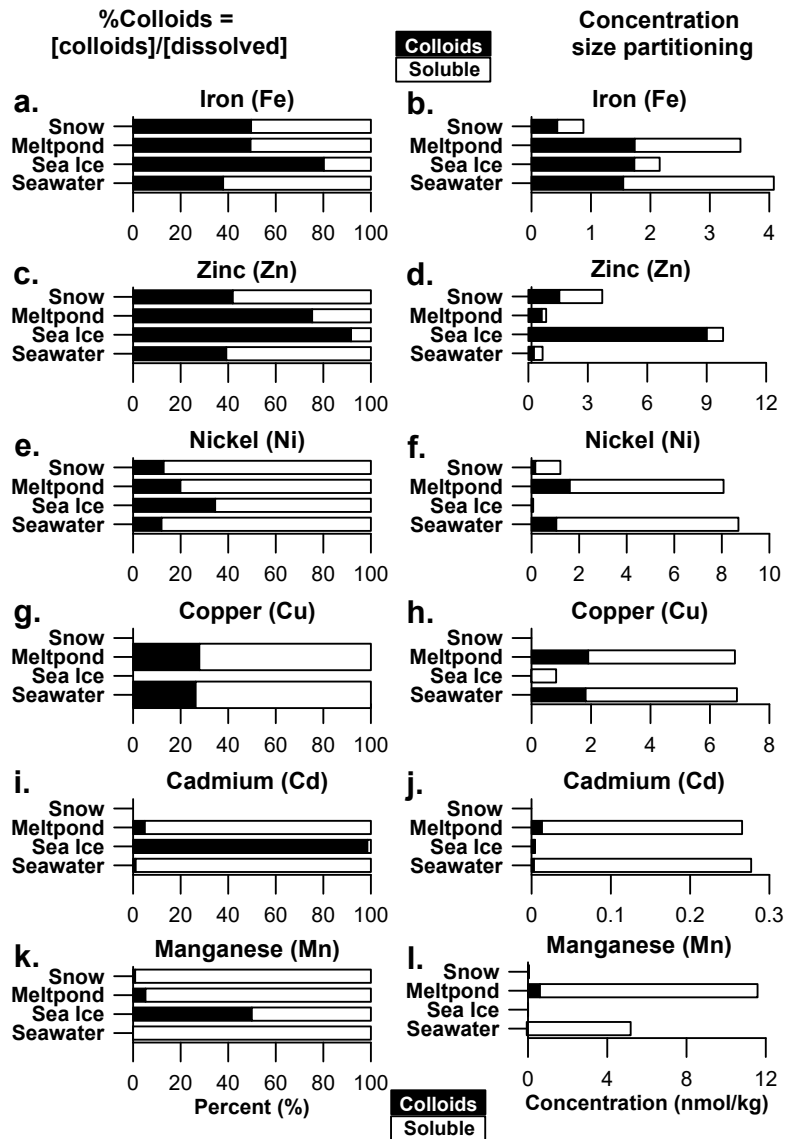


**Figure 6.8** Station 43 %Colloidal = [colloid]/[dissolved] for each metal (left) and the size partitioned concentrations (right) across each cryospheric pool. Colloids are represented by black bars and the soluble phase by white bars. This station was chosen as an example to illustrate an “TPD-dominated” station where snow inputs of lithogenic metals were high, which was also true at Stations 39 and 42. Note that Copper has no data for the snow pool.

#### **6.4.1. Question 1: Do cryospheric freshwater pools have higher %colloids than seawater?**

Freshwater pools appear to have a higher and more variable %colloids across the three cryospheric entities – snow, sea ice, and melt ponds – compared to surface seawater (Table 6.2). Melt ponds are a good metric of mixing between cryospheric freshwaters and seawater (see Section 6.2.2 below), but as such have variable salinity (Marsay et al., 2018b) and are not necessarily good metrics for average freshwater in the cryosphere. Thus, we examine here the %colloids in snow and sea ice in comparison to the underlying seawater at each station for each element.

Only Fe, Ni, and Cd have statistically significantly higher ( $p < 0.05$ ) %colloids in snow and sea ice compared to seawater across all six stations. For snow and sea ice together, this translated to %cFe of  $69 \pm 16\%$ , a %cNi of  $35 \pm 19\%$ , and a %cCd of  $40 \pm 44\%$ , which were close to the overall averages across all three cryospheric pools (listed in Table 6.2). Zinc and Mn also had statistically significantly higher %colloids than seawater when melt ponds were considered (Table 6.2), but without them they were not statistically distinguishable from surface seawater %colloids ( $p = 0.05$  for Zn and  $p = 0.06$  for Mn). Colloidal Cu contributions, in contrast, were fairly similar between sea ice, melt ponds, and seawater (Table 6.2). This was somewhat surprising, as we understand Cu colloids, particularly within freshwater environments such as estuaries, to be higher than in seawater and removed during flocculation (Sholkovitz, 1978; Dai and Martin, 1995; Gunnars et al., 2002). It has also been suggested that Cu complexation by organic ligands may also impart a proclivity to be in the colloidal phase (Dammshäuser and

Croot, 2012). The template for this hypothesis was Fe, which is known to be >99% organically complexed, especially in surface waters (Rue and Bruland, 1995; Gledhill and Buck, 2012) and is also often found in the colloidal phase. We then might expect Cu to follow a similar trend, as it is likewise significantly organically complexed (Moffett and Dupont, 2007; Vraspir and Butler, 2009). Instead, the low and consistent %cCu here and in other similar studies (Roshan and Wu, 2018; Jensen et al., 2020) is suggestive of some equilibrium partitioning of Cu between soluble and colloidal phases, which would have to be facilitated by ligand exchange if our assumption of >99% ligand complexation of dissolved Cu for seawater is also true for cryospheric freshwaters.

In that same vein, we find that metals like Cd and Mn do not typically have any colloids across multiple different environments, assessed using similar methods (Jensen et al., 2020). Thus, it was surprising to find %colloids above even 5% for both cCd and cMn in snow, melt ponds, and sea ice. As described in (Lannuzel et al., 2014) this is not without precedent for cMn in sea ice, which the authors attributed to the aggregation and decrease in colloids as salinity increased, which is also observed in estuaries for Fe, Zn, Mn, Cu, Ni in particular (Sholkovitz, 1978; Dai and Martin, 1995; Hölemann et al., 2005). This could indicate either removal to the particulate phase during flocculation/aggregation (as one would expect in an estuarine environment) or disaggregation back to the soluble phase. In the case of disaggregation, we would expect that the (colloids) trend would follow the %colloids. In this study, we observed that for elements such as Cd and Mn, while freshwater %colloids were high, the underlying seawater was 95-100% soluble and in much higher concentrations, and so [cMn] and

[cCd] were relatively unchanged between pools (Figures 3 and 4). Any potential change to the concentration of Cd and Mn colloids in freshwater due to aggregation is not likely to affect the underlying seawater.

The question still remains, why are %colloids so high for many metals, even Cd and Mn, in the snow at Stations 31, 33, and 46? Particulate data suggests high Fe and Al particle concentrations at these stations (Kadko et al., 2018), indicative of increased dust inputs, and air mass back trajectories support a European aerosol origin that may also contain higher levels of contaminants such as Zn (Marsay et al., 2018a). Previous studies in the North Atlantic observed high %cFe associated with high dust fluxes into the surface ocean (Bergquist et al., 2007; Fitzsimmons and Boyle, 2014b; Fitzsimmons et al., 2015; Kunde et al., 2019). While this surface peak in cFe is absent in the Arctic Ocean, where dust inputs are lower than the North Atlantic (Table 6.2, Chapter 4), snow that is influenced by significant aerosol inputs appears to carry this higher colloidal load for Fe, Zn, Cd and Mn, and this snow may not have melted into the surface seawater that we observe at these stations. Thus, the large %colloids we see across all elements in snow may be the result of disaggregated inorganic (amorphous/crystalline) aerosols that have not solubilized with any organic ligands that might be present in the snow; this would be especially true for Stations 31 and 33 that had received recent, direct aerosol inputs, based on the particulate data (Kadko et al., 2018). Likewise, reversible scavenging of equilibrated particles may augment the dissolved phase in the form of colloids (Fitzsimmons et al., 2017).

However, relatively “pure” Station 46 snow did not have high particle loads that might indicate recent aerosol inputs but still had high %colloids, and also at this station %colloids in snow were much higher for all metals than they were in the other freshwater and seawater pools. One possible explanation is a high organic loading. Arctic snow has been found to be rich in organics that have primarily terrestrial and anthropogenic sources (Grannas et al., 2007) as a result of wet and dry deposition (Sempere and Kawamura, 1994; Lei and Wania, 2004; Roth et al., 2004). Additionally, labile DOM with terrestrial origin has been found in Antarctic snow (Antony et al., 2014). This could serve to promote metal aggregation from the soluble to the colloidal phase (Wilkinson et al., 1997; Wells, 2002) or provide ligands in the colloidal phase to stabilize metal colloids, as well as influence photochemical reactions occurring in the snow phase (Grannas et al., 2007). Alternatively, the high %colloids for metals such as Mn in snow and even sea ice (this study and (Lannuzel et al., 2014)), which historically does not have a large colloidal phase in seawater, may also be an artifact of the freezing and thawing process during sample deposition and collection, as this has been shown to increase %colloids in laboratory experiments for metals such as Zn and Cd (Jensen et al., 2020); unfortunately, we cannot currently sample snow’s metal speciation *in situ* without this thawing treatment.

**6.4.2. Question 2: Could aggregation and/or colloidal scavenging be a pathway for metal loss during the incubation of waters in cryospheric freshwater reservoirs before it is sourced to seawater?**

To examine the second question, we first examined the size partitioning trends station-by-station moving from snow, to melt pond and sea ice, and finally to surface seawater in order to assess the potential for colloid fluxes and aggregation. Throughout the sections above, we have framed the change in colloids as a change in %colloids, which remains a useful metric in parsing reactivity and availability. However, aggregation during incubation in cryospheric freshwaters can only occur if there is likewise a decrease in [colloids] across these pools, since an ingrowth of [soluble] can also create a decreasing %colloidal trend. Thus, we also examine here changes in total metal concentrations from snow, to sea ice and melt pond, to seawater. Colloidal transformations across these freshwater reservoirs are only significant if they have sufficient concentration to influence the partitioning in the underlying seawater.

Aerosol-influenced Stations 31 and 33 again provide the clearest template for decrease in %colloids for Fe, Ni, Cu, Zn, Mn, and Cd from snow to seawater, but this is not necessarily reflected as a decrease in [colloids]. At Stations 31 and 33, there is a clear decrease in [colloids] for Fe, Zn, Cd, and Mn (Figure 6.4). Since these pools are physically distinct at these locations (no evidence of mixing within melt ponds, for example), these patterns would suggest that future mixing/melting of these cryospheric freshwaters into the melt ponds and/or seawater would provide a source of these colloids, which may then be subject to aggregative losses.. In contrast,, [colloids]

actually increased from snow, to sea ice, to seawater for Ni, Cu, at Stations 31 and 33, indicating a separate colloidal source to this seawater (such as rivers, shelf sediments, mixing from other ocean basins, etc.). This would suggest that, upon melting, cryospheric freshwaters would not add to the metal inventories and speciation of underlying seawater for Ni, Cu, Cd, and Mn but instead would dilute it.

At Stations “TPD-influenced” 39, 42, and 43 (Figures 6.6, 6.7, 6.8), there was no decreasing trend of %colloid nor [colloid] across any elements. For Fe and Zn, the concentration of colloids remained consistent and “seawater-like” across the cryosphere (illustrated at Station 42, Figure 6.6). Importantly, elements such as Ni and Cu, but also Cd and Mn, all share large concentrations of both colloids and soluble species in the underlying seawater at Stations 39, 42, and 43. As referenced above, these stations are known to be heavily affected in the upper 50 m by the Transpolar Drift (TPD) current that bisects the Arctic Ocean and stays primarily north of 84°N (Charette et al., 2020). The TPD carries seawater heavily influenced by Eurasian rivers (up to 20% meteoric water) and thus rapidly transports river-sourced elements like Fe, Ni, Cu, and Cd across the Arctic to reach these otherwise extremely remote sites (Charette et al., 2020). This is reflected in relatively higher total concentrations for Fe, Ni, Cu, and Cd in particular in the underlying seawater at these stations (Figure 6.6, 6.7, 6.8), despite that the size partitioning of TPD and non-TPD surface seawater is quite constant (Table 6.2). Thus, cryospheric freshwater pools would not likely supply much colloidal metal flux to these already-high seawater colloid concentrations, and thus aggregation across the cryospheric freshwaters at these stations would not be relevant.

Finally, relatively “pure” Station 46 (Figure 6.5) shows a distinct decrease in %colloids for Fe, Zn, Ni, Cd, and possibly Mn moving snow to seawater (Figure 6.5). However, only Fe and Zn show a decrease in [colloids], similar to “aerosol-influenced” Stations 31, 33. Nickel, Cu, and Cd all have a gain in [colloids], similar to the “TPD-influenced” Stations 39, 42, and 43 moving from freshwaters to seawater. This suggests that absent these unique TPD or aerosol influences, only Fe and Zn colloids at Station 46 are perhaps being aggregated and removed via scavenging, moving from the cryosphere to seawater. Elements such as Ni, Cu, Cd and Mn, in turn, do not have cryospheric freshwater concentrations high enough to affect the underlying seawater, whose dissolved concentrations are much higher because they are dominated by soluble-sized species at these stations.

Importantly, in these above analyses of trends in size partitioning across reservoirs, it is impossible to determine the exact extent to which the snow, sea ice, and surface seawater have mixed at any given station, which makes it difficult to attribute any of the trends discussed so far to “aggregation” or “disaggregation” specifically. Melt ponds, however, are a unique pool where snow, sea ice, and seawater actively mix together and incubate over various timescales, all the while influenced by scavenging onto particles and both phytoplankton and microbial processes (Marsay et al., 2018b). Using oxygen isotopes in water and salinity measurements, an assignment of the volume partitioning of sea ice, snow, and seawater into each melt pond in this study was calculated previously (Marsay et al., 2018b). Thus, here we use those tracer-derived source partitioning estimates in a mass balance approach with our size partitioning data

for each “cryospheric end member” to investigate potential speciation transformations occurring within melt ponds, and we attempt to attribute those to particulate supply fluxes/features.

We first used measured salinity in the melt ponds as a marker of mixing between the different water reservoirs. For instance, the melt pond at Station 33 had the lowest salinity (1.40) and highest percent contribution to volume from snow (94%) (Marsay et al., 2018b) and high %colloids for Fe, Ni, Zn, and Cd. In contrast, Station 43 had the highest salinity (25.76) and high contribution from seawater (79%) and accordingly presented with more “seawater-like” distribution of %colloids and [colloids] (Figure 6.8). Together, the results from snow and melt ponds suggest that incubation time in a melt pond may result in decreases in colloids over time and that mixing between seawater and cryospheric pools may play a controlling role for some metal colloids.

We can probe this hypothesis further by modeling the melt pond [colloid] and [soluble] based on the fractional contribution from each freshwater pool as described in Marsay et al. (2018b) (Figure 6.9):

$$f_{\text{SW}} * [\text{colloid}]_{\text{SW}} + f_{\text{SNOW}} * [\text{colloid}]_{\text{SNOW}} + f_{\text{ICE}} * [\text{colloid}]_{\text{ICE}} = [\text{colloid}]_{\text{MP,model}} \quad (6.2)$$

where  $f_{\text{SW}}$  is the fractional volume of melt pond (MP) water from seawater (SW),  $f_{\text{SNOW}}$  is the fractional volume of MP water from snow,  $f_{\text{ICE}}$  is the fractional volume of MP water from sea ice. When added together these should equal the colloidal concentration in the meltpond ( $[\text{colloid}]_{\text{MP,model}}$ ) and can be compared to the measured meltpond concentrations ( $[\text{colloid}]_{\text{MP,meas}}$ ). The same equation can be written for the soluble metal concentrations as well. Then, if measured melt pond colloids ( $[\text{colloids}]_{\text{MP,meas}}$ ) are lower

than expected based on the [colloids] supplied by each pool ( $[\text{colloids}]_{\text{MP,model}}$ ), then aggregation, biological uptake, or scavenging of colloids to the particulate phase or colloidal disaggregation to the soluble phase may have occurred; an analogous comparison of the measured and modeled [soluble] mass balance would help distinguish colloidal disaggregation from colloidal scavenging losses. In contrast, if the  $[\text{colloids}]_{\text{MP,model}} < [\text{colloids}]_{\text{MP,meas}}$ , this could indicate that colloids are generated within the melt pond from particle disaggregation or soluble aggregation. We assume here that the metal concentrations measured in each cryospheric freshwater pool at each site are representative of the waters that melted to form the melt pond; thus, we cannot ignore the fact that any disagreements between the measured and modeled concentrations may reflect that our measured end member concentrations are not fair representations of the melted material in any particular melt pond, for reasons of either spatial or temporal variability.

From this analysis, we see that  $[\text{cFe,cZn}]_{\text{MP,model}} \gg [\text{cFe,cZn}]_{\text{MP,meas}}$  at all stations except Station 43 (both) and Station 46 (cZn aggregation only). This is accompanied by  $[\text{sFe, sZn}]_{\text{MP,model}} \gg [\text{sFe, sZn}]_{\text{MP,meas}}$  at those same stations, which suggests strong biological uptake or scavenging from both soluble and colloidal phases to the particulate phase. Given that Station 33 had such strong aerosol inputs from snow, this “missing” dissolved Fe and Zn could have arisen from aggregation of aerosol-laden Fe and Zn. The melt pond particle data reported in Marsay et al. (2018) indicate that Station 33 stood out as having the highest particulate Mn/P and Fe/P ratios, after lithogenic corrections, suggesting the presence of Mn and Fe oxides at these sites.

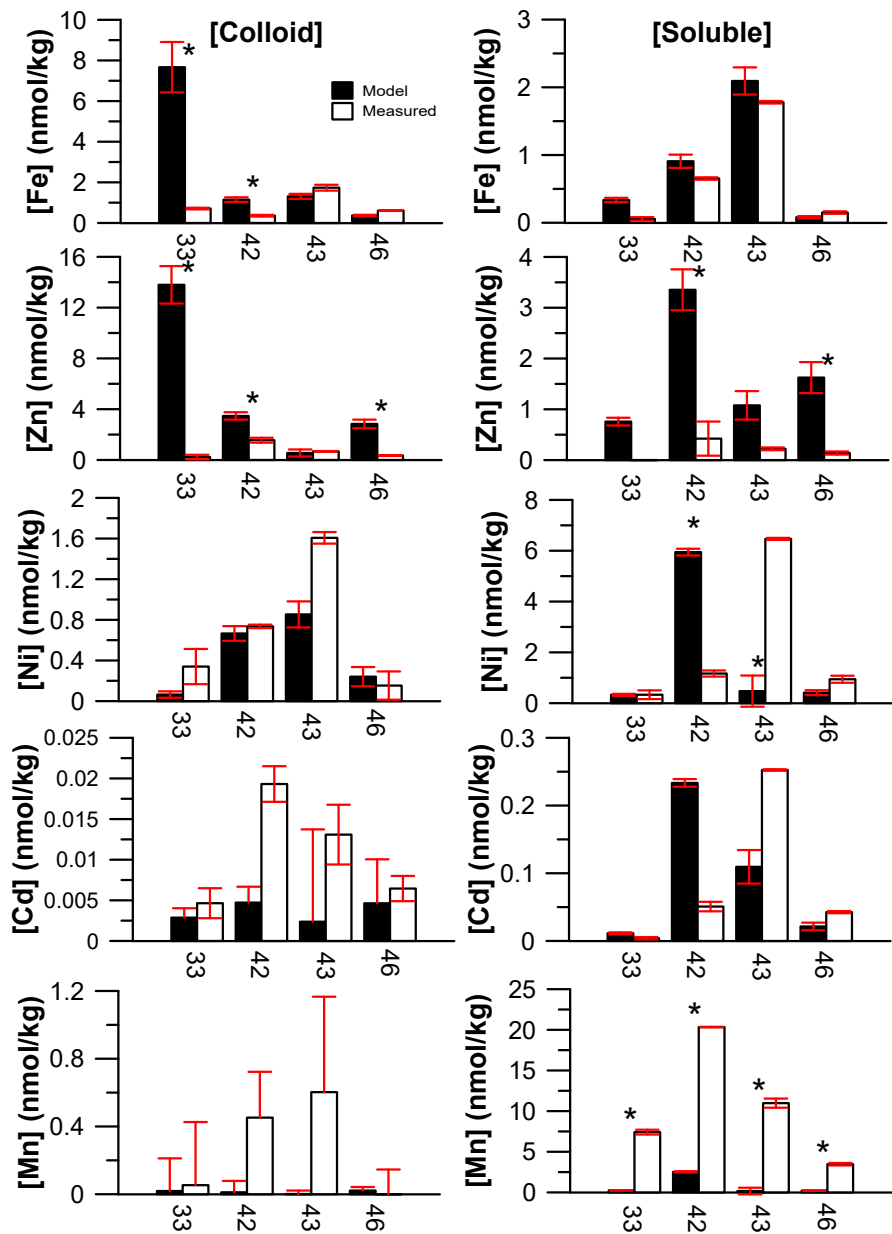


**Figure 6.9** Results of [colloid] and [soluble] concentrations in modeled (black) and measured (white) meltponds for Stations 33, 42, 43, and 46. Meltpond 39 is excluded due to poor snow recovery and Cu is omitted throughout for the same reason. Propagated error is shown as red bars in both directions unless doing so will cause the graph to plot negative error values (Cd and Mn colloids). Error was assessed based on duplicate samples, long-term variability, and a baseline 10% error in fractions calculated by Marsay et al. [2018b]. \*indicates modeled and measured values are significantly different by 2-tailed z-test ( $p < 0.05$ ).

However, Station 42 also recorded “missing” dissolved Fe and Zn, which must be attributed to either aggregation into particles or biological uptake but had more normal particulate Fe/P and Mn/P ratios, perhaps representative of cellular material. Without POC or chlorophyll a concentrations at these melt ponds, we cannot distinguish abiotic scavenging from biological uptake mechanisms for the different stations. It is important to note that Station 42 also saw the only aggregation of soluble Cd and Ni of any station, perhaps pointing to stronger biological uptake at that particular station.

With the soluble/colloidal metal partitioning data, one question that we hoped to answer was whether we could record aggregation or disaggregation between soluble and colloidal compounds specifically. At TPD-influenced Station 43, there was  $\sim 0.3$  nmol/kg of “missing”  $[sFe]_{MP,meas}$  compared to the  $[sFe]_{model}$ , which was about equal to the  $\sim 0.4$  nmol/kg “extra”  $[cFe]_{MP,meas}$  compared to the  $[cFe]_{MP,model}$ . Without any knowledge of changes to the particulate pool, this would suggest sFe aggregation into cFe during incubation in the melt pond of this site.

The largest discrepancy in  $[colloids, soluble]_{MP, model}$  and  $[colloids, soluble]_{MP, meas}$  in melt ponds, particularly for Fe and Zn, was at Station 33 where snow samples were collected after recently fallen snow between 80 and 90°N (Marsay et al., 2018a). Not only do Stations 31 and 33 have high aerosol deposition rates via snow based on tracers of atmospheric flux, such as  $^7Be$  (Kadko et al., 2018), they were also collected the most recently after snow fall (12 and 15 days, respectively, (Marsay et al., 2018a)). Both %colloids and  $[colloids]$  happened to be the highest at these stations for metals such as Fe, Ni, Zn, Cd, and Mn, perhaps suggesting that colloids may be more abundant

in recently fallen snow. Particulate Fe and Zn in melt ponds both had high contribution from the crustal phase at Station 33 (Marsay et al., 2018b), which perhaps served to scavenge or aggregate these elements more efficiently at this station. Additionally, photochemical reduction could serve to solubilize colloidal Fe and Mn after deposition (Sunda et al., 1983; Sunda and Huntsman, 1994; Kuma et al., 1996), as suggested above. Concentrations and %colloids continue to decrease steadily in snow for elements like Fe, Ni, and Zn although there is a peak in %colloids again at Station 46 despite 27 days elapsing since last snow fall (Marsay et al., 2018a), perhaps due to low overall concentrations across the board.

In contrast to Fe and Zn, Mn almost always had  $[cMn]_{MP,model} < [cMn]_{MP,meas}$  and  $[sMn]_{MP,model} < [sMn]_{MP,meas}$ , indicating that measured melt pond Mn concentrations were unexpectedly higher than their source freshwater concentrations suggest that they should be, in both the soluble and colloidal size fractions. Manganese is the only element for which this pattern persisted across nearly all stations. This “extra Mn” was much more abundant in the soluble size fraction (>5 nmol/kg more measured than expected based on end members) than in the colloidal size fraction, in line with minimal observed colloidal Mn in the samples of this study. Greater measured Mn concentrations than the modeled produces could only occur if Mn particles were disaggregating into these smaller (soluble) phases. This is plausible as photoreduction is known to solubilize particulate Mn oxides in surface waters such as melt ponds on the timescale of hours and would explain the higher measured concentrations of soluble Mn in melt ponds of all

stations, relative to what we would expect from mixing (Figure 6.9; Sunda et al., 1983; Marsay et al., 2018b).

Nickel and Cd both had  $[\text{colloids}]_{\text{MP,model}}$  within error of  $[\text{colloids}]_{\text{MP, meas}}$  at each station, except at Station 52 (Cd only) and Station 43 (Ni only), suggesting that mixing may largely explain the colloidal concentrations for these elements in meltponds (Figure 6.9) and that no additional colloidal aggregation/disaggregation processes were at play in the melt ponds. This aligns well with results from the dissolved phase that showed a correlation between salinity and dNi and dCd, indicative of mixing as a dominant control (Marsay et al., 2018b). The soluble comparison, while more statistically distinct, points to ingrowth of the soluble phase at Stations 43 and 46. This is in opposition to elements such as Fe and Zn that largely show aggregation or scavenging of both phases across all meltponds. As noted above, the unique trend at Station 42 of  $[\text{sNi}, \text{sCd}]_{\text{MP, model}} \gg [\text{sNi}, \text{sCd}]_{\text{MP, meas}}$  is likely due to biological uptake of sNi and sCd at this station.

It is difficult from these observations to make any conclusions about how the particulate phases may be influenced by meltpond mixing or aggregative losses. As summarized in Marsay et al. (2018b), Fe and Mn particles were primarily lithogenic while Zn, Ni, and Cd were primarily non-lithogenic and had Metal/P ratios in agreement with cellular measurements taken within these meltpond samples. However, Fe and Zn showed the most similarities here, particularly at Station 33 where crustal contribution was high for both particulate phases, although Mn, with large crustal contribution, did not. The fact that Ni and Cd did not see significant aggregative loss of colloids perhaps

indicates that the corresponding particulate phases (primarily biogenic) are more stable to aggregation and instead promote dissolution into smaller colloidal and soluble phases.

## 6.5. Conclusions

We originally set out to answer 1) if %colloids were higher in cryospheric freshwaters compared to seawater at our study sites, and 2) if aggregation or decrease in colloids was a major sink of colloids moving from snow/ice to melt ponds to seawater. This required a detailed look at both the relative speciation (%colloids) and concentration ([colloids]) across each station for each metal. We found that the size partitioning of dissolved Fe, Mn, Ni, Cu, Zn, and Cd was remarkably consistent in the surface seawater (<20m) of the Western Arctic Ocean at these six study sites, and, to answer the first question, there were significantly higher %colloids found in the cryospheric freshwaters compared to the underlying seawater for all metals except Cu. However, this observation was partially driven by snow samples, which had high %colloids for most metals, particularly at Stations 31 and 33 where the influence of aerosol deposition was high. Iron and Zn were most significantly affected, although %colloids were very high for Mn and Cd (~50-70%) in snow as well, which do not normally have a significant colloidal fraction.

Surface seawater at Stations 39, 42, and 43 appeared more heavily influenced by river water carried by the TPD current, which is known to hold elevated concentrations of elements such as Fe, Cu, Ni, and Cd. Concentrations and size partitioning for Ni, Cu, Mn, and Cd at these stations appeared to be less affected by the overlying cryosphere as they are elevated in the TPD. In contrast, Fe and Zn had elevated or comparable

[colloids] and %colloids in the cryosphere compared to seawater, even at Stations 39, 42, and 43 indicating that mixing between the freshwater and seawater could result in changes to the underlying seawater partitioning. The same was not true for Ni, Cu, Mn, and Cd.

This was reflected in modeled concentrations of melt ponds that demonstrate aggregative or scavenging effects clearly for Fe and Zn at a majority of stations, but little to no significant losses for other metals. Likewise, snow deposition in both quantity and timing seemed to play a role in the contribution of colloids to the dissolved pool as well as overall concentration. Samples from Stations 31 and 33 that had high aerosol deposition were also most recently collected and the effects of photochemistry and dissolution may not have had a chance to disaggregate or scavenge Fe and Zn colloids, which showed the most significant trend.

This was reflected at Station 46 where aerosol deposition was not necessarily high and the influence of the TPD was negligible. Here, only Fe and Zn showed signs of aggregation or decrease in colloids moving from snow to seawater in both %colloids and [colloids]. While Ni, Cd and Mn had some decrease in %colloids moving from snow to seawater, their [colloids] remained low compared to the underlying seawater, which was again dominated by soluble species. Thus, any perceived “loss” due to a decrease in %colloids couldn’t be attributed to changes in speciation as a result of mixing and transformations occurring within the cryosphere.

It is important to note here that we are only able to make conclusions on speciation and aggregation based on six stations within an ice-covered region of the

Arctic Ocean. There is clearly some geographic variation and the potential dependence on incubation time as a result of sampling timing could exert a large influence on colloid behavior and distribution. As climate change accelerates melting of snow, sea ice and melt ponds, mixing between each pool and with the underlying seawater will become more important. We present here baseline measurements and predictions of how the cryosphere may affect seawater with the assumption that increased melting will occur. Future sampling efforts to collect more data on dissolved and colloidal trace metals across the Arctic will help ascertain the influence of important factors such as river water and snow deposition on controlling speciation within the cryosphere and underlying seawater.

## 6.6. References

- Aguilar-Islas, Ana M., Robert Rember, Shigeto Nishino, Takashi Kikuchi, and Motoyo Itoh. 2013. "Partitioning and lateral transport of iron to the Canada Basin." *Polar Science* 7 (2):82-99. doi: <http://dx.doi.org/10.1016/j.polar.2012.11.001>.
- Aguilar-Islas, A. M., R. D. Rember, C. W. Mordy, and J. Wu. 2008. "Sea ice-derived dissolved iron and its potential influence on the spring algal bloom in the Bering Sea." *Geophysical Research Letters* 35 (24):n/a-n/a. doi: [10.1029/2008GL035736](https://doi.org/10.1029/2008GL035736).
- Aleksi, Nummelin, Ilicak Mehmet, Li Camille, and Smedsrud Lars H. 2016. "Consequences of future increased Arctic runoff on Arctic Ocean stratification, circulation, and sea ice cover." *Journal of Geophysical Research: Oceans* 121 (1):617-637. doi: [doi:10.1002/2015JC011156](https://doi.org/10.1002/2015JC011156).

- Antony, Runa, Amanda M Grannas, Amanda S Willoughby, Rachel L Sleighter, Meloth Thamban, and Patrick G Hatcher. 2014. "Origin and sources of dissolved organic matter in snow on the East Antarctic ice sheet." *Environmental science & technology* 48 (11):6151-6159.
- Arrigo, Kevin R., Donald K. Perovich, Robert S. Pickart, Zachary W. Brown, Gert L. van Dijken, Kate E. Lowry, Matthew M. Mills, Molly A. Palmer, William M. Balch, Frank Bahr, Nicholas R. Bates, Claudia Benitez-Nelson, Bruce Bowler, Emily Brownlee, Jens K. Ehn, Karen E. Frey, Rebecca Garley, Samuel R. Laney, Laura Lubelczyk, Jeremy Mathis, Atsushi Matsuoka, B. Greg Mitchell, G. W. K. Moore, Eva Ortega-Retuerta, Sharmila Pal, Chris M. Polashenski, Rick A. Reynolds, Brian Schieber, Heidi M. Sosik, Michael Stephens, and James H. Swift. 2012. "Massive Phytoplankton Blooms Under Arctic Sea Ice." *Science*. doi: 10.1126/science.1215065.
- Bergquist, B. A., J. Wu, and E. A. Boyle. 2007. "Variability in oceanic dissolved iron is dominated by the colloidal fraction." *Geochimica et Cosmochimica Acta* 71 (12):2960-2974. doi: <http://dx.doi.org/10.1016/j.gca.2007.03.013>.
- Bruland, K. W., R. Middag, and M. C. Lohan. 2014. "8.2 - Controls of Trace Metals in Seawater." In *Treatise on Geochemistry (Second Edition)*, edited by Heinrich D. Holland and Karl K. Turekian, 19-51. Oxford: Elsevier.
- Byrne, Robert H. 2002. "Inorganic speciation of dissolved elements in seawater: the influence of pH on concentration ratios." *Geochemical Transactions* 3 (1):11. doi: 10.1186/1467-4866-3-11.

Charette, Matthew A., Lauren E. Kipp, Laramie T. Jensen, Jessica S. Dabrowski, Laura M. Whitmore, Jessica N. Fitzsimmons, Tatiana Williford, Adam Ulfsbo, Elizabeth Jones, Randelle M. Bundy, Sebastian M. Vivancos, Katharina Pahnke, Seth G. John, Yang Xiang, Mariko Hatta, Mariia V. Petrova, Lars-Eric Heimbürger-Boavida, Dorothea Bauch, Robert Newton, Angelica Pasqualini, Alison M. Agather, Rainer M.W. Amon, Robert F. Anderson, Per S. Andersson, Ronald Benner, Katlin L. Bowman, R. Lawrence Edwards, Sandra Gdaniec, Loes J.A. Gerringa, Aridane G. González, Mats Granskog, Brian Haley, Chad R. Hammerschmidt, Dennis A. Hansell, Paul B. Henderson, David C. Kadko, Karl Kaiser, Patrick Laan, Phoebe J. Lam, Carl H. Lamborg, Martin Levier, Xianglei Li, Andrew R. Margolin, Chris Measures, Rob Middag, Frank J. Millero, Willard S. Moore, Ronja Paffrath, H el ene Planquette, Benjamin Rabe, Heather Reader, Robert Rember, Micha J.A. Rijkenberg, Matthieu Roy-Barman, Michiel Rutgers van der Loeff, Mak Saito, Ursula Schauer, Peter Schlosser, Robert M. Sherrell, Alan M. Shiller, Hans Slagter, Jeroen E. Sonke, Colin Stedmon, Ryan J. Woosley, Ole Valk, Jan van Ooijen, and Ruifeng Zhang. 2020. "The Transpolar Drift as a Source of Riverine and Shelf-Derived Trace Elements to the Central Arctic Ocean." *Journal of Geophysical Research: Oceans* n/a (n/a):e2019JC015920. doi: 10.1029/2019jc015920.

Chen, Min, Robert C. H. Dei, Wen-Xiong Wang, and Laodong Guo. 2003. "Marine diatom uptake of iron bound with natural colloids of different origins." *Marine*

*Chemistry* 81 (3–4):177-189. doi: [http://dx.doi.org/10.1016/S0304-4203\(03\)00032-X](http://dx.doi.org/10.1016/S0304-4203(03)00032-X).

Chen, Min, and Wen-Xiong Wang. 2001. "Bioavailability of natural colloid-bound iron to marine plankton: Influences of colloidal size and aging." *Limnology and Oceanography* 46 (8):1956-1967. doi: 10.4319/lo.2001.46.8.1956.

Cid, Abigail Parcasio, Seiji Nakatsuka, and Yoshiki Sohrin. 2012. "Stoichiometry among bioactive trace metals in the Chukchi and Beaufort Seas." *Journal of oceanography* 68 (6):985-1001.

Cullen, Jay T, Bridget A Bergquist, and James W Moffett. 2006. "Thermodynamic characterization of the partitioning of iron between soluble and colloidal species in the Atlantic Ocean." *Marine Chemistry* 98 (2-4):295-303.

Dai, Min-Han, and Jean-Marie Martin. 1995. "First data on trace metal level and behaviour in two major Arctic river-estuarine systems (Ob and Yenisey) and in the adjacent Kara Sea, Russia." *Earth and Planetary Science Letters* 131 (3):127-141. doi: [http://dx.doi.org/10.1016/0012-821X\(95\)00021-4](http://dx.doi.org/10.1016/0012-821X(95)00021-4).

Dammshäuser, Anna, and Peter L. Croot. 2012. "Low colloidal associations of aluminium and titanium in surface waters of the tropical Atlantic." *Geochimica et Cosmochimica Acta* 96:304-318. doi: <http://dx.doi.org/10.1016/j.gca.2012.07.032>.

Dickson, Bob, Igor Yashayaev, Jens Meincke, Bill Turrell, Stephen Dye, and Juergen Holfort. 2002. "Rapid freshening of the deep North Atlantic Ocean over the past four decades." *Nature* 416 (6883):832.

- Dieckmann, Gerhard, Gernot Nehrke, Christiane Uhlig, J Göttlicher, Sebastian Gerland, Mats A Granskog, and David N Thomas. 2010. "Ikaite (CaCO<sub>3</sub> · 6H<sub>2</sub>O) discovered in Arctic sea ice." *The Cryosphere* 4:227-230.
- Erickson, Harold P. 2009. "Size and Shape of Protein Molecules at the Nanometer Level Determined by Sedimentation, Gel Filtration, and Electron Microscopy." *Biological Procedures Online* 11 (1):32. doi: 10.1007/s12575-009-9008-x.
- Fitzsimmons, Jessica N., and Edward A. Boyle. 2012. "An intercalibration between the GEOTRACES GO-FLO and the MITESS/Vanes sampling systems for dissolved iron concentration analyses (and a closer look at adsorption effects)." *Limnology and Oceanography: Methods* 10 (6):437-450. doi: 10.4319/lom.2012.10.437.
- Fitzsimmons, Jessica N, and Edward A Boyle. 2014. "Assessment and comparison of Anopore and cross flow filtration methods for the determination of dissolved iron size fractionation into soluble and colloidal phases in seawater." *Limnol. Oceanogr. Methods* 12:246-263.
- Fitzsimmons, Jessica N., and Edward A. Boyle. 2014. "Both soluble and colloidal iron phases control dissolved iron variability in the tropical North Atlantic Ocean." *Geochimica et Cosmochimica Acta* 125:539-550. doi: <http://dx.doi.org/10.1016/j.gca.2013.10.032>.
- Fitzsimmons, Jessica N., G. G. Carrasco, J. Wu, S. Roshan, M. Hatta, C. I. Measures, T. M. Conway, S. G. John, and E. A. Boyle. 2015. "Partitioning of dissolved iron and iron isotopes into soluble and colloidal phases along the GA03

- GEOTRACES North Atlantic Transect." *Deep-Sea Research Part II: Topical Studies in Oceanography* 116:130-151. doi: 10.1016/j.dsr2.2014.11.014.
- Fitzsimmons, Jessica N., Seth G John, Christopher M Marsay, Colleen L Hoffman, Sarah L Nicholas, Brandy M Toner, Christopher R German, and Robert M Sherrell. 2017. "Iron persistence in a distal hydrothermal plume supported by dissolved–particulate exchange." *Nature Geoscience* 10 (3):195.
- Frey, Karen E., and James W. McClelland. 2009. "Impacts of permafrost degradation on arctic river biogeochemistry." *Hydrological Processes* 23 (1):169-182. doi: 10.1002/hyp.7196.
- Gledhill, Martha, and Kristen N. Buck. 2012. "The Organic Complexation of Iron in the Marine Environment: A Review." *Frontiers in Microbiology* 3:69. doi: 10.3389/fmicb.2012.00069.
- Grannas, A. M., A. E. Jones, J. Dibb, M. Ammann, C. Anastasio, H. J. Beine, M. Bergin, J. Bottenheim, C. S. Boxe, G. Carver, G. Chen, J. H. Crawford, F. Dominé, M. M. Frey, M. I. Guzmán, D. E. Heard, D. Helmig, M. R. Hoffmann, R. E. Honrath, L. G. Huey, M. Hutterli, H. W. Jacobi, P. Klán, B. Lefer, J. McConnell, J. Plane, R. Sander, J. Savarino, P. B. Shepson, W. R. Simpson, J. R. Sodeau, R. Von Glasow, R. Weller, E. W. Wolff, and T. Zhu. 2007. "An overview of snow photochemistry: evidence, mechanisms and impacts." *Atmospheric Chemistry and Physics Discussions* 7 (2):4165-4283.
- Gunnars, Anneli, Sven Blomqvist, Peter Johansson, and Christian Andersson. 2002. "Formation of Fe(III) oxyhydroxide colloids in freshwater and brackish seawater,

- with incorporation of phosphate and calcium." *Geochimica et Cosmochimica Acta* 66 (5):745-758. doi: [https://doi.org/10.1016/S0016-7037\(01\)00818-3](https://doi.org/10.1016/S0016-7037(01)00818-3).
- Guo, Laodong, and Peter H. Santschi. 1997. "Composition and cycling of colloids in marine environments." *Reviews of Geophysics* 35 (1):17-40. doi: [doi:10.1029/96RG03195](https://doi.org/10.1029/96RG03195).
- Hölemann, J. A., M. Schirmacher, and A. Prange. 2005. "Seasonal variability of trace metals in the Lena River and the southeastern Laptev Sea: Impact of the spring freshet." *Global and Planetary Change* 48 (1–3):112-125. doi: <http://dx.doi.org/10.1016/j.gloplacha.2004.12.008>.
- Holmes, R. M., J. W. McClelland, S. E. Tank, R. G. M. Spencer, and A. I. Shiklomanov. 2019. Arctic Great Rivers Observatory. Water quality dataset.
- Jensen, L. T., N. J. Wyatt, W. M. Landing, and J. N. Fitzsimmons. 2020. "Assessment of the stability, sorption, and exchangeability of marine dissolved and colloidal metals." *Marine Chemistry* 220:103754. doi: <https://doi.org/10.1016/j.marchem.2020.103754>.
- Jensen, L. T., N. J. Wyatt, B. S. Twining, S. Rauschenberg, W. M. Landing, R. M. Sherrell, and J. N. Fitzsimmons. 2019. "Biogeochemical Cycling of Dissolved Zinc in the Western Arctic (Arctic GEOTRACES GN01)." *Global Biogeochemical Cycles* 33 (3):343-369. doi: [10.1029/2018gb005975](https://doi.org/10.1029/2018gb005975).
- Kadko, David, Ana Aguilar-Islas, Channing Bolt, Clifton S Buck, Jessica N Fitzsimmons, Laramie T Jensen, William M Landing, Christopher M Marsay, Robert Rember, and Alan M Shiller. 2018. "The residence times of trace

elements determined in the surface Arctic Ocean during the 2015 US Arctic GEOTRACES expedition." *Marine Chemistry*.

- Karcher, Michael, John N Smith, Frank Kauker, Rüdiger Gerdes, and William M Smethie. 2012. "Recent changes in Arctic Ocean circulation revealed by iodine-129 observations and modeling." *Journal of Geophysical Research: Oceans* 117 (C8).
- Klunder, M. B., D. Bauch, P. Laan, H. J. W. de Baar, S. van Heuven, and S. Ober. 2012. "Dissolved iron in the Arctic shelf seas and surface waters of the central Arctic Ocean: Impact of Arctic river water and ice-melt." *Journal of Geophysical Research: Oceans* 117 (C1):n/a-n/a. doi: 10.1029/2011JC007133.
- Klunder, M. B., P. Laan, R. Middag, H. J. W. de Baar, and K. Bakker. 2012. "Dissolved iron in the Arctic Ocean: Important role of hydrothermal sources, shelf input and scavenging removal." *Journal of Geophysical Research: Oceans* 117 (C4):n/a-n/a. doi: 10.1029/2011JC007135.
- Kondo, Yoshiko, Hajime Obata, Nanako Hioki, Atsushi Ooki, Shigeto Nishino, Takashi Kikuchi, and Kenshi Kuma. 2016. "Transport of trace metals (Mn, Fe, Ni, Zn and Cd) in the western Arctic Ocean (Chukchi Sea and Canada Basin) in late summer 2012." *Deep Sea Research Part I: Oceanographic Research Papers* 116:236-252. doi: <http://dx.doi.org/10.1016/j.dsr.2016.08.010>.
- Kuma, Kenshi, Jun Nishioka, and Katsuhiko Matsunaga. 1996. "Controls on iron (III) hydroxide solubility in seawater: the influence of pH and natural organic chelators." *Limnology and Oceanography* 41 (3):396-407.

- Kunde, K, NJ Wyatt, D González-Santana, A Tagliabue, C Mahaffey, and MC Lohan. 2019. "Iron Distribution in the Subtropical North Atlantic: The Pivotal Role of Colloidal Iron." *Global Biogeochemical Cycles*.
- Lagerström, Maria, M. Field, Marie Seguret, Fisher E, Clark, and Robert Sherrell. 2013. "Automated on-line flow-injection ICP-MS determination of trace metals (Mn, Fe, Co, Ni, Cu and Zn) in open ocean seawater: Application to the GEOTRACES program." *Marine Chemistry* 155:71-80. doi: 10.1016/j.marchem.2013.06.001.
- Lannuzel, Delphine, Pier C. van der Merwe, Ashley T. Townsend, and Andrew R. Bowie. 2014. "Size fractionation of iron, manganese and aluminium in Antarctic fast ice reveals a lithogenic origin and low iron solubility." *Marine Chemistry* 161:47-56. doi: <https://doi.org/10.1016/j.marchem.2014.02.006>.
- Lei, Ying D, and Frank Wania. 2004. "Is rain or snow a more efficient scavenger of organic chemicals?" *Atmospheric Environment* 38 (22):3557-3571.
- Macdonald, RW, ZA Kuzyk, and SC Johannessen. 2015. "It is not just about the ice: a geochemical perspective on the changing Arctic Ocean." *Journal of Environmental Studies and Sciences* 5 (3):288-301.
- Macdonald, R.W., Z. A. Kuzyk, and S. C. Johannessen. 2015. "It is not just about the ice: a geochemical perspective on the changing Arctic Ocean." *Journal of Environmental Studies and Sciences* 5 (3):288-301. doi: 10.1007/s13412-015-0302-4.

Marsay, Chris M., Ana Aguilar-Islas, Jessica N. Fitzsimmons, Mariko Hatta, Laramie T. Jensen, Seth G. John, David Kadko, William M. Landing, Nathan T. Lanning, Peter L. Morton, Angelica Pasqualini, Sara Rauschenberg, Robert M. Sherrell, Alan M. Shiller, Benjamin S. Twining, Laura M. Whitmore, Ruifeng Zhang, and Clifton S. Buck. 2018. "Dissolved and particulate trace elements in late summer Arctic melt ponds." *Marine Chemistry* 204:70-85. doi: <https://doi.org/10.1016/j.marchem.2018.06.002>.

Marsay, Chris M., David Kadko, William M. Landing, Peter L. Morton, Brent A. Summers, and Clifton S. Buck. 2018. "Concentrations, provenance and flux of aerosol trace elements during US GEOTRACES Western Arctic cruise GN01." *Chemical Geology* 502:1-14. doi: <https://doi.org/10.1016/j.chemgeo.2018.06.007>.

Measures, C. I. 1999. "The role of entrained sediments in sea ice in the distribution of aluminium and iron in the surface waters of the Arctic Ocean." *Marine Chemistry* 68 (1–2):59-70. doi: [http://dx.doi.org/10.1016/S0304-4203\(99\)00065-1](http://dx.doi.org/10.1016/S0304-4203(99)00065-1).

Middag, R., HJW De Baar, P Laan, and K Bakker. 2009. "Dissolved aluminium and the silicon cycle in the Arctic Ocean." *Marine Chemistry* 115 (3):176-195.

Middag, R., H. J. W. de Baar, P. Laan, and M. B. Klunder. 2011. "Fluvial and hydrothermal input of manganese into the Arctic Ocean." *Geochimica et Cosmochimica Acta* 75 (9):2393-2408. doi: <http://dx.doi.org/10.1016/j.gca.2011.02.011>.

- Moffett, James W, and Christopher Dupont. 2007. "Cu complexation by organic ligands in the sub-arctic NW Pacific and Bering Sea." *Deep Sea Research Part I: Oceanographic Research Papers* 54 (4):586-595.
- Nakayama, Yuta, Satoshi Fujita, Kenshi Kuma, and Koji Shimada. 2011. "Iron and humic-type fluorescent dissolved organic matter in the Chukchi Sea and Canada Basin of the western Arctic Ocean." *Journal of Geophysical Research: Oceans* 116 (C7):n/a-n/a. doi: 10.1029/2010JC006779.
- Nishimura, Shotaroh, Kenshi Kuma, Satoko Ishikawa, Aya Omata, and Sei-ichi Saitoh. 2012. "Iron, nutrients, and humic-type fluorescent dissolved organic matter in the northern Bering Sea shelf, Bering Strait, and Chukchi Sea." *Journal of Geophysical Research: Oceans* 117 (C2):n/a-n/a. doi: 10.1029/2011JC007355.
- Oldham, Véronique E., Alfonso Mucci, Bradley M. Tebo, and George W. Luther Iii. 2017. "Soluble Mn(III)–L complexes are abundant in oxygenated waters and stabilized by humic ligands." *Geochimica et Cosmochimica Acta* 199:238-246. doi: <http://dx.doi.org/10.1016/j.gca.2016.11.043>.
- Opsahl, Stephen, Ronald Benner, and Rainer M. W. Amon. 1999. "Major flux of terrigenous dissolved organic matter through the Arctic Ocean." *Limnology and Oceanography* 44 (8):2017-2023. doi: 10.4319/lo.1999.44.8.2017.
- Peterson, Bruce J., Robert M. Holmes, James W. McClelland, Charles J. Vörösmarty, Richard B. Lammers, Alexander I. Shiklomanov, Igor A. Shiklomanov, and Stefan Rahmstorf. 2002. "Increasing River Discharge to the Arctic Ocean." *Science* 298 (5601):2171-2173. doi: 10.1126/science.1077445.

- Pokrovsky, O. S., L. S. Shirokova, J. Viers, V. V. Gordeev, V. P. Shevchenko, A. V. Chupakov, T. Y. Vorobieva, F. Candaudap, C. Causserand, A. Lanzanova, and C. Zouiten. 2014. "Fate of colloids during estuarine mixing in the Arctic." *Ocean Sci.* 10 (1):107-125. doi: 10.5194/os-10-107-2014.
- Rijkenberg, Micha J. A., Hans A. Slagter, Michiel Rutgers van der Loeff, Jan van Ooijen, and Loes J. A. Gerringa. 2018. "Dissolved Fe in the Deep and Upper Arctic Ocean With a Focus on Fe Limitation in the Nansen Basin." *Frontiers in Marine Science* 5 (88). doi: 10.3389/fmars.2018.00088.
- Roshan, Saeed, and Jingfeng Wu. 2018. "Dissolved and colloidal copper in the tropical South Pacific." *Geochimica et Cosmochimica Acta* 233:81-94. doi: <https://doi.org/10.1016/j.gca.2018.05.008>.
- Roth, Christine M, Kai-Uwe Goss, and René P Schwarzenbach. 2004. "Sorption of diverse organic vapors to snow." *Environmental science & technology* 38 (15):4078-4084.
- Rue, Eden L, and Kenneth W Bruland. 1995. "Complexation of iron (III) by natural organic ligands in the Central North Pacific as determined by a new competitive ligand equilibration/adsorptive cathodic stripping voltammetric method." *Marine chemistry* 50 (1-4):117-138.
- Sempere, Richard, and Kimitaka Kawamura. 1994. "Comparative distributions of dicarboxylic acids and related polar compounds in snow, rain and aerosols from urban atmosphere." *Atmospheric Environment* 28 (3):449-459.

- Sholkovitz, Edward R. 1978. "The flocculation of dissolved Fe, Mn, Al, Cu, NI, Co and Cd during estuarine mixing." *Earth and Planetary Science Letters* 41 (1):77-86.
- Slagter, Hans A., Luis M. Laglera, Camila Sukekava, and Loes J. A. Gerringa. 2019. "Fe-Binding Organic Ligands in the Humic-Rich TransPolar Drift in the Surface Arctic Ocean Using Multiple Voltammetric Methods." *Journal of Geophysical Research: Oceans* 124 (3):1491-1508. doi: 10.1029/2018jc014576.
- Spencer, Robert GM, Paul J Mann, Thorsten Dittmar, Timothy I Eglinton, Cameron McIntyre, R Max Holmes, Nikita Zimov, and Aron Stubbins. 2015. "Detecting the signature of permafrost thaw in Arctic rivers." *Geophysical Research Letters* 42 (8):2830-2835.
- Sunda, WG, SA Huntsman, and GR Harvey. 1983. "Photoreduction of manganese oxides in seawater and its geochemical and biological implications." *Nature* 301 (5897):234-236.
- Sunda, William G. 2012. "Feedback interactions between trace metal nutrients and phytoplankton in the ocean." *Frontiers in Microbiology* 3. doi: 10.3389/fmicb.2012.00204.
- Sunda, William G, and Susan A Huntsman. 1994. "Photoreduction of manganese oxides in seawater." *Marine chemistry* 46 (1-2):133-152.
- Taylor, Rebecca L, David M Semeniuk, Christopher D Payne, Jie Zhou, Jean-Éric Tremblay, Jay T Cullen, and Maria T Maldonado. 2013. "Colimitation by light, nitrate, and iron in the Beaufort Sea in late summer." *Journal of Geophysical Research: Oceans* 118 (7):3260-3277.

- Tovar-Sánchez, Antonio, Carlos M. Duarte, Juan C. Alonso, Silvia Lacorte, Romà Tauler, and Cristobal Galbán-Malagón. 2010. "Impacts of metals and nutrients released from melting multiyear Arctic sea ice." *Journal of Geophysical Research: Oceans* 115 (C7):n/a-n/a. doi: 10.1029/2009JC005685.
- Vraspir, Julia M, and Alison Butler. 2009. "Chemistry of marine ligands and siderophores."
- Weeks, Wilford F, and Stephen F Ackley. 1986. "The growth, structure, and properties of sea ice." In *The geophysics of sea ice*, 9-164. Springer.
- Wells, Mark L. 2002. "Marine colloids and trace metals." *Biogeochemistry of marine dissolved organic matter*:367-404.
- Wilkinson, K. J., J. C. Negre, and J. Buffle. 1997. "Coagulation of colloidal material in surface waters: the role of natural organic matter." *Journal of Contaminant Hydrology* 26 (1):229-243. doi: [https://doi.org/10.1016/S0169-7722\(96\)00071-X](https://doi.org/10.1016/S0169-7722(96)00071-X).
- Wu, Jingfeng, Edward Boyle, William Sunda, and Liang-Saw Wen. 2001. "Soluble and Colloidal Iron in the Oligotrophic North Atlantic and North Pacific." *Science* 293 (5531):847-849. doi: 10.1126/science.1059251.
- Zhang, Ruifeng, Laramie T. Jensen, Jessica N. Fitzsimmons, Robert M. Sherrell, and Seth John. 2019. "Dissolved cadmium and cadmium stable isotopes in the western Arctic Ocean." *Geochimica et Cosmochimica Acta* 258:258-273. doi: <https://doi.org/10.1016/j.gca.2019.05.028>.

## 7. SUMMARY AND CONCLUSIONS

The goal of this dissertation was to use the strength of a multielement method to explore the biogeochemical processes governing the behavior of trace metals in the Western Arctic Ocean and place them in a global context. We went in with a limited understanding of trace metal distribution in the Arctic, particularly within the central basin. However, it was evident that riverine input, sea ice melt, the broad continental shelves, and restrictive bathymetry that all typify the Western Arctic Ocean have a large effect on trace metal distributions. It was immediately clear that the typical “nutrient”, “scavenged”, “hybrid”-type profile behaviors that we are used to seeing in the global ocean were entirely absent in the Arctic Ocean. Instead, trace metals such as Fe, Zn, Ni, Cu, and Mn had high surface concentrations that decreased to constant, low values at depth. This is primarily due to the key factors controlling trace metal distribution within the Arctic Ocean: high riverine input that maintains elevated metals in the surface ocean in the absence of strong biological uptake; a strong shelf-derived flux of elements such as Fe, Zn, and Mn that are carried into the central basin by a subsurface water mass; and a stark absence of typical remineralization signals at depth.

In a global context, the Arctic trace metal profiles summarized here are entirely unique. Likewise, the strong relationship of many elements to macronutrients (like Zn to Si) is weak or absent in the Western Arctic Ocean. Within the deep water column the metals are low and governed primarily by slow mixing of Atlantic-derived waters that are sparingly ventilated. Importantly, many classic global biogeochemical processes and

interfaces such as river input and continental shelf exchange are present in the Arctic Ocean, but the nature of the particle-poor, advective basin belies significant biological cycling as well strong scavenging signals. As climate change continues to release freshwater to the surface Arctic, the exchange between the more dynamic upper water column and deep water will likely become increasingly limited.

The studies summarized in this dissertation help lay the groundwork for more studies involving trace metals in the Arctic Ocean in the future. It is important to establish these baseline distributions in a rapidly changing environment. With the wealth of established oceanic tracers from this study, it is our hope that future studies will further synthesize processes previously less well understood, such as the seasonality and variability of water mass circulation on the Chukchi Shelf. Future work should also be done on better characterizing the origin and ages of Arctic deep water and whether trace metal concentrations are affected primarily by preformed, Atlantic-derived values or influenced by scavenging and sporadic ventilation. The observations in the Arctic Ocean serve to upend our classical view of trace metals and highlight the controls on biogeochemical cycling in an important conduit to the North Atlantic that is disproportionately affected by ongoing climate change.